

Estimation Of Surface Fluxes Using Bulk Transfer
Methods Over Lake Surface: An Example Of Lake
Kasumigaura

Zhongwang Wei

2013/07/08

Abstract

Studying atmospheric dynamics like evaporation is quite important for water resources management, meteorology and hydrology. Owing to difficulties in field observations, the related researches over water surfaces especially lake surfaces have generally been received less attention and the lake-atmosphere interaction is not as well understood as compared to the land-atmospheric interaction. To combat this lack of knowledge, 10 Hz fluxes data, 30 min averaged atmospheric data and wave data have been obtained since June of 2007 at the observatory located in the center of Lake Kasumigaura which is the second largest lake in Japan.

The lake-atmosphere interaction in atmospheric dynamics mainly includes those processes that influence the transport of momentum, heat and moisture fluxes over lake surface. The eddy correlation technique is a method of direct measurement of these fluxes, but it is not always applicable and needs gap filling in case of data gap due to e.g. rainfall. Therefore, to determine the fluxes for a long period or for gap filling purpose, the bulk transfer method is an attractive alternative since it uses routinely measured mean meteorological quantities. However, since the turbulent structure and geographic condition are complex, there are still several problems that need to be solved to apply this method over lake surface. In this thesis, the influence of lake current, stability, large scale convection and wave on bulk transfer methods was investigated. Furthermore, the fluxes and evaporation over three years were estimated in order to estimate hydrological characteristics of lake Kasumigaura by applying eddy correlation method and bulk transfer method. The main findings are summarized as follows:

1. Bulk transfer method related to the locally generated turbulence

By using the measurement of lake current for one and half months, it was shown that the surface current was quite small and negligible in estimating a relative wind speed to a moving water surface due to lake current. The current is mainly induced by the wind and was two orders of magnitude smaller than that of wind speed. In the moderate to high wind speed region, the neutral bulk coefficients derived from eddy correlation method were found in agreement with those reported in the previous studies. Over lake surface the heat fluxes are

relatively small, and the stability is mainly dominated by the friction velocity or wind speed. Therefore the atmosphere over the lake surface is near neutral and the stability has smaller effect on the bulk coefficients as computed to the land surfaces.

2. Bulk transfer method related to the large-scale convection

The characteristics of large-scale convection were investigated by applying cospectral and ogive analysis. It was found that the bulk coefficient increased with decrease of wind speed under weak wind speed range. The mismatch of time scale between fluxes and wind speed was found to be responsible for this. To partially solve this mismatch, modified bulk transfer methods related to an gustiness factor were added to improve the fluxes estimation under light wind condition when we consider both locally generated turbulence and large-scale convection. The convective boundary layer depth was estimated by a slab model agrees with that determined by the pilot balloon measurement, and was used to estimate effective wind speed. Furthermore, an alternative method using scalar averaged wind speed was investigated as well. By applying these methods, the estimated fluxes became closer to the measurement value than traditional method under weak wind speed region.

3. The wave influence in lake-atmosphere interaction

By applying the wind profile method, the roughness length expressed as Charnock equation was found to depend only on the wind friction velocity u_* , and the acceleration of gravity, g . The wind profile relation was tested by field experiment, where it shows in agreement with those reported in previous studies over lands, and the correction for wind profile relation is not necessary. Above all, in measurement height (10 m), the turbulence was mainly controlled by the atmosphere flow, the water surface state was negligible in the application of bulk transfer method. This study presented evidence showing that the influence of wind wave over lake surface is negligible in air-lake exchange.

4. Fluxes and evaporation over lake surface

The energy budget and evaporation were estimated by eddy correlation method with gap filling applied by the bulk transfer method. The storage of energy in the lake is a very important which is different from over land. The vertical profile of water temperature was measured each month, indicating that the water in different depth is well mixed, and the vertical temperature gradient was not found during observation month. This well mixture

of water could absorb more energy. Since the water surface temperature is always higher than air temperature, evaporation occurred all the time which is also different from other lake fluxes studies. Finally, the long term fluxes and evaporation were summarized. The sensible heat and latent heat were always positive. A seasonal variation of latent heat was found similar to that of the net radiation. Sensible heat fluxes tended to keep a constant value and quite smaller compared to latent heat.

KEYWORDS: bulk coefficient, evaporation, flux, lake current, large scale convection, wave

Contents

Abstract	i
Contents	
Contents of tables	vi
Contents of figures	vii
1 Introduction.....	1
1.1 The interaction between lake-land-atmosphere.....	1
1.2 Lake evaporation and energy balance	2
1.3 The bulk transfer method.....	3
1.4 Outline of the thesis.....	5
2 Study area.....	9
2.1 Study site	9
2.2 Outline of observation	10
3 Methodology	21
3.1 Methods	21
3.2 Data processing and selection	22
3.3 Gap filling for long term fluxes and evaporation estimation.....	27
3.4 Summary and outline of data selection	27
4 Bulk coefficients estimated from eddy correlation data and wind profile.....	36
4.1 Estimation of neutral bulk coefficients.....	36
4.2 Diabatic bulk coefficient.....	37
4.3 Errors in sensible heat bulk coefficients estimation	38
5 Factors controlling bulk coefficients variation over water surface	47
5.1 Surface current.....	47
5.2 wave impact on roughness length and TKE energy budget	48
5.3 Large scale convection	57

6	Application: estimation of Surface Heat Fluxes over Kasumigaura combining bulk transfer methods and eddy correlation method	116
6.1	Fluxes and evaporation estimation over lake surface	116
6.2	Daily variation	117
6.3	Long term variation	117
7	Conclusions.....	128
	Acknowledgements.....	132
	References.....	133
	Appendix A.....	144
	Appendix B.....	147
	Appendix C.....	149
	Appendix D.....	167

Contents of tables

1.1	Previous studies of bulk coefficients estimation	6
1.2	Previous studies of bulk coefficients estimation (continued)	7
2.1	Long term data collection by MLIT (The Ministry of Land, Infrastructure and Transport and Tourism of Japan)	11
2.2	Long term data collection by Univ of Tsukuba	12
2.3	Short term observation	13
3.1	Classification of the data quality by the stationarity test and the integral turbulence characteristics according to Foken et al.(2005)	29
5.1	Charnock paramter proposed for power-law relation, $z_{0m}g/u_*^2 = A(u_*/c_p)^B$	76
5.2	pilot balloon observation.....	89
5.3	High wind speed cases for ogive analysis (2h averaging period).....	93
5.4	Low wind speed cases for ogive analysis (2h averaging period).....	94
5.5	High wind speed cases for estimation of convective time scale (2h averaging period)	108
5.6	Low wind speed cases for estimation of convective time scale (2h averaging period)	109
5.7	Trend condition for high wind speed cases	112
5.8	Trend condition for low wind speed cases.....	113
5.9	Various definitions of time scale for high wind speed cases (min)	114
5.10	Various definitions of time scale for low wind speed cases (min).....	115

Contents of figures

1.1	Schematic view of the atmospheric boundary layer over lake surface.....	8
2.1	Kasumigaura basin and Pilot balloon observation. Black circles represents Koshin observatory, red circle represents Ushiwata, blue squares represents Rinkojiken, and green triangles represents Tennonshi	14
2.2	Observatory at the center of Kasumigaura (Photo was taken on 2012/12/03)	15
2.3	Schematic view of observatory	16
2.4	The fetch of Lake Kasumigaura (Unit: km)	17
2.5	The wind direction over observatory during 2008-2010 (30 min interval)	18
2.6	The wind speed over observatory during 2008-2010 (30 min interval)	19
2.7	The stability over observatory during 2008-2010 (30 min interval).....	20
3.1	Spectral analysis for giving a general view of dataset (2009/01/15 09:00-09:30 JST). u , v and w are the three component of wind speed, t is for temperature, q is for moisture and c is for CO_2	30
3.2	The integral turbulence characteristic test for wind speed, sensible heat, latent heat and carbon dioxide flux. subscribe w is for vertical wind speed, t is for temperature, q is for moisture and c is for CO_2 . $-z/L$ is stability and σ is standard variation .	31
3.3	Stationarity test for v component wind speed (2009, 30 min interval)	32
3.4	Stationarity test for u component wind speed (2009, 30 min interval)	33
3.5	The procedure of data analysis	34
3.6	Stability functions verse stability, derived by different authors: Paulson (1970), Fairall (1996) and Brutsaert (1992)	35
4.1	Neutral 10-m drag transfer coefficient C_{dn} as a function of 10-m wind speed, in comparison with previous studies.....	41
4.2	Neutral 10-m temperature transfer coefficient C_{hn} as a function of 10-m wind speed, in comparison with previous studies.....	42

4.3	Neutral 10-m moisture transfer coefficient C_{en} as a function of 10-m wind speed, in comparison with previous studies.....	43
4.4	Transfer coefficients as a function of dt	44
4.5	Transfer coefficient as a function of bulk Richardson number.....	45
4.6	The probable error analysis for sensible heat bulk coefficient in high wind speed region. σ_{Ch} is the probable error for C_h , wt is sensible heat flux and dt it temperature difference between water surface and air.....	46
5.1	Photos about Acoustic Doppler Current Profiler (Figure by The Ministry of Land, Infrastructure and Transport and Tourism of Japan).....	75
5.2	Comparison of wind speed and water surface current speed for the period of 2008/2/22-2008/3/18	76
5.3	Comparison of wind speed and a relative wind speed by considering the surface current	77
5.4	The surface current speed as a function of wind speed	78
5.5	The growth of wave by the wind over lake surface	79
5.6	The height of the dominant wave as a function of wind speed.....	80
5.7	The period of the dominant wave as a function of wind speed	81
5.8	The phase speed of the dominant wave as a function of wind speed	82
5.9	Roughness Reynolds number Rr verse friction velocity, blue circles for $Rr \geq 2.3$, red squares for $0.13 \leq Rr < 2.3$, green triangles for $Rr < 0.13$	83
5.10	Typical schematic of a wind profile over the water surface (redraw from Sjoblom and Smedman (2003)).....	84
5.11	Variation of momentum roughness length with Charnock parameter u_*^2/g , the slope derived from origin through regression of each 0.02 x-axis bin median value	85
5.12	Charnock parameter versus inverse of wave age for rough surface ($Rr > 3.2$). The curve are from Smith et al. (1992), Johnson et al. (1998) and Drennan et al. (2003)..	86
5.13	Dependence of the shear correction function ψ on the wave age parameter c_p/u_*	87
5.14	Dimensional presentation of the Charnock formula. (Figure by Toba et al. (1990))...	88
5.15	In comparison with friction velocity driver from a constant Charnock parameter and empirical wave information method by Taylor and Yelland (2001).....	89
5.16	Drag coefficient under weak wind speed.....	90
5.17	The drag coefficient related to wind direction, net radiation and temperature between the air and water surface.....	91

5.18	Schematic of energy spectrum in the atmosphere boundary layer showing distinct regions of energy production (A) and dissipation (C) and the inertial subrange (B), where both energy production and dissipation are negligible. (Redrawn from Kaimal and Finnigan (1994)).....	92
5.19	Normalized surface layer cospectral of uw . The bold red line represents the standard cospectra by Kaimal et al. (1972)	95
5.20	Ogives of momentum flux cospectral as a function of frequency. The dotted lines from right to left represents the time scale of 10-min, 30-min, 60-min and 120-min..	96
5.21	Mean wind speed as a function of frequency, the dotted lines from right to left represent the time scale of 10-min, 30-min, 60-min and 120-min.	97
5.22	Drag coefficient estimated from the ogive and wind speed as a function of frequency, the dotted lines from right to left represent the time scale of 10-min, 30-min, 60-min and 120-min.	98
5.23	The pilot balloon observation. The red line represents the height of CBL depth.	99
5.24	Schematic diagram of potential temperature and sensible heat flux profile in slab model. θ is temperature, $\overline{w'\theta'}$ is the sensible heat flux, the subscribe h and s represent convection height and land surface. γ is a constant value of dry adiabatic lapse rate.	100
5.25	The sensible heat at Lake center (Koshin), Ushiwata and Terrestrial Environment Research Center (TERC) at 2011/08/26.	101
5.26	The CBL depth derived from different data sets (2011/08/26).	102
5.27	CBL depth estimated using Terrestrial Environment Research Center data in comparison with observation	103
5.28	Comparison of CBL depth estimated from Mie lidar and slab model (Figure by Saotome (2009)). Dotted line represents the CBL depth derived from slab model, and solid line represents the CBL depth derived from Mie lidar	104
5.29	Comparison of CBL depth estimated from ozone lidar and slab model (2008/02/08)	105
5.30	Scalar averaged wind speed U_{scalar} and effective wind speed U_e related to vector averaged wind speed U	106
5.31	Bulk coefficients derived from vector averaged wind speed U , scalar averaged wind speed U_{scalar} and effective wind speed U_e	107
5.32	Normalized variance versus time scale using a averaging time of $T=120$ min, the black line indicates $\sigma^2/\sigma_{60}^2 = 1$	110

5.33	Miltiresolustion decomposition of the momentum flux as a function of the averaging time scale.	111
6.1	Daily variation of radiation in summer and winter.....	119
6.2	Daily variation of energy in summer and winter	120
6.3	Daily variation of vertical temperature in summer and winter.....	121
6.4	Monthly measured water temperature in variation water depth	122
6.5	Monthly averaged temperature in air, water surface and 1.0 m water depth.....	123
6.6	Monthly sum of energy balance over lake surface during 2008-2010	124
6.7	Daily sum of net radiation, precipitation, evaporation and daily averaged water level: 2008.....	125
6.8	Daily sum of net radiation, precipitation, evaporation and daily averaged water level: 2009.....	126
6.9	Daily sum of net radiation, precipitation, evaporation and daily averaged water level: 2010.....	127

1 Introduction

1.1 The interaction between lake-land-atmosphere

Lakes cover only about 3% of the earth's surface (Downing et al., 2006), but the interaction among land-atmosphere-lake surface is very sensitive to changes in the basins' hydrological cycle, water resources management and meteorology. Due to difficulties in field work, usually we assume that the boundary layer over the lake surface behaves in the same way as the boundary layer over the land or over the sea surface, but recently few findings (e.g. Drennan et al., 2003; Read et al., 2012; Sun et al., 1997) revealed that the processes over the water surface are significantly different from those of the land and the sea surface. Since it is generally received less attention and the lake-atmosphere-land interaction is not as well understood, the impacts on the exchange of momentum, moisture and temperature brought by the interaction among land-atmosphere-lake surface were focused on in the thesis.

To investigate the difference of the boundary layer over lake, land and sea surface, the main process of lake-atmosphere-land exchange schematic was depicted in Fig.1.1. The main differences and remaining issues are summarized as follows:

1. The lake-atmosphere dynamics are different from those of land-atmosphere dynamics, which is manifested chiefly by wind-wave interaction. The surface wave creates boundary conditions for the atmospheric flow, and the varying characteristics of the wave field exert profound influence on the structure of the marine atmospheric boundary layer (Sjoblom and Smedman, 2003). Until now, wave influence on turbulence is still open to discussion. The layer named wave boundary layer where the wave directly influenced the flux is not clearly understood (Sjoblom and Smedman, 2003). Furthermore the characteristic of wave is different from that of sea surface: the swell plays very important role over sea surface but wave over the medium-sized lake surface is mainly induced by the local wind.
2. Lake-land interaction mainly reflected by the large scale convection, which is induced by temperature uneven distribution between lands and lake surface. Since the lakes are sur-

rounded by lands, in most of cases the spatial extent of a lake is too small to strictly expect equilibrium conditions of the atmospheric turbulence with the local water surface (Vesala et al., 2012). The turbulence over lake surface presented in the surface layer does not merely consist of the mechanical turbulence, but associates with the thermal convection (Vercauteren, 2011). Physical prediction model is difficult to establish and verification due to unknown factors encountered in the actual large-scale convective exchange process.

1.2 Lake evaporation and energy balance

Lake-atmosphere-land interaction in atmospheric dynamics mainly includes those processes that influence the transport of momentum, heat and moisture fluxes over lake surface. Accurate estimates of surface energy exchange components are critical for understanding various physical processes of large lakes and their atmospheric environment (Lofgren and Zhu, 2000). Lake surface energy fluxes and evaporation have been investigated by many authors using various methods, Blanken et al. (2000) described the direct eddy covariance measurements of evaporation from Great Slave Lake during segments of the 1997 and 1998 in ice-free periods. Thermal energy budget components and monthly evaporation in Lake Superior were estimated using mass transfer and water budget methods by Schertzer (1978). Similarly, 10-year analysis of seasonal, intraseasonal, and interannual variations in lake evaporation for Sparkling Lake in northern Wisconsin were investigated by Lenters et al. (2005). Derecki (1975) used a water balance method to estimate the evaporation. Momentum and heat fluxes over lakes Tämnaaren and Råksjö were determined by the bulk-aerodynamic and eddy-correlation methods by Heikinheimo et al. (1999). Recently, the isotope mass balance method was developed to estimate the energy exchange components (Gibson, 2002). Various climatic approaches (Penman method, Bowen ratio method and the complementary relationship lake evaporation model) were applied at a monthly time-step for annual evaporation estimates at Lake Ziway (Vallet-Coulomb et al., 2001).

Among these methods, eddy correlation technique is a method of direct measurement of these fluxes, but it is not always applicable and needs gap filling in case of raining time. Isotope mass balance method is hard to apply since the influence of water inflow and runoff is difficult to estimate. Since the storage energy in water is difficult to calculate, water budget methods cannot produce a reasonable result. Therefore the bulk transfer method is an attractive alternative to estimate the fluxes using routinely measured mean meteorological quantities.

1.3 The bulk transfer method

The bulk transfer method is widely used in numerical models; for instance, it is commonly included into GCM (General Circulation Model) models (e.g. GEOS-5 AGCM) to help us understand the air-sea interaction and perform an accurate large scale simulation of the atmosphere and ocean. Also it is used to help us manage the local water balance more effectively (Ikura, 2010).

In bulk transfer methods, the fluxes are parameterized in terms of the mean meteorological quantities (wind speed, water temperature, air temperature and humidity) and empirical transfer coefficients derived from the eddy correlation method. In these methods, the bulk coefficients are the only unknown parameters. Sensible heat and latent bulk coefficients, are sometimes treated as a constant value associated with the wind speed (e.g. Brut et al., 2005; DeCosmo et al., 1996), but also in some cases expressed as a function of wind speed (e.g. Oost et al., 2000; Rutgersson et al., 2007). In general, however, the bulk coefficient for momentum is estimated as a function of wind speed. In a summary, expressions have been proposed by each author are summarized in Table 1.1 and Table 1.2.

In stationarity and homogeneous condition, the fluxes estimated by the bulk transfer method matches well with those of estimated by the eddy correlation method. Since there are complicated turbulent structure and geographic condition, there are still several problems need to be solved to apply this method over water surface:

1. What does the role of surface current play in the bulk transform methods?

The surface current may not be zero and may contribute to the fluxes. Until now, most studies focused on the sea surface, and few cases were done over lake. The influence of lake surface current in bulk transfer method is still not well known (e.g. Ataktürk and Katsaros, 1999; Dupuis et al., 1997).

2. How to include the stability effect into bulk transfer methods?

Most studies (e.g. Taylor and Yelland, 2001) chose a neutral atmosphere condition when they estimated the bulk coefficient from the eddy correlation method. Since the atmosphere is not always neutral, estimation of transfer coefficients in diabatic condition are quite important and should be investigated.

3. Are fluxes influenced by wave state ?

Different from land surface, flux varies upon the surface state (e.g. wave). The influence

of water state is a remaining issue. For instance, some authors suggested that the roughness length is influenced not only by the smooth surface roughness length and gravity wave which is associated to atmosphere condition, but also wave age: c_p/u_* (e.g. Drennan et al., 2003; Oost et al., 2002; Smith et al., 1992), where u_* is friction velocity and c_p is the phase velocity of wave. Wu (1994) has suggested that capillary waves associated with surface tension to explain the large drag coefficients at weak winds observed by Geernaert et al. (1988) and Bradley et al. (1991). Wu (1994)'s result was also adopted and was modified by Bourassa et al. (1999) in BVW model (Bourassa-Vincent-Wood Flux and Sea State Model). Brutsaert (1973) suggested a correction function for the wave influence in flux estimation. On the contrary, some authors suspected that the wave state has small influence in bulk coefficient. Janssen (1997) claimed that theories of wave age related to the bulk coefficients are still incomplete and it is questionable whether the sea-state effect, which is of the order of 10%, can be separated from experimental noise, which is of the order of 20%. Findings from Lake Washington (Ataktürk and Katsaros, 1999) indicated the wave age has limitations in describing the observation from a small body of water. Similar suggestion also can be found in Taylor and Yelland (2001) and Johnson et al. (1998). Therefore, using the theory equations, to understand which parameter affects bulk coefficients and to estimate bulk coefficients as functions of wind speed are significant challenge.

4. How to add the influence of large-scale convection into our studies ?

The large-scale flow was proposed to understand the large scatter of bulk coefficient at weak wind speed. A lot of evidence (e.g. Businger, 1973; Fairall et al., 2003 1996; Godfrey and Beljaars, 1991; Mahrt and Sun, 1995; Mahrt et al., 1996; Schumann, 1988; Stull, 1994) have shown that the fluxes are enhanced by the convective circulation under weak wind speed and make the MOST (Monin-Obukhov similarity theory) abnormal. Even if it is the reason of the cause the large scatter, how to separate the turbulence from the large-eddy is still not well known. Furthermore, a bulk formulation to consider the large scale circulation is also significant challenge.

Since there are problems mentioned above, to develop a reliable bulk transfer method has become essential, which is based on understanding the influencing factors of the exchange process.

1.4 Outline of the thesis

In the present thesis, our objective is to develop improved lake-atmosphere interaction parameterizations. More specifically, the influence of atmosphere condition (e.g. stability, large-scale convection) in bulk transfer methods is more clearly understood and to investigate the effect of water surface state (e.g. wave, surface current) on bulk transfer method. Based on the bulk transfer method and eddy correlation method, the long term fluxes and evaporation over lake surface would be estimated in order to provide more detail information about local water balance and to help us manage the water resource effectively.

The outline of this thesis is as follows: A brief description of the study area is presented in chapter 2. The description of eddy correlation method and bulk transfer method are introduced, and the data processing and data control are described in chapter 3. In chapter 4 and 5, the influence of surface current and stability in bulk coefficient estimation are investigated. Bulk coefficients related to the locally generated turbulence equations is proposed. Furthermore, in order to include the influence of large-scale convection into our bulk coefficients, the convective boundary layer depth and the convective velocity are focused on. The wave impact is revealed as well. The long term fluxes balance based on both the eddy correlation method and bulk transfer methods are also depicted in chapter 6. The conclusions were summarized in chapter 7. The appendix showed rotation calculation mentioned in chapter 3, neutral bulk coefficient mentioned in Chapter 4 and trend estimation mentioned in Chapter 5.

Table 1.1 Previous studies of bulk coefficients estimation

Reference	Equations	Range of velocity	Study area	Year
Brut et al. (2005)	$C_{DN} \times 10^3 = (0.084U + 0.5548) \pm 0.213$	$C_{DN} : 4 < U < 11$	Equatorial Atlantic basin	2005
	$C_{EN} \times 10^3 = (0.055U + 0.63) \pm 0.1324$	$C_{EN} : 4 < U < 11$		
	$C_{HN} \times 10^3 = 1.3 \pm 0.37$	$C_{HN} : 4 < U < 10$		
DeCosmo et al. (1996)	$C_{HN} \times 10^3 = 1.14 \pm 0.35$	$6 < U < 27$	Dutch coast	1996
	$C_{EN} \times 10^3 = 1.12 \pm 0.24$			
Dupuis et al. (1999)	$C_{DN} \times 10^3 = 11.7U^{-2} + 0.668$	$C_{DN} : U < 5.5$	South of the Azores	1999
	$C_{EN} \times 10^3 = 2.79 \times U^{-1} + 0.66 (U < 5.2)$			
	$C_{HN} \times 10^3 = C_{HN} \times 10^3 = 1.2 (U > 5.2)$			
Oost et al. (2000)	$C_{HN} \times 10^3 = 0.079U + 0.471$	$C_{HN} : 7 < U < 13$	9 km off the Dutch coast	2000
	$C_{EN} \times 10^3 = 1.10 \pm 0.22$	$C_{EN} : 2 < U < 18$		
Atakturk and Katsaros (1999)	$C_{DN} \times 10^3 = 0.078U + 0.87$	$2 < U < 9$	Lake Washington	1999

Table 1.2 Previous studies of bulk coefficients estimation (continued)

Reference	Equations	Range of velocity	Study area	Year
Tsukamoto et al. (1991)	$C_D \times 10^3 = 1.69$			
	$C_H \times 10^3 = 2.58$	-	Coast of the sea of Japan	1991
	$C_E \times 10^3 = 1.51$			
Oost et al. (2002)	$C_{DN} \times 10^3 = 0.138U + 0.18$			
	$C_{DN}^{0.5} = 0.4 / \{4.52 \ln(wa) + \ln(2\pi)\}$ 3.91}	-	Southern north sea	2002
Rutgersson et al. (2007)	$C_{HN} \times 10^3 = 1.0$ ($0 < U < 9$)			
	$C_{HN} \times 10^3 = (0.12U - 0.08)$ ($9 < U < 14$)	$0 < U < 14$	Baltic sea	2007
	$C_{EN} \times 10^3 = 1.12$ 1.5 / $\{6 + (U - 4.5)^2\}$ +			
	0.002U			
Large and pond (1981)	$C_{DN} \times 10^3 = 1.2$ ($4 < U < 11$)			
	$C_{DN} \times 10^3 = 0.49 + 0.065U$ ($11 < U < 25$)	-	Nova scotia	1981
Smith et al (1992)	$C_{DN} \times 10^3 = 0.27 + 0.116U$	-	Dutch offshore	1992
U : wind speed	wa : wave age			

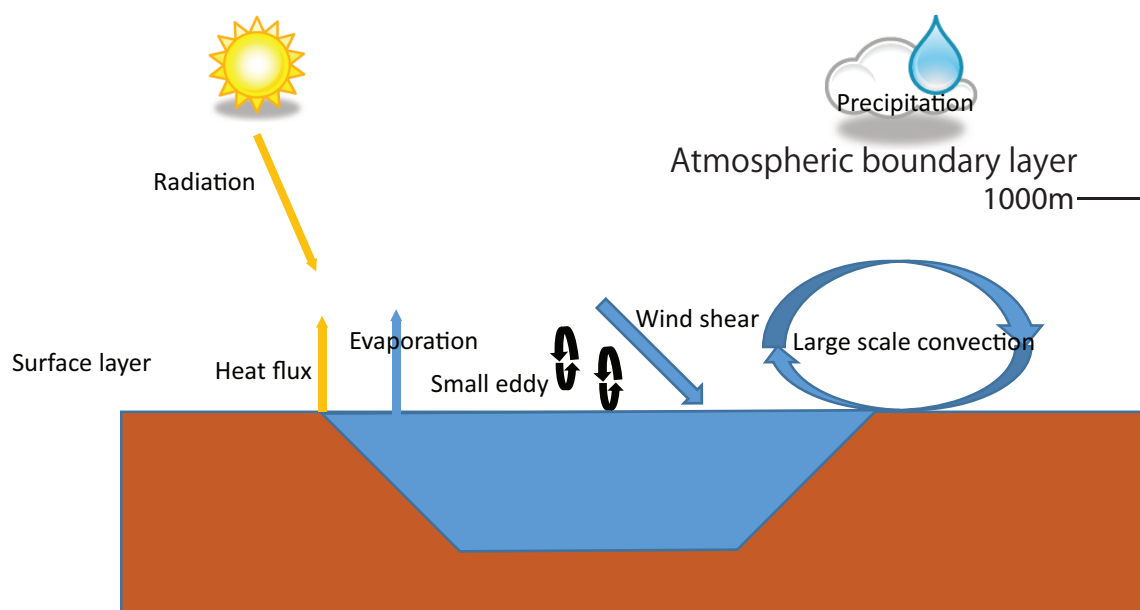


Fig 1.1 Schematic view of the atmospheric boundary layer over lake surface

2 Study area

2.1 Study site

2.1.1 Description of study site

The Lake Kasumigaura (35:52-36:09N, 140:13-140:38E) is the second largest lake in Japan (Fig.2.1), with a surface area of 219.9 km², maximum depth of about 7 m and mean depth of 4 m. The lake is mainly recharged by 56 inlet rivers and the water level is controlled by the floodgate (Data source: http://www.kasumigaura.pref.ibaraki.jp/04_kenkyu/introduction/documents/06.pdf). As one of the important reservoirs for water resource, lake Kasumigaura provides over 60 tons of water per second, of which the most goes to agriculture (83%). The rest is provided to local industry (13%) and public (4%) in the prefecture of Ibaraki. It plays a very important role in the local environment and economy (Data source: <http://www.worldlakes.org/lakedetails.asp?lakeid=8394>).

The observation site (36 02'35"N, 140 24'42"E) is located at the center of the Lake Kasumigaura (Fig.2.2). The fetch (Fig.2.4) varies between 4 km-12 km. The wind on lake center is complicated. The pressure induced wind, sea/land wind and lake/land wind play very important roles in this area. The prevailing wind direction is between northern and eastern (Fig.2.5). The most frequent wind speed was about 3-4 m/s (Fig.2.6), with an averaged value of 4 m/s, and standard deviation 3 m/s (during 2008-2010). In general, the lake Kasumigaura was under slightly unstable atmospheric conditions (Fig.2.7), except in very light winds, the wind speed $U < 2.5$ m, where the stability $-z/L > 3$ was found. Precipitation was less than 1000 mm/year on average. Highest water temperature can be found at 2 pm and the lowest is at about 5 am in daily variation. The annual temperature varies within 5 and 30 degree (Data source: http://www.kasumigaura.pref.ibaraki.jp/04_kenkyu/introduction/kahology_top.html).

2.2 Outline of observation

The main construction of observation was depicted in Fig.2.3. 10 Hz wind speed, moisture, temperature and 30 min atmospheric data have been collected by University of Tsukuba since July 2007 (Table 2.2). Also some data from MLIT (The Ministry of Land, Infrastructure and Transport and Tourism of Japan) collected at the same time were used in our study (Table 2.1). The water surface current was measured by MLIT during 2008/2/22-2008/3/17 at the lake center. In order to understand the convective circulation over lake area, convective boundary layer depth was observed by Pilot balloon experiment, and the observation location can be found in Fig.2.1. A mobile station was set in Ushiwata for the period of 2011/8/22-2011/8/29 for more accurate understanding the convective circulation. These observations are shown in Table 2.3.

Table 2.1 Long term data collection by MLIT (The Ministry of Land, Infrastructure and Transport and Tourism of Japan)

Item	Equipment	Observation height	Sampling interval	Average time
Rainfall amount	Tipping bucket Rain Gauge	8.85 m	1 hour	integrated value
Atmospheric pressure	Aneroid barometers	6.75 m	1 hour	instantaneous value
Wind direction, Wind speed	Windmill anemometer	9.45 m	0.25 s	Last 1 hour
Solar insolation	Pyranometer	8.75 m	1 s	Last 1 hour
Air temperature	platinum resistance thermometer sensor	8.25 m	1 s	Last 1 hour
dew-point temperature	Lithium chloride thermometer	8.25 m	1 s	Last 1hour
Water temperature	platinum resistance thermometer sensor	-0.5 m, -5.5 m	5 s	Last 1 hour
Water temperature	platinum resistance thermometer sensor	About 0-1 m	30 min	instantaneous value
water level	Crystal type water level meter	N/A	1 s	Last 1hour
Wave high, Period	Aquatic capacity wave height meter	N/A	0.05 s	Last 10 min
Evaporation	Pan	6.75 m	1 hour	integrated value

Table 2.2 Long term data collection by Univ of Tsukuba

Items	Equipment	Observation height	Sampling time	Average time
3 components wind speed and temperature	Sonic and Anemometer-Thermometer (Gill Instruments Ltd., R3A)	9.80 m	0.1 s	Last 30 min
H ₂ O concentration and CO ₂ concentration	Open Path Analyzer (LI-COR, Inc., LI-7500)	9.80 m	0.1 s	Last 30 min
Short wave radiation and Long wave radiation	Radiometer (Kipp and Zonen B.V., CNR-1)	4.29 m	5 s	Last 30 min
Air temperature and Humidity	Ventilated in Radiation (REBS, Inc., AEM)	2.00 m, 3.72 m	5 s	Last 30 min
Water surface temperature	Infrared (Minorta, CML-303N)	4.27 m	5 s	Last 30 min
Water temperature	Platinum resistance thermometer sensor	-0.1 m, -1.0 m, -2.5 m	30 min interval	instantaneous value

Table 2.3 Short term observation

Item	Author	Location	Equipment	Observation period	Average time
Lake current	MLIT (The Ministry of Land, Infrastructure and Transport and Tourism of Japan)	Lake center	Ultrasonic flow meter(WH-ADCP)	2008/2/22-2008/3/17 min	30 min
Pilot balloon experiment	Univ. of Tsukuba	Rinkojiken, Ushiwata, Tennonsu	Pibal Theodolite	2011/08/26	N/A
Fluxes and atmosphere	Univ. of Tsukuba	Ushiwata	Same as Lake center	2007/6-	30 min

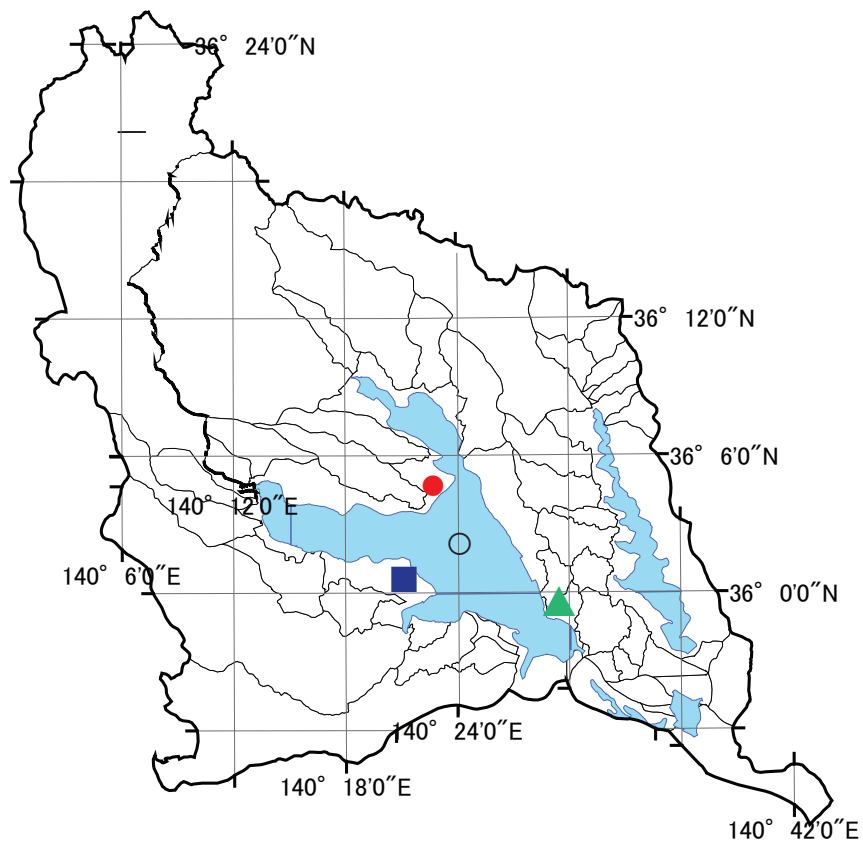


Fig 2.1 Kasumigaura basin and Pilot balloon observation. Black circles represents Koshin observatory, red circle represents Ushiwata, blue squares represents Rinkojiken, and green triangles represents Tennonshi



Fig 2.2 Observatory at the center of Kasumigaura (Photo was taken on 2012/12/03)

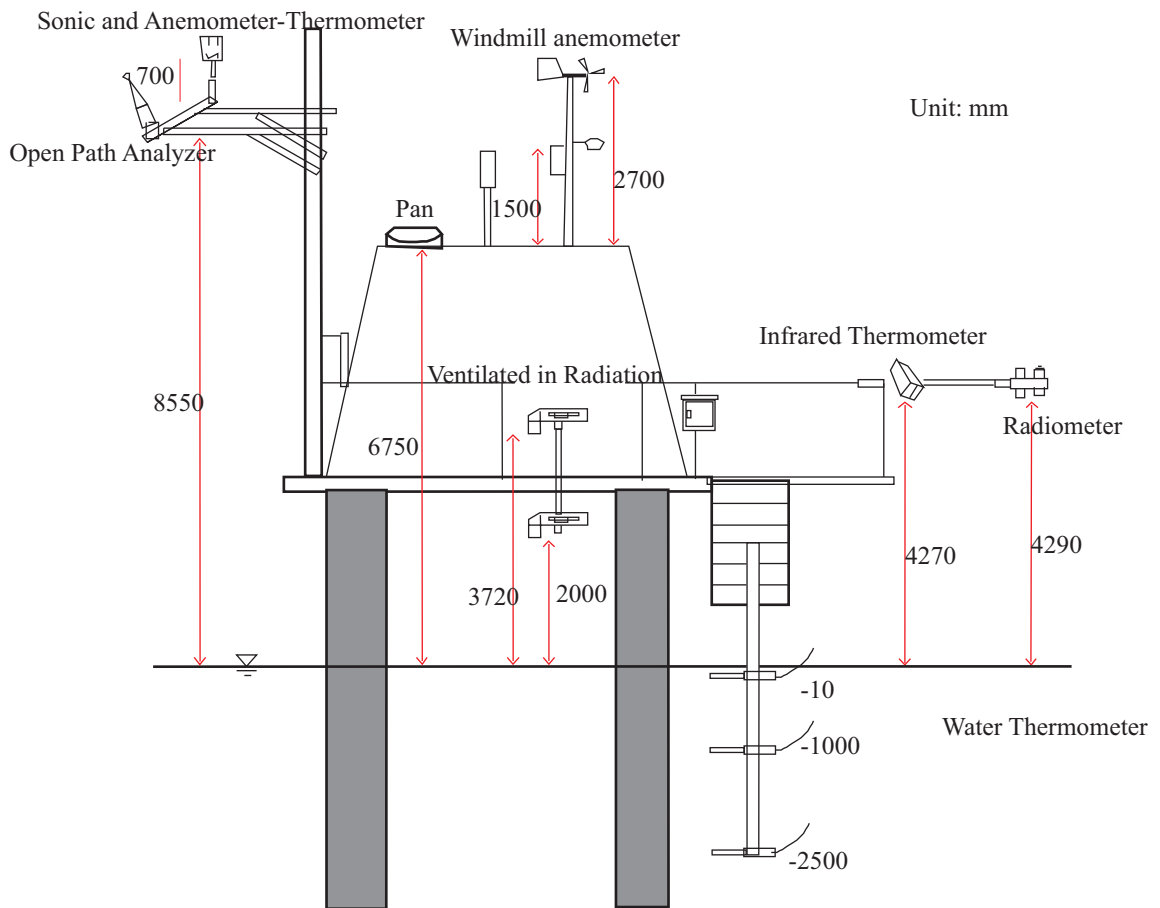


Fig 2.3 Schematic view of observatory

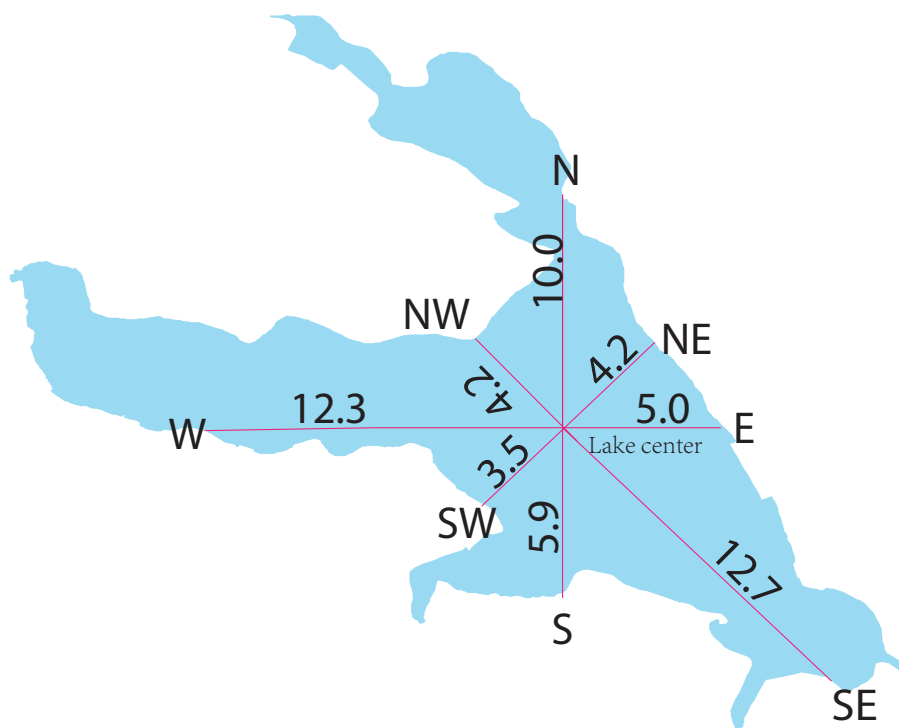


Fig 2.4 The fetch of Lake Kasumigaura (Unit: km)

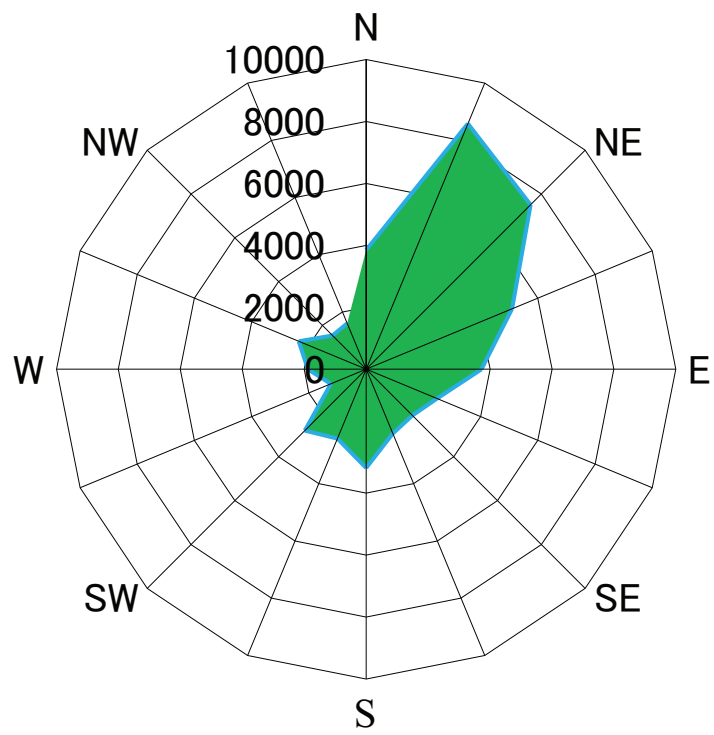


Fig 2.5 The wind direction over observatory during 2008-2010 (30 min interval)

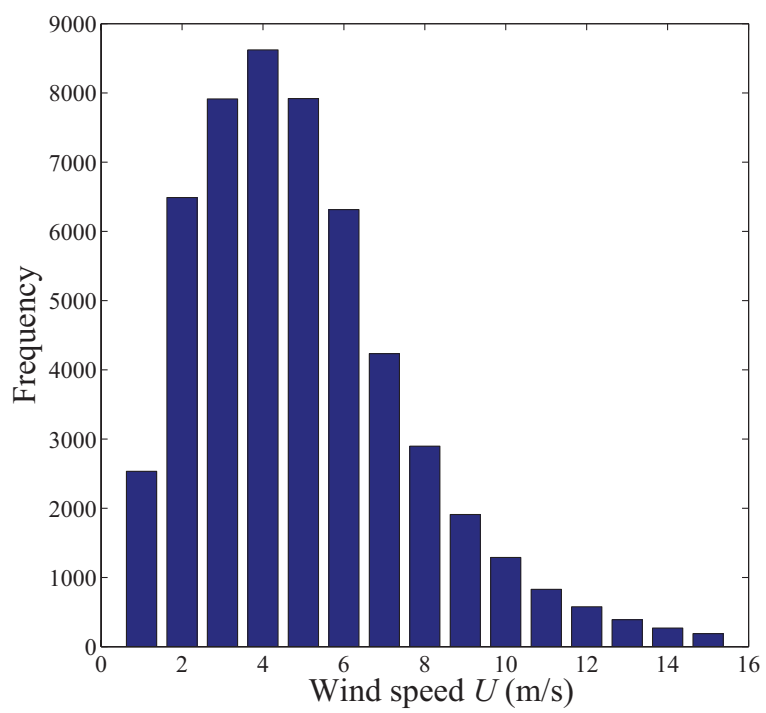


Fig 2.6 The wind speed over observatory during 2008-2010 (30 min interval)

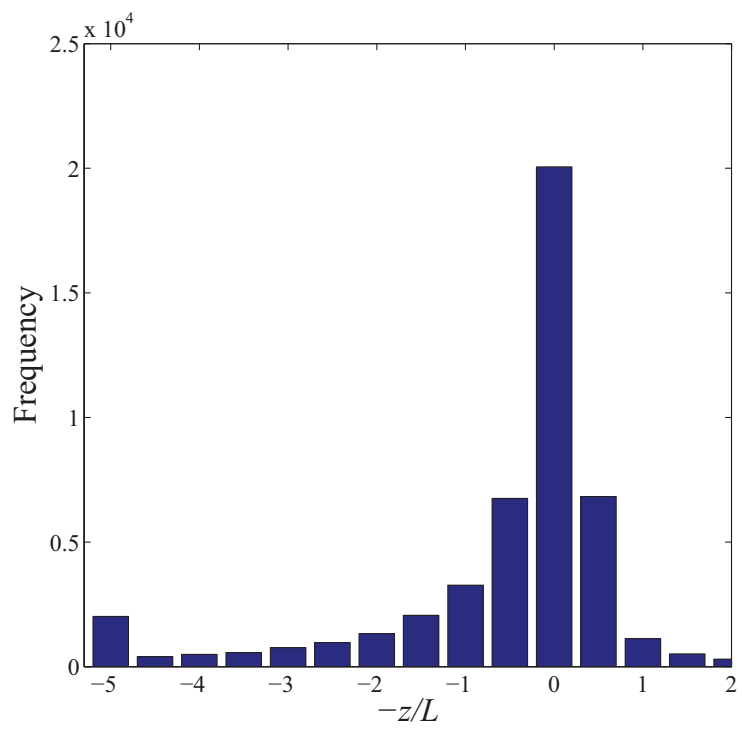


Fig 2.7 The stability over observatory during 2008-2010 (30 min interval)

3 Methodology

3.1 Methods

In this study, the fluxes were estimated by eddy correlation method. Based on this method, the bulk transfer method and wind profile method were applied. Here the bulk transfer method and eddy correlation method are introduced as follows.

3.1.1 Eddy correlation method

The eddy correlation utilizes Reynolds averaging and decomposition. The eddy flux is computed as a covariance between instantaneous deviation in vertical wind speed (w') from the mean value ($\overline{w(t)}$) and instantaneous fluctuation in other meteorological quantities x . The time average operator is defined as

$$\overline{x(t)} = \bar{x} = \frac{1}{T} \int_0^T x(t) \quad (3.1)$$

where T is consecutive segments of length, and the overline is an averaging operation. Then the obtained flux is calculated as follows,

$$\overline{w'x'} = \overline{(w - \bar{w})(x - \bar{x})} \quad (3.2)$$

3.1.2 Bulk transfer method

Bulk transfer method are expressed as routinely measured mean meteorological quantities and bulk coefficients. The main methods to estimate the bulk coefficients were introduced as follows: With homogeneous stationary condition, the traditional bulk coefficients can be estimated from eddy correlation method.

$$C_d = \frac{u_*^2}{U^2} \quad (3.3)$$

$$C_h = \frac{\overline{w't'}}{U\Delta t} \quad (3.4)$$

$$C_e = \frac{\overline{w'q'}}{U\Delta q} \quad (3.5)$$

where u_* is friction velocity, U is the mean wind speed, $\overline{w't'}$ is the variation of sensible heat, $\overline{w'q'}$ is the variation of latent heat, Δt and Δq are the temperature and humidity difference between the air and water surface, C_d is the drag coefficient, C_h and C_e are the transfer coefficients for sensible heat and humidity. By applying Monin-Obukhov similarity theory, the bulk coefficients also can be expressed as:

$$C_d = \frac{k^2}{\{\ln(z/z_{0m}) - \Psi_m(z/L)\}^2} \quad (3.6)$$

$$C_h = \frac{k^2}{\{\ln(z/z_{0m}) - \Psi_m(z/L)\} \{\ln(z/z_{0h}) - \Psi_h(z/L)\}} \quad (3.7)$$

$$C_e = \frac{k^2}{\{\ln(z/z_{0m}) - \Psi_m(z/L)\} \{\ln(z/z_{0q}) - \Psi_q(z/L)\}} \quad (3.8)$$

In which z is observation height which is related to water surface, z_{0m} , z_{0h} and z_{0q} are the roughness for momentum, sensible heat and latent heat, the stability function is given by:

$$z/L = \frac{z(kg/T)(\overline{w'T'} + 0.61T\overline{w'q'})}{-u_*^3} \quad (3.9)$$

3.2 Data processing and selection

To create a reliable data set is a first prerequisite for modeling and forecasting the surface-air exchange. Micro-meteorological data processing techniques in the past have been proposed for ideal flow conditions and thus they must be carefully re-evaluated for the more challenging conditions of flux observation (Law and Verma, 2005). Here the necessary techniques such as coordinate rotation, instrument correction and data quality assurance are covered in this study. The main procedure is shown in Fig.3.5 and some steps are introduced as follows.

3.2.1 Correction

3.2.1.1 Rotation correction

Application of coordinate rotation is a necessary step in micro-meteorological studies of surface-air exchange before the observed fluxes can be meaningfully interpreted (Lee et al., 2005). The rotation procedure for turbulence fluxes was adopted (Kaimal and Finnigan, 1994). Using the measured three components wind speed from sonic anemometer thermometer u_1 , v_1 and w_1 (30 minutes averaged), 2-time rotations were done in this study. The first step swings the x_1 and y_1 axis around z_1 to produce a new axis x_2 , y_2 and z_2 . This step forces the lateral component $v = 0$. Since ideally the wind flow should be horizontal and the mean value of w should be zero, the second

rotation swings x_2 and z_2 about y_2 into new direction x_3, y_3 and z_3 in order to force $w_3 = 0$. After the rotation, the friction velocity is

$$u_* = \sqrt{-\overline{u'w'}} \quad (3.10)$$

Similar to friction velocity, the scalar fluxes can also be done by the same steps, and a more detail is explained in Appendix B.

3.2.1.2 WPL correlation

The density correction theory of the Webb-Pearman-Leuning theory (hereafter WPL) is a principle underpinning the experimental investigation of surface fluxes of energy and masses in the atmospheric boundary layer (Lee and Massman, 2011). According to Lee et al. (2005), the moisture flux after correlation is given by

$$\overline{w'\rho_v'} = \left(1 + \mu \frac{\rho_v}{\rho_a}\right) \left(\overline{w'\rho_v'} + \frac{\rho_v}{T} \overline{w't'}\right) \quad (3.11)$$

Where μ is ratio of molecular mass relative to dry air, ρ_a is the molar concentration of atmospheric water vapour, ρ_v is the molar concentration of atmospheric water vapour.

3.2.1.3 Height adjustment

Since bulk transfer methods are usually applied at 10 m, the humidity and wind speed and temperature were adjusted to 10 m by (3.12)-(3.14):

$$t_{10} = t_m + \frac{t_*}{k} \left[\ln \left(\frac{10}{z_m} \right) - \psi_h \left(\frac{10}{L} \right) + \psi_h \left(\frac{z_m}{L} \right) \right] \quad (3.12)$$

$$q_{10} = q_m + \frac{q_*}{k} \left[\ln \left(\frac{10}{z_m} \right) - \psi_q \left(\frac{10}{L} \right) + \psi_q \left(\frac{z_m}{L} \right) \right] \quad (3.13)$$

$$U_{10} = U_m + \frac{u_*}{k} \left[\ln \left(\frac{10}{z_m} \right) - \psi_m \left(\frac{10}{L} \right) + \psi_m \left(\frac{z_m}{L} \right) \right] \quad (3.14)$$

where z_m is measurement height. The detail operations are given in Appendix A.

3.2.2 Stability functions

The bulk coefficients over water surface depend on the stratification, relative height and various roughness lengths related to the surface condition. Since the relative height was adjusted to

10 m, here we focused on the stability function and roughness length. As an important parameter in the estimation of coefficients, stability functions derived from the dimensionless gradients of the wind speed, temperature and humidity can be expressed by following the Monin-Obukhov similarity theory (hereafter MOST) as:

$$\frac{kz}{x_*} \frac{d\bar{U}}{dz} = \phi_x\left(\frac{z}{L}\right) \quad (3.15)$$

$$\psi_x\left(\frac{z}{L}\right) = \int_0^{z/L} [1 - \phi_x(y)] dy/y \quad (3.16)$$

where y is a dummy integration variable, and x refers to wind speed, temperature and humidity. The functional relationships between Ψ and z/L have been investigated by many authors over land surfaces (e.g. Businger et al., 1971; Paulson, 1970).

For unstable situation,

$$\Psi_m = \ln \left\{ \left(\frac{1+x^2}{2} \right) \left(\frac{1+x}{2} \right)^2 \right\} - 2 \tan^{-1} x + \frac{\pi}{2} \quad (3.17)$$

$$\Psi_h = \Psi_e = \ln \left(\frac{1+x^2}{2} \right)^2 \quad (3.18)$$

where $x = (1 - \gamma\zeta)^{1/4}$, γ has the range of 11 – 18. For the stable situation, $\Psi_m = -\beta_M\zeta$, $\Psi_h = \Psi_e = -\beta_M\zeta$. A value of $\gamma = 16$; $\beta_M = \beta_h = \beta_e = 5$ is widely used (Kraus and Businger, 1994). Recent findings have revealed that this summary may be invalid under strong unstable condition when the requirements of the stationarity and horizontal homogeneity are not satisfied, which is very common status over the water surface. MOST become invalid under strongly convective conditions. To solve this problem, two methods were commonly used in fluxes estimation. Brutsaert (1992) updated Kader and Yaglom (1990)'s result and proposed a reasonable expression,

$$\psi_m(-y) = \ln(a+y) - 3by^{1/3} + \frac{ba^{1/3}}{2} \ln \left[\frac{(1+x)^2}{1-x+x^2} \right] \quad (3.19)$$

$$+ 3^{1/2}ba^{1/3}\tan^{-1} [(2x-1)/3^{1/2}] + \psi_0 \text{ for } y \leq b^{-3} \quad (3.20)$$

$$\psi_m(-y) = \psi_m(b^{-3}) \text{ for } y > b^{-3} \quad (3.21)$$

For temperature and humidity,

$$\psi_h(-y) = [(1-d)/n] \ln[(c+y^n)/c] \quad (3.22)$$

where $y = -z/L$, $a = 0.33$, $b = 0.41$, $x = (y/a)^{1/3}$ and $\psi_0 = (-\ln a + 3^{1/2}ba^{1/3}\pi/6)$. These equations seem reasonable since they are supported by experimental evidence in dynamic convective and a convective sublayer (Brutsaert, 2005). Another method for sea fluxes was suggested by

Fairall et al. (1996) in strong convective status. It is suggested that the form of Ψ_m should include free convection correct limits,

$$\Psi_{conv} = \frac{3}{2} \ln \left\{ \frac{x^2 + x + 1}{3} \right\} - \sqrt{3} \tan^{-1} \frac{2x + 1}{\sqrt{3}} + \frac{\pi}{\sqrt{3}} \quad (3.23)$$

$$\Psi_{kansas} = \ln \left\{ \left(\frac{1 + x^2}{2} \right) \left(\frac{1 + x}{2} \right)^2 \right\} - 2 \tan^{-1} x + \frac{\pi}{2} \quad (3.24)$$

$$\Psi_m = \frac{\Psi_{kansas} + \zeta^2 \Psi_{conv}}{1 + \zeta^2} \quad (3.25)$$

where $x = (1 - 12.87\zeta)^{1/3}$. It is claimed that this equation gives good agreement with Kansas-type profile (Paulson, 1970) for near neutral condition and obeys the -1/3 asymptotic convective limit dependence on stability. These three types of equations are shown in Fig.3.6. For slightly unstable and neutral condition, they are not significantly different. For extremely unstable, Fairall et al (1996)'s result still converge to the traditional type, while the Brutsaert equation shows a relatively small. The Brutsaert formulation has been studied by Sugita et al. (1995) which showed that it describes measurements of the sensible heat flux under strongly unstable conditions better than the equation derived from Paulson (1970). Therefore, it is better to choose Brutsaert's formulation in this study since the fluxes in our study area may be affected by the large-scale convection under unstable situation.

3.2.2.1 Calibration of equipment

The error that arisen in measurement by the instruments deviation or equipment should be carefully calibrated. The water thermometers for 2.5 m and 1.0 m were correlated according to Miyano (2010) as follows :

$$tw_1 = 0.999902Tw_1 - 0.56058 \quad (2.5m) \quad (3.26)$$

$$tw_2 = 0.994736Tw_2 - 0.63304 \quad (1.0m) \quad (3.27)$$

3.2.3 Data assurance

A consistent procedure for quality control of meteorological data is essential for measurement networks and long term measurement sites (Foken et al., 2005). As shown in Fig.3.5, we applied several steps to make sure our data are reliable in this studies.

3.2.3.1 Spectral analysis test

After the spike removal, the spectral analysis was applied to understand the general data conditions. Spectral analysis is a widely used method to identify whether the data are reliable in flux observation. Here Blackman-Tuckey method mentioned by Hino (1977) was applied in this study by using random data. The analysis showed that the slopes are closed to $-5/3$ (Fig. 3.1) which satisfy the requirement of fluxes. These results indicated that the data quality appears well in general. In detail, for each 30 min data record, the stationarity test and the integral turbulence characteristics test were applied. Classification of the data quality is listed in Tab.3.1 and the tests are explained below.

3.2.3.2 Stationary test for momentum flux

Typical non-stationarity is driven by the change of meteorological variables through the time of the day, change of weather patterns, significant meso-scale variability, or changes of the measuring point relative to the measuring events such as the phase of a gravity wave (Foken et al., 2005). The stationary test compares the statistical parameters determined for the averaging period and for a short interval of this period. According to Foken and Wichura (1996), the time series for the determination of the measured signals w (vertical wind) and x (horizontal wind component or scalar), 30 minutes data would be divided into $M = 6$ intervals of about 5 minutes. If the result is within the usual range, the data can be judged as of 'good quality' or 'stationarity'. The test statistics was given by

$$RN_{\overline{x'w'}} = \left| \frac{\overline{x'w'}(5 \text{ min}) - \overline{x'w'}(30 \text{ min})}{\overline{x'w'}(30 \text{ min})} \right| \times 100\% \quad (3.28)$$

The results indicated that under weak wind speed region (3.3 and Fig. 3.4), only half of data can be justified as normal class. For high quality data (\leq Class2), it was only 10%.

3.2.3.3 Integral turbulence characteristics test

The integral turbulence characteristics test (hereafter ITC) is based on similarity characteristics of the atmospheric turbulence. According to this theory, a similar parameter is the correlation coefficient between the time series of two turbulent parameters. If this correlation coefficient is within the usual range, a well-developed turbulence can be assumed (Foken et al., 2005). The empirical relations were obtained from the Kansas experiment results, reexamined and refined through comparison with other observations (e.g. Dyer, 1974). The functions proposed by Kaimal

and Finnigan (1994) are expressed as:

$$\frac{\sigma_w}{u_*} = \begin{cases} 1.25(1 - 3z/L)^{1/3} & -2 \leq z/L \leq 0 \\ 1.25(1 + 0.2z/L)^{1/3} & 0 \leq z/L \leq 1 \end{cases} \quad (3.29)$$

$$\frac{\sigma_t}{|t_*|} = \frac{\sigma_q}{|q_*|} = \begin{cases} 2(1 - 9.5z/L)^{-1/3} & -2 \leq z/L \leq 0 \\ 2(1 + 0.5z/L)^{-1} & 0 \leq z/L \leq 1 \end{cases} \quad (3.30)$$

where σ is the standard deviation, subscript w , q and t represent vertical velocity, humidity and temperature. In this data assurance method, the measured values in the left hand side and the modeled parameters in the right hand side would be compared according to,

$$ITC = \left| \frac{(\varphi/X^*)_{\text{model}} - (\varphi/X^*)_{\text{measurement}}}{(\varphi/X^*)_{\text{model}}} \right| \times 100\% \quad (3.31)$$

The results are found in Fig.3.2. The data near the neutral condition show large errors in our dataset, and only about 15% can be judged as good quality except for Carbon dioxide showing huge errors (and were not used in this study).

3.3 Gap filling for long term fluxes and evaporation estimation

To complete time series for long term fluxes estimation, the gap filling is necessary since the eddy correlation method may be invalid in some occasion (e.g. unreliable wind direction, precipitation). To estimate credible and reliable fluxes, the half-hour eddy correlation data were replaced by the results estimated from the bulk transfer methods in the following cases:

- Presence of spike induced by system or sensor breakdown, calibration, maintenance.
- Wind direction in the range of 60-160 degree (to avoid tower influence,).
- Precipitation (3 hour before and after each event).
- In the case of management activities of sensors.

3.4 Summary and outline of data selection

In this chapter, the eddy correlation method and bulk transfer method are introduced. The rotation correction, and WPL correction were applied in our dataset. The height was adjusted to

the standard of 10 m. Stability function was chosen based on Brutsaert (2005) and the thermometer was calibrated. For obtaining reliable fluxes data, ITC and stationarity test were applied. In general, the selected data excludes weak turbulence case: ($u_* < 0.05$, $\overline{w'q'} < 0.015$, $\overline{w't'} < 0.015$). For different objectives the data selection are different in each chapter. In Chapter 4, in order to estimate accurate bulk coefficients, only Class1,2 in ITC and stationarity test for momentum, moisture and temperature data are used. The night time data are also removed. In Chapter 5, data quality tests were not applied, but only the day time (8:00-11:00 JST) data is used to estimate fluxes under strong convective condition. Since we try to investigate the impact of the wave on momentum flux, only tests for momentum are applied and Class1,2 data were selected in Chapter 6.

Table 3.1 Classification of the data quality by the stationarity test and the integral turbulence characteristics according to Foken et al.(2005)

Range	Class	Flag
0-15%	Class1	Excellent
16-30%	Class2	Excellent
31-50%	Class3	Normal
51-75%	Class4	Normal
76-100%	Class5	Normal
101-250%	Class6	Low
251-500%	Class7	Low
501-750%	Class8	Low
751-1000%	Class9	Low
$\geq 1001\%$	Class10	Bad

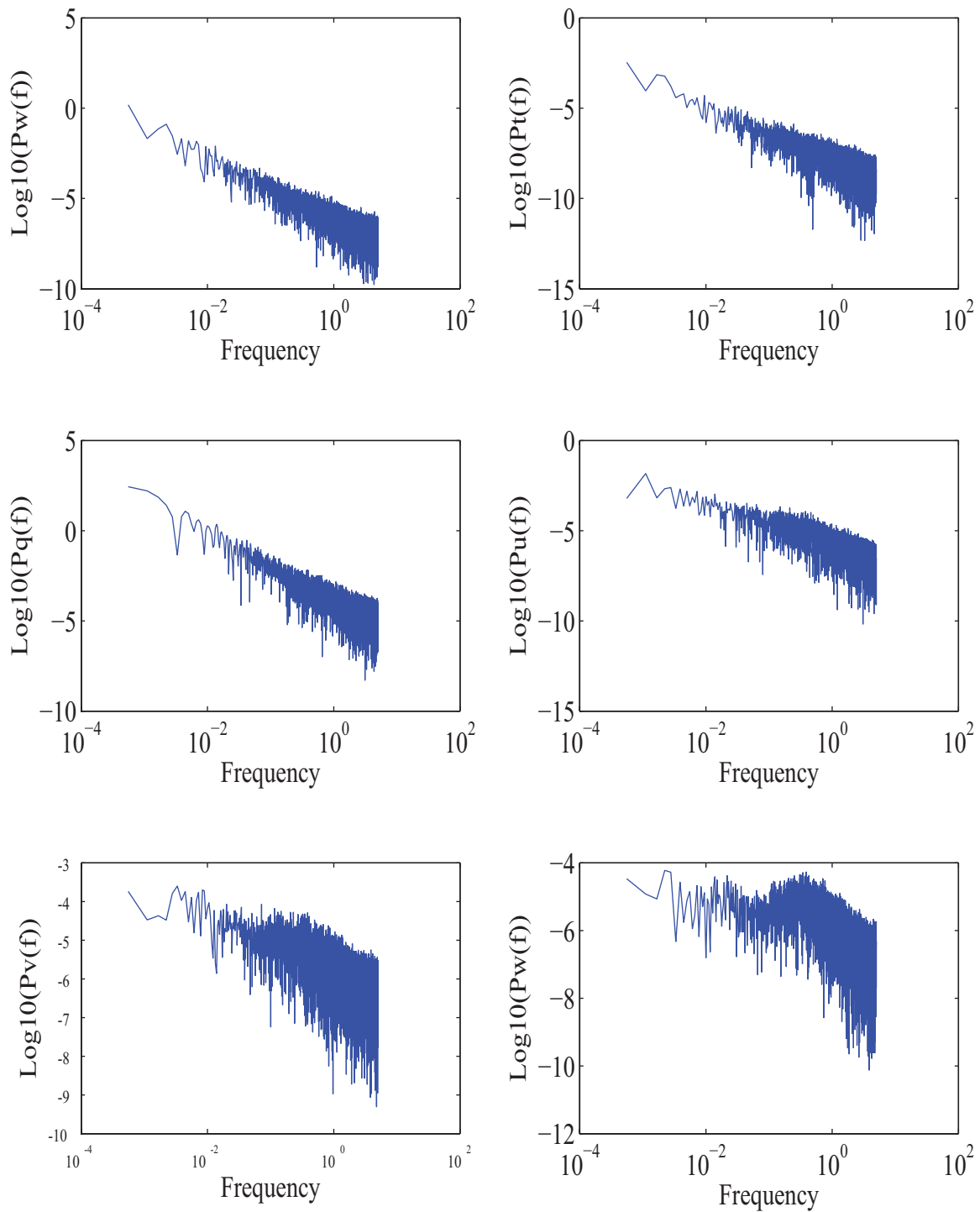


Fig 3.1 Spectral analysis for giving a general view of dataset (2009/01/15 09:00-09:30 JST). u , v and w are the three component of wind speed, t is for temperature, q is for moisture and c is for CO_2 .

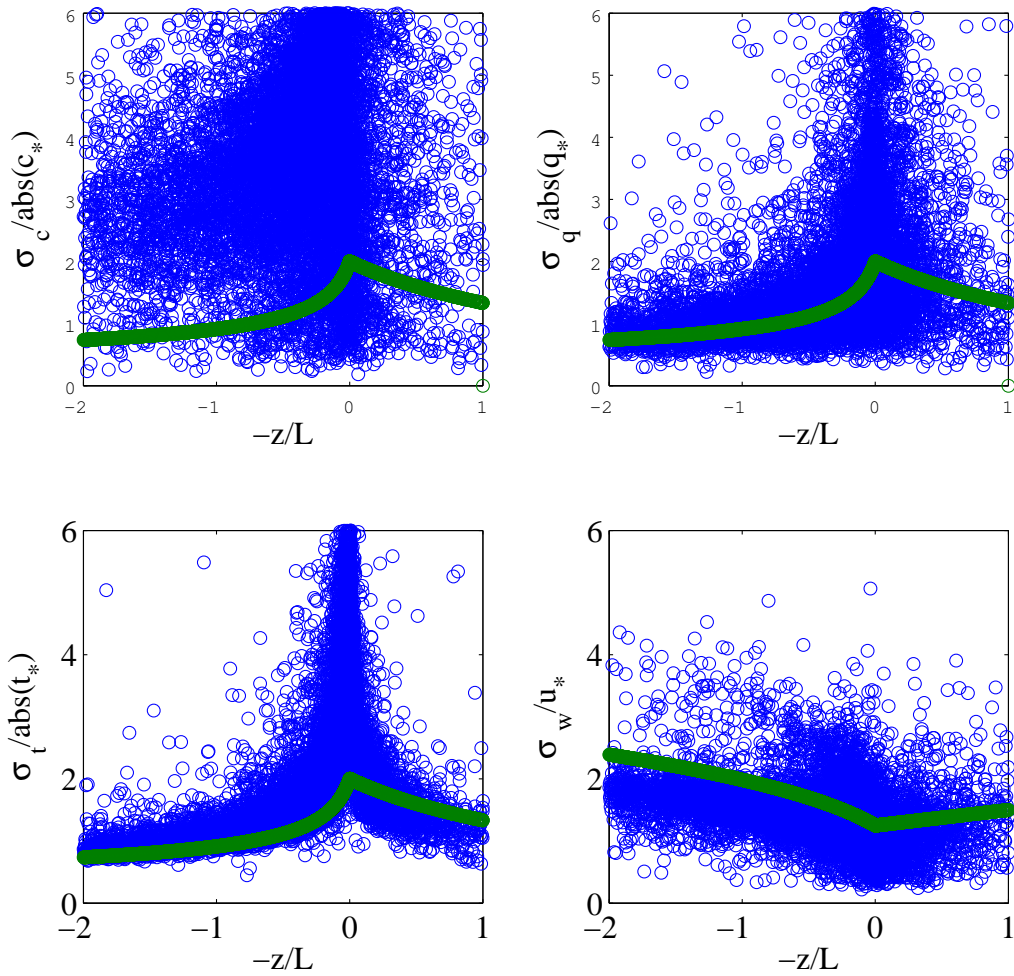


Fig 3.2 The integral turbulence characteristic test for wind speed, sensible heat, latent heat and carbon dioxide flux. subscribe w is for vertical wind speed, t is for temperature, q is for moisture and c is for CO_2 . $-z/L$ is stability and σ is standard variation

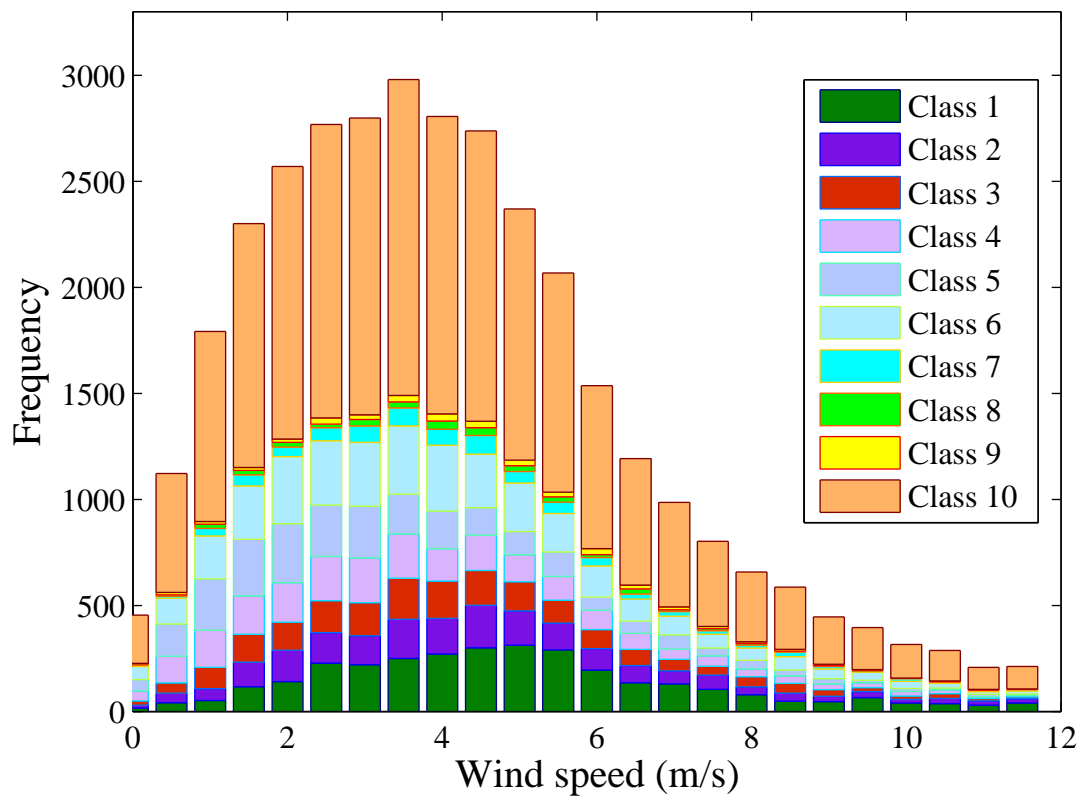


Fig 3.3 Stationarity test for v component wind speed (2009, 30 min interval)

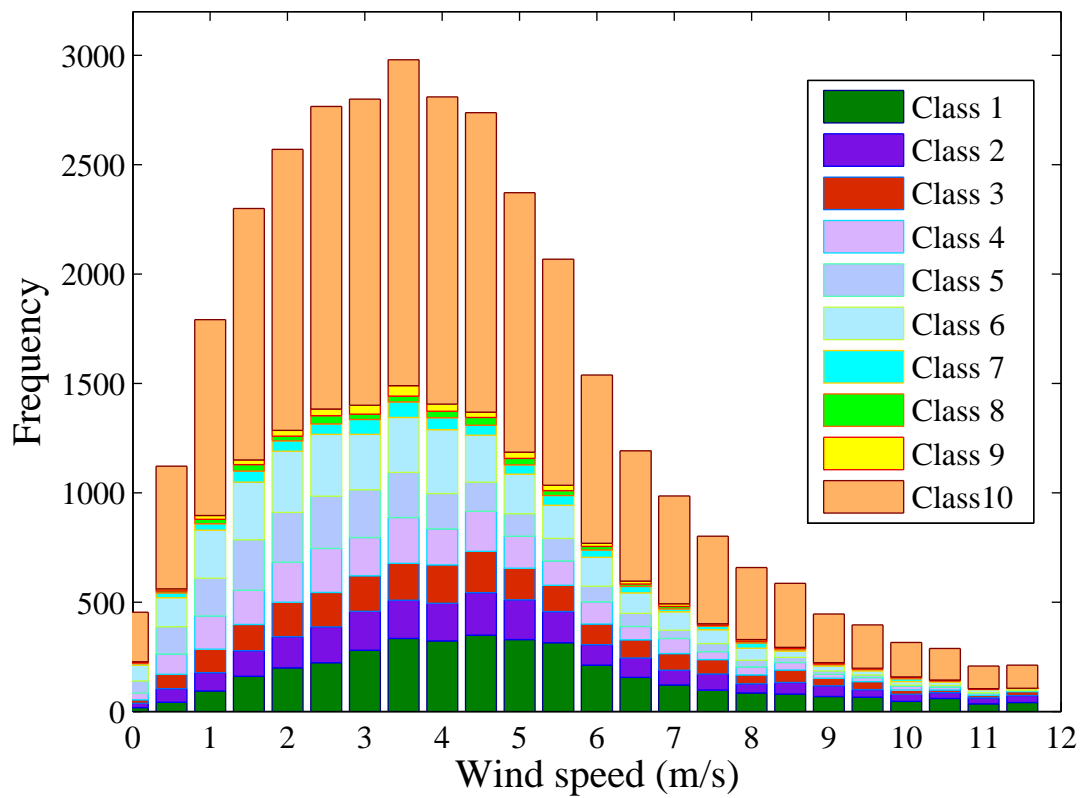


Fig 3.4 Stationarity test for u component wind speed (2009, 30 min interval)

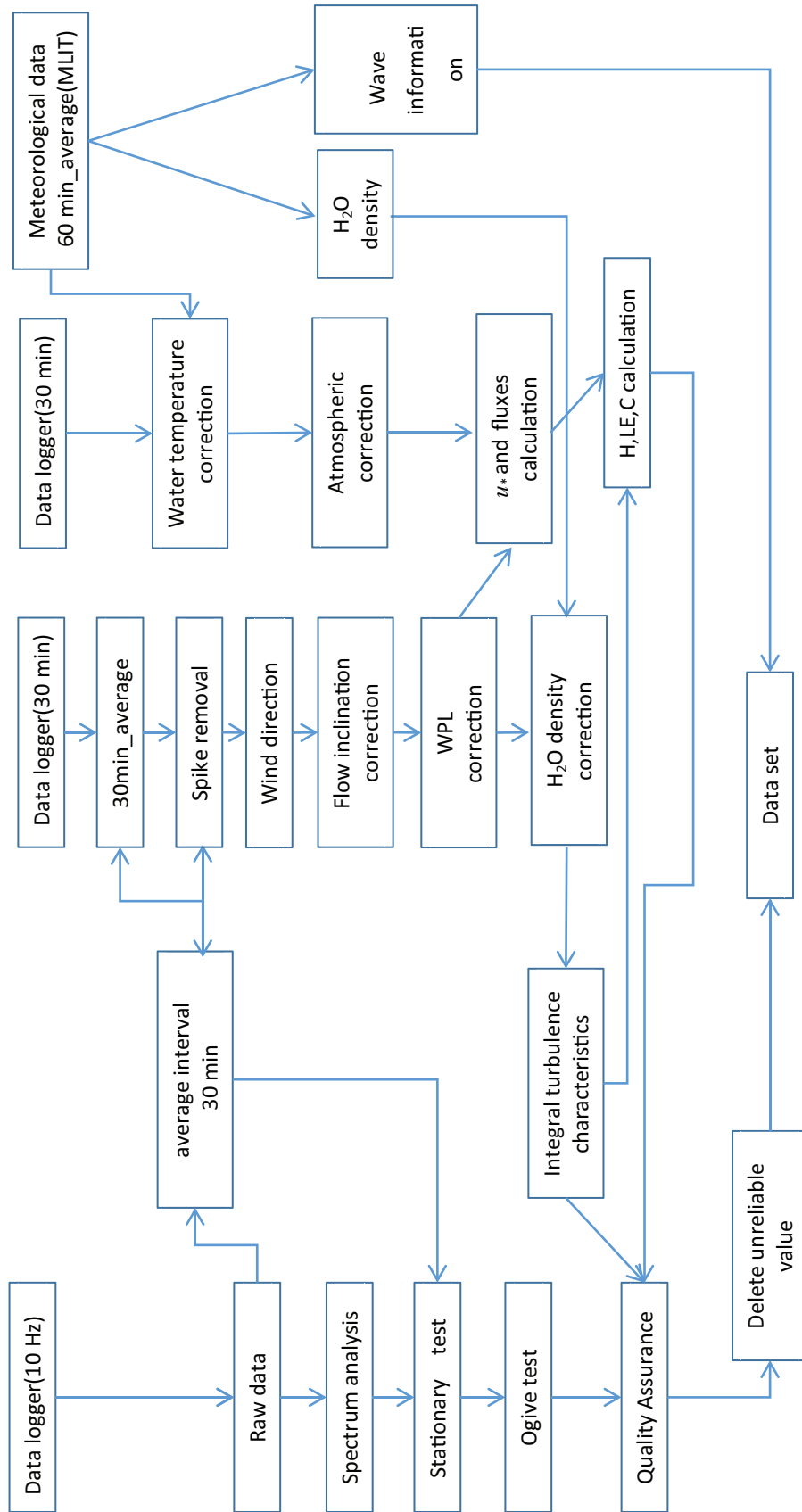


Fig 3.5 The procedure of data analysis

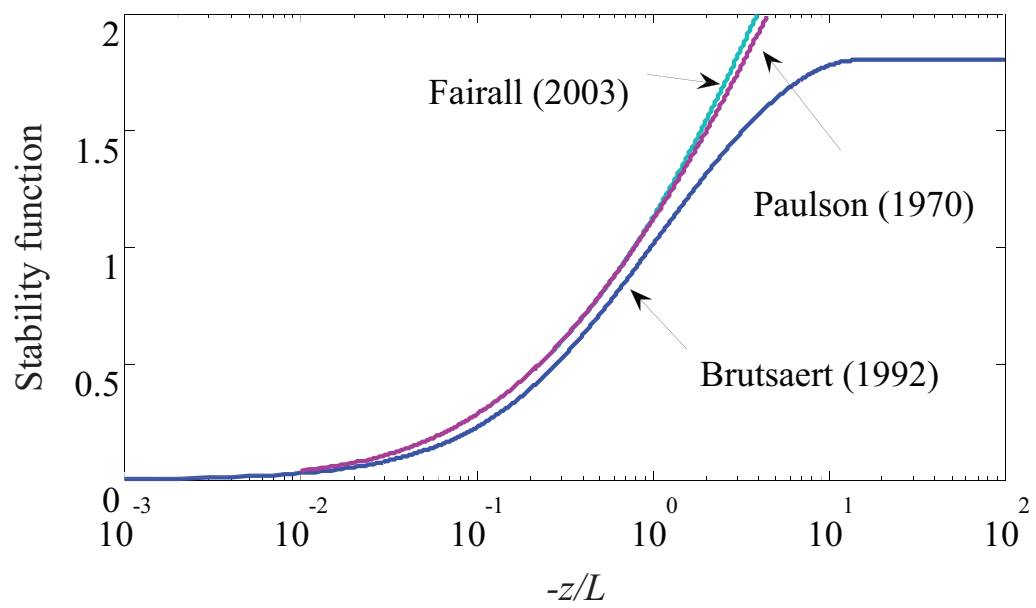


Fig 3.6 Stability functions verse stability, derived by different authors: Paulson (1970), Fairall (1996) and Brutsaert (1992)

4 Bulk coefficients estimated from eddy correlation data and wind profile

4.1 Estimation of neutral bulk coefficients

As mentioned in 3.1, the bulk coefficients clearly depend on the measurement height and the atmosphere stability. Therefore, usually we choose a neutral atmosphere and 10-m height as standard conditions. The neutral bulk coefficients derived from wind profile method have been introduced by many authors (e.g. Brut et al., 2005; Fairall et al., 1996). The neutral bulk coefficients are given by

$$C_{dn} = \frac{u_*^2}{(U_{10n})^2} \quad (4.1)$$

$$C_{hn} = \frac{\overline{w't'}}{(U_{10n}) \Delta t_{10n}} \quad (4.2)$$

$$C_{en} = \frac{\overline{w'q'}}{(U_{10n}) \Delta q_{10n}} \quad (4.3)$$

C_{dn} , C_{en} and C_{hn} are the neutral bulk coefficients for momentum, moisture and temperature, which are derived from the 10 m neutral meteorological quantities (A detail is explained in Appendix A).

To perform more reliable estimation of bulk coefficients, data quality test introduced in Section 2 were applied. Only very high quality data were selected in this chapter. The neutral bulk coefficient as a function of wind speed are shown in Fig. 4.1. C_{dn} shows linear-dependent on the wind speed for the range of $U=2-14$ m/s, which is similar with previous studies (e.g. Ataktürk and Katsaros, 1999; Brut et al., 2005; Oost et al., 2002; Taylor and Yelland, 2001) in same wind speed range. Different from C_{dn} , C_{en} shown in Fig. 4.3 is independent with wind speed and with small errors. The average values of C_{en} is about 0.0011. This value is identical to that of many previous studies. For instance, the value of 0.0012 ± 0.00024 was found by DeCosmo et al. (1996) for the range of $U=6-27$ m/s, 0.00111 ± 0.00014 was obtained by Smith et al. (1995) and 0.0011 was suggested by Oost et al. (2000). C_{hn} related to the U_{10n} is shown in Fig. 4.2, which indicates similar results in the range of 2-9 m/s. It is noted that the temperature bulk coefficient

increase with increasing wind speed after $U=9$ m/s. In theory, the behavior of C_{en} and C_{hn} should be similar. The increasing of C_{hn} at high wind speed region are also reported by some studies and showed same tendency (e.g. Rutgersson et al., 2007). One possibility for this cause is that it might be influence by the temperature between the water surface and air dt . Fig.4.4(b) revealed C_{en} is also independent with dt but C_{hn} in Fig.4.4(a) showed large scale under $dt < 6$ °C. Nevertheless, assuming C_{en} and C_{hn} are independent on the wind speed under weak wind speed (The C_{hn} under high wind speed region will be discussed later), C_{en} and C_{hn} were given by:

$$C_{en} \times 10^3 = C_{hn} \times 10^3 = 1.1(U > 2m/s) \quad (4.4)$$

C_{hn} at high wind speed was also expressed here as a reference:

$$C_{hn} \times 10^3 = \begin{cases} 1.1 & 2 < U_{10n} < 9m/s \\ 0.1922U_{10n} - 0.828 & U_{10n} \geq 9m/s \end{cases} \quad (4.5)$$

4.2 Diabatic bulk coefficient

Since we found the C_{en} and C_{hn} are independent of the wind speed, the influence of stability becomes essential. The stability can be parameterized by the Obukhov length or the Richardson number. The Richardson number Ri is introduced here since it is only related to commonly measured variables:

$$Ri = \frac{gz}{273.15 + T_a} \cdot \frac{T_s - T_a}{U^2} \quad (4.6)$$

Where g is gravity acceleration speed, z is observation height, T_a is the air temperature and T_s is the water surface temperature. The diabatic bulk coefficient C_e and C_h related to Richardson number (Fig.4.5) can be expressed as

$$C_e \times 10^3 = C_h \times 10^3 = 1.1(U > 2m/s) \quad (4.7)$$

C_e and C_h are almost a constant, but large scatter of C_h was found near the neutral condition. The stability has small effect on bulk coefficient. This is because over water surface, the heat fluxes are relatively small, and z/L or Ri is almost dominated by the friction velocity or wind speed. The neutral atmospheric condition can thus be found for most of the time. Indeed, the correction function ψ is quite small in profile equations and can be neglected for near neutral condition.

Overall, derived values agree with those reported in the past, perhaps with one exception. It is an increase of C_{dn} in weak wind speed range. However, we did not have any reliable data to

confirm the characteristic of bulk coefficients under 2 m/s. The theoretical value of smooth surface (e.g. Kondo, 1975; Nikuradse, 1933) under weak wind speed was adopted, and the bulk transfer methods related to locally generated turbulence were given by

$$\overline{u'w'} = \begin{cases} 1.08U^2/1000U^2 & U < 2.2\text{m/s} \\ (0.0767U + 0.6931)/1000U^2 & U \geq 2.2\text{m/s} \end{cases} \quad (4.8)$$

$$\overline{w't'} = \begin{cases} 1.185U^{-0.15}/1000Udt & U < 2.2\text{m/s} \\ 1.1/1000Udt & U \geq 2.2\text{m/s} \end{cases} \quad (4.9)$$

$$\overline{u'w'} = \begin{cases} 1.185U^{-0.15}/1000Udt & U < 2.2\text{m/s} \\ 1.1/1000Udt & U \geq 2.2\text{m/s} \end{cases} \quad (4.10)$$

4.3 Errors in sensible heat bulk coefficients estimation

Above all, the bulk coefficients showed reasonable results and similar with those of previous studies. One of the most interesting findings is that the sensible heat bulk coefficient increased at high wind speed. In general, direct estimation of the transfer coefficients for sensible heat flux are particularly problematic for near-neutral conditions because relatively small errors in the air-sea temperature difference may strongly contaminate the estimated transfer coefficient (Mahrt et al., 2012). Using the error analysis, we could exclude the unreliable data induced by the measurement error. The probable error analysis was applied in our study. The probable error σ_{C_h} in a function of $x = f(y_1, y_2, \dots, y_i)$ which consists of several variable y_i with its own absolute error σ_{y_i} can be evaluated in general by (Bevington, 1969; Sugita et al., 1996):

$$\sigma_x \simeq \left[\sigma_{y_1}^2 \left(\frac{\partial x}{\partial y_1} \right)^2 + \sigma_{y_2}^2 \left(\frac{\partial x}{\partial y_2} \right)^2 + \dots + \sigma_{y_i}^2 \left(\frac{\partial x}{\partial y_i} \right)^2 \right]^{0.5} \quad (4.11)$$

since $C_h = \overline{w't'}/Udt$, the probable error σ_{C_h} is given by:

$$\sigma_{C_h}^2 \simeq \sigma_{\overline{w't'}}^2 \left(\frac{\partial C_h}{\partial \overline{w't'}} \right)^2 + \sigma_U^2 \left(\frac{\partial C_h}{\partial U} \right)^2 + \sigma_{dt}^2 \left(\frac{\partial C_h}{\partial dt} \right)^2 \quad (4.12)$$

Since $\sigma_{\overline{w't'}}$ and σ_U are quite small, neglecting these terms of $\sigma_{wt}^2 \left(\frac{\partial C_h}{\partial wt} \right)^2$ and $\sigma_U^2 \left(\frac{\partial C_h}{\partial U} \right)^2$, we have

$$\sigma_{C_h}^2 \simeq \sigma_{dt}^2 \left(\frac{\partial C_h}{\partial dt} \right)^2 \quad (4.13)$$

when $U > 9$ m/s, dt varied from 1-7 degree, $\overline{w't'}$ varied from 0.015 to 0.15, $\sigma_{dt} = \pm 0.65K$. The error is shown in Fig.4.6. Large error was found within this range. Therefore, by neglecting the high wind speed case, C_h was suggested to take the same value as C_e (equal to 0.0011) at high wind speed cases.

Since the large error of C_h for the high wind speed range, the value of C_h is still unknown. Recently it got great attention because of more accurate temperature can be measured. It may be quite important because such condition is common in our study area. Here we discussed the relation among the sensible heat, wind speed and water-air temperature difference, to try to reduce error in sensible heat flux estimation under high wind speed condition:

1. Temperature difference dependence.

In this study site, the measurement error of temperature different between water surface and air is about ± 0.65 K. This value is large enough to result in considerable error. However, even measurements of the sea surface-air temperature difference are accurate to within 0.1 K, the sensible heat coefficient still increased with increasing wind speed (Ann-Sofi et al., 2007). It is questioned that the water surface temperature and air temperature measurement error is not only caused by the equipment error, but also occurred due to several physical reasons:

- Spray can lead to counterargument transfer of sensible heat for strong wind (e.g. Andreas, 2011; Mahrt et al., 2012), and the measurement of air temperature may be influenced by the spray. Furthermore, spray evaporation causes the lower part of the atmosphere to experience cooling and moistening. This cooling process increases the air-sea temperature difference, destabilizes the surface layer, and enhances the surface layer turbulence (Zhang et al., 2006).
- The influence of errors in the measured water surface temperature due to reflect downward longwave radiation could be correlated with wind speed if cloud cover decreased with increasing wind speed (e.g. Mahrt et al., 2012). This may reflect the sensor and result in a considerable error.
- The patches of foam is observed to be cooler than surrounding water surface and resulting underestimation of surface temperature (Marmorino and Smith, 2005).

2. Wind speed dependence.

Large et al. (1995) suggested under a strong wind condition, the wave boundary layer (to be introduced in chapter 6) may be higher than the measurement height. As a result, the wind speed in the wave boundary layer is smaller than that predicted by Monin-Obukhov similarity theory, which resulted an underestimated neutral wind speed estimated using the wind profile method. This resulted in the neutral wind speed estimated from wind profile method in bulk coefficient is underestimated. However, the cospectral and ogive analysis in Chapter 5 and the wave analysis in chapter 6 indicated that for high wind speed, the influence of wave in wind profile method was negligible.

3. Turbulence dependence.

- The sensor measurement error. Burns et al. (2012) found for $U > 8$ m/s, the sensible heat measured from eddy correlation sensor becomes larger than that calculated with the thermocouple, reaching a maximum difference of about 250 W/m^2 at about $U \approx 18$ m/s. From his study, cospectral analysis of sensible heat flux suggested that spurious correlation is a problem during high winds which leads to increased sensible heat in the eddy correlation method.
- Ann-Sofi et al. (2007) and Smedman et al. (2007) demonstrated that when the Obukhov length is less than about -150 m a regime with very specific characteristics, a large-scale transport process enhanced the sensible and latent heat and caused Monin-Obukhov relations for the exchange of sensible heat to break down. Therefore $\overline{w't'}$ and $\overline{w't'q}$ showed higher value than the locally generate turbulence. This suggestion was still questioned in our study. Based on this suggestion, the latent heat should also be increased at high wind speed region, but indeed, we only found the sensible heat increased under high wind speed region.

Until now, we could not answer the question about the issue mentioned about because of the measurement limitation. However, it is hoped that the more accurate temperature and wave measurement can be done in future and C_h can be estimated in a robust way at high wind speed range.

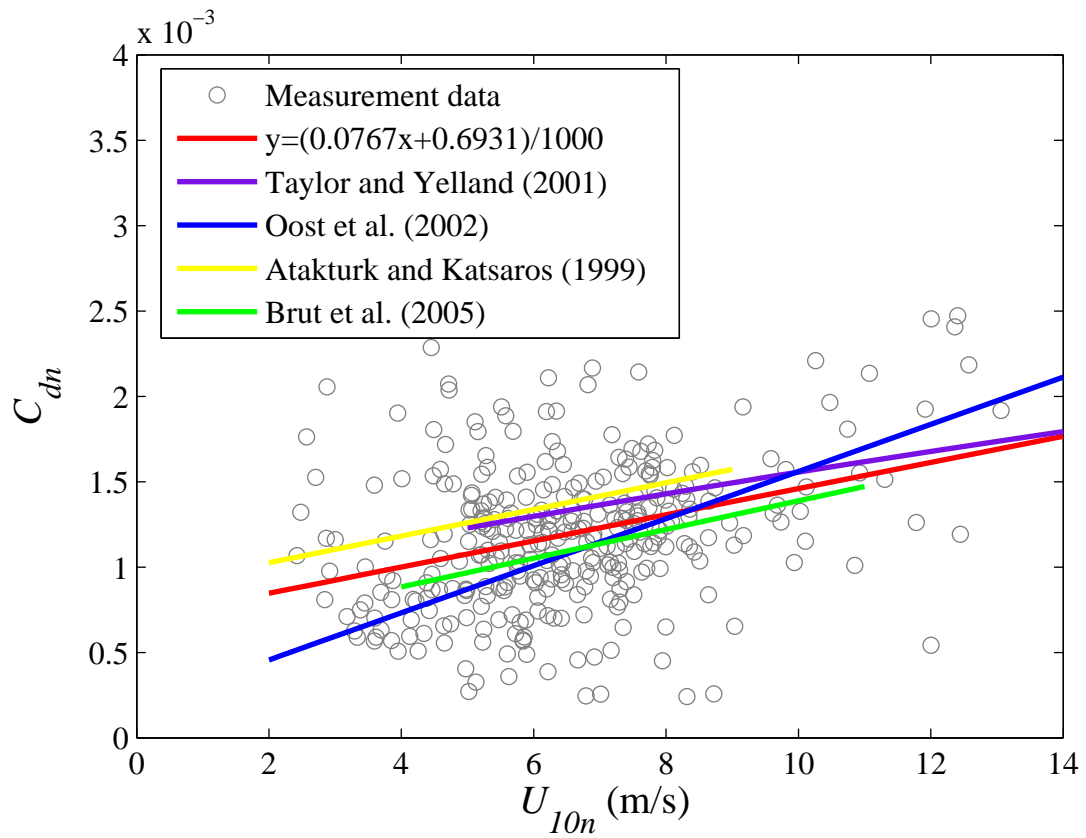


Fig 4.1 Neutral 10-m drag transfer coefficient C_{dn} as a function of 10-m wind speed, in comparison with previous studies

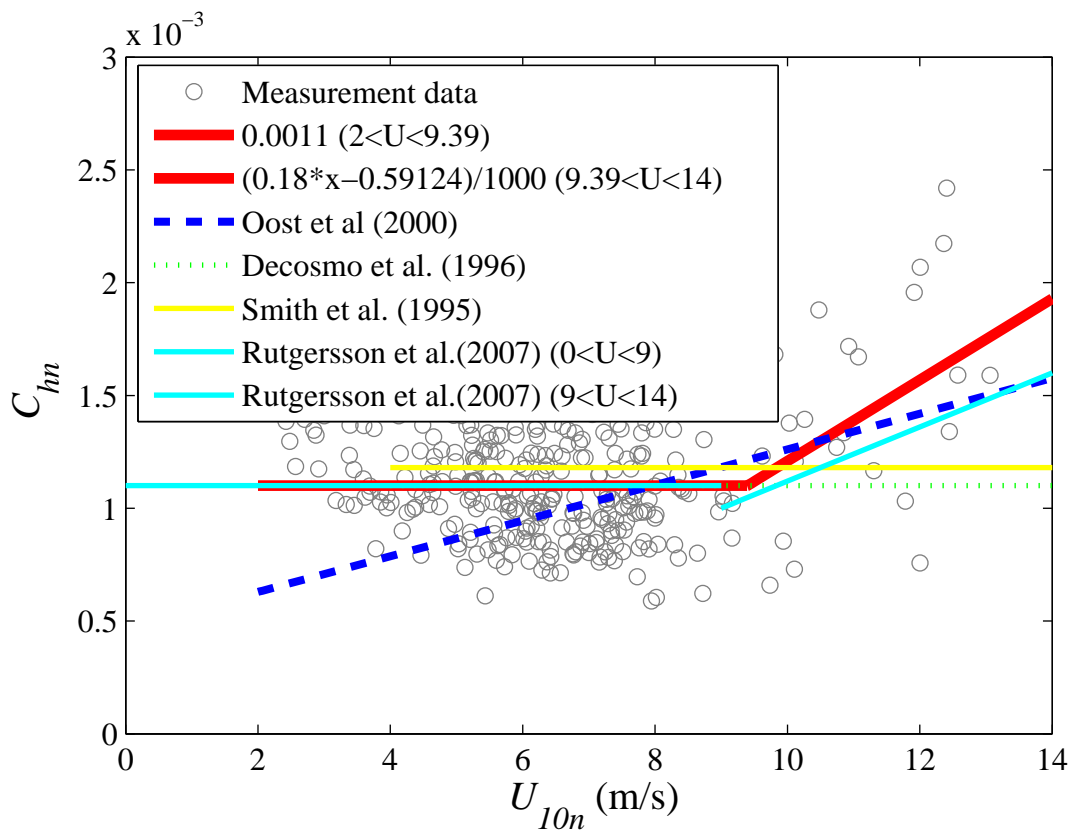


Fig 4.2 Neutral 10-m temperature transfer coefficient C_{hn} as a function of 10-m wind speed, in comparison with previous studies

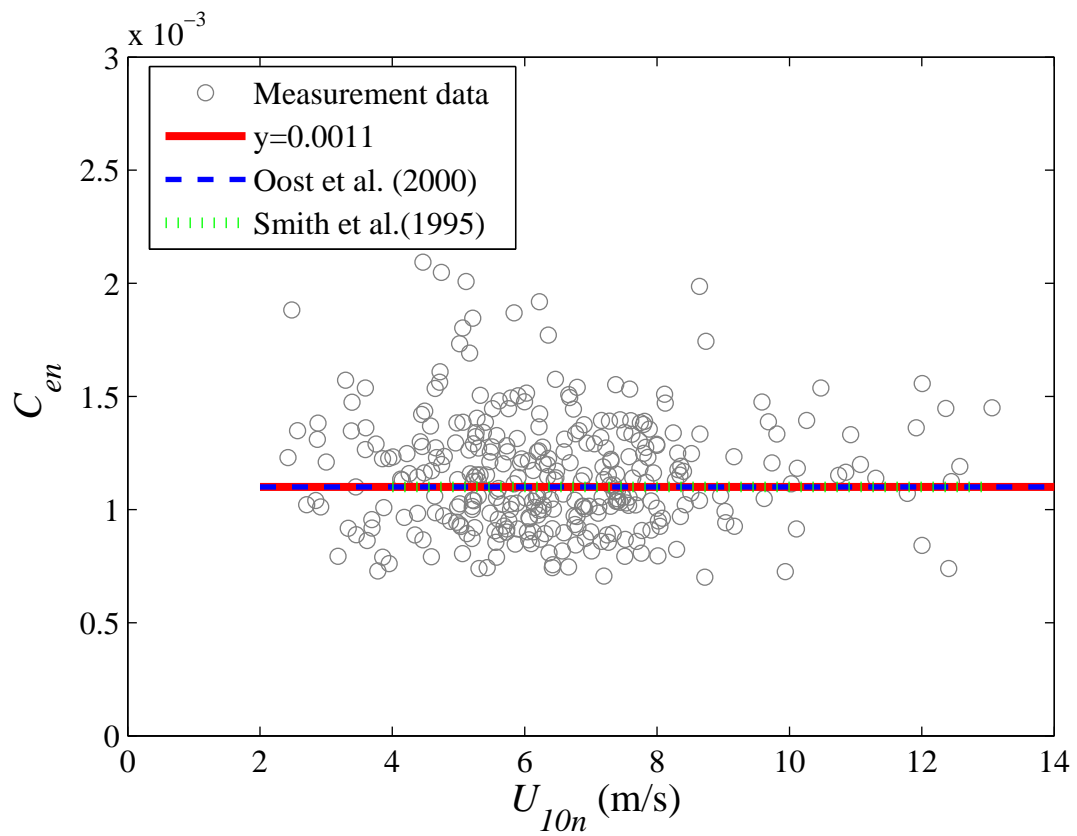
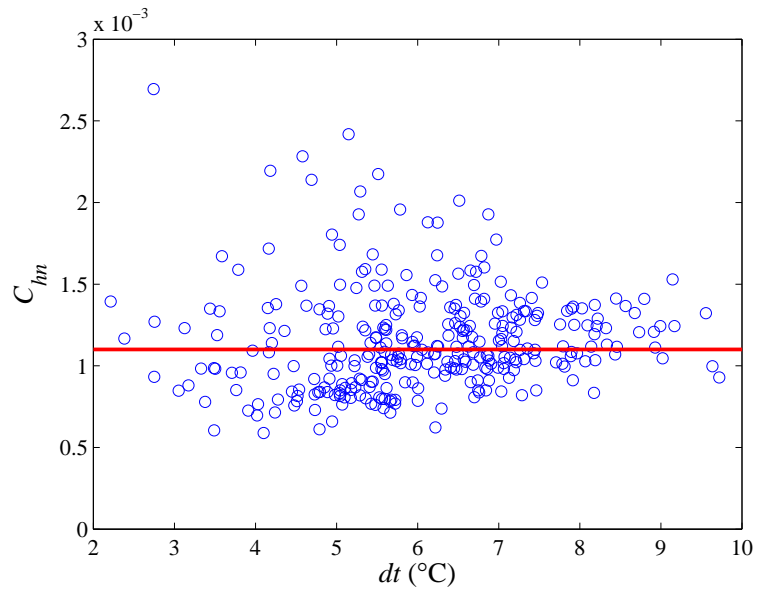
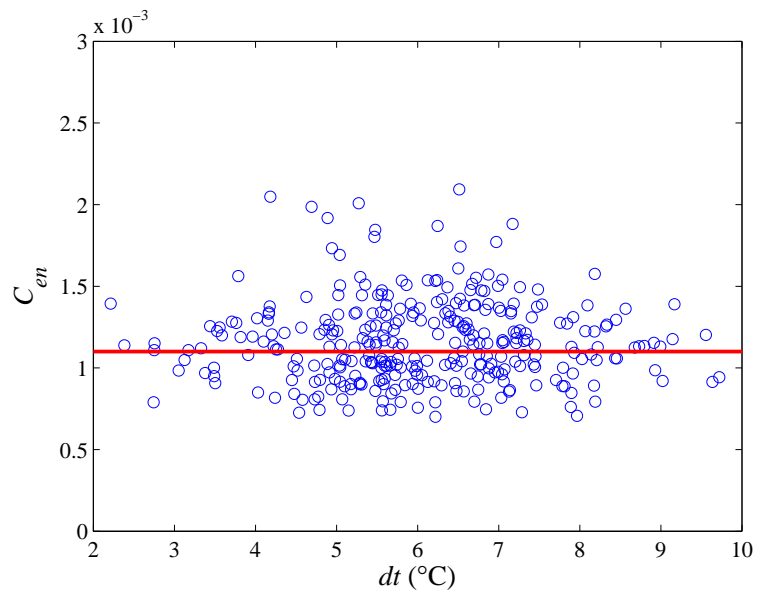


Fig 4.3 Neutral 10-m moisture transfer coefficient C_{en} as a function of 10-m wind speed, in comparison with previous studies

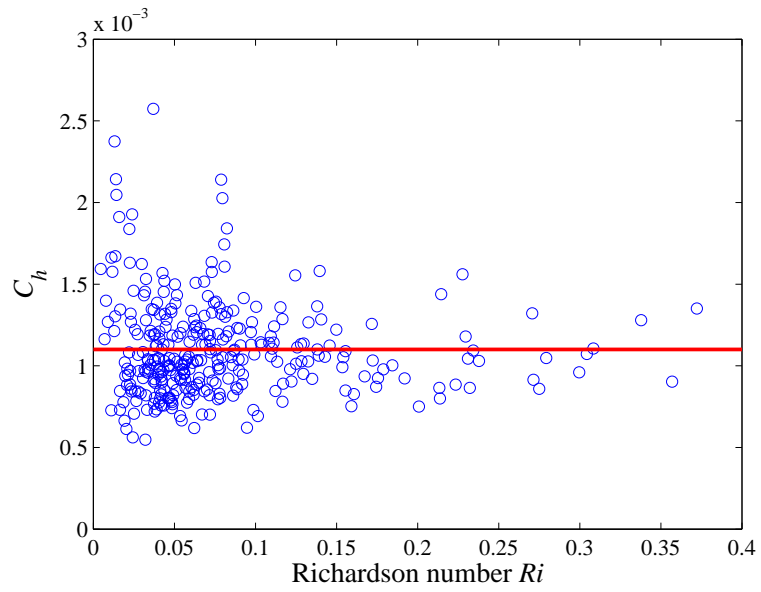


(a) Temperature transfer coefficient as a function of dt

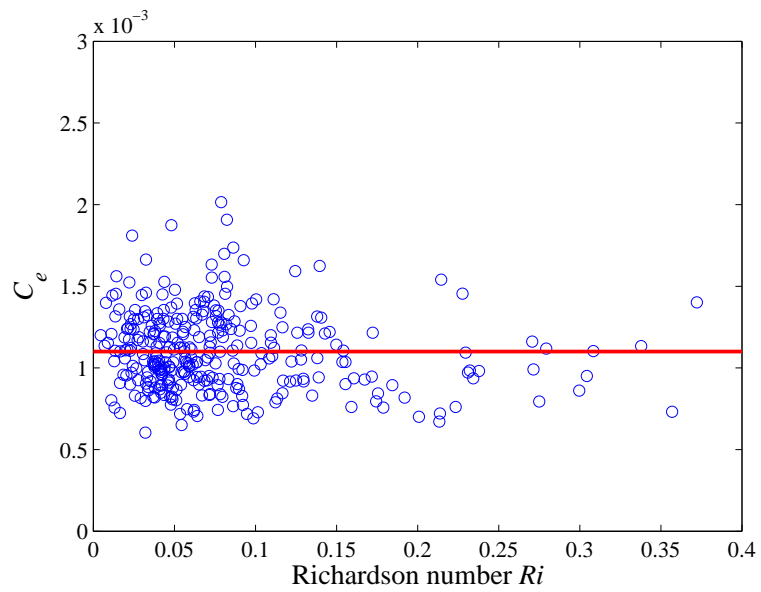


(b) Moisture transfer coefficient as a function of dt

Fig 4.4 Transfer coefficients as a function of dt



(a) Temperature transfer coefficient as a function of bulk Richardson number



(b) Moisture transfer coefficient as a function of bulk Richardson number

Fig 4.5 Transfer coefficient as a function of bulk Richardson number

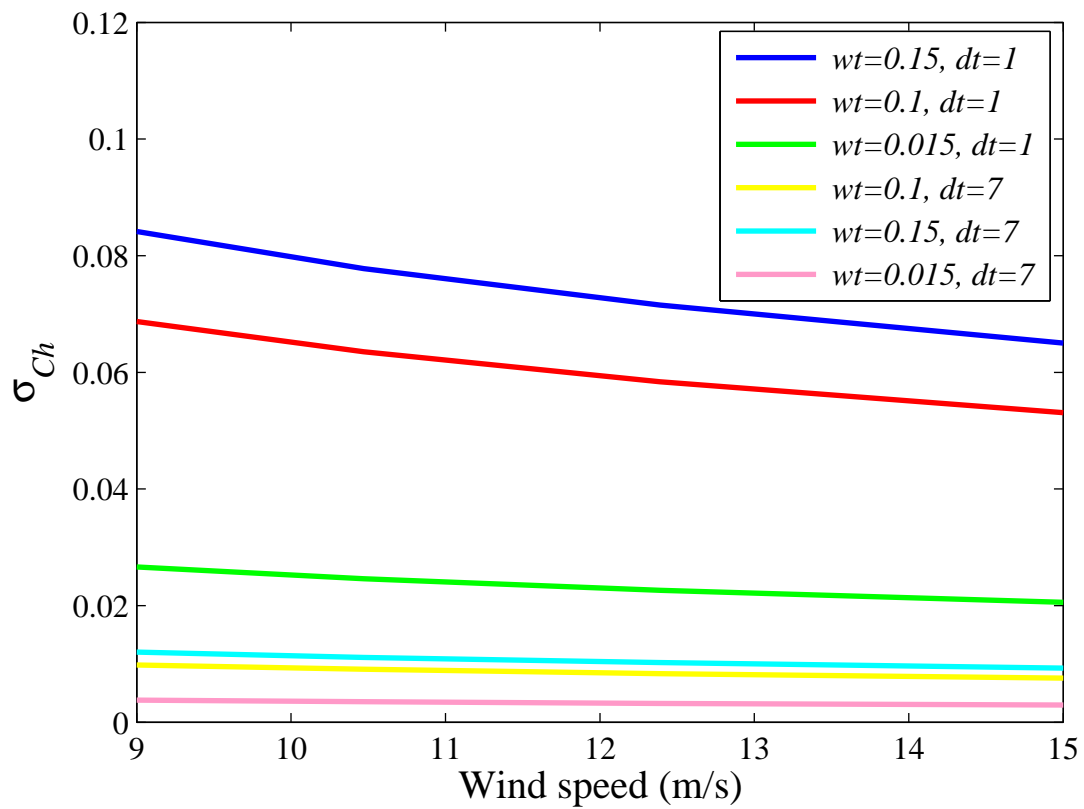


Fig 4.6 The probable error analysis for sensible heat bulk coefficient in high wind speed region. σ_{C_h} is the probable error for C_h , wt is sensible heat flux and dt it temperature difference between water surface and air.

5 Factors controlling bulk coefficients variation over water surface

In chapter 4, it is noted that there was still considerable uncertainty in the estimation of drag coefficient. First, commonly we assumed that the atmosphere over the water surface is in the same way as that over the land (e.g. Stability function, without surface current and wave). However, the drag coefficient was plotted as a function of wind speed which is different from land surface (a constant). Second, although the drag coefficient increased with increasing wind speed, the scatter is still large in comparison with heat coefficients. Obviously, the factors controlling bulk coefficients variation should be further investigated. Meanwhile, heat and moisture coefficients appeared different characteristics, Fig.4.1 revealed heat and moisture bulk coefficients were independent on the wind speed. Some previous studies also showed similar tendency. It means over lake surface, the heat and moisture were directly related to the turbulence diffusion by locally generate turbulence but not surface condition (we can assume the bulk coefficients for heat fluxes have same characteristic with land surface). Therefore, the factors controlling the variation of drag coefficient are essential in this chapter. It is noted that it does not mean that heat exchange is a standalone system, indeed, the C_{en} and C_{hn} are partly dependent on the momentum exchange, for instance the momentum roughness.

5.1 Surface current

Different from land surface, the mean flow in the bulk transfer method in general should be computed by relating to surface current over lake surface. The lake current is mainly induced by the wind (Muraoka and Fukushima, 1981), runoff (Ellis et al., 1997), and spatial uneven temperature distribution (Green and Terrell, 1978). Since it is comparatively small, most of studies neglected it in the air-water exchange process. However, under weak wind region, the influence may become significant. With inclusion of the effect of surface current, bulk coefficients are given by

$$C_d = \frac{u_*^2}{(U - U_s)^2} \quad (5.1)$$

$$C_h = \frac{\overline{w't'}}{(U - U_s) \Delta t} \quad (5.2)$$

$$C_e = \frac{\overline{w'q'}}{(U - U_s) \Delta q} \quad (5.3)$$

where U_s is the surface current speed in the wind direction. In this study, the lake surface current was measured by MLIT with the Acoustic Doppler Current Profiler (ADCP, 1200KHZ, Fig. 5.1 (a)) which measures horizontal current velocities and direction as a function of depth (Fig.5.1 (b)). From the observation, we found the wind was the main source of current, and surface current speed increased with increasing wind speed for most of the cases. However, the surface current velocity was less than 25 cm/s during our experimental period, which is two orders of magnitude smaller than that of the wind speed (Fig.5.2). The linear regression between wind speed and surface current speed was shown in Fig.5.3. In addition, the current direction sometimes did not coincide with the wind direction. Muraoka and Fukushima (1981) noted this disagreement may be caused by the horizontal circulation current which is induced by the spatial non-uniform nature of wind distribution over lake Kasumigaura. This suggestion was verified by Toyota et al. (2006), who simulated the surface current over the Lake Suwa. Nevertheless, since it was quite small in comparison with wind speed, the lake surface current can be judged negligible in this research.

5.2 wave impact on roughness length and TKE energy budget

Wave is known to have a significant influence over water surface, generally shown a relationship with the momentum roughness: since the stratification function is decided (?) and reference height is adjusted to standard 10 m, the roughness length being a direct function to reflect the interaction of the wind and water surface. It has been tacitly assumed that this parameter reflects the integrated effects of wave formation, wave breaking and dissipation on the transfer of momentum to the surface (Kraus and Businger, 1994). In this section, the wind profile method and the TKE budget method were applied for understanding the wave influence on lake-atmosphere interaction.

5.2.1 The water state over lake Kasumigaura

5.2.1.1 The wave state over Lake surface

To answer the question about the wave influencing on fluxes, we need to concentrate on the wave state. Phenomenally, the surface condition is related to the wave. Although the wave is exist both over lake surface and the sea surface, but since lake surface has a limit fetch and depth (about

6 m at our observatory), the wave over lake surface is significantly different from the ocean. The crucial difference is that the swell is not exist over the lake surface, the water surface is mainly dominated by the shear at the air-water interface. Photos in Fig.5.5 were taken at variable wind speed. As shown in Fig.5.5, under weak wind speed the water surface is almost smooth, and as wind increasing, the wave grows. Fig.5.6 showed the measured significant wave height H_s increase with increasing wind speed, and could be expressed as:

$$H_s = 0.0114U^{1.623} \quad (5.4)$$

Similar to H_s , the period of wave T_p showed high correlation with the wind speed (Fig.5.7)

$$T_p = 0.44U^{1.292} \quad (5.5)$$

In addition, the c_p estimated from T_p and H_s is a main parameter to reflect the wave state (e.g. Brutsaert, 1973; Cheng and Brutsaert, 1972) in history. Here the c_p is estimated from iteration of dispersion relation (e.g. Smedman et al., 2003). The main procedure was introduced as follows:

1. First guess set $L_p = 20$
2. A new L_p was estimated by:

$$L_p = \frac{gT_p^2}{2\pi} \tanh\left(\frac{2\pi h_d}{L_p}\right) \quad (5.6)$$

3. Repeat until the value of L_p close to the new L_p
4. The phase speed should be

$$c_p = \frac{L_p}{T_p} \quad (5.7)$$

where L_p is the wave length. c_p also shows high correlation with the wind speed (Fig.5.8).

$$c_p = 0.8982U^{0.605} \quad (5.8)$$

The calculated wave age shows that the long wave where $c_p/u_* > 40$ (Toba et al., 1990) is not exist in our study. It's noted that these features of wave information suggest the water surface is mainly dependent on the local shear. Different from lake surface, the swell existed over sea surface is generated from a distant place. It will show high values of wave age and will not maintain an equilibrium condition with local wind shear.

5.2.1.2 Roughness Richardson number

Fundamentally, the water surface also could be expressed as roughness Richardson number which is related to the friction velocity. Since the friction velocity mainly depends on the wind speed, the roughness length varies with the wind speed but not a constant. When the calm weather, the surface becomes aerodynamically smooth (smooth surface region) and as the wind speed increases, the surface changes from smooth to rough. The air flow tends to attach to the surface, but when the waves become very steep, or break, flow separation occurs (Kraus and Businger, 1994). When this happens, the stress increases dramatically and the surface is effectively rougher than in other areas (transition region). Consequently, with increasing wind, the roughness increases with the flow separation (roughness region). Here the surface states could be applied by using a roughness Reynolds number Rr , which was introduced by Nikuradse (1933):

$$Rr = \frac{u_* z_0}{\nu} \quad (5.9)$$

where z_0 is the surface roughness length and it should be a function of z_{0m} , z_0 is calculated according to Sugita et al. (1995):

$$z_0 = \begin{cases} z_{0m} & Rr \geq 3.32 \\ z_{0m}/(k_1 + k_2(\ln Rr) + k_3(\ln Rr)^2 + k_4(\ln Rr)^3 + k_5(\ln Rr)^4) & Rr \leq 3.32 \end{cases} \quad (5.10)$$

where $k_1 = 0.799$, $k_2 = 0.224$, $k_3 = 0.00206$, $k_4 = 0.0490$, $k_5 = 0.00956$, the first Rr is estimated by the $Rr = u_* z_{0m}/\nu$, if $Rr \geq 3.32$, the $z_0 = z_{0m}$; else if $Rr \leq 3.32$ the Rr should be recalculated and be used to estimate the new z_0 (The process repeated until the value of z_0 close to z_{0m}). Using the measured friction velocity was used and the kinematic viscosity could be estimated by Kondon (1994):

$$\nu = 1.328 \times 10^{-5} \times \frac{1013.25}{P} \times \left(\frac{273.15 + T_{10}}{273.15} \right)^{1.754} \quad (5.11)$$

The roughness Reynolds shown as a function of friction velocity was plotted in Fig. 5.9, the smooth surface main occurred when the $u_* \leq 0.3$, the surface became complete rough when $u_* \geq 0.5$, but when u_* located between 0.3 and 0.5, the surface state was very complicated, it was a mixture of smooth surface, transition surface and completely rough surface.

5.2.1.3 The theory of wave boundary layer

Over land surface, the logarithmic wind law is assumed to be related to local generated turbulence flux where $\tau = \tau_t$, but over water surface, τ should be described as:

$$\tau = \tau_t + \tau_w + \tau_v \quad (5.12)$$

Where τ is total stress, τ_t is stress induced by the locally generated turbulence, τ_w is stress induced by the wave, τ_v is viscous stress. Here τ_v is important only in the viscous layer which is only about 1mm height (Drennan et al 2003), and is negligible. Hence the τ_w become essential. The main dispute is that whether τ_w can be neglected at our measurement height. According to Sjoblom and Smedman (2003), the wind profile can be divided into three height intervals, and the depth of this layer varies due to the wave state (Fig.5.10). The lowest layer is a direct wave influenced layer where the layer with constant wind speed (Smedman et al., 2003). It indicates that $\tau = \tau_w$ in this layer. The highest layer is the surface layer which wind profile is logarithmic during neutral condition ($\tau = \tau_t$). A "transition layer" appears between these two layers, both τ_t and τ_w need to be consider in this layer ($\tau = \tau_t + \tau_w$). In brief, the wave influenced layer and transition layer are named wave boundary layer.

The height of the wave boundary layer is quite important here, since if the wave boundary layer where the surface wave has direct influence on the atmospheric flow is higher than measurement height, τ_w is significant and should be treated more carefully in estimating bulk coefficients. Cheng and Brutsaert (1972) decided the height by $z_c = z_{0m} \exp(kc_p/u_*\phi)$, where ϕ is a dimensionless shear function in neutral condition, z_c is the wave boundary layer (hereafter WBL) height. However, ϕ and z_{0m} inhere is quite difficult to define since the characteristics of three layer mentioned above have different characteristics. To investigate WBL height, several experiments and simulation were done recently. For pure wind condition, numerous studies indicated this layer is much lower than measurement height. Makin and Mastenbroek (1996) found that under high wind speed, τ_w is under 5% of the total stress at the height of 1 m, and reduce to 1% at 3m. Using tower data in Lake Ontario, Drennan et al.(2003) calculated the velocity spectra and cospectra measured at 3m and found they follow established universal scaling laws, indicating τ_w is negligible. On the contrast, Smedman et al. (1994), Grachev et al. (2003) have shown that WBL extend much higher. By combining simultaneous data from an instrumented Air-Sea Interaction Spar (ASIS) buoy and a 30-m tower, Höglström et al. (2009) and Smedman et al. (2009) revealed under a very large wave age condition the wind is very nearly constant up to the highest measuring level. Although their

observation and simulation gave us some information about WBL height in different situation, but until now, to quantify WBL height in a robust way is still unknown. The main solution until now is assumed that the wind profile method valid by applying several correction, typically roughness length or correction function:

- The turbulent flux is constant with height and the stability function is as same as that estimated from the land surface (e.g. Brutsaert, 1992), but the wave age should be included into roughness length estimation. This assumption is widely used in previous studies. For instance, Smith et al. (1992) found that the roughness length is strong wave age dependent over the sea surface. Donelan et al. (1993) also contributed the wave influence to a wave age dependent roughness length.
- A wave age independent roughness is assumed. The traditional stability function is invalid. A new correction function should include both stability and wave age parameter. For instance, based on several assumption, an enforceable solution was proposed by Brutsaert (1973) that the dimensionless shear function ϕ can be decided by $1 + 0.006(c_p/u_* - 29)$ when $C_p/u_* > 29$ in neutral condition.

As mentioned above, the wave impact on the fluxes is still not well understood. In this chapter, assuming the wind profile is valid, the wave influence on roughness length and correction function were investigated in our study area.

5.2.2 Wave age in estimation of roughness length

Historically, the mismatch of z_{0m} estimated from wind profile method and wind-wave interaction equation has triggered debate that whether the influence of the water surface waves on roughness can be negligible. In this section, wave data were analyzed for more clearly understanding of whether and how the state of wave effect roughness length.

5.2.2.1 Roughness length derived from wind profile method

The roughness length z_0 is the height above the displacement plane at which the mean wind becomes zero when extrapolating the logarithmic wind-speed profile downward through the surface layer. Since the stratification function is decided and reference height is adjusted to standard 10 m, the momentum roughness length can be derived from wind profile equation:

$$z_{0m} = \exp(\ln(z) - (\frac{kU}{u_*} + \psi_m)) \quad (5.13)$$

where ψ_m follow Brutsaert (1992), z is measurement high, $k = 0.4$ and u_* is the friction velocity.

5.2.2.2 Roughness length derived from wind-water interaction models

As mentioned above, the momentum roughness length estimated by back calculation from the eddy correlation measurement is not a constant value but depends on the surface condition. For aerodynamically smooth surface ($Rr < 0.13$) and it is entirely determined by the viscous shear, have been found by many authors (e.g. Brutsaert, 1982; Kondo, 1975; Nikuradse, 1933):

$$z_{0m} = \frac{0.11\nu}{u_*} \quad (5.14)$$

As u_* increases, the viscous sublayer get thinner, hence momentum roughness length first decreases, consequently, the wave start to penetrate through the viscous sublayer and interact with the outer turbulent flow (Ataktürk and Katsaros, 1999). Following this transition of the surface from a relatively smooth to a rough state, the roughness length increases. The most widely used roughness length for rough surface ($Rr > 0.13$) was proposed by Charnock (1955)

$$z_{0m} = \frac{au_*^2}{g} \quad (5.15)$$

Where a is an empirically derived constant which was found to depend on the geographic condition and varied with in 0.012 and 0.035 (Garratt et al., 1992). For instance, in open sea observation, $a \approx 0.011$ was usually used (e.g. Fairall et al., 2003 1996; Smith et al., 1992), but in near shore $a \approx 0.0185$ (Wu, 1980). Another way, the wave age dependent view suggested that a constant value a may describe the asymptotic roughness lengths for some special cases only. They cannot predict the variation of the measured wind stress with the surface state, fetch and depth. They attempted to relate the Charnock parameter a to the wave age ($w_a = c_p/u_*$). The relationship was given by

$$a = \alpha \left(\frac{c_p}{u_*} \right)^{-\beta} \quad (5.16)$$

where c_p is the phase speed of the dominant wave mentioned at 6.1.

A constant Charnock parameter a , shown as the slope derived from the median value of each 0.02 x-axis bin in Fig.5.11, is a good representation of the overall trend in rough surface. $a = 0.032$ is much higher than the results obtained from the sea. In wind profile method, the higher roughness length resulted in higher drag coefficient. This have been discussed by Smith et al. (1992) and Ataktürk and Katsaros (1999): the drag coefficient of the sea surface does not depend on wind speed alone, in open-sea conditions the drag coefficient is 10-15% lower than in

coastal or shallower situations and this difference is believed to be due to at difference in typical sea states, i.e. wave age. The wave age dependent roughness length has been investigated by many author (Tab.5.1), the back calculated a was always represented as $z_{0m}g/u_*^2$ and plotted as a function of inverse wave age u_*/c_p . This result was represented in Fig.5.12. A bin-averaging plot was used for trend investigation. The trend of increasing Charnock parameter with inverse wave age was not found. Different from sea surface, the inverse of the wave age varied in a very narrow region and was shown no relation between the wave and roughness. The wave information is not necessary to consider into roughness length estimation in our study area. In another words, in roughness length estimation, a constant Charnock parameter $a = 0.032$, which is expressed with only atmospheric state, was found described the roughness length well over lake surface.

5.2.3 The wave age in estimation of nondimension correction function

To estimate a wave age dependent nondimension correction function, the TKE budget should be understood first. In a stationary and horizontally homogeneous surface layer conditions, the normalised TKE budget was given by

$$0 = -\frac{kz}{u_*^3} \left(\overline{u'w'} \frac{\partial \bar{u}}{\partial z} + \overline{v'w'} \frac{\partial \bar{v}}{\partial z} \right) + \frac{kz}{u_*^3} \frac{\overline{gw'q_v'}}{T} - \frac{kz}{u_*^3} \frac{\overline{gw'e'}}{\partial z} - \frac{kz}{u_*^3} \frac{\partial \overline{w'P'}}{\partial z} - \varepsilon \frac{kz}{u_*^3} \quad (5.17)$$

In brief, it is written as:

$$\phi_m - \phi_{z/L} - \phi_t - \phi_p - \phi_\varepsilon = 0 \quad (5.18)$$

Where terms 1 and 2 corresponds to the shear and the buoyant production and loss, respectively. Term 3 is relate to turbulence transport, term 4 is pressure transport and 5 is molecular dissipation. Term 3 and term 4 is quite small and negligible over land surface, then TKE budget can be expressed as:

$$0 = \phi_m - \phi_{z/L} - \phi_\varepsilon \quad (5.19)$$

but when τ_w can not be neglected, the function becomes:

$$\phi_w = \phi_m - \phi_{z/L} - \phi_\varepsilon \quad (5.20)$$

Furthermore, assuming ϕ_w is only wave age dependent but not observation height, from the energy budget we have the integration form of $\phi_m + \phi_w$:

$$\psi = \psi_w(c_p/u_*) + \psi_m(z/L) \quad (5.21)$$

What we need to do is that to understand the form of $\psi_w(c_p/u_*)$. Here assuming the roughness length is given by $z_{0m} = 0.032u_*^2/g$ which is obtained in last section. For a rough surface, no clear relation between ϕ_w and c_p/u_* was found and the ϕ_w almost close to 0 on average (Fig.5.13).

5.2.4 Summary and discussion of this subsection

The focus of this section was on the dynamics of the locally generated turbulence over the water surface of the lake. Specifically, the aim was to answer whether the wave affects the turbulence over lake surface. From the analysis of measurements of wave, it was shown that the atmosphere boundary layer over lake surface has several different characteristics from land or from sea.

1. Different from the land.

One of the most important differences is that the z_{0m} is no longer a constant value, which depends on the surface condition. For rough surface, the roughness length was dominated by the gravity wave and expressed as Charnock equation. A constant Charnock parameter ($a = 0.032$) was found to adequately describe the momentum roughness length.

2. Different from the sea

Several findings were found different from the sea surface. One of them was that the wave age varied in a narrow range. Owing to this characteristic, wave age dependent momentum roughness length was not found in our study. The other one was that wind profile equation was valid in our study site at moderate and high wind speed. A wave age dependence correction function is not necessary.

Although these findings confirmed that the dynamics of the water surface exchanges were mainly controlled by the atmospheric flow, in order to understand the wave's impact on fluxes, several questions should be answered in reasonable ways:

1. Why the wave age varied in a narrow range and was not necessary in our analysis?

Over lake surface, the wave is dominated by the wind since absence of the swell. In another word c_p is controlled by the wind speed or friction velocity. Indeed, the wave parameters: H_s, T_p, c_p showed high correlation with the wind speed, indicating the wave information could be expressed as a function of wind speed. Consequently, only wind speed is remained in bulk transfer estimation.

2. When wave age dependent roughness length can be found?

Although a constant value of the Charnock parameter was obtained from our study site, for more wide range of u_*^2/g (see Fig.5.14), the situation is more complicated. Historically, the concept of wave age was introduced to answer the scatter located in 0.01-0.1 of u_*^2/g in Fig.5.14 (Toba et al., 1990), but in our study, a wave age dependence Charnock parameter was not found here. It is suggested here the Charnock parameter a should be estimated in gradually. For instance, when 0.01-0.1 of u_*^2/g , $a = 0.032$. For 0.1-1 of u_*^2/g , $a = 0.0185$

3. Self correlation in scaling with u_* in wave dependence Charnock equation.

The Charnock equation suffers a serious problem in self correlation in scaling with u_* . Since direct measurement of roughness length is unavailable, usually it is calculated from the flux using wind profile method. u_* is used in both sides in Charnock equation. Therefore, for a wave age dependent roughness length, seriously self-correlation problem could be found: $z_{0m}(z, U, u_*)g/u_*^2 = A(u_*/c_p)^B$. Ataktürk and Katsaros (1999), Smith et al. (1992) and Janssen (1997) mentioned that if the variables were confined in a narrow range, self-correlation of u_* may lead to spurious result. To reduce the influence of self-correlation, a wide region of inverse wave age in wave age dependent Charnock parameter is necessary. Since it was invalid in our study site, it is better to take care in analyzing the relation between wave age and roughness length.

4. Beside of Charnock equation, is there any other methods to estimate roughness length?

For avoiding the self-correlation, an empirical equation predicted from the height and steepness of waves was proposed by Talyor and Yelland (2001):

$$z_{0m} = Ah_s(h_s/L_p)^B \quad (5.22)$$

in our dataset $A = 720$ and $B = 4.5$ was found. It produced similar result with Charnock equation (Fig.5.15). It is a good addition for estimating friction velocity and validation of Charnock equation. It is more reliable since the self-correlation problem is avoided.

5. The wave boundary height over lake surface can be higher than the measurement high?

From our results, we found the wind profile method worked well in our measurement height in moderate and high wind speed. This means the wave boundary height was lower than the measurement height. The cospectral analysis in chapter 5 also provided an additional

evidence that in moderate and high wind speed, the turbulent is governed by atmospheric turbulence and shown a similar curve with standard cospectral curve (Kaimal et al., 1972) derived from the vegetation surface. For much higher wind speed ($U > 14$ m/s), since we do not have reliable data, the situation is still unknown.

5.3 Large scale convection

In chapter 4, the data were selected by applying several data quality control tests. These data tests merely reflected the locally generated turbulent part in the atmosphere. As a result, all data under weak wind speed were excluded in the analysis. Vesala et al. (2012) suggested a critical notice is necessary with respect to widely established empirical concepts to screen eddy covariance data which may not be appropriate for lake fluxes studies because of the complicated geographical condition. In this subsection, these kinds of tests were not applied, since they are ambiguous and empirical. The data were checked manually: unreliable wind direction, rain periods (3 hours before and after raining) and spike were discarded before the analyses. The new data selection resulted in large scatter in estimation of bulk coefficients under weak wind speed region. For instance, the drag coefficient are plotted in Fig.5.16. It has been argued by some investigators that this large scatter caused by numerous factors. Some authors (e.g., Moncrieff et al., 2006) related this phenomenon to the sensor noise or system errors. However, since the improvement of sensor and careful correction, it seems to be unreasonable to attribute the underestimation of the eddy covariance fluxes to only the reasons mentioned above. On the other hand, the opinion that this may be caused by the convective circulation creates random perturbation gusts near the surface has been suggested by several authors. Stull (1994) found in the limit of free convection, the traditional bulk transfer method fails because zero fluxes are predicted with zero mean wind. Indeed in the real atmosphere, heat moisture and tracer fluxes can be nonzero because of the vertical transport action of convective circulations induced by thermal of warm rising air. Schumann (1988) mentioned that the spatial temperature difference causes hydrostatic pressure difference and induces the convection. This convection would lead to the large-scale circulation which increases the fluxes. Through flight experiments, Sun and Mahrt (1994) and Sun et al. (1996) have already verified the influence of meso-scale flux in bulk formulation and suggested that a modified formula is necessary. Many findings indicated that under weak wind speed, the impact of convection should be taken into account in bulk transfer method. Since the influence of convection in both momentum and heat should be parameterized into U or u_* , momentum exchange process is expected to

be a good indicator of the characteristic of large scale convection. In this chapter, we focused on analysis of the momentum flux and wind speed which are influenced by the large scale convection. Furthermore, the results were applied for estimating the heat fluxes in bulk transfer methods.

5.3.1 The characteristics of large scale convection

An inherent characteristic of the study area in this study is that it is surrounded by land, the spatial temperature difference between lands and water surfaces may induce thermal convection. In addition, it may be affected greatly by sea-land breeze since lake is nearby the sea. Since the complicated geographic condition, several factors were investigated to study the reasons causing the large scatter under weak wind speed. Here the main possibilities can be mentioned as wind direction WD related to fetch, radiation Rn , wind speed U , temperature difference between air and water surface dt which is related to the stability, were investigated during day time. In Fig.5.17, no relation was found between WD and dt , but most of the cases were found in high radiation and weak wind speed which indicated that the atmosphere is under strong unstable condition. Furthermore, the higher values of drag coefficient was found at higher radiation and lower wind speed. This indicates that the large scatter of C_{dn} under weak wind is properly caused by the large scale convection which is induced by the spatial temperature difference.

As mentioned above, large-scale convection may play a very important role under weak wind speed region. To understand the characteristic of large scale convection in a quantitative way is thus an important subject. One of the ways is to perform analysis by Fourier analysis which is a very useful tool for deriving information on energy development, transfer and dissipation of turbulence. Here we investigated the large-scale convection by applying two method: cospectral analysis and ogive analysis, both of them are based on Fourier analysis.

5.3.1.1 Cospectral and Ogive analysis

Eddy covariance flux data obtained during 3 years' measurements were divided into two datasets. One contained various erroneous and suspicious data which may be influenced by large scale convection under weak wind speed region. The other one, for comparison, high wind speed cases were collected, in which showing similar C_{dn} with the previous studies. Of the day time runs recorded during the study period, ten runs for each dataset, each of 2-hour duration were selected. All of the runs excluded unreliable wind direction, raining day in which aliasing errors are huge. A detail are listed in Table 5.3 and Table 5.4.

Before employing the Fourier Transfer Algorithm, the wind velocity was rotated into a new wind velocity, in order to force the averaging cross and vertical wind component equal to 0. Noted that no de-trending or filtering process was applied in here since this would affect the low frequency characteristics that we wish to investigate. The trends curves can be found in Appendix C and Appendix D.

Meanwhile, the trend problem should be taken care because the trend is not only caused by large-scale convection, but also the diurnal variation. Here the Mann-Kendall (hereafter, MK) trend test were introduced here. The Mann-Kendall trend test is one of the most popularly applied test to detect trends in hydrologic time-series (Yue and Wang, 2004). The MK statistic test, S is give by

$$S = \sum_{k=1}^{n-1} \sum_{j=k+1}^n \text{sign}(x_j - x_k) \quad (5.23)$$

where the x_j is the sequential data values, n is the length of the data set and the $\text{sign}(\theta)$ is given by

$$\text{sign}(\theta) = \begin{cases} 1 & \theta > 0 \\ 0 & \theta = 0 \\ -1 & \theta < 0 \end{cases} \quad (5.24)$$

Under the assumption that the data are independent and identically distributed, the mean and variance of the S statistic are given by (Kendall, 1975)

$$\text{Var}[S] = \frac{n(n-1)(2n+5)}{18} - \sum_{j=1}^k \frac{t_j(t_j-1)(2t_j+5)}{18} \quad (5.25)$$

Where k is the number of groups of tied ranks, each with t_j tied observations (Hamed, 2008). Furthermore, the standardized test statistic Z is respectively given by

$$Z = \begin{cases} \frac{S-1}{\text{Var}(S)^{1/2}} & S > 0 \\ 0 & S = 0 \\ \frac{S+1}{\text{Var}(S)^{1/2}} & S < 0 \end{cases} \quad (5.26)$$

If the Z is small enough, the trend is not found by random sampling. A positive and negative Z values indicate an upward and downward trend, respectively. At the significance level of Gaussian distribution 5% which is a value of 3.92, if $Z \leq \pm 3.92$, then the existing trend is considered to be statistically significant. The results showed that the trend existed in both strong and weak wind cases (Table 5.8 and Table 5.7). For similar trend condition, we tried to use Fourier transform to find out the difference between weak and strong wind cases.

In this study, Fourier transform was calculated by using Complex Fast Fourier Transform method. For each run, the FFT algorithm produced 72000 complex points. The last of them represents the spectral energy at the Nyquist frequency (5 HZ), and the first represents the spectral energy at the inverse of sampling rate which is 2 hour. Their real and imaginary parts were combined to calculate spectral, cospectral. To demonstrate the definition of cospectral, the following algorithm was given by Stull (1988):

$$Co = F_{Ar}F_{Br} + F_{Ai}F_{Ai} \quad (5.27)$$

where the A and B are meteorological variations, subscripts r and i denote the real and the imaginary parts of FFT, respectively. The cospectral results were smoothed by averaging in non-overlapping frequency bands equally spaced on a logarithmic scale. Here we divided one decade into 10 bands. The smoothed cospectral results were compared with the standard cospectral proposed by Kaimal et al. (1972) which would be introduced later.

5.3.1.2 Theory of Cospectral and Ogive analysis

Cospectral of the turbulence offers a convenient way of investigating the behavior of fluxes since its representation is associated with each scale of motion the amount of kinetic energy, variance, or eddy flux which contributes to the whole and provides a new and invaluable perspective on boundary layer structure (Kaimal and Finnigan, 1994). To understand the theory of cospectral analysis, a particularly useful conceptual picture of the distribution of energy in wave number space was drawn by Kaimal and Finnigan (Fig.5.18). In this figure, they assumed the homogeneous turbulence is provided by the scalar energy spectrum $E(K)$. $E(K)$ represents the contribution to the total kinetic energy from Fourier modes with wavenumber magnitudes between K and $K + dK$ with decreasing of frequency. In low frequency region, $E(K)$ peaks in the energy-containing region, by definition, and drops to zero at both ends of the spectrum. This can be identified into three major regions (Kaimal and Finnigan, 1994):

- Range A, the energy-containing range, which contains the bulk of the turbulent energy and where energy is produced by buoyancy and shear.
- Range B, the inertial sub-range, where energy is neither produced nor dissipated but handed down to smaller and smaller scales.
- Range C, the dissipation range, where kinetic energy is converted to internal energy.

The wave length at the spectral peak in this figure, is a length scale of greater importance to boundary layer meteorologists than the integral length since it is representative of the size of eddies with most energy. A cospectral peak is often found within 30 min in wavenumber-energy plot. This indicates that all the fluxes are collected within 30 min. Otherwise, the data may be influenced by the large scale convection since it fixes the cospectral gap.

In this study, since most measurements were performed in time scale, the wave number should be converted into frequency. Furthermore, since the spectral forms tend to be different for each variable, the non-dimensional frequency and non-dimensional form of energy based on dimensionless similarity theory were applied, which provide same information with wavenumber-energy plot ($-\frac{fC_{uw}(f)}{u_*^2}$). A classical universal curve for momentum flux was plotted by Kaimal et al. (1972), and the normalized curve can be approximated by:

$$-\frac{fC_{uw}(f)}{u_*^2} = \frac{12n}{(1 + 9.6n)^{7/3}} \quad (5.28)$$

A clear cospectral peak could be found between $n=0.1-0.01$. This was obtained over short vegetated surface and regarded as the standard model for comparison. Comparisons of cospectral in this study allowed us to illustrate the differences in mechanisms associating with the impacts of different surface (e.g. land; lake surface; sea surface).

The second method for investigating characteristics of turbulence was introduced by Oncley et al. (1996). This method used ogive plots that integrate under the cospectral curve to show the cumulative contribution eddies to the total transport by increasing the period (Moncrieff et al., 2005). This curve of so called ogive curve is defined by

$$Og_{uw}(f_0) = \int_{\infty}^{f_0} C_{o_{uw}}(f)df \quad (5.29)$$

where $C_{o_{uw}}$ is the cospectral of the vertical wind velocity and horizontal wind velocity. The convergence of ogive at low frequencies indicates that all relevant eddies are collected. The ogive curve contains same information with cospectral, but the advantage of the ogive presentation is that we can determine whether we have sampled for long enough by observing whether the ogive curve has reached its asymptote, and the empirical curve (e.g. the Kansas cospectral proposed by Kaimal et al, (1972)) is no longer necessary for comparison. Furthermore, the ogive value, equals the covariance between meteorological quantities, is also useful when discussing the influence of low frequency fluxes on surface exchange (Moncrieff et al., 2005).

5.3.1.3 Mismatch of time scale of fluxes and mean quantities caused by large scale convection

Fig.5.19 shows the average of the normalized momentum flux cospectral, $-fC_{uw}(f)/u_*$. The standard cospectral (Kaimal et al., 1972) is also plotted. The observed cospectral for high wind cases had a peak at about the same normalized frequency with standard cospectral. It indicates that all the fluxes were caught for 30 min or less since the first peaks in the spectrum indicate the eddy sizes that contribute most to turbulent kinetic energy. Furthermore, there is no difference between the water surfaces or vegetations for 10 m heights in the surface layer, the large scale convection contribution was much smaller than the local generated turbulence. On the contrast, under weak wind speed cases, it is clear that there was no any significant peaks in the scales associated with turbulence. The large scale convection might fix the cospectral gap, and tended the curve increasing.

For Ogive analysis, as shown in Fig.5.20, for high wind speed cases, the ogive curve increased during integration from high frequency to low frequencies until a certain time, at about 10 min then remained more or less constant, suggesting that 10 min might be an adequate period for capture all frequencies contributing to the fluxes. Similar to cospectral result, the ogive function did not reach a constant value after a certain frequency in weak wind speed cases. The energy keeps increase with decreasing frequency. To investigate the cause of large value of C_{dn} , mean velocity associated with the frequency are also plotted in Fig.5.21. Both of weak and strong wind cases, were found almost kept a constant value at low frequency. The wind speeds were not influenced by the large scale convection. Furthermore, the bulk coefficients can be calculated based on the ogive results as follows

$$C_{dn}(f_0) = \frac{\int_{\infty}^{f_0} C_{o_{uw}}(f) df}{U(f_0)} \quad (5.30)$$

where $U(f_0)$ is the mean velocity in the current frequency. As shown in Fig.5.22, the bulk coefficient varied in a small region at high wind speed cases, but under weak wind speed, since the fluxes were still increasing in our investigated time scale, the mismatch of time scale between the fluxes and velocity was found (to be introduced later). This is the reason that the bulk coefficient shows a larger value than the value of smooth surface.

5.3.2 Modified wind speed by applying gustiness theory

5.3.2.1 Gustiness theory

As mentioned above, the common assumption of smooth surface would underestimate fluxes under weak wind region because of large scale convection. As Redelsperger et al. (2000) mentioned, for wind speed below 3 m/s, exchanges between ocean and atmosphere are predominantly due to convective driven motion. Since such case is rare in the ocean, it is neglected in large scale exchange process studies. Different from ocean, the low speed cases are very common over lake surface, and it is necessary to develop a method for estimating this effect. Here we regarded the measured fluxes as the effective fluxes resulting from both turbulence and large scale convection flux. A general approach to solve this mismatch of time scale was presented by Godfrey and Beljaars (1991) who suggested using an effective wind speed U_e instead of the traditional vector-averaged mean wind speed in bulk transfer methods

$$\overline{u'w'} = C_d U_e^2 \quad (5.31)$$

where $U_e = (U^2 + u_g^2)^{0.5}$. u_g is the influence of large-scale convection circulation which is called the gustiness defined by the free convection velocity w_* and an empirical coefficient β . β implies the ratio between horizontal scale and vertical scale of the convection circulation (Schumann, 1988). w_* was defined by Deardorff (1970) as

$$w_* = (F_b z_i)^{1/3} \quad (5.32)$$

where F_b is the buoyancy flux:

$$F_b = \frac{g}{T} (\overline{w'T'_v}) \quad (5.33)$$

z_i is the height of the convective boundary layer (hereafter CBL), g is gravitational acceleration, T is the temperature and $T_v = T(1 + 0.61q)$ is the virtual temperature, here q is humidity. Since the temperature and sensible heat flux can be obtained from the eddy correlation data, $\beta \approx 0.8$ can be found in numerous large eddies simulation studies (e.g. Schumann, 1988; Sykes et al., 1993). Therefore, the difficulty of this approach is to estimate the depth of z_i . Here both observation and modelling were done to obtain accurate z_i .

5.3.2.2 CBL depth estimation

The CBL depth z_i is an important scaling variable in boundary layer meteorology. CBL mainly grows by sensible heat input from the land surface during day time. Marked changes in

either wind speed or direction between atmospheric layers are often used to separate the surface layer and convective boundary layer. Based on these characteristics, the observation and modelling of CBL were carried out.

Observations of pilot balloons were made for the purpose of determining wind direction and velocity at various altitudes. Observations were made by following the ascent of a helium-filled balloon with a theodolite. The balloon was inflated with an amount of helium so as to rise the balloon at 120 m/min and accurately reflect the direction and speed of the wind presents at the altitudes where it climbs through. The angles of azimuth and elevation from the theodolite to the balloon were observed and recorded at 5 second interval. Several places (Fig.2.1: Ushiwata, Rinkojiken, Tennousukouen) were chosen to obtain the general CBL depth around the lake.

An example of CBL measurement at Rinkojiken is depicted in Fig.5.32. A significant change of wind speed and wind direction were found at about 100 m: the wind speed changed from 2.2 to 1.8 m, the wind direction also changed from 20 degree to 340 degree. This was regarded as the CBL depth based on these changes. A second inversion was found at about 300 m, which indicated the depth of the boundary layer. The rest of 2 times measurement were defined in the same method. A detail about these measurements is shown in Tab.5.2. From this result, a brief schemas of z_i growth before afternoon was defined in time series. Since the observation times were limited, a modelling based on the regional sensible growth was introduced and the model was validated using the measurements by pilot balloon.

If one assumes a purely thermodynamic process, the CBL depth increases by the warming of boundary layer air continue input from the land surface (neglects any contribution from other mechanical turbulence. Based on this concept, the slab model which based on the zero-order scheme (Deardorff, 1979) could be outlined in Fig.5.24 and basic equations of this model were expressed as follows

$$\frac{d\theta}{dt} = \frac{\overline{(w'\theta'_q)_s} - \overline{(w'\theta')_{z_i}}}{z_i} \quad (5.34)$$

$$\frac{d\Delta\theta}{dt} = \gamma \frac{dz_i}{dt} - \frac{d\theta}{dt} \quad (5.35)$$

$$\frac{dh}{dt} = \frac{\overline{(w'\theta'_q)_{z_i}}}{\Delta\theta} \quad (5.36)$$

$$\overline{(w'\theta'_q)_{z_i}} = -\varepsilon \overline{(w'\theta'_q)_s} \quad (5.37)$$

then

$$\frac{d\theta}{dt} = \frac{\overline{(w'\theta'_q)_s} - \varepsilon \overline{(w'\theta'_q)_s}}{z_i} \quad (5.38)$$

where θ is temperature, t is time, $\overline{w'\theta'}$ is the sensible heat flux, the subscript z_i and s represent convection height and land surface. If we assume the temperature jump is not exist, $\overline{(w'\theta'_q)}_{z_i} = 0$, $\frac{d\Delta\theta}{dt} = 0$. Based on equation (5.34), we have

$$\gamma \frac{dz_i}{dt} - \frac{\overline{(w'\theta'_q)}_s}{z_i} = 0 \quad (5.39)$$

Regarding γ is a constant value of dry adiabatic lapse rate, the CBL depth z_i is estimated from time-integrated surface sensible heat flux which is given by

$$\int_0^t \frac{dz_i^2}{2} = \int_0^t \frac{\overline{(w'\theta'_q)}_s}{\gamma} \quad (5.40)$$

and

$$z_i^2 = \frac{2}{\gamma} \int_0^t \overline{(w'\theta'_q)}_s \quad (5.41)$$

where 0 denotes sunrise and t is the current time. Although z_i can be calculated from the surface sensible heat flux, the complicated geographic condition let us more careful in choosing the measurement location. Since a lake is surrounded by land, in most of cases the spatial extent of the lake is too small to strictly expect equilibrium conditions of the atmospheric turbulence with the local water surface (Vesala et al., 2012). Thus z_i may be influenced by the heat flux from the land surface, paddy field, and/ or lake. Therefore several datasets were calculated and compared to the observation data. A typical grassland surface flux (1.6m) at Terrestrial Environment Research Center (hereafter TERC), dataset from a mobile station set in Ushiwata over a paddy field and the dataset from Lake center observatory were used to estimate z_i . For almost same radiation condition, the sensible heat from different dataset showed large difference (Fig.5.25). This resulted in large differences of z_i which were estimated from different datasets. In the afternoon, several hundred meters of z_i difference was found (Fig.5.26). The paddy field showed largest value which might be terminated by local geographic condition; in lake center, a large part of energy was absorbed by the water and z_i showed smallest value. The TERC data resulted in a little lower z_i than paddy field's which completely affected by the land surface. Compare to the observation result, we found the CBL depth derived from TERC dataset has high correlation with the observation data ($y=1.2x$, Fig.5.27). This might caused by the face that the sensible heat over a water surface was very small compare to the land surface and might can be neglected in the whole area. Therefore TERC's data were chosen for estimating CBL depth. Meanwhile, since all of measurements were done before 12 am, the afternoon condition is still not well known. Saotome (2009) estimated the CBL depth using the Mie lidar located near lake Kasumigaura

(Source: <http://www-lidar.nies.go.jp/>), and compared to slab model's result. He found the best match occurred during 8:00-11:00 AM. These results also support our analysis using data from the ozone lidar (Fig.5.29). The Center for Global Environmental Research (CGER) ozone lidar system was constructed at Tsukuba in 1988 for measuring vertical profiles of stratospheric ozone which is able to measure ozone in the lower and middle stratosphere with high accuracy (data source: <http://db.cger.nies.go.jp/gem/moni-e/ozon/lidar/lidar01.html>). The CBL depth estimated from the ozone lidar was in agreement with the modelled value before afternoon, but several hundred meters difference was found in the afternoon. Main reason is that slab model utilizing our study was too simple to model the real atmosphere. In our model, the z_i was decided by the locally generated sensible heat fluxes. However in the afternoon, the horizontal heat transfer may play a very important role. Incorporating the results mentioned above, we only choose the time period for 8-11 JST in fine day in gustiness analysis.

5.3.2.3 Bulk coefficients estimated from modified wind speed

Since z_i has been decided, the gustiness term could be determined by $u_g = \beta(F_b z_i)^{1/3}$. The effective wind speed can then be estimated. Note that since z_i is hard to obtain, an alternative method was developed. Mahrt and Sun (1995) suggested using the scalar averaged wind speed U_{scalar} instead of the vector averaged wind speed U . Based on this concept, the time averaging instantaneous speed was defined as:

$$\overline{U^2} = \overline{\bar{u}^2 + 2\bar{u}u' + u'^2 + \bar{v}^2 + 2\bar{v}v' + v'^2} \quad (5.42)$$

since the cross terms $\bar{u}u'$ and $\bar{v}v'$ vanished after simple unweight averaging. Therefore the scalar averaged wind speed can be expressed as:

$$\overline{U^2} = \overline{\bar{u}^2 + u'^2 + \bar{v}^2 + v'^2} \quad (5.43)$$

In this equation, $U_{vector}^2 = \bar{u}^2 + \bar{v}^2$. By neglecting the difference between the average of the square root and the square root of the average, the equation becomes

$$U_{scalar}^2 = U_{vector}^2 + (u'^2 + v'^2) \quad (5.44)$$

In the free convection case, the standard deviation of the horizontal wind fluctuations can be expressed as $u' = v' = 0.67w_*$ (Panofsky et al., 1977). Based on this concept, horizontal wind fluctuations is close to the gustiness factor mentioned in Godfrey and Beljaars (1991): $(u'^2 + v'^2)^{0.5} \approx \beta w_*$.

Compared to vector averaged wind speed, we found the gustiness term was very small compare to vector averaged wind speed at moderate and high wind speed, whereas it might play very important role under weak wind speed (Fig.5.30). Both U_e and U_{scalar} showed larger values than vector averaged wind speed under weak wind speed, but U_e and U_{scalar} were not match each other. The drag coefficient estimated from U_e , U_{scalar} , U_{vector} and smooth surface are depicted in Fig.5.31. The results shows that bulk coefficients is still different from that for the smooth surface after using modified wind speed. Although the effective wind speed using modified wind speed did not completely solve weak wind speed issue in estimation bulk coefficients, compared to using U_{vector} , we still suggest using a scalar wind speed in bulk transfer method under strong convective condition, since the fluxes derived from scalar wind speed is closer to the measurement value.

5.3.3 Remaining issue

Although the method improved the flux estimation under weak wind speed, However, indeed we did not successful estimate fluxes under strong convective condition completely. The main reasons may be answered by several questions.

1. Does z_i estimated from TERC dataset really express the CBL depth over lake surface?

Although the results depicted that z_i based on the TERC's data match our observation well, this result might be applicable only in similar atmospheric condition (e.g. radiation). Considering the distance between them (about 20 km), the convection height may be totally difference.

2. A simple slab model is good enough for modelling the CBL depth?

In this study, the model was quite simple: with assumption that all the heat comes from the local surface. In other words, advection should be zero. Actually, the heat transferred by the wind is very important. A more accurate model (e.g. Lee, 1986) is hoped to be used in the further analysis.

3. $U_{scalar} \approx ((\beta w_*)^2 + U^2)^{0.5}$?

The scalar averaged wind speed was assumed to be close to the value of $((\beta w_*)^2 + U^2)^{0.5}$. This should be questioned since $\sigma_u = \sigma_v = 0.67w_*$ is too approximate for estimating the gustiness. To derive an accurate gustiness factor, more studies are necessary.

4. Another way to evaluate the influence of large scale convection in bulk transfer method?

There are several methods to evaluate the influence. For example, Abdella and D'Alessio (2003) proposed a new parameterization for momentum roughness length which extends the Charnock formula down to zero friction velocity. The new formula is expressed as:

$$z_{0m} = \frac{0.015}{g}(u_*^2 + \chi w_*^2) \quad (5.45)$$

Where χ is a empirical parameter. This method had same problem, and z_i should be decided by an accurate method. Metzger and Holmes (2008) estimated z_i using the method of Liu and Ohtaki (1997). In their method, z_i was estimated from the horizontal u velocity spectrum:

$$z_i = 0.53(\lambda_{max})_u \quad (5.46)$$

Where $(\lambda_{max})_u$ is the peak wavelength in the u spectrum. Nevertheless, an accurate z_i is indispensable in this study. It is also one of the further works.

5. A simple bulk transfer equation sheared the same bulk coefficient which is derived from the locally generated turbulence?

In this study, the bulk transfer method was applied by

$$-\overline{u'w'} = u_*^2 = C_d(U^2 + (\beta w_*)^2) \quad (5.47)$$

U and βw_* shared the same bulk coefficient. No relevant study was found to discuss whether it is adequately accurate. Since the different characteristics exist between the locally generated turbulence and large scale convection, the solution is still unknown. It may need to develop a new bulk transfer coefficient to include the contribution from convection. For instance, it should be expressed as $-\overline{u'w'} = u_*^2 = C_d U^2 + C_{dl}(\beta w_*)^2$. Where C_{dl} is drag coefficient for large scale convection. This question be answered by a large eddy simulation (e.g., Vercauteren et al., 2008).

6. The accuracy of measurement of turbulence under weak wind speed region? Similar with most of previous studies, the measured fluxes were regarded as standard value with small error. However, since the non-stationary under weak wind situation, the accuracy of measurements become a question, the re-parameterization is necessary.

5.3.4 Summary and discussion of this subsection

In this subsection, the characteristics of large scale convection were investigated by cospectral and ogive analysis. Under strong wind speed, the energy mainly comes from the locally

generated turbulence, but under weak wind speed, the fluxes were influenced by the large scale convection. Since wind speed converged at a constant value at about 30 min under weak wind speed, the mismatch of time scale between flux and wind speed was found. In order to solve this mismatch, a convective velocity was taken account into wind speed. Aim to estimate the convective velocity, the pilot balloon observation was done and a slab model was used to estimate the CBL depth. Furthermore, an alternative which is using the scalar averaged wind speed instead of the vector averaged wind speed was also investigated. Both methods were found to make the bulk coefficients estimation under weak wind speed under strong convective condition closer to that for smooth surface. A scalar averaged wind speed was suggested for estimating fluxes and evaporation under strong convective conditions.

Although we found the mismatch of time scale between the flux and wind speed, the reason that caused this mismatch should be answered. To answer this mismatch, the mechanism of turbulent averaging should be understood clearly. To define the fluctuation x' in 3.1, which is quite important term in eddy correlation flux calculation, a reasonable time scale should be decided first. Since the atmosphere typically contains motions and coherent vertical transports (fluxes) on a wide range of timescales, the selection of averaging time is not always straightforward (Vickers and Mahrt, 2003). The choice of averaging timescale depends on the objective of research and mainly summarize as follows:

- (a) The study relates to turbulence only.

When relating fluxes to the local mean wind shear and temperature stratification, as in similarity theory, the prescribed time scale would ideally include transports on all turbulence time scales and exclude all meso-scale and large motions (Vickers and Mahrt, 2003). To include transport on all the turbulence, 30 min average time scale is suggested by many authors (e.g. Kaimal and Finnigan, 1994; Rannik and Vesala, 1999). Furthermore, mesoscale motion do not obey similarity theory and are poorly sampled on time scale on time scale of a few hours or less (e.g. Mahrt et al., 2001; Vickers and Mahrt, 2003). To exclude the data influenced by the large scale convection for 30 min, several empirical data tests which is based on similarity relationship should be applied. This study was done in chapter 4, the results showed quite match with previous studies.

- (b) The study relates to both turbulence and large scale convection.

For surface energy study, it is found by many studies, the fluxes are underestimated

when we only consider the locally generated turbulence. Using the 50 sites in FLUXNET, Wilson et al. (2002) found about 20% of available energy on average. Using TOGA array mooring data, Esbensen and McPhaden (1996) found that the enhancement of evaporation due to meso-scale motions can reach up to 30% of the total amount of evaporation over sea surface. Indeed, the underestimation of heat fluxes were reported at almost all the measurement sites regardless of the type of the land cover and external conditions (Saito., 2007).

5.3.5 To defined a reasonable time scale

As mentioned above, for long term fluxes estimation, the influence of large scale convection could not be neglected. Therefore, to define a reasonable time scale is essential in this subsection. To decide the averaging timescale, Lumley and Panofsky (1964) proposed the average period should be decided by:

$$T = \frac{2\sigma_U^2 T_u}{\bar{U}^2 \eta^2} \quad (5.48)$$

Where σ_U^2 is the variance of quantities $U(t)$, and T_U is an integral time scale. These equations provided us several information:

- The required averaging times for turbulence moments increase with the order of the moment, and that any moment probably requires longer time to determine than the mean. For instance, the momentum flux (2nd moment) needs much longer time than the mean wind speed (1st moment). Furthermore, the mismatch will occur since the averaging time difference between different moments. In our study, for most of cases, the fluxes increased but the mean wind speed decreased at the same frequency. The mismatch was found under weak wind speed.
- The averaging time depends on the time scale of the eddy. For typical daytime wind speed values over the land ($\sigma_U = 1$ m/s, $T_u = 10$ s and $U = 5$ m/s), and specifying $\eta = 0.02$, we have $T = 2000$ sec = 30 min (Kaimal and Finnigan,1994). However for large-scale eddies which have longer time scale (larger T_u), the average time should be extended to capture all eddies.

The equation mentioned above could not be used in determining the time scale in a quantitative way, since several parameters are usually unknown. In order to catch all the turbulence

fluxes, and to yield local turbulent fluxes that appear to be statistically stationary, Metzger and Holmes (2008) investigated the physically relevant time scales in unstable atmospheric boundary layer using four convection-removal time scale methods:

- (a) Based on the location of the maximum in the ogive of the flux: t_c

It is most robustness method to define the time scale (Vercauteren et al., 2008). The convergence of ogive at low frequencies indicates that all relevant eddies were collected. If the ogive reaches an asymptote at some frequency f_c , we can decide the averaging time to include all the relevant flux contributions.

- (b) The ratio of the mixed-layer depth over the convective velocity: t_*

The ratio of the mixed-layer depth over the convective velocity, t_* is defined following Lilly (1968):

$$t_* = z_i/w_* \quad (5.49)$$

where z_i is the convective depth, and w_* is the convective velocity. Physically, the convective time scale t_* represents a characteristic time for the thermally driven eddies to be transported from the bottom to the top of the mixed layer (Stull, 1988).

- (c) The convergence time of the vertical velocity and temperature variance: \tilde{t}

\tilde{t} relates to the convergence time \tilde{t} for the velocity and temperature variance is often used as a measure to establish that a "sufficient" averaging time has been selected (Sakai et al., 2001). If the time series were statistically stationary, the variance σ^2 would be expected to increase monotonically with increasing averaging time T and asymptotically converge to its "true" variance(Lenschow et al., 1994).

- (d) The location of the zero crossing in the multiresolution decomposition of the flux: $\tilde{t}_M R$

Howell and Mahrt (1997) and Vickers and Mahrt (2003) suggested the multiresolution decomposition (MR) method to defined a reasonable averaging time period. In this method, geophysical variables are orthogonally decomposed by averaging time series using different averaging lengths, referred to as a (Haar) multiresolution decomposition (Howell and Mahrt, 1997) .

The four methods mentioned above address the issue of selecting a time scale to define accurate fluxes in averaging process of eddy correlation method. Using the same data as ogive analysis, they are discussed here:

- The location of the maximum in the ogive of the flux: t_c .

For high wind speed cases, the flux converged at about 30min, indicating that 30 min is a reasonable time scale for estimating fluxes. In the other words, the influence of large eddies is quite small, compare with the locally generated turbulence. In contrast, for low wind speed cases, the fluxes even could not converged until 2 hours. The influence of large eddies played very important role on this region. The results can be found in Fig. 5.19 and ??

- The ratio of the mixed-layer depth over the convective velocity: t_*

t_* was much smaller than t_c (Table5.6) and (Table5.6) both in high wind speed cases and low wind speed cases, indicating the uncertainty in z_i cannot explain the discrepancy between t_* and t_c . Indeed, (Metzger and Holmes, 2008) found in order to obtain a value near t_c , the mixed-layer depth would have to be on the order of 4000m. Because of this ambiguity in the appropriate measure of z_i and w_* , results of t_* are presented here for illustrative purposes only.

- The convergence time of the vertical velocity and temperature variance: \tilde{t}

\tilde{t} is defined as the time scale where the variance reaches 99.5% of σ_{60}^2 which represents the variance calculated using a mean-removal time of 60 min. In the present study, averaging time scale is defined by the convergence time of the vertical and horizontal velocity variance. The σ_{60}^2 was assumed as a convergence criterion. What is more, we can find the variance converged to the σ_{60}^2 at about 30 min for high wind speed cases. For low wind speed, the variance do not typically to the fixed value. Metzger and Holmes (2008) mentioned that this definition of \tilde{t} is problematic since the horizontal velocity variances do not typically 'converge' to a fixed value. Furthermore, although σ_{60}^2 has been suggested previously as a convergence criterion (Sakai et al., 2001), no physical justification exists for doing so in general (Metzger and Holmes, 2008).

- The location of the zero crossing in the multiresolution decomposition of the flux:

Assume the time series wind component w and u each consisting of 2^M points (in the present study, M=16, about 109 min). To estimate multiresolution decomposition, sub-record averages over a window of 2^m points are defined by Howell and Mahrt (1997):

$$\overline{w_n}(2^m) = \frac{1}{2^m} \sum_{i=(n-1)2^m}^{n2^m-1} w_i \quad (5.50)$$

Where $n = 1, \dots, 2^{M-m}$. The integer n identifies the position of the 2^{M-m} different averaging windows of 2^m points. Based on the Reynolds averaging length of z^m points, the momentum flux is defined as

$$\langle u' (2^m) w' (2^m) \rangle = \frac{1}{2^M} \sum_{i=0}^{2^M-1} [w_i - \bar{w}_n(2^m)] [u_i - \bar{u}_n(2^m)] \quad (5.51)$$

Where the angle brackets $\langle \rangle$ represent the averaging over the whole record length. The observed w and u deviations from local averages over windows of 2^m points is given by

$$u_i' (2^m) w_i' (2^m) = [w_i - \bar{w}_n(2^m)] [u_i - \bar{u}_n(2^m)] \quad (5.52)$$

Therefore, the Reynolds flux produces the same value with the total fluxes calculated within each of the $2^{(M-m)}$ windows of 2^m points. The total fluxes within the n^{th} window is given by

$$\frac{1}{2^m} \sum_{i=(n-1)2^m}^{n2^m-1} u_i' (2^m) w_i' (2^m) \quad (5.53)$$

In this equation, $u_i' (2^m) w_i' (2^m)$ is calculated following

$$u_i' (2^m) w_i' (2^m) = [w_i - \bar{w}_n(2^m)] [u_i - \bar{u}_n(2^m)] \quad (5.54)$$

The flux based on an averaging length of 2^M points is given by

$$\langle u' (2^M) w' (2^M) \rangle = \sum_{m=0}^M \{ \langle u' (2^m) w' (2^m) \rangle - \langle u' (2^{m-1}) w' (2^{m-1}) \rangle \} \quad (5.55)$$

Then

$$\langle u' (2^M) w' (2^M) \rangle = \sum_{m=1}^M \langle \Delta u (2^m) \Delta w (2^m) \rangle \quad (5.56)$$

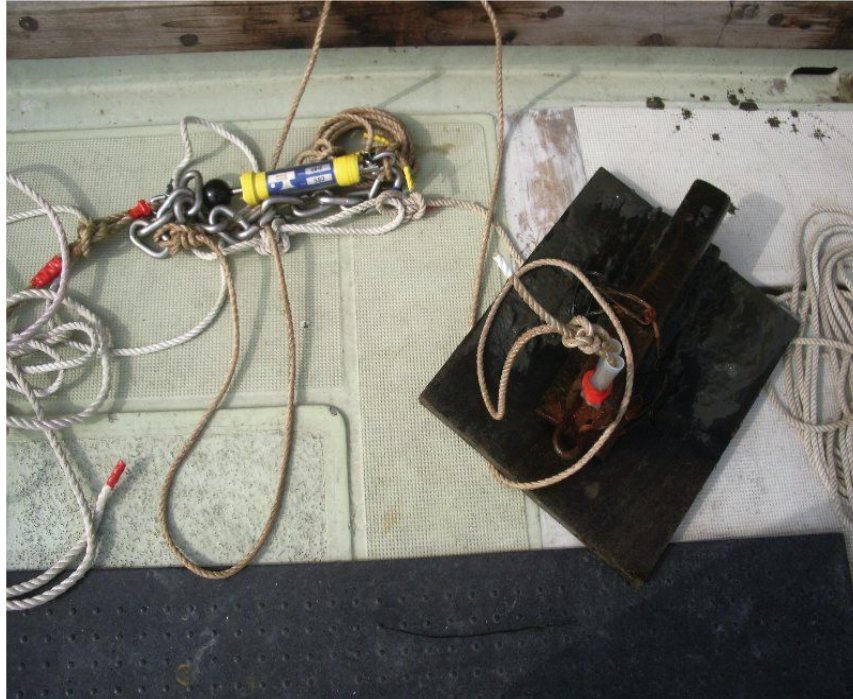
Where

$$\langle \Delta u (2^m) \Delta w (2^m) \rangle = \frac{1}{2^{M-m}} \sum_{n=1}^{2^{M-m}} [\bar{u}_{2n} (2^{m-1}) - \bar{u}_n (2^m)] \times [\bar{w}_{2n} (2^{m-1}) - \bar{w}_n (2^m)] \quad (5.57)$$

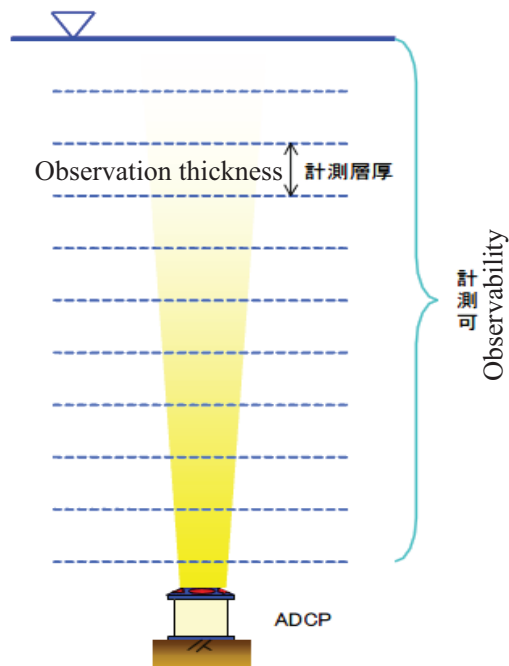
is a multiresolution cospectral for an 2^m interval averaging length. $\langle u' (2^M) w' (2^M) \rangle$ relates the total record flux to a sum of difference terms and always was plotted as *MRcospectral*. Indeed, this method can be regarded as a highpass filter that, with each application, removes increasingly shorter averaging time scale fluctuations Vickers and Mahrt (2003).

The results were plotted in Fig.5.33. For high wind speed, the time scale estimated by the MR analysis agree well with those reported by the ogive analysis. For low wind speed cases, it is so noise and we could not decide a reasonable time scale. However, due to the limit accuracy of the multiresolution decomposition method (for 109 min time scale, only 16 points can be obtained, furthermore, fewer in low frequency region), it is not suggested for deciding a quantitative time scale.

Time scales defined by various methods were summarized at Table 5.9 and Table 5.10. Similar time scales were not obtained, furthermore, it is unable give a definition under weak wind speed. The results showed longer averaging time are necessary. However, extending the averaging period too long does not reduce the error (Kaimal and Finnigan, 1994), since the wind becomes non-stationary due to diurnal variation. For short time, on the other hand, give rise to increase sampling error and lead to mismatch of time scale between the flux and wind speed. Therefore the usually used 30-min averaging time scale is a good choice. A modified mean wind speed should be applied in estimation of bulk coefficients. In our study, the effective wind speed and scalar averaged wind speed were applied.



(a) Acoustic Doppler Current Profiler



(b) The measurement theory of ADCP

Fig 5.1 Photos about Acoustic Doppler Current Profiler (Figure by The Ministry of Land, Infrastructure and Transport and Tourism of Japan)

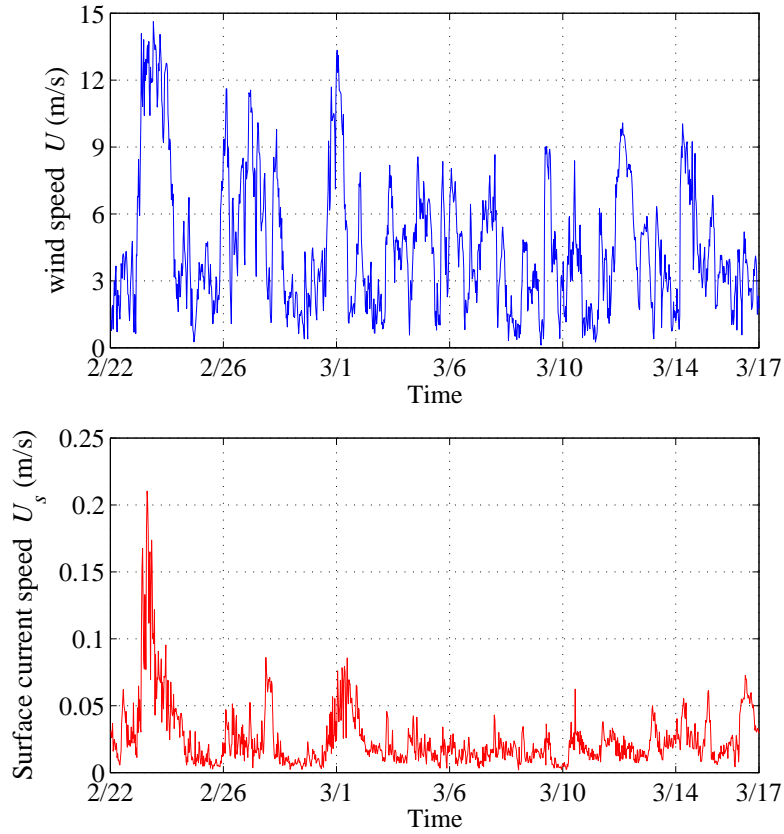


Fig 5.2 Comparison of wind speed and water surface current speed for the period of 2008/2/22-2008/3/18

Table 5.1 Charnock paramter proposed for power-law relation, $z_{0m}g/u_*^2 = A(u_*/c_p)^B$

Source	A	B
Toba et al. (1990)	0.02	-0.5
Maat et al. (1991)	0.8	1
Smith et al. (1992)	0.48	1
Monbaliu (1994)	2.87	1.69
Vickers and Mahrt (1997)	2.9	2.0
Johnson et al. (1998)	1.89	1.59
Drennan et al. (2003)	1.7	1.7

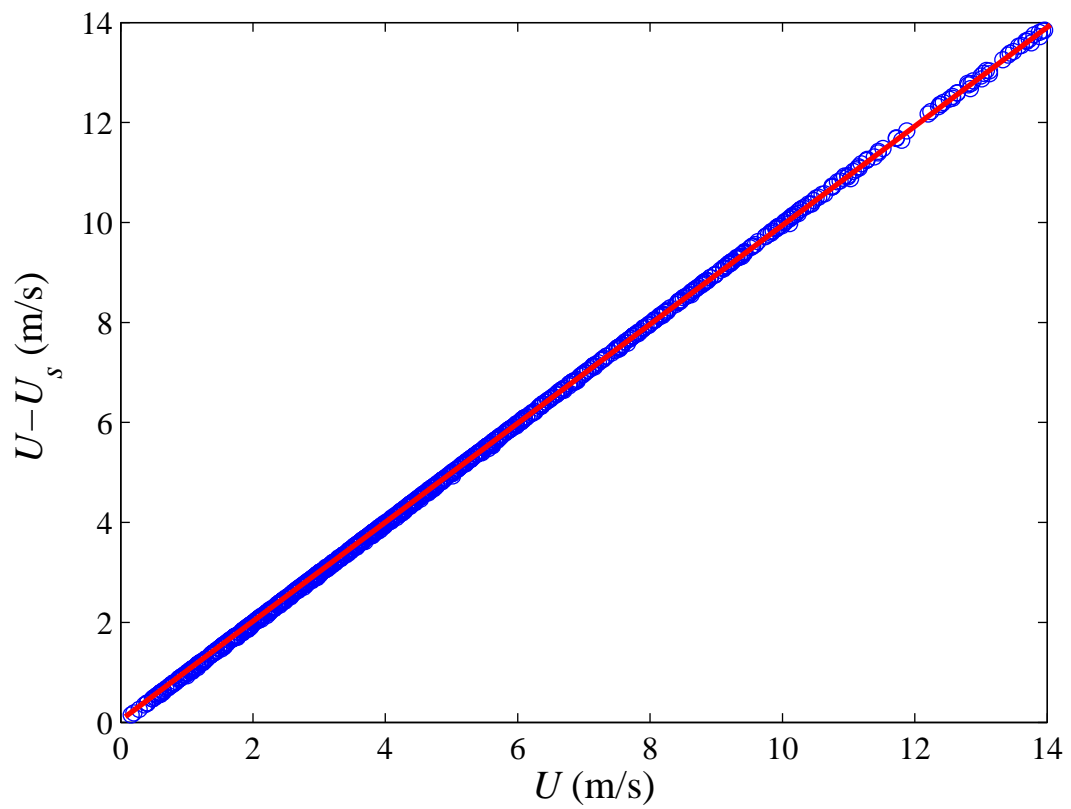


Fig 5.3 Comparison of wind speed and a relative wind speed by considering the surface current

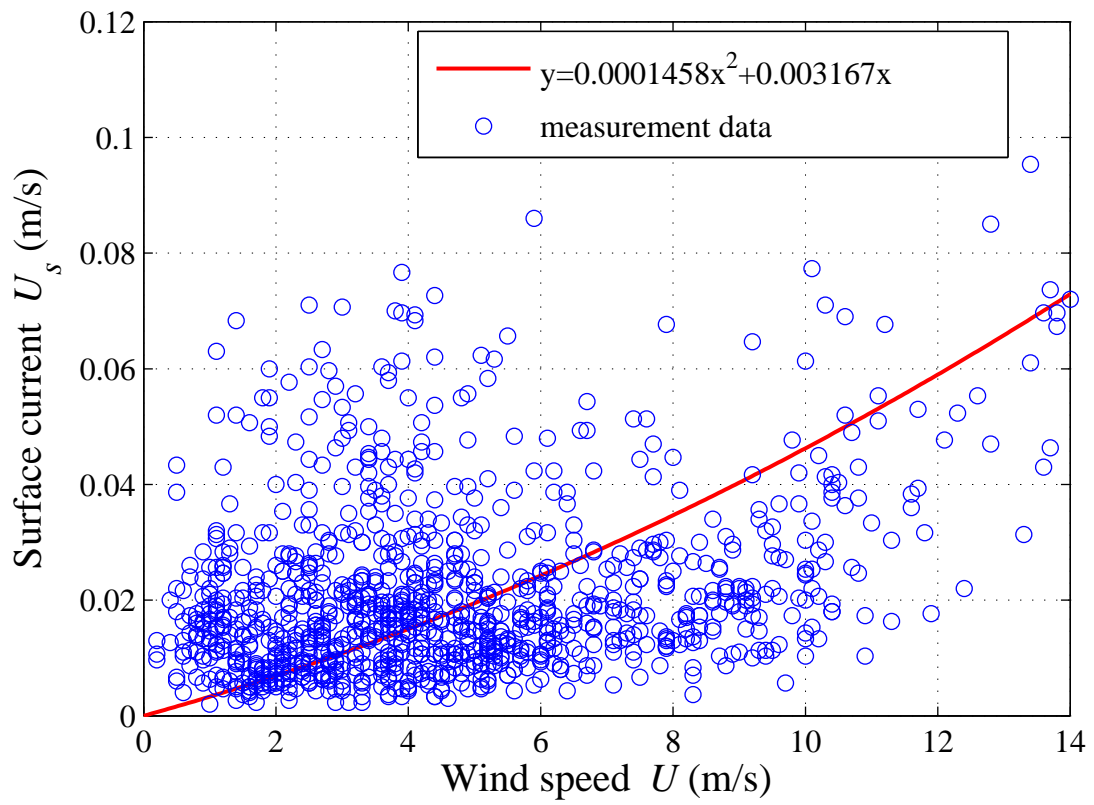


Fig 5.4 The surface current speed as a function of wind speed

 <p>Smooth surface</p>		
<p>Photo was taken at $U=0.25\text{m/s}$</p>	<p>Photo was taken at $U=2.35\text{m/s}$</p>	<p>Photo was taken at $U=7.5\text{m/s}$</p>

Fig 5.5 The growth of wave by the wind over lake surface

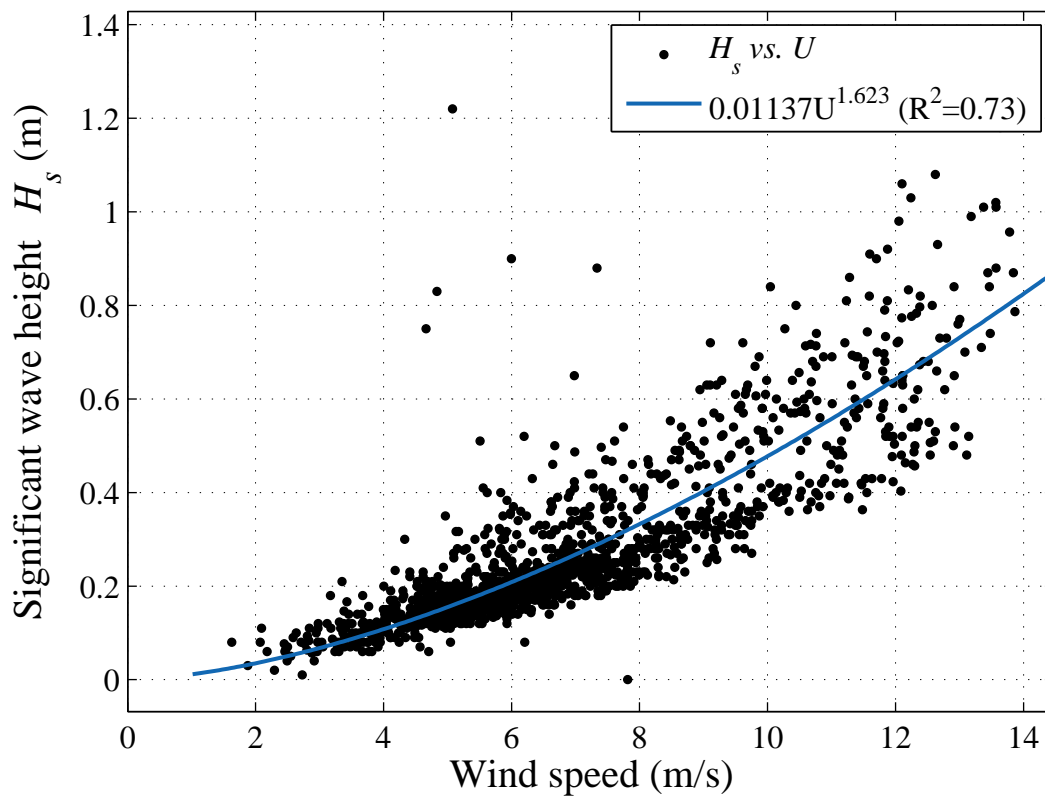


Fig 5.6 The height of the dominant wave as a function of wind speed

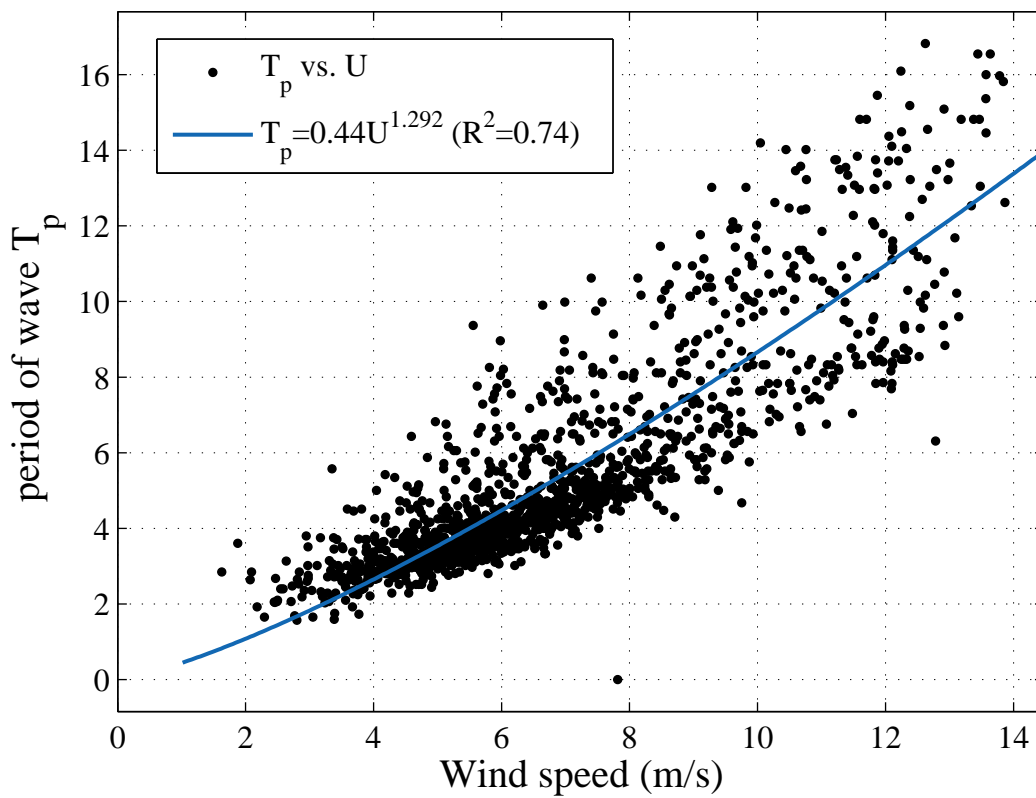


Fig 5.7 The period of the dominant wave as a function of wind speed

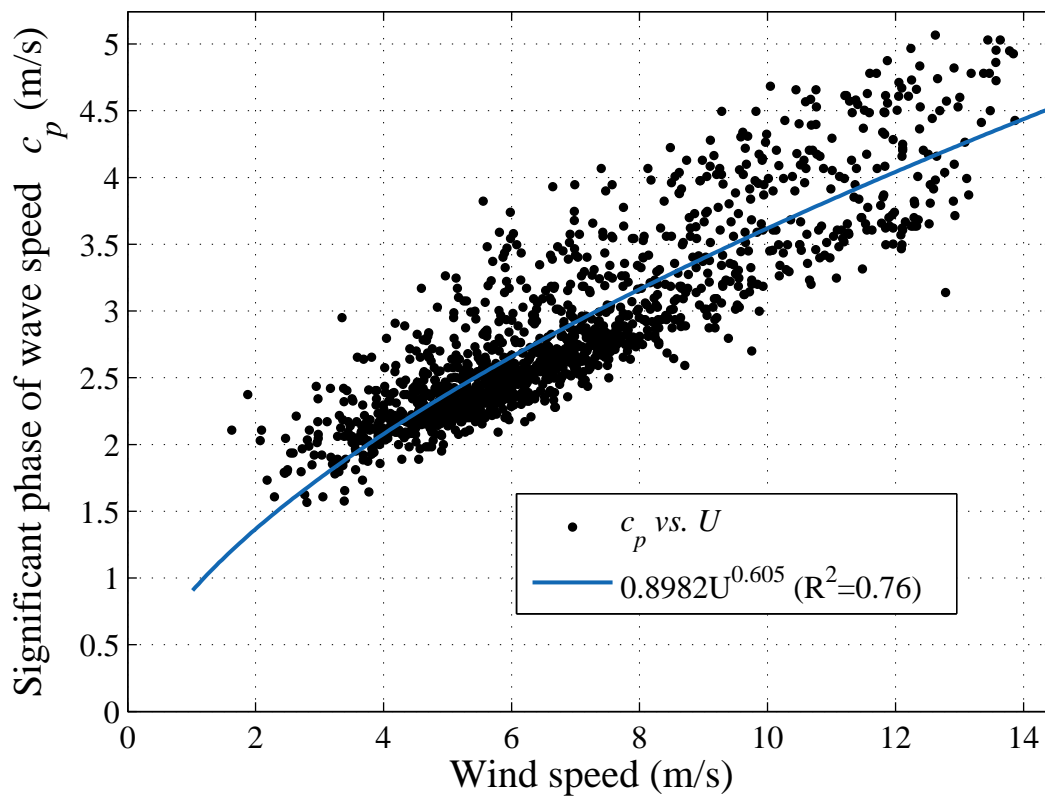


Fig 5.8 The phase speed of the dominant wave as a function of wind speed

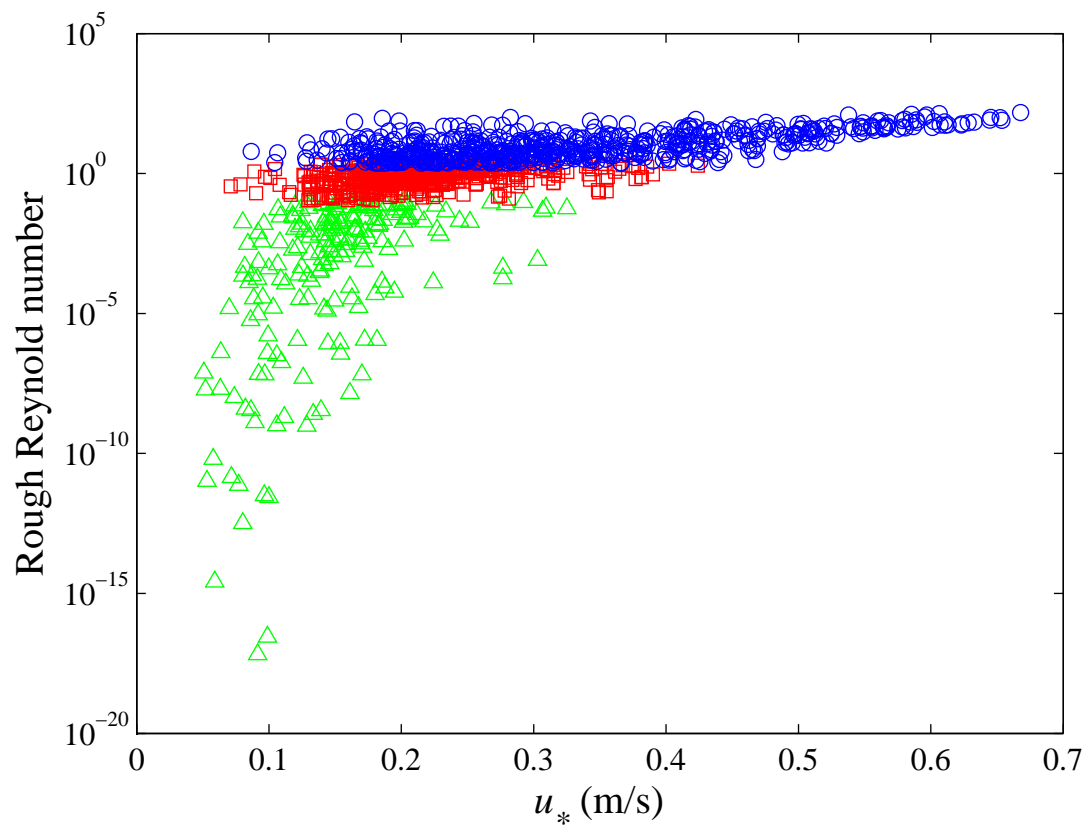


Fig 5.9 Roughness Reynolds number Rr verse friction velocity, blue circles for $Rr \geq 2.3$, red squares for $0.13 \leq Rr < 2.3$, green triangles for $Rr < 0.13$

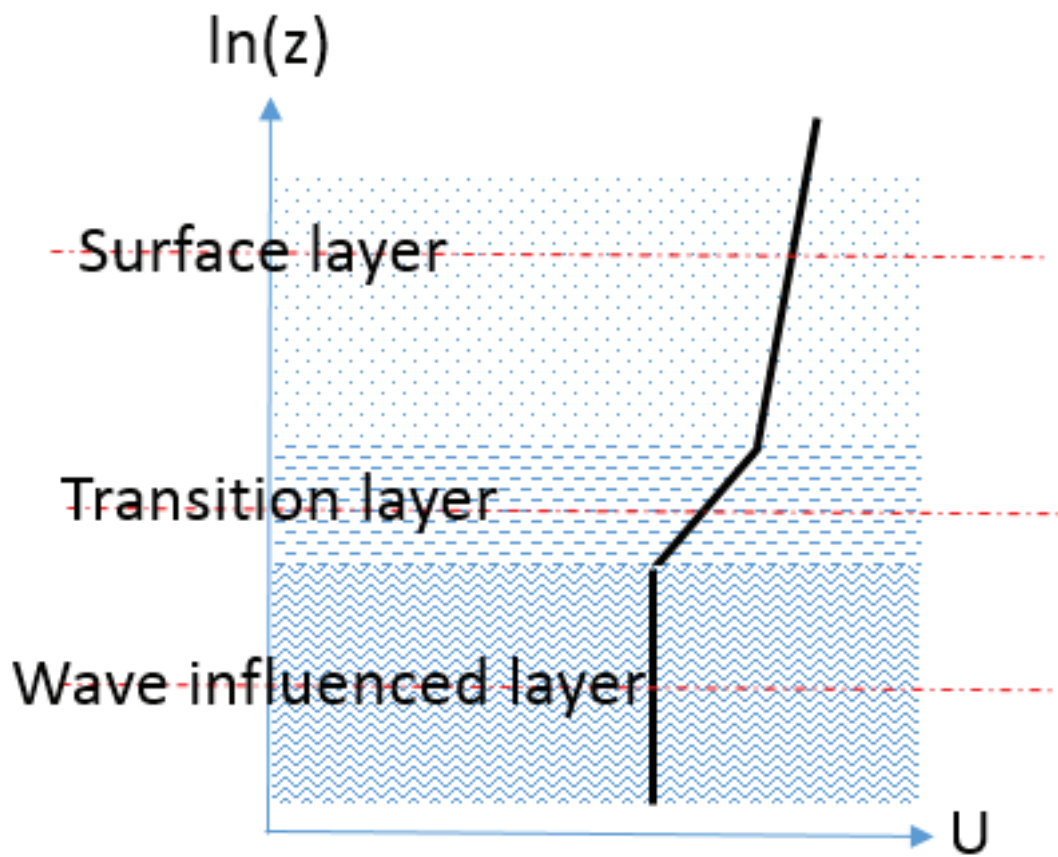


Fig 5.10 Typical schematic of a wind profile over the water surface (redraw from Sjoblom and Smedman (2003))

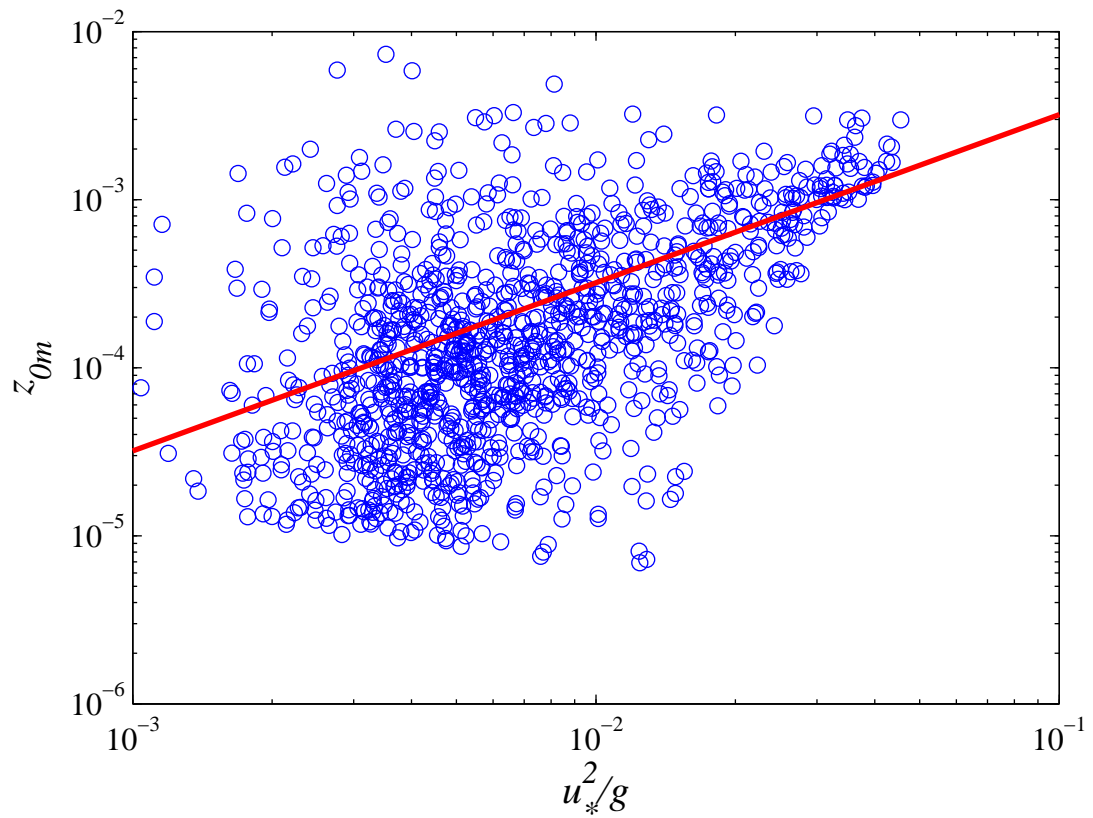


Fig 5.11 Variation of momentum roughness length with Charnock parameter u_*^2/g , the slope derived from origin through regression of each 0.02 x-axis bin median value

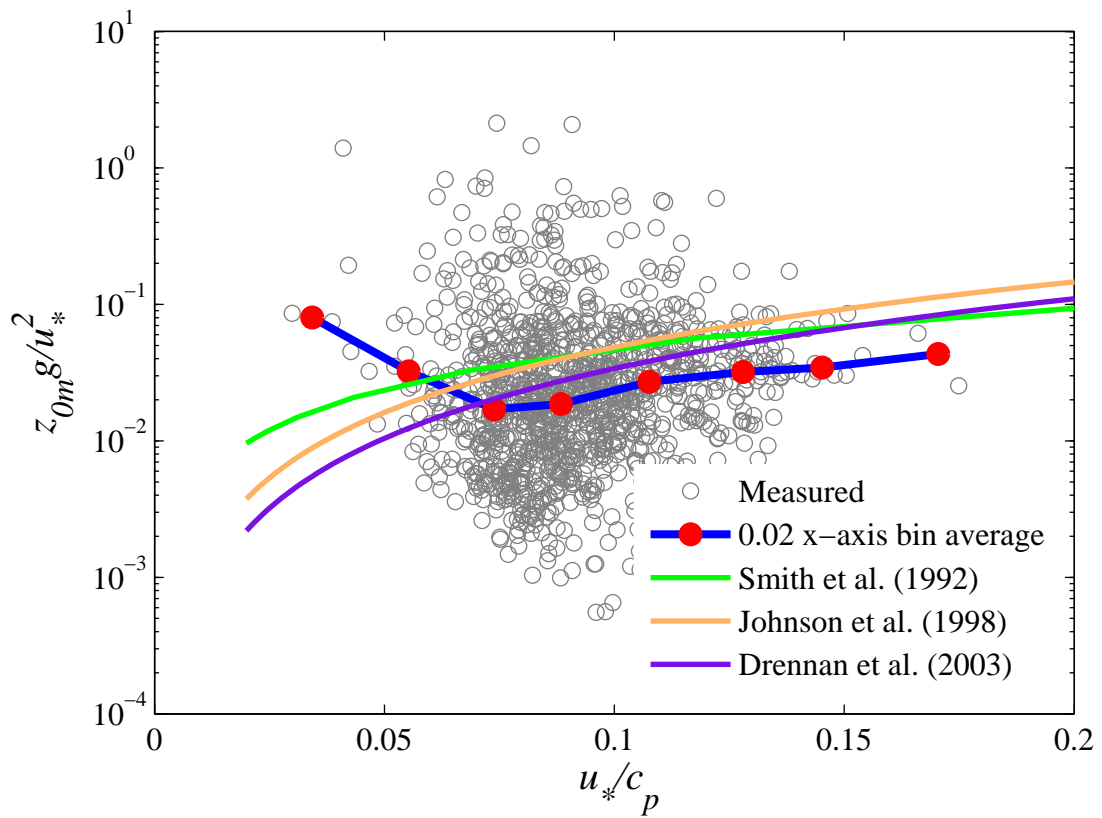


Fig 5.12 Charnock parameter versus inverse of wave age for rough surface ($Rr > 3.2$). The curve are from Smith et al. (1992), Johnson et al. (1998) and Drennan et al. (2003)

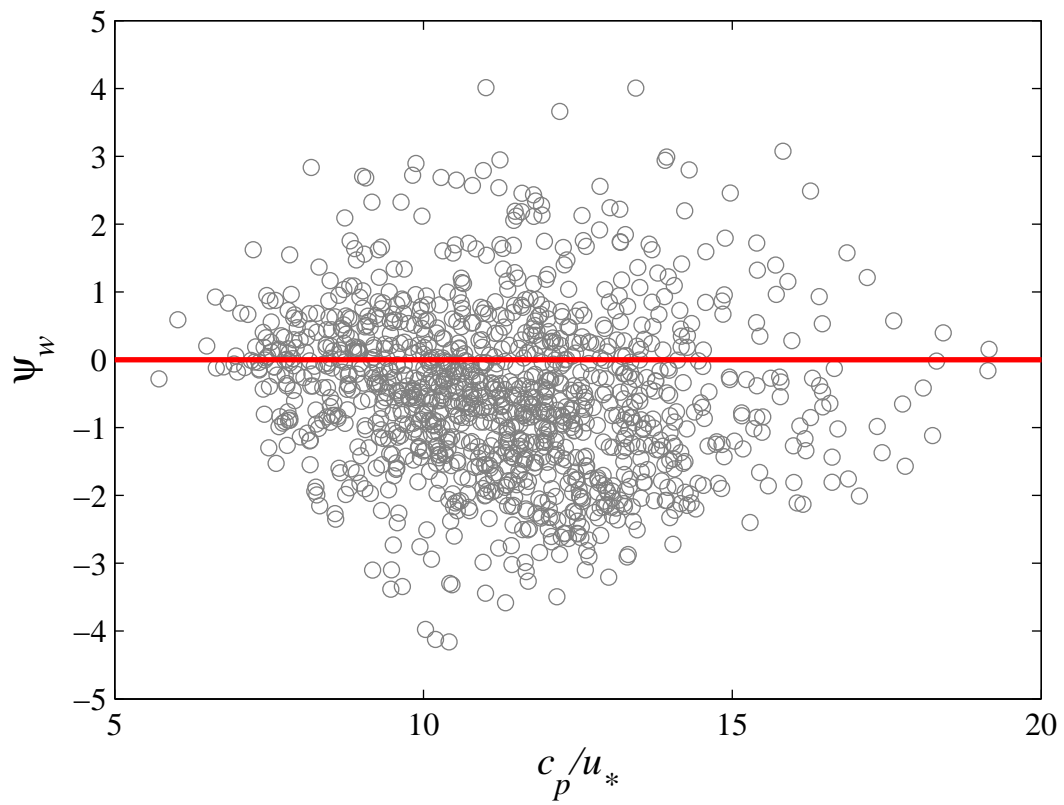


Fig 5.13 Dependence of the shear correction function ψ on the wave age parameter c_p/u_*

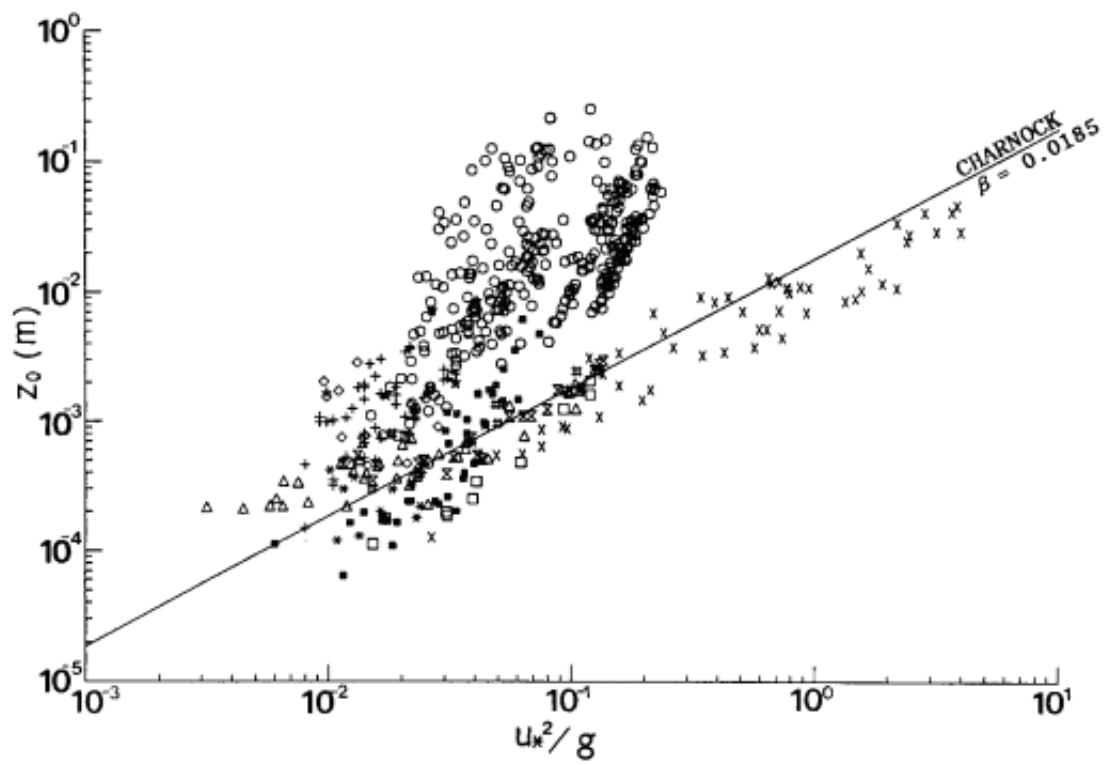


Fig 5.14 Dimensional presentation of the Charnock formula. (Figure by Toba et al. (1990))

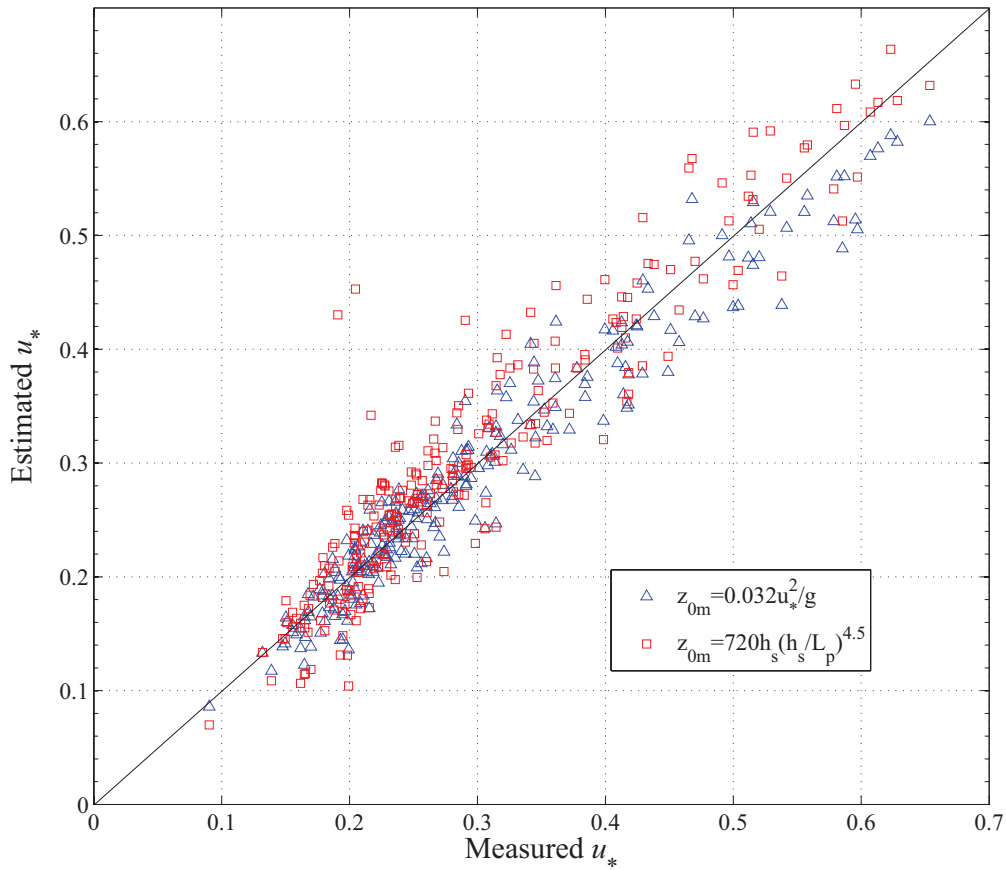


Fig 5.15 In comparison with friction velocity driver from a constant Charnock parameter and empirical wave information method by Taylor and Yelland (2001)

Table 5.2 pilot balloon observation

Observation site	Date and time (JST)	Wind direction	Wind speed(m/s)	Weather	CBL depth(m)
Rinkojiken	2011/8/26 08:15	45	1.1	Fine	250
Rinkojiken	2011/8/26 11:16	275	5.8	Fine	530
Ushiwata	2011/8/26 07:40	225	1.3	Fine	200
Tennonsu	2011/8/26 09:40	300	2	Fine	290

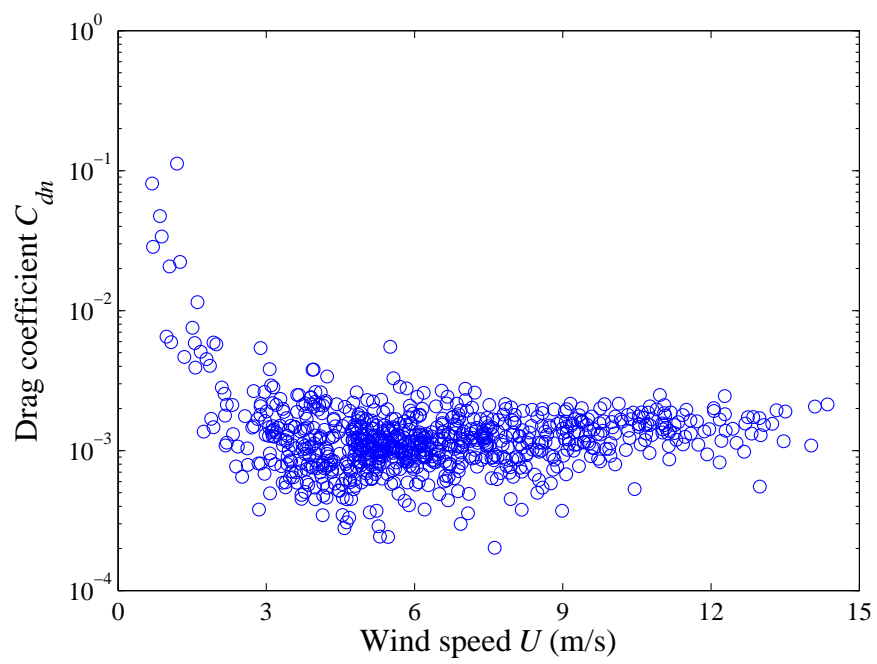


Fig 5.16 Drag coefficient under weak wind speed

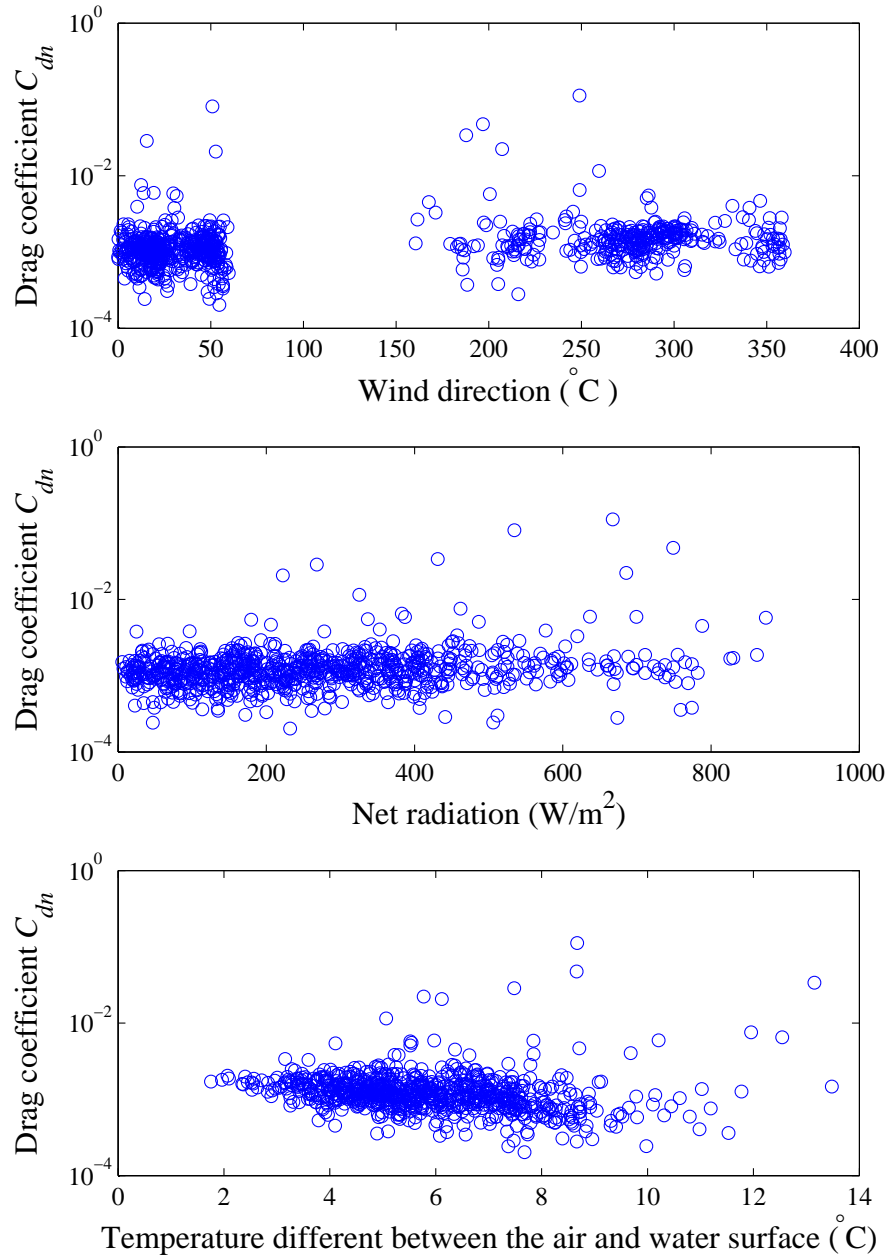


Fig 5.17 The drag coefficient related to wind direction, net radiation and temperature between the air and water surface

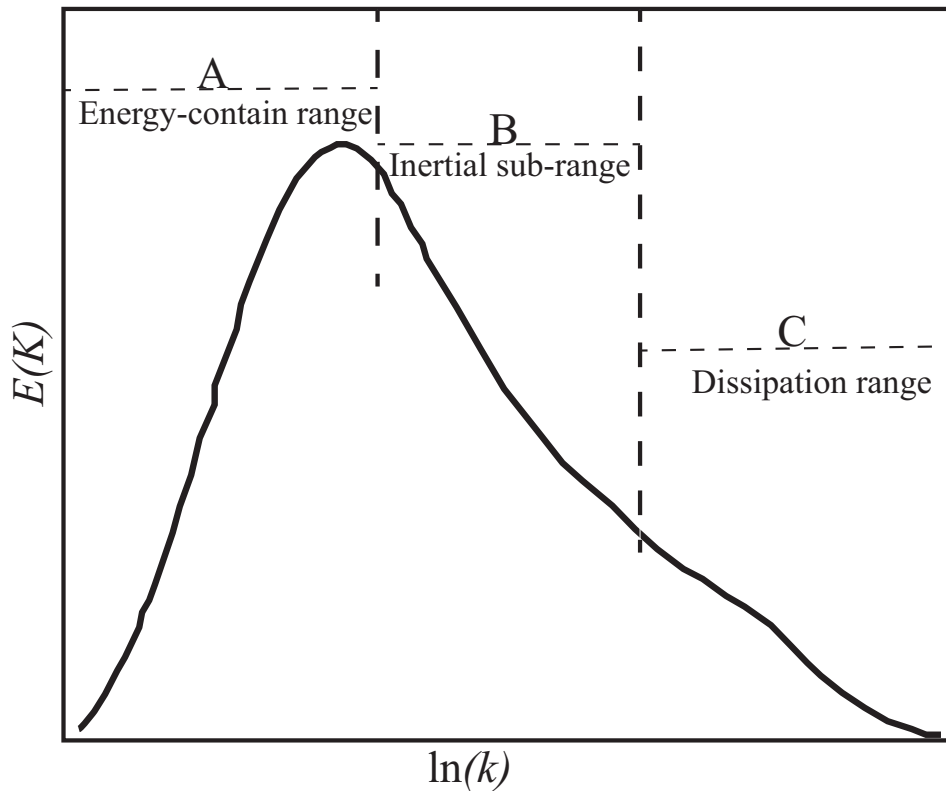


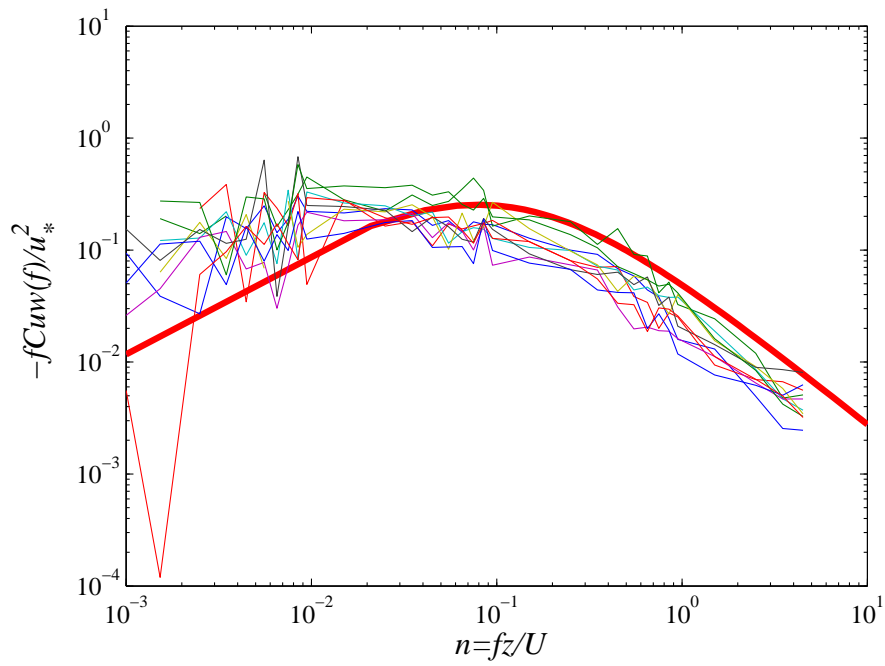
Fig 5.18 Schematic of energy spectrum in the atmosphere boundary layer showing distinct regions of energy production (A) and dissipation (C) and the inertial subrange (B), where both energy production and dissipation are negligible. (Redrawn from Kaimal and Finnigan (1994))

Table 5.3 High wind speed cases for ogive analysis (2h averaging period)

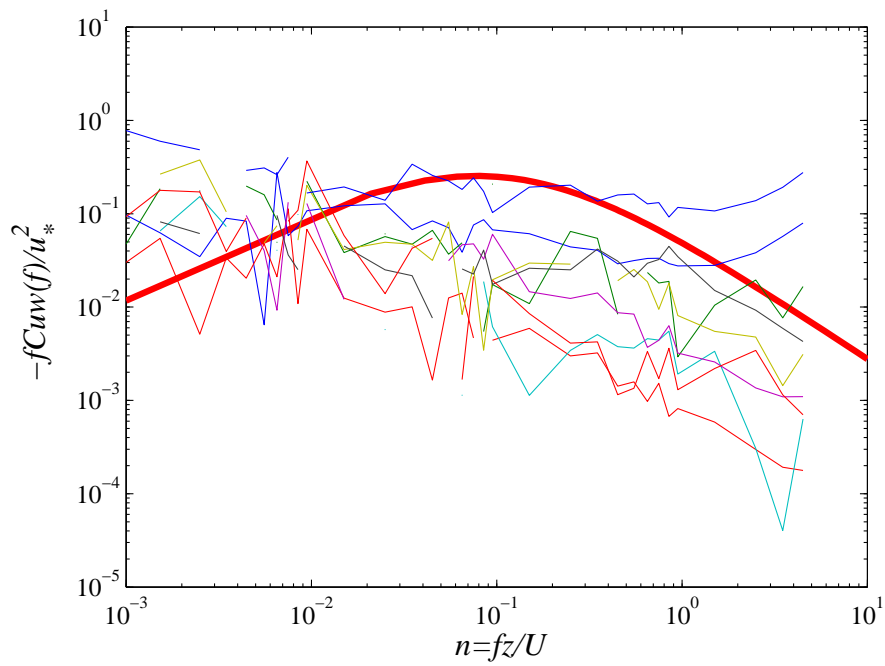
Data number	Date and time (JST)	WD	$-u'w'$ (m^2/s^2)	Uscalar (m/s)
Data1	2008-01-01 08:00:00	279	0.0886	7.1772
Data2	2008-11-22 09:00:00	301	0.0537	4.5500
Data3	2009-09-18 12:00:00	36	0.0504	6.0839
Data4	2009-12-18 08:00:00	238	0.0675	4.8949
Data5	2010-02-17 07:30:00	23	0.0637	5.6101
Data6	2010-12-25 08:30:00	246	0.0595	5.3429
Data7	2008-05-08 05:30:00	40	0.0608	5.5895
Data8	2008-05-16 06:00:00	47	0.0847	8.0327
Data9	2008-12-13 07:30:00	15	0.0226	6.1112
Data10	2009-03-30 06:30:00	18	0.0558	7.0868

Table 5.4 Low wind speed cases for ogive analysis (2h averaging period)

Data number	Date and time (JST)	WD	$-u'w'$ (m^2/s^2)	Uscalar (m/s)
Data1	2008-06-01 10:30:00	182	0.0308	2.0482
Data2	2008-07-27 12:00:00	23	0.0177	2.5633
Data3	2008-08-07 09:00:00	243	0.1097	0.2003
Data4	2008-09-13 08:00:00	39	0.0323	0.8927
Data5	2008-09-25 09:30:00	315	0.0225	2.5723
Data6	2009-02-19 10:30:00	94	0.0474	2.0645
Data7	2009-03-27 12:00:00	125	0.1551	2.0831
Data8	2009-09-22 13:00:00	161	0.0125	0.7662
Data9	2009-10-09 13:30:00	49	0.0076	0.4263
Data10	2010-01-16 14:00:00	31	0.0837	3.5266

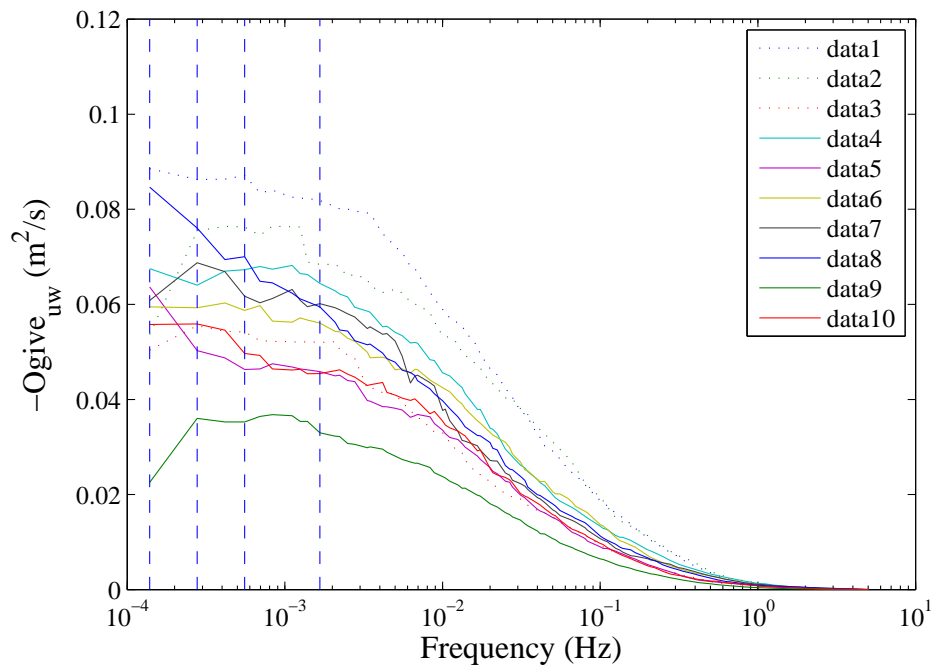


(a) High wind speed cases

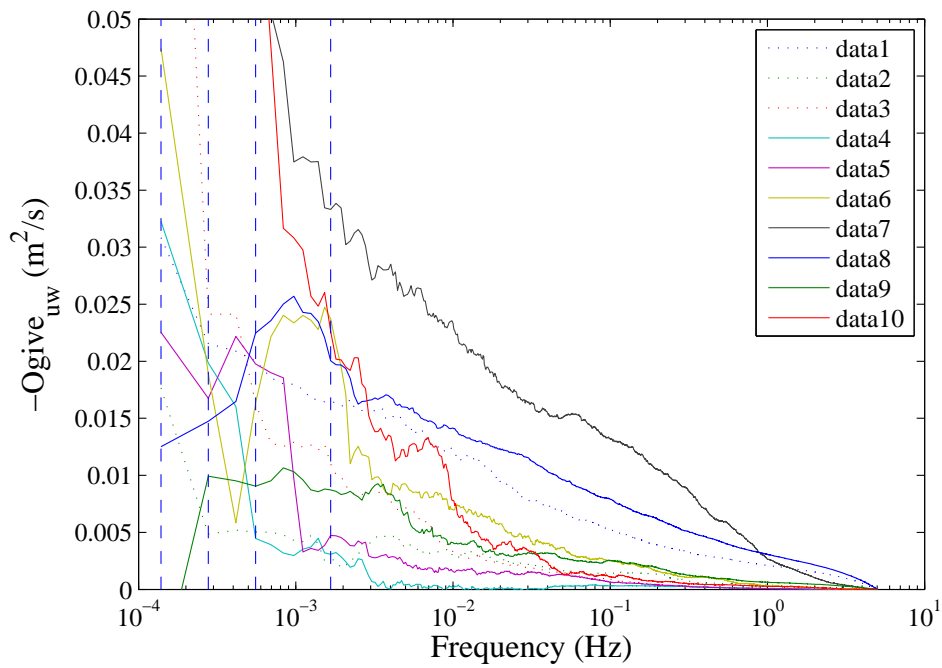


(b) Low wind speed cases

Fig 5.19 Normalized surface layer cospectral of uw . The bold red line represents the standard cospectra by Kaimal et al. (1972)

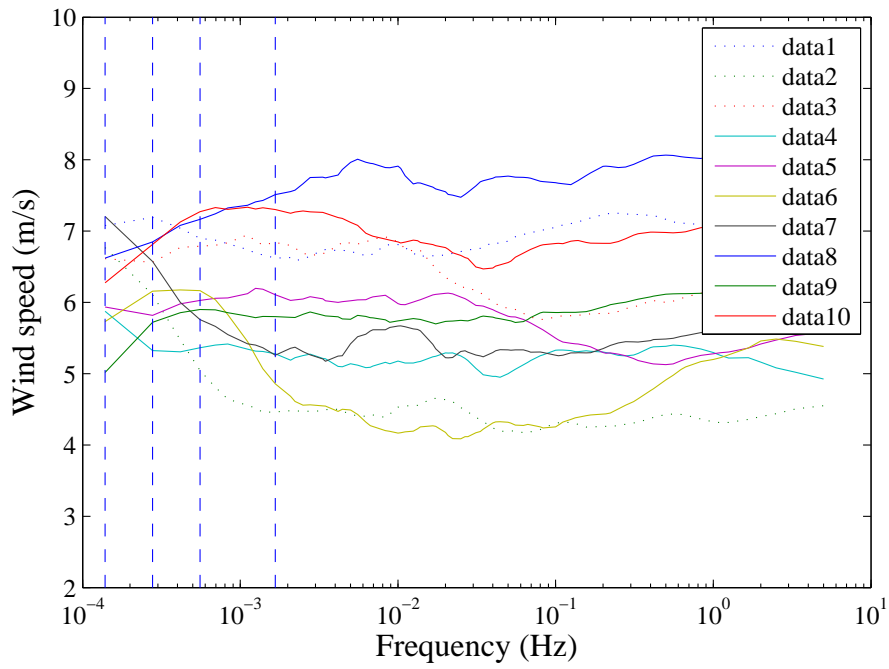


(a) High wind speed cases

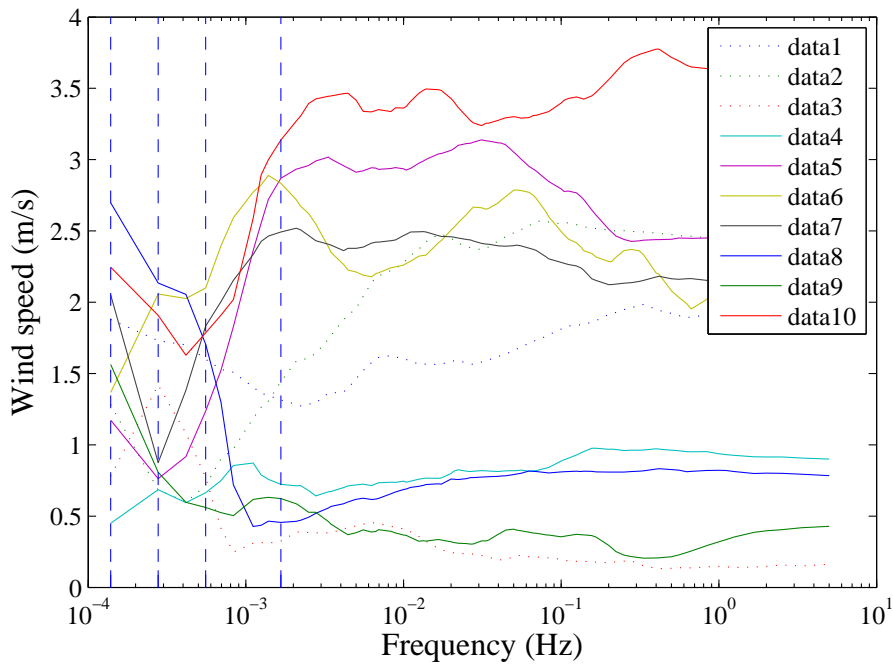


(b) Low wind speed cases

Fig 5.20 Ogives of momentum flux cospectral as a function of frequency. The dotted lines from right to left represents the time scale of 10-min, 30-min, 60-min and 120-min.

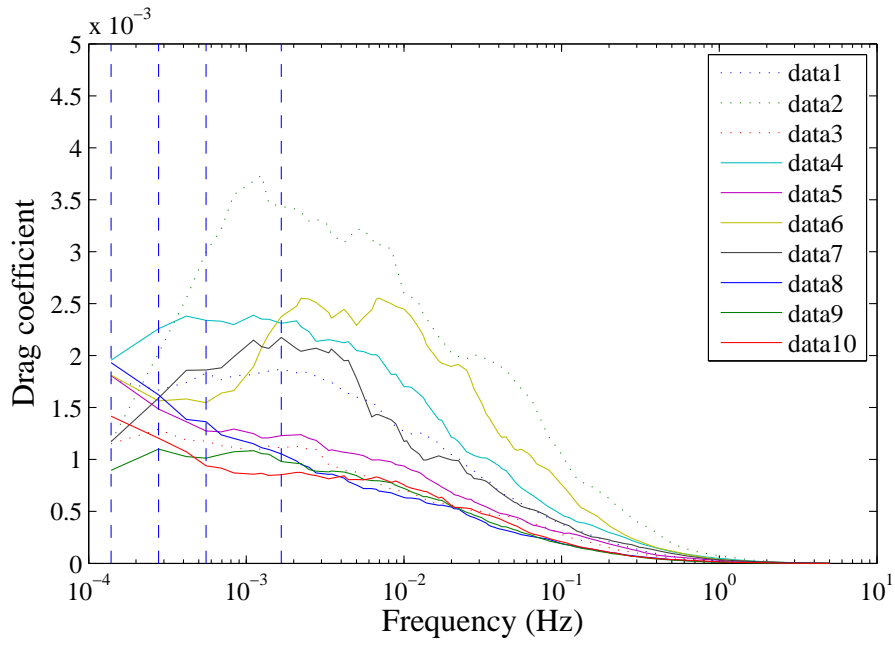


(a) High wind speed cases

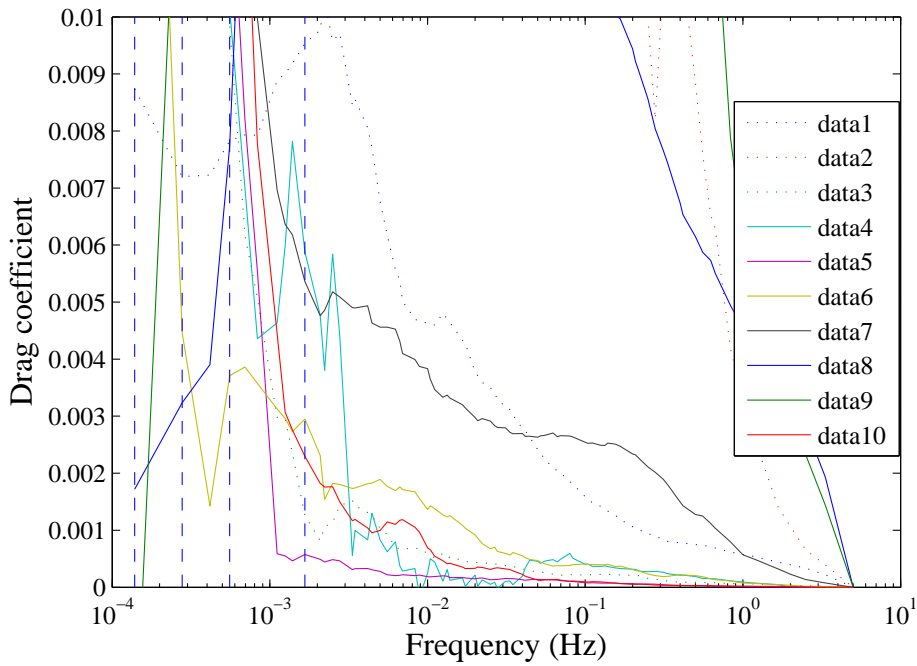


(b) Low wind speed cases

Fig 5.21 Mean wind speed as a function of frequency, the dotted lines from right to left represent the time scale of 10-min, 30-min, 60-min and 120-min.

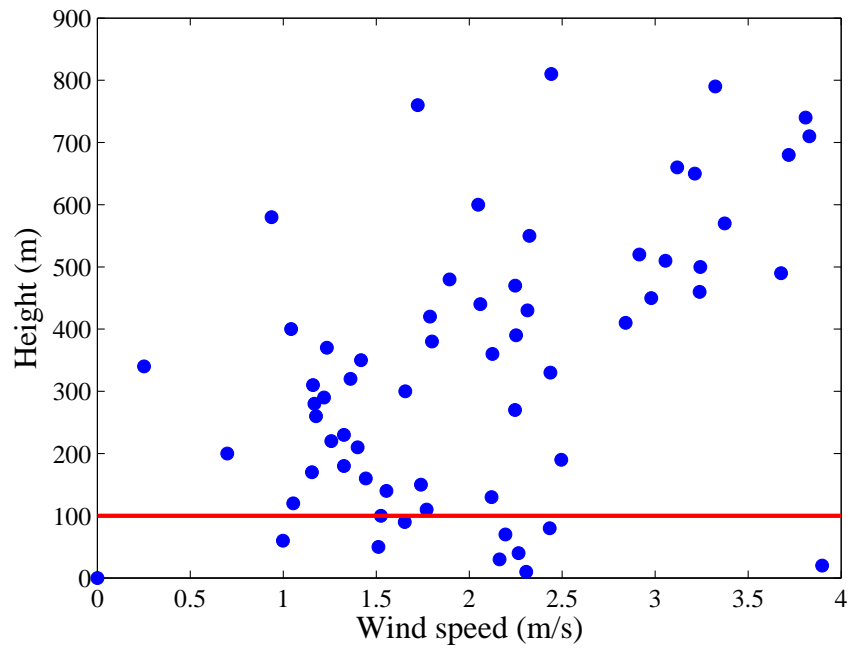


(a) High wind speed cases

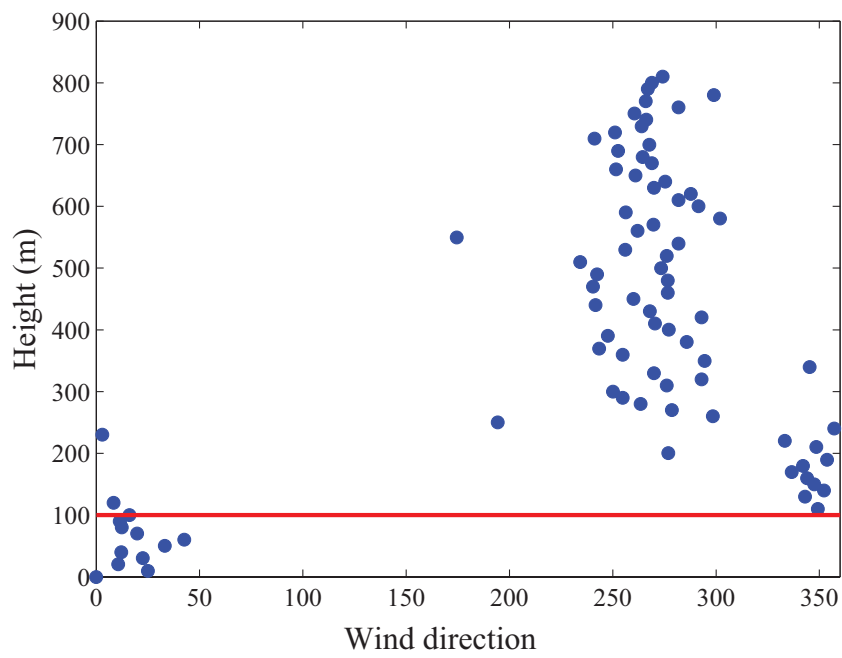


(b) Low wind speed cases

Fig 5.22 Drag coefficient estimated from the ogive and wind speed as a function of frequency, the dotted lines from right to left represent the time scale of 10-min, 30-min, 60-min and 120-min.



(a) The wind speed at different height



(b) The wind direction at different height

Fig 5.23 The pilot balloon observation. The red line represents the height of CBL depth.

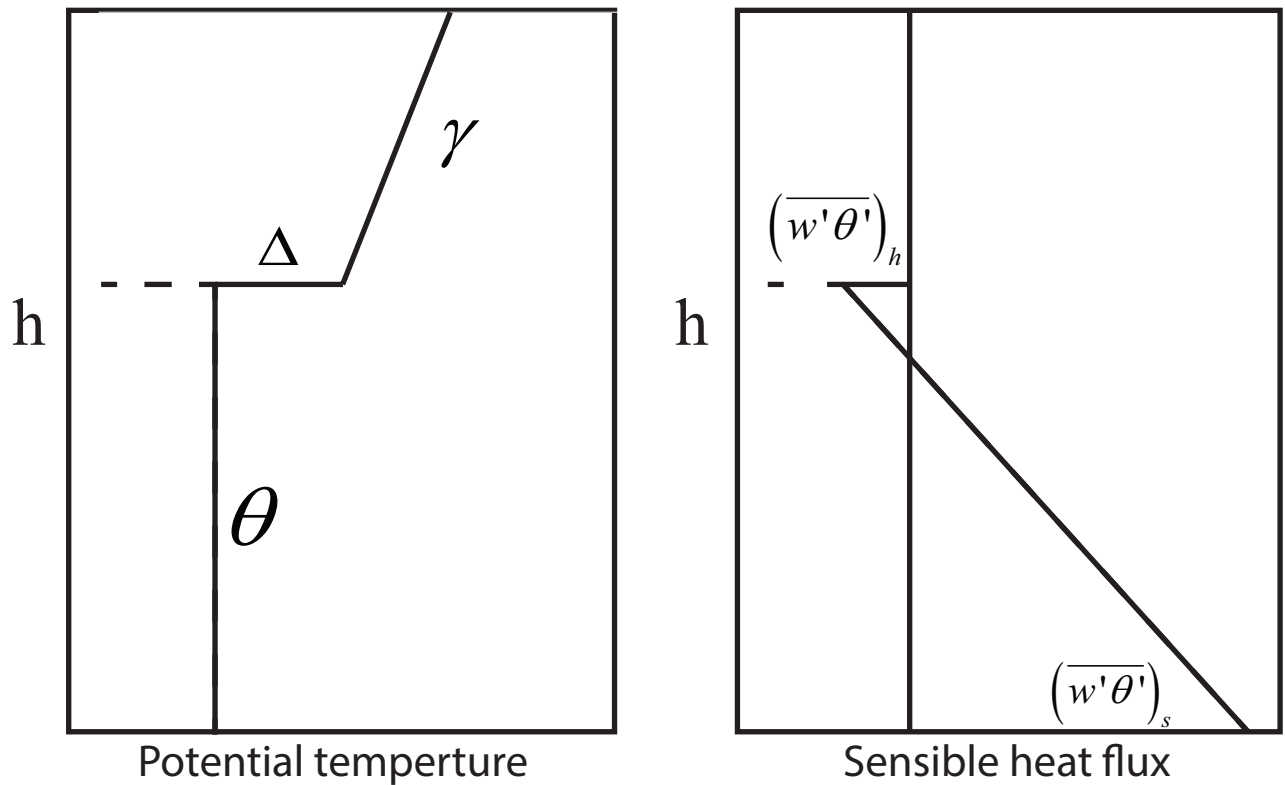


Fig 5.24 Schematic diagram of potential temperature and sensible heat flux profile in slab model. θ is temperature, $\overline{w'\theta'}$ is the sensible heat flux, the subscribe h and s represent convection height and land surface. γ is a constant value of dry adiabatic lapse rate.

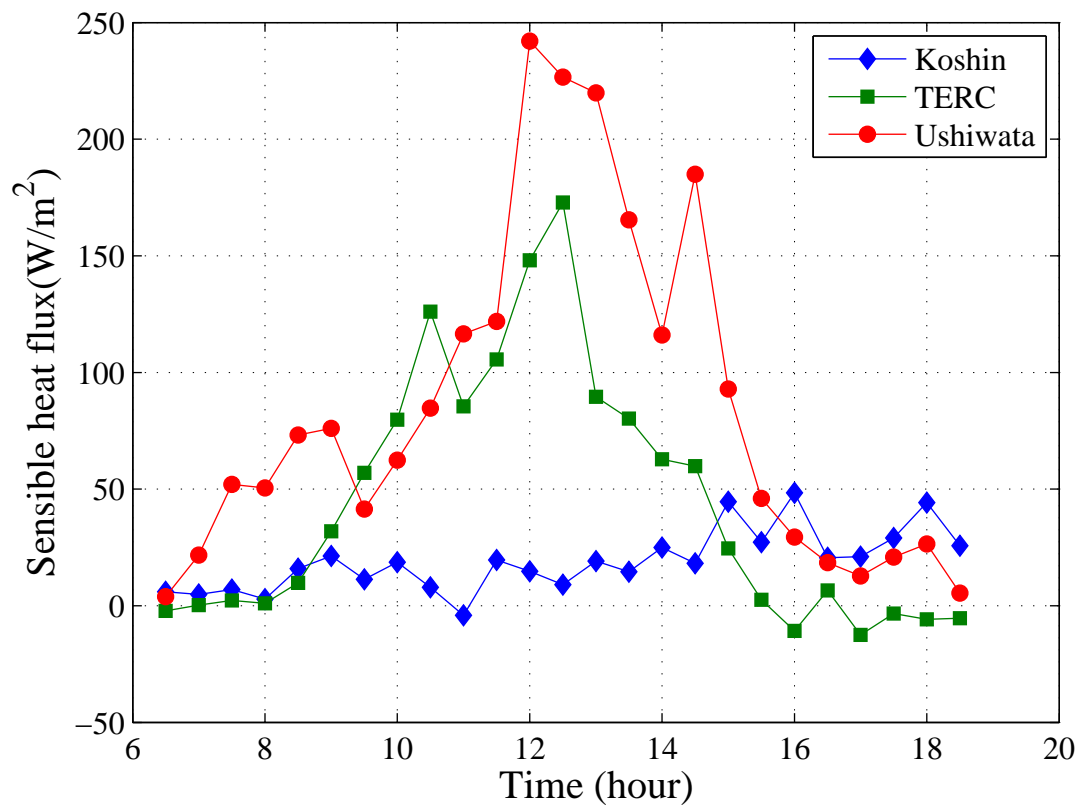


Fig 5.25 The sensible heat at Lake center (Koshin), Ushiwata and Terrestrial Environment Research Center (TERC) at 2011/08/26.

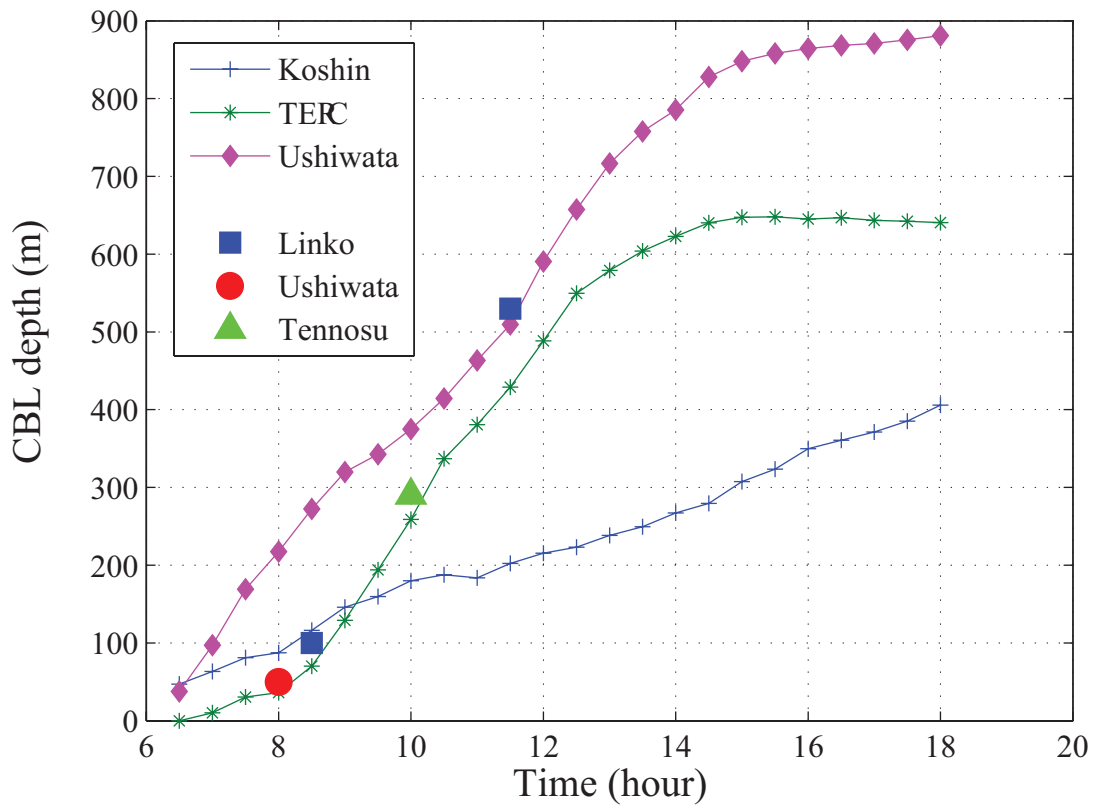


Fig 5.26 The CBL depth derived from different data sets (2011/08/26).

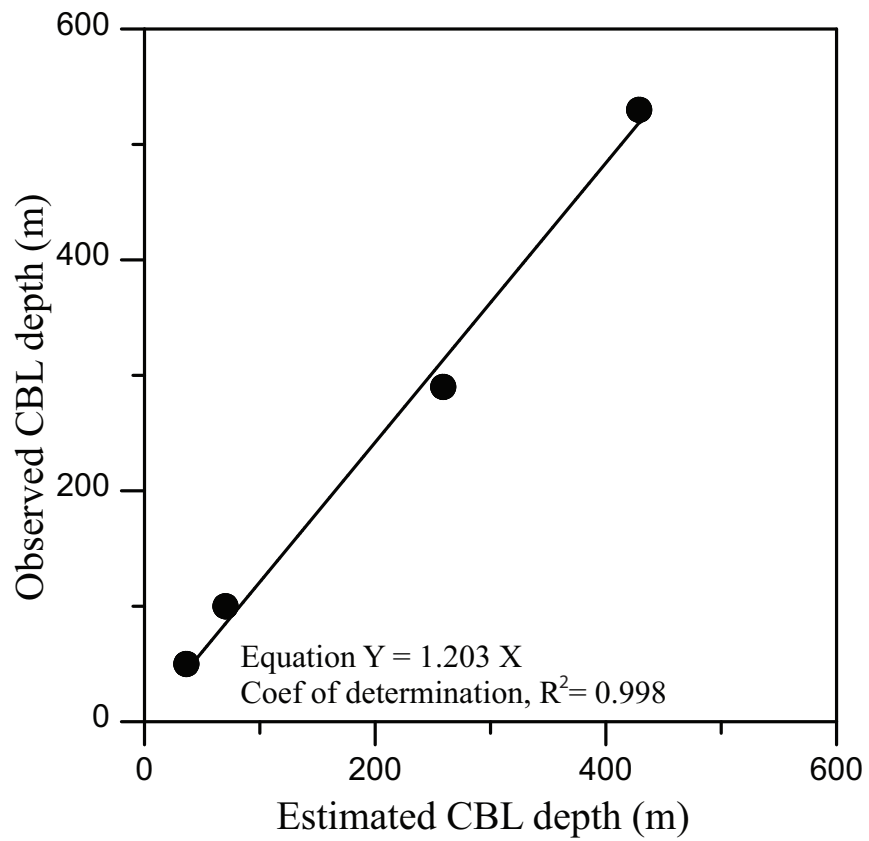


Fig 5.27 CBL depth estimated using Terrestrial Environment Research Center data in comparison with observation

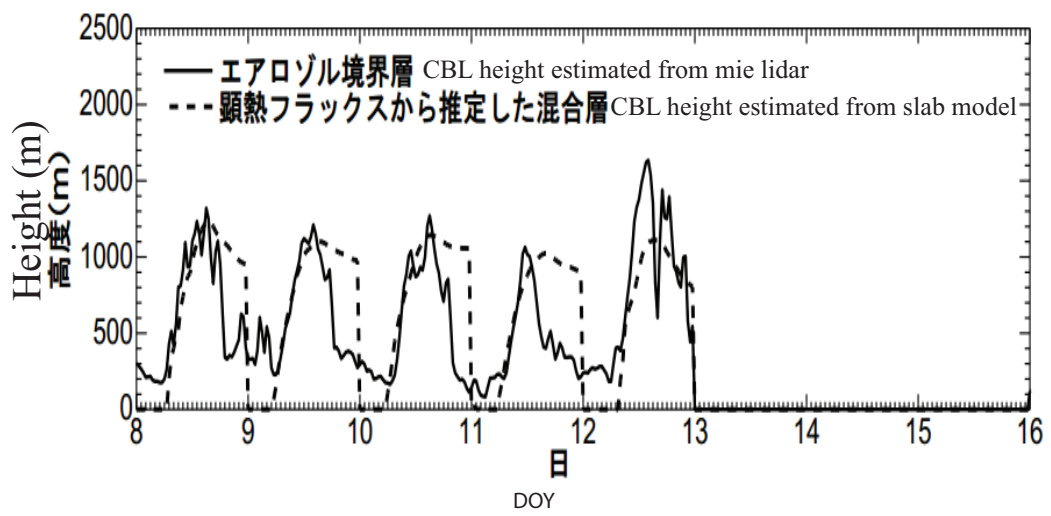


Fig 5.28 Comparison of CBL depth estimated from Mie lidar and slab model (Figure by Saotome (2009)). Dotted line represents the CBL depth derived from slab model, and solid line represents the CBL depth derived from Mie lidar

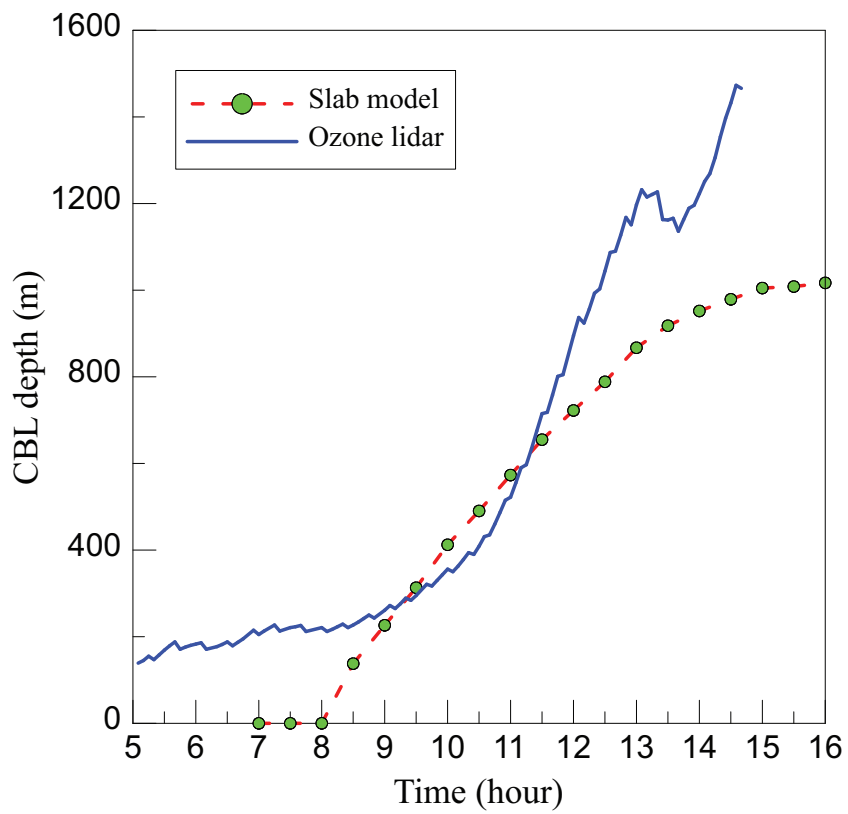


Fig 5.29 Comparison of CBL depth estimated from ozone lidar and slab model (2008/02/08)

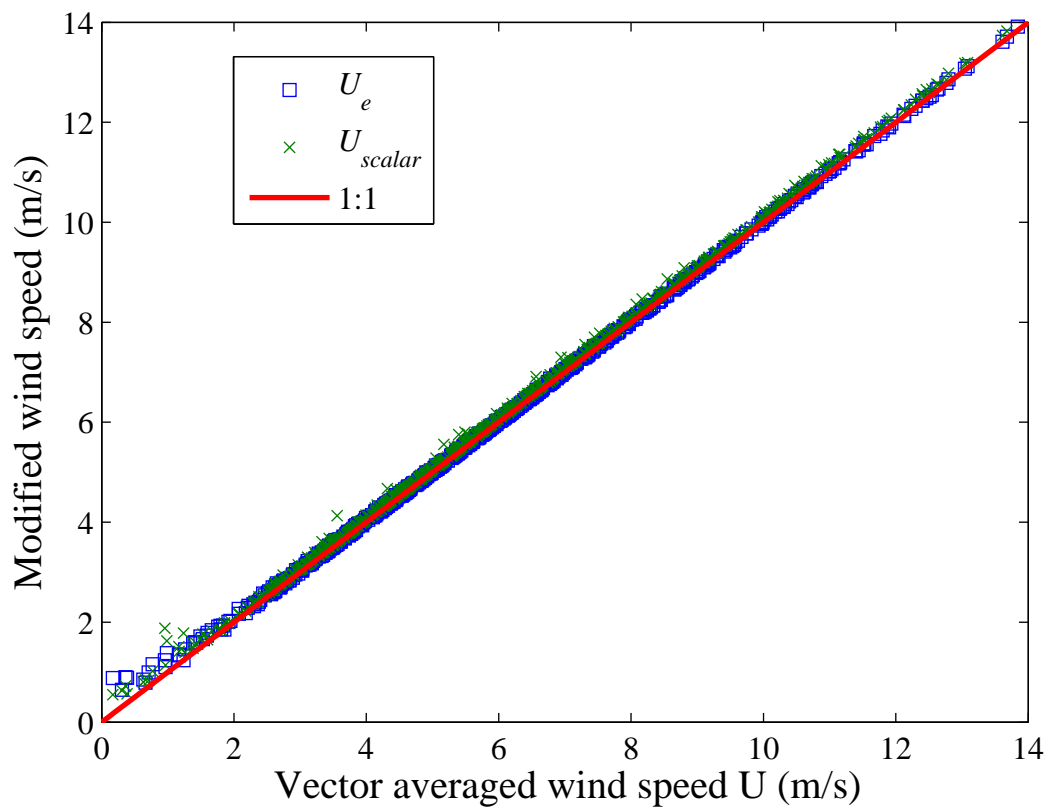


Fig 5.30 Scalar averaged wind speed U_{scalar} and effective wind speed U_e related to vector averaged wind speed U

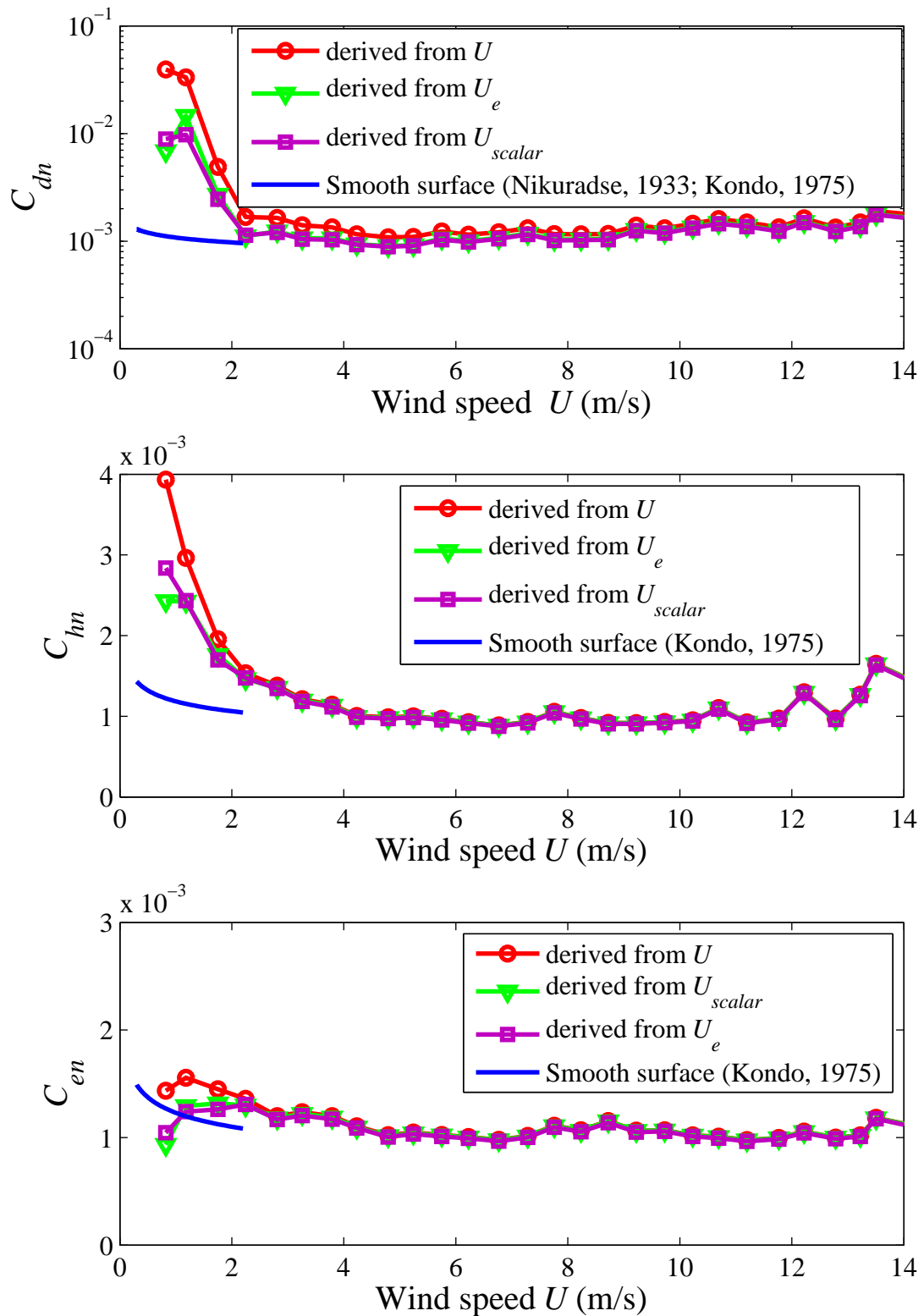


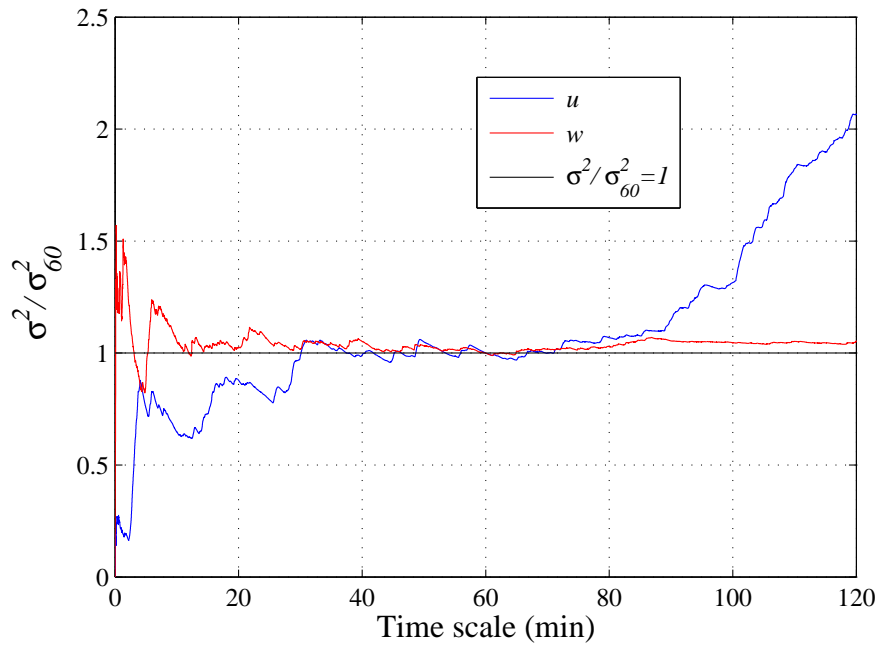
Fig 5.31 Bulk coefficients derived from vector averaged wind speed U , scalar averaged wind speed U_{scalar} and effective wind speed U_e .

Table 5.5 High wind speed cases for estimation of convective time scale (2h averaging period)

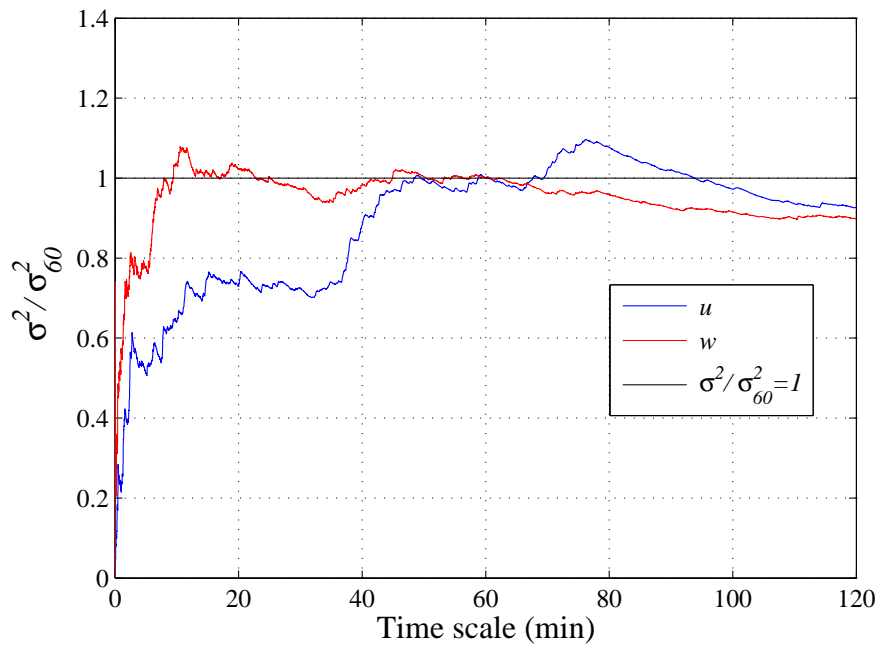
Data number	Date and time (JST)	z_i (m)	w_* (m/s)	t_* (min)
Data1	2008-01-01 08:00:00	254	1.0514	4.02
Data2	2008-11-22 09:00:00	695	1.8629	6.21
Data3	2009-09-18 12:00:00	424	1.1124	6.35
Data4	2009-12-18 08:00:00	320	1.6479	3.23
Data5	2010-02-17 07:30:00	334	1.2752	4.36
Data6	2010-12-25 08:30:00	355	1.8361	3.32
Data7	2008-05-08 05:30:00	95	1.4522	1.09
Data8	2008-05-16 06:00:00	332	1.0805	5.12
Data9	2008-12-13 07:30:00	179	1.0489	2.84
Data10	2009-03-30 06:30:00	405	1.2865	5.24

Table 5.6 Low wind speed cases for estimation of convective time scale (2h averaging period)

Data number	Date and time (JST)	z_i (m)	w_* (m/s)	t_* (min)
Data1	2008-06-01 10:30:00	942	0.8873	17.69
Data2	2008-07-27 12:00:00	574	1.3218	7.23
Data3	2008-08-07 09:00:00	765	1.4887	8.56
Data4	2008-09-13 08:00:00	424	0.8438	8.31
Data5	2008-09-25 09:30:00	289	1.2875	3.74
Data6	2009-02-19 10:30:00	818	1.7882	7.62
Data7	2009-03-27 12:00:00	1143	2.4149	7.88
Data8	2009-09-22 13:00:00	N/A	1.4083	N/A
Data9	2009-10-09 13:30:00	754	1.0712	11.73
Data10	2010-01-16 14:00:00	914	1.7732	8.59

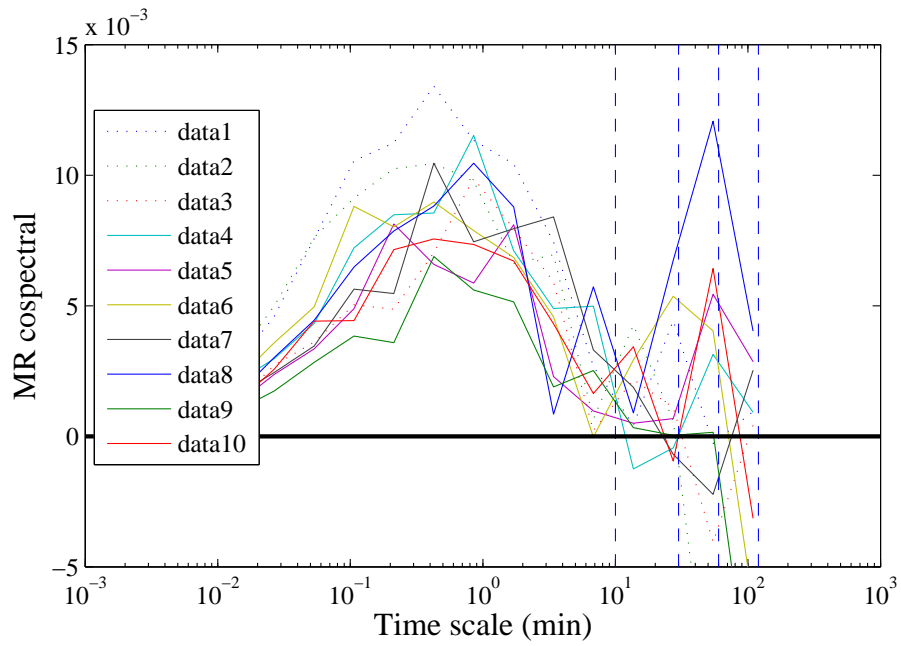


(a) High wind speed cases

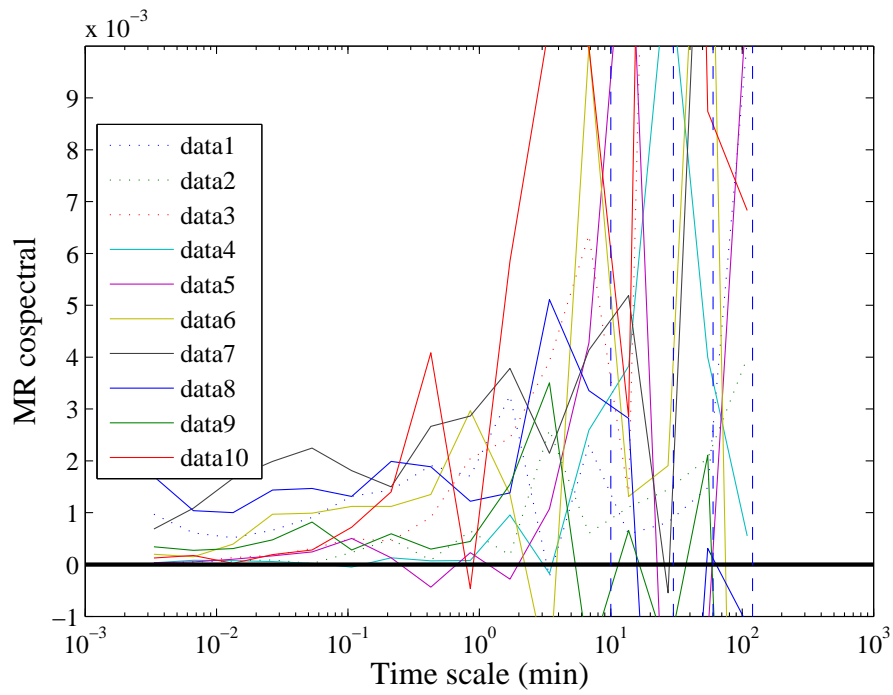


(b) Low wind speed cases

Fig 5.32 Normalized variance versus time scale using a averaging time of $T=120$ min, the black line indicates $\sigma^2/\sigma_{60}^2 = 1$



(a) High wind speed cases



(b) Low wind speed cases

Fig 5.33 Multiresolution decomposition of the momentum flux as a function of the averaging time scale.

Table 5.7 Trend condition for high wind speed cases

Data number	Date and time (JST)	Z	<i>Trend</i>
Data1	2008-01-01 08:00:00	19.6786	+
Data2	2008-11-22 09:00:00	143.0825	+
Data3	2009-09-18 12:00:00	5.8302	+
Data4	2009-12-18 08:00:00	187.8112	+
Data5	2010-02-17 07:30:00	66.4436	+
Data6	2010-12-25 08:30:00	-92.1405	-
Data7	2008-05-08 05:30:00	191.3615	+
Data8	2008-05-16 06:00:00	-112.8270	-
Data9	2008-12-13 07:30:00	-252.5632	-
Data10	2009-03-30 06:30:00	-164.8446	-

Table 5.8 Trend condition for low wind speed cases

Data number	Date and time (JST)	Z	<i>Trend</i>
Data1	2008-06-01 10:30:00	169.6436	+
Data2	2008-07-27 12:00:00	210.7358	+
Data3	2008-08-07 09:00:00	-116.3172	-
Data4	2008-09-13 08:00:00	-110.5695	-
Data5	2008-09-25 09:30:00	163.1658	+
Data6	2009-02-19 10:30:00	-165.5500	+
Data7	2009-03-27 12:00:00	298.3690	+
Data8	2009-09-22 13:00:00	171.2786	+
Data9	2009-10-09 13:30:00	198.1467	+
Data10	2010-01-16 14:00:00	126.9701	+

Table 5.9 Various definitions of time scale for high wind speed cases (min)

Data number	Date and time (JST)	t_*	t_c	t_{MR}	\tilde{t}
Data1	2008-01-01 08:00:00	4.02	30	54.61	50
Data2	2008-11-22 09:00:00	6.21	30	27.31	N
Data3	2009-09-18 12:00:00	6.35	30	6.83	55
Data4	2009-12-18 08:00:00	3.23	N	27.31	N
Data5	2010-02-17 07:30:00	4.36	10	13.65	55
Data6	2010-12-25 08:30:00	3.32	60	6.83	N
Data7	2008-05-08 05:30:00	1.09	N	27.31	N
Data8	2008-05-16 06:00:00	5.12	N	3.41	N
Data9	2008-12-13 07:30:00	2.84	30	27.31	55
Data10	2009-03-30 06:30:00	5.24	60	27.31	60

Table 5.10 Various definitions of time scale for low wind speed cases (min)

Data number	Date and time (JST)	t_*	t_c	t_{MR}	\tilde{t}
Data1	2008-06-01 10:30:00	17.69	<i>N</i>	<i>N</i>	50
Data2	2008-07-27 12:00:00	7.23	<i>N</i>	<i>N</i>	<i>N</i>
Data3	2008-08-07 09:00:00	8.56	<i>N</i>	<i>N</i>	<i>N</i>
Data4	2008-09-13 08:00:00	8.31	<i>N</i>	<i>N</i>	<i>N</i>
Data5	2008-09-25 09:30:00	3.74	<i>N</i>	<i>N</i>	<i>N</i>
Data6	2009-02-19 10:30:00	7.62	<i>N</i>	<i>N</i>	45
Data7	2009-03-27 12:00:00	7.88	<i>N</i>	<i>N</i>	<i>N</i>
Data8	2009-09-22 13:00:00	<i>N</i>	<i>N</i>	<i>N</i>	<i>N</i>
Data9	2009-10-09 13:30:00	11.73	<i>N</i>	<i>N</i>	<i>N</i>
Data10	2010-01-16 14:00:00	8.59	<i>N</i>	<i>N</i>	<i>N</i>

6 Application: estimation of Surface Heat Fluxes over Kasumigaura combining bulk transfer methods and eddy correlation method

Variations in lake evaporation have a significant impact on the energy and water budgets of lakes. Understanding these variations and the role of climate is important for water resource management as well as predicting future changes in lake hydrology as a result of climate change (Lenters et al. 2004). In this chapter, the energy variation and evaporation were estimated to give a general hydrological characteristics of lake Kasumigaura.

6.1 Fluxes and evaporation estimation over lake surface

Solar radiation is one of the most important variables that influence the climate and environment in our life. Fig.6.1 showed the daily variation of the radiation budget. In this figure, S_u , S_d , L_u and L_d represented upward shortwave radiation, downward shortwave radiation, upward longwave radiation and downward longwave radiation, respectively. The net radiation is estimated from

$$Rn = S_d - S_u + L_d - L_u \quad (6.1)$$

The radiation energy is absorbed and convert to different energy types: sensible heat, latent heat and the storage term in water. The heat energy fluxes are estimated as follows

$$H = C_t \rho_a \overline{w' t'} \quad (6.2)$$

$$LE = L_e \overline{w' \rho'_v} \quad (6.3)$$

The storage term Q is estimated from

$$Q = Rn - H - LE \quad (6.4)$$

where

$$C_t = 1005(1 - 0.84)q \quad (6.5)$$

$$L_e = 3151 - 2.38(T + 273.15) \quad (6.6)$$

The evaporation over water surface is given by

$$E = \frac{\overline{w' \rho_v'}}{\rho_w} \Delta t \quad (6.7)$$

where Δt is the observations interval (1800 second in here)

6.2 Daily variation

Rn and S_d shown clear diurnal cycles both in summer and winter day indicated that Rn was mainly decided by S_d . S_u is almost close to 0 whether summer or winter day indicates that most of energy were absorbed by the water body (short wave albedo of water is about 0.07 (Budyko, 1974)). About 300 W/m² difference of net radiation was found between the summer and winter. Daily temperature variation were also illustrated in Fig.6.3, minimum and maximum showed at nighttime and noontime, respectively. For most of the time, T_s which was shown larger value than T_a indicated the water surface was warmer than the air and resulted an unstable atmosphere.

The diurnal heat balance was implied in Fig.6.2. The latent heat flux and sensible heat were always positive, and latent heat showed a diurnal variation and much larger than the sensible heat flux in summer. In winter, both sensible and latent flux were quite small and did not show apparent diurnal cycles. Q showed a similar variation with Rn . It is quite important in our study since the latent and sensible heat fluxes are representing minor part of Rn . One complexity of water bodies comes from the fact that the thermal capacity of water is much higher than that of many other materials such as soil, a much greater quantity of energy can thus be stored in water bodies than in soils. The energy budget of lakes and the consequent evaporation patterns was impacted by this characteristic. It is very different from ground surfaces where the storage term is small and often neglected. Some studies based on the energy budget (e.g. Priestley and Taylor, 1972; Rosenberry et al., 2007) and assume the $Q = 0$ would produce a significant error in estimation heat fluxes or evaporation in similar atmospheric condition. In addition, the vertical profile of water temperature was measured each month (Fig.6.4), the measurement indicated that the water in different depth was well mixture, a temperature gradient was not found during all the year. This well mixture of water resulted in more energy absorbed.

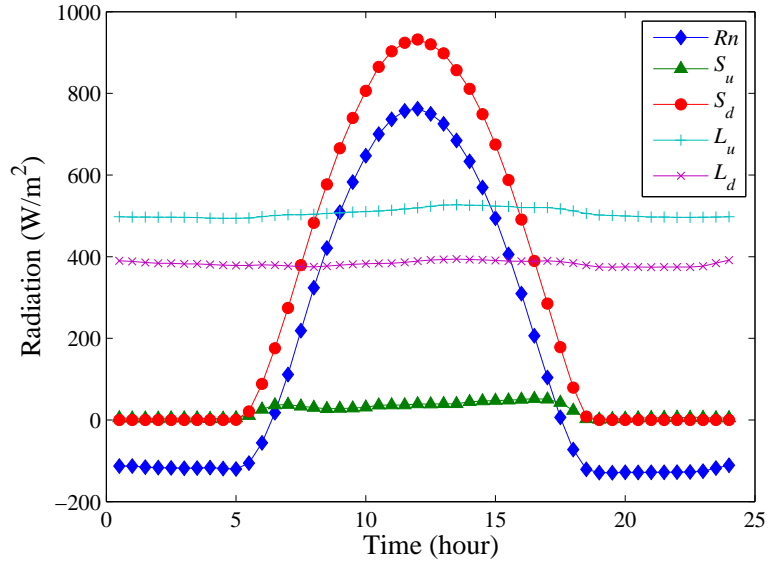
6.3 Long term variation

The monthly variation of temperature in Lake Kasumigaura center was plotted in Fig.6.5. The minimum and maximum, in August to February of both water surface temperature and air

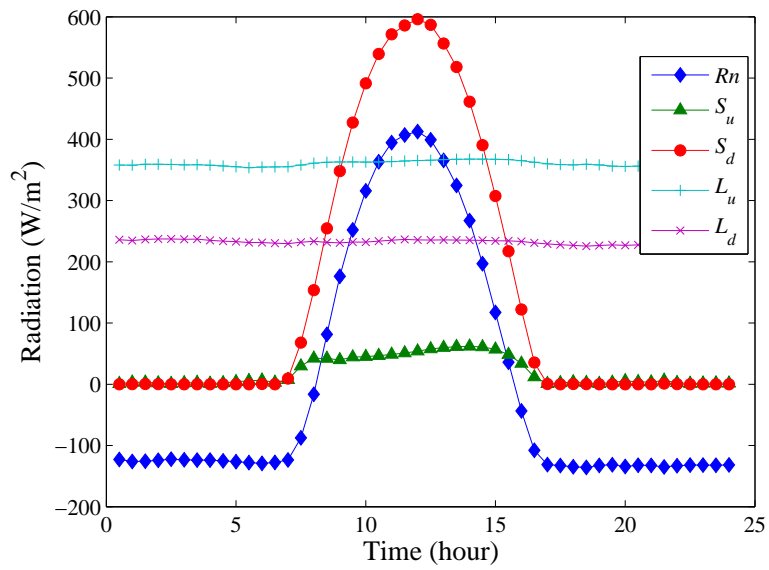
temperature and water temperature, which were similar with R_n . The temperature difference between the air and water surface was very small and resulted in relatively small sensible heat.

Monthly sum heat fluxes were illustrated in Fig.6.6. Similar to the daily change, the sensible heat and latent heat were always positive. A seasonal variation of latent heat was found similar to the R_n . But sensible heat tended to keep a constant value and was quite small compare to latent heat. A constant value of dt through all the year might response to the stable value of sensible heat. Furthermore, this difference also indicated Bowen ratio over lake surface is quite smaller than 1.

Daily averaged annual radiation, precipitation, evaporation and water level were plotted in Fig.6.7, Fig.6.8 and Fig.6.9. The water level was not change through the years about 1.3m on average. The annual amount of rainfall was about 929mm, 996mm and 1112mm. 721mm, 781mm and 813mm were found for evaporation, respectively.

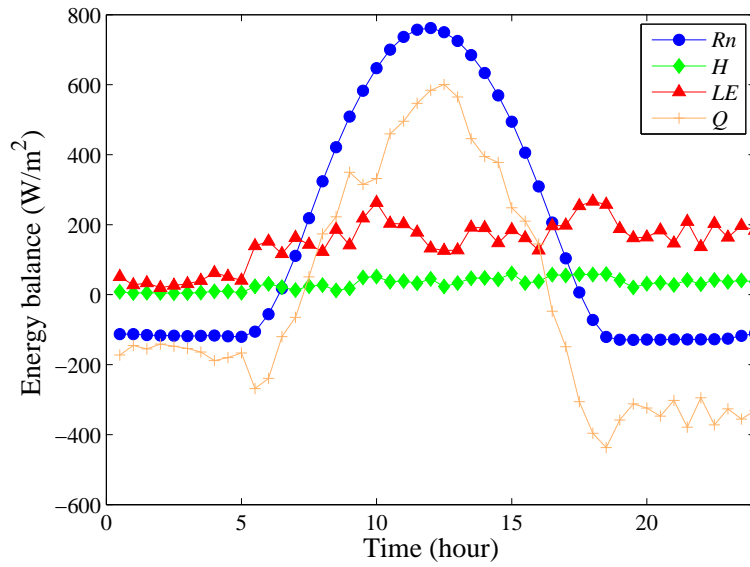


(a) Summer (2009/08/15)

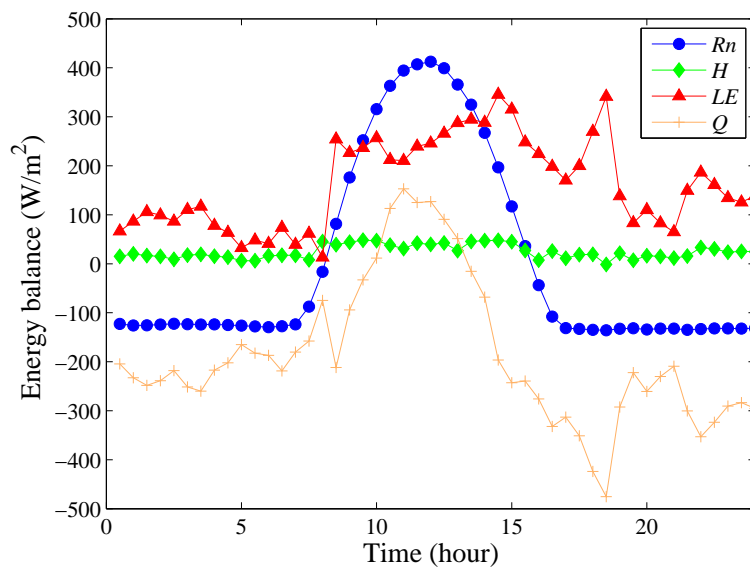


(b) Winter (2009/01/15)

Fig 6.1 Daily variation of radiation in summer and winter

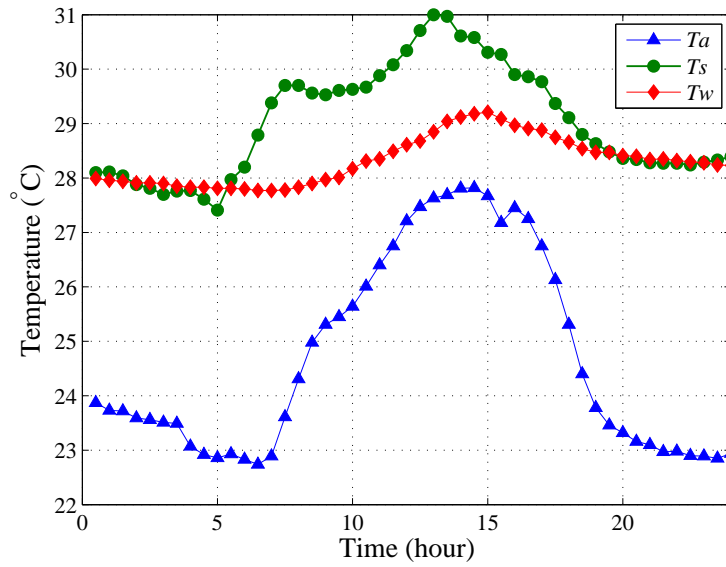


(a) Summer (2009/08/15)

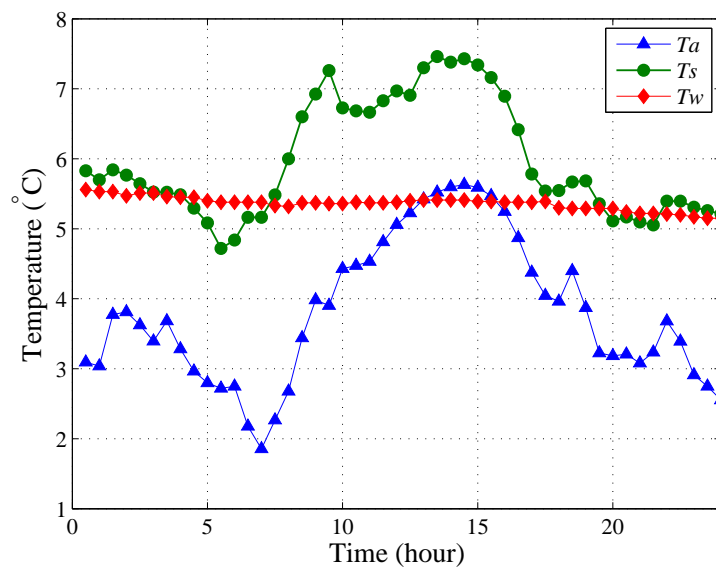


(b) Winter (2009/01/15)

Fig 6.2 Daily variation of energy in summer and winter



(a) Summer (2009/08/15)



(b) Winter (2009/01/15)

Fig 6.3 Daily variation of vertical temperature in summer and winter

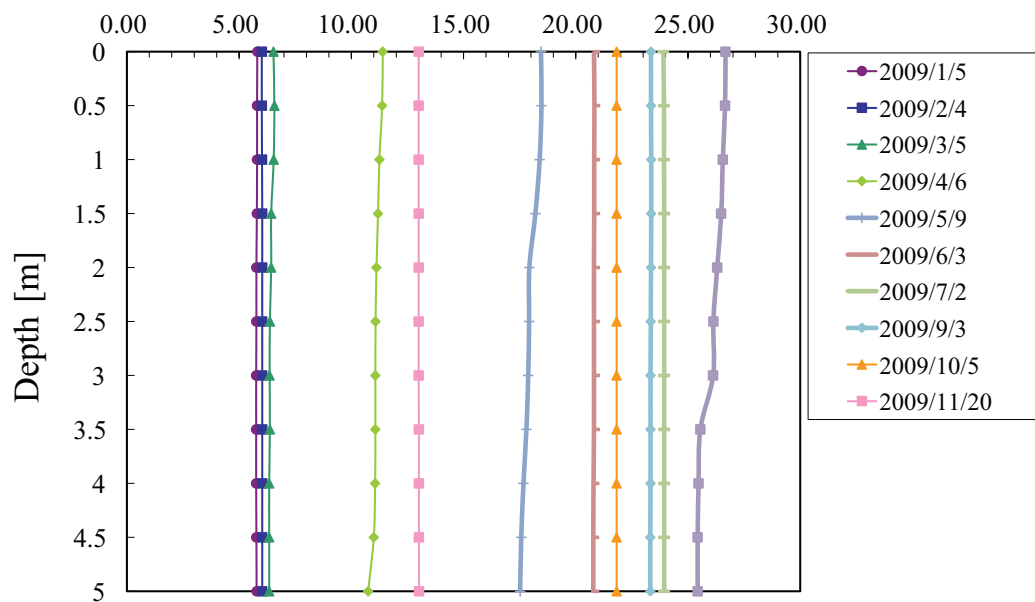


Fig 6.4 Monthly measured water temperature in variation water depth

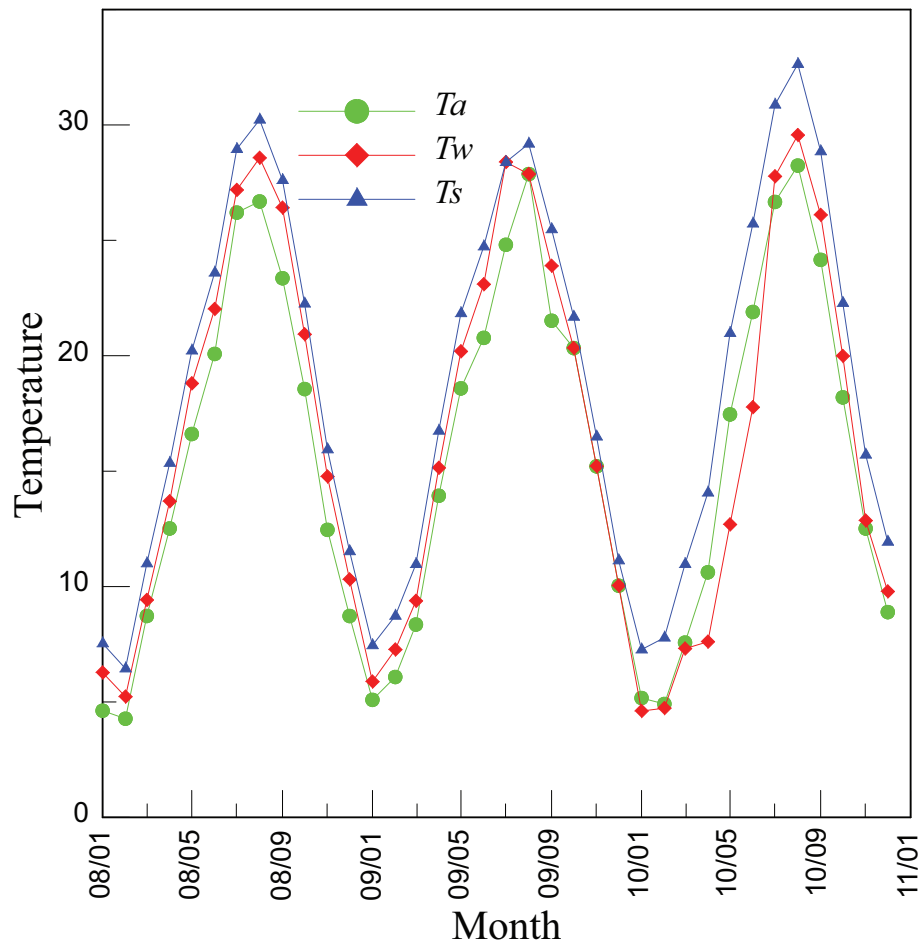


Fig 6.5 Monthly averaged temperature in air, water surface and 1.0 m water depth

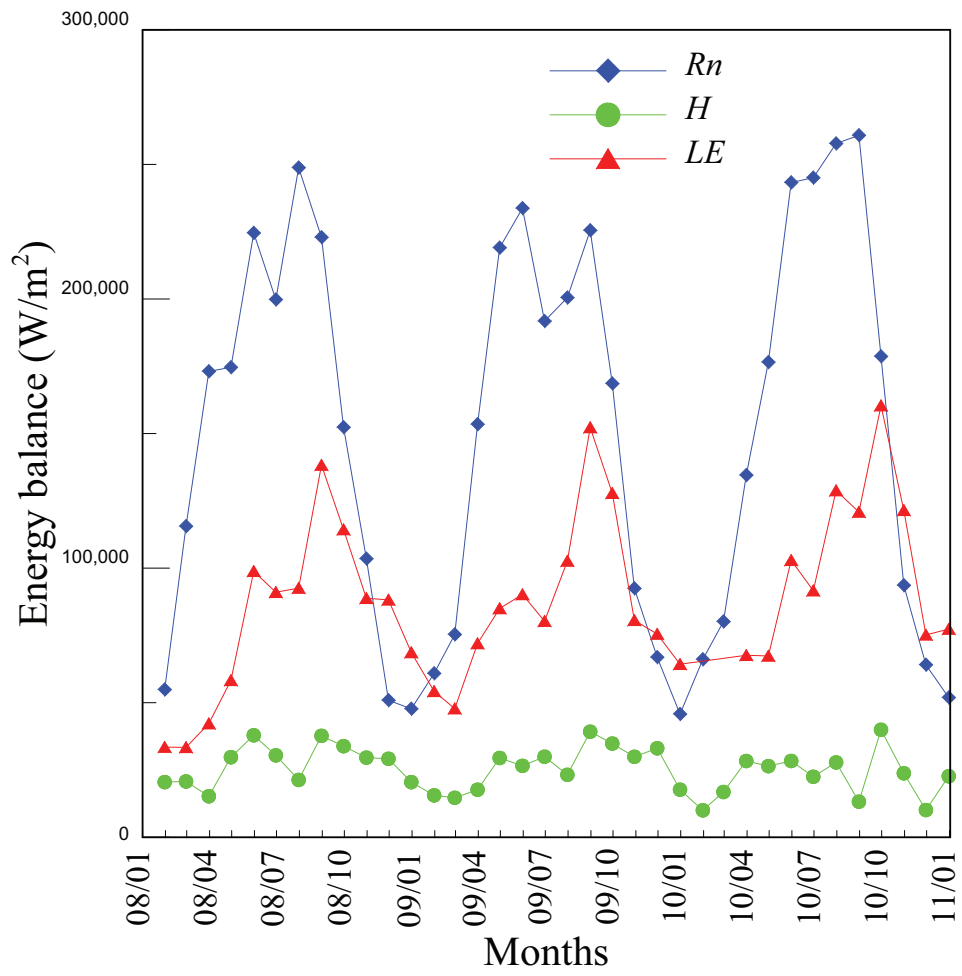


Fig 6.6 Monthly sum of energy balance over lake surface during 2008-2010

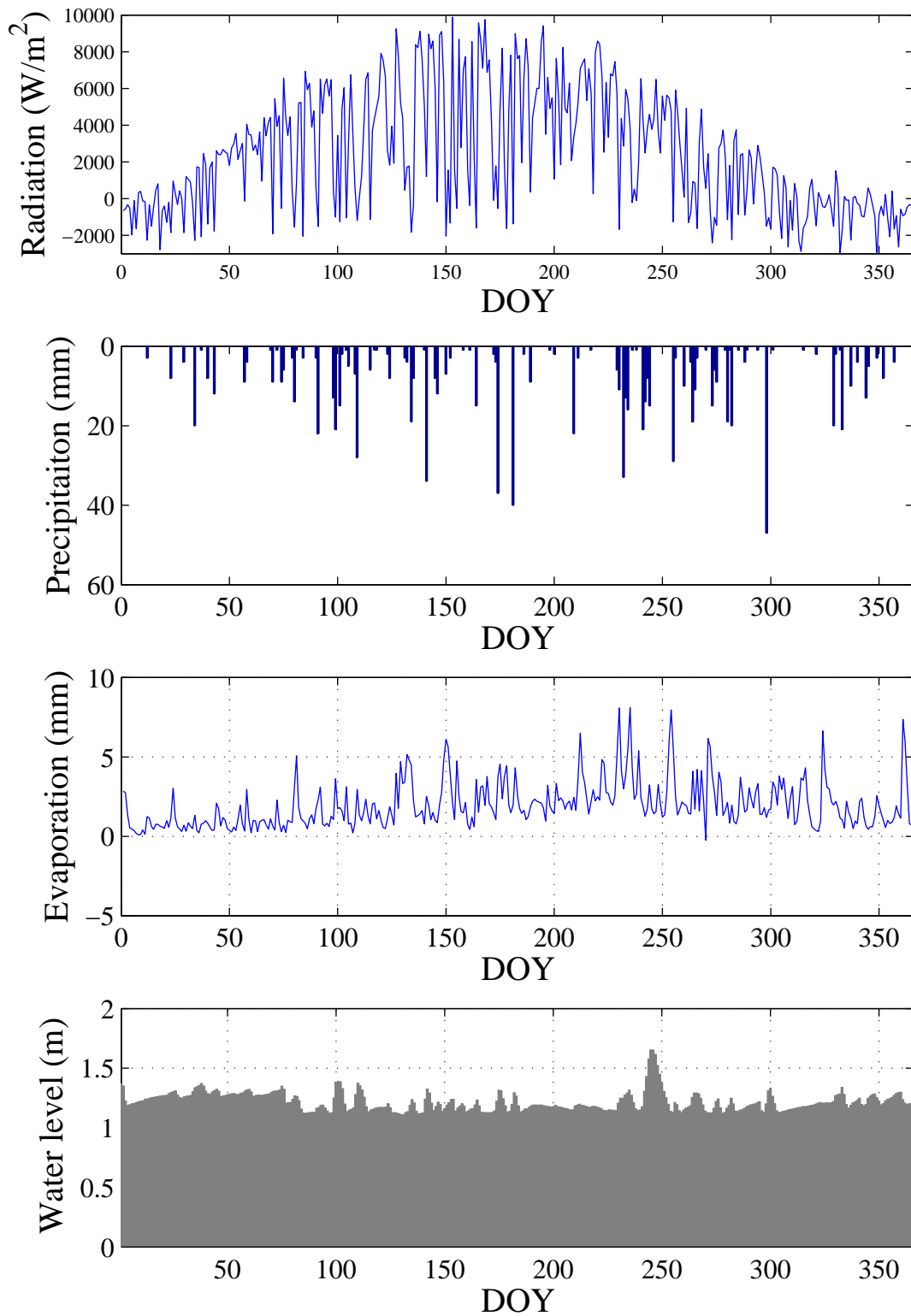


Fig 6.7 Daily sum of net radiation, precipitation, evaporation and daily averaged water level:

2008

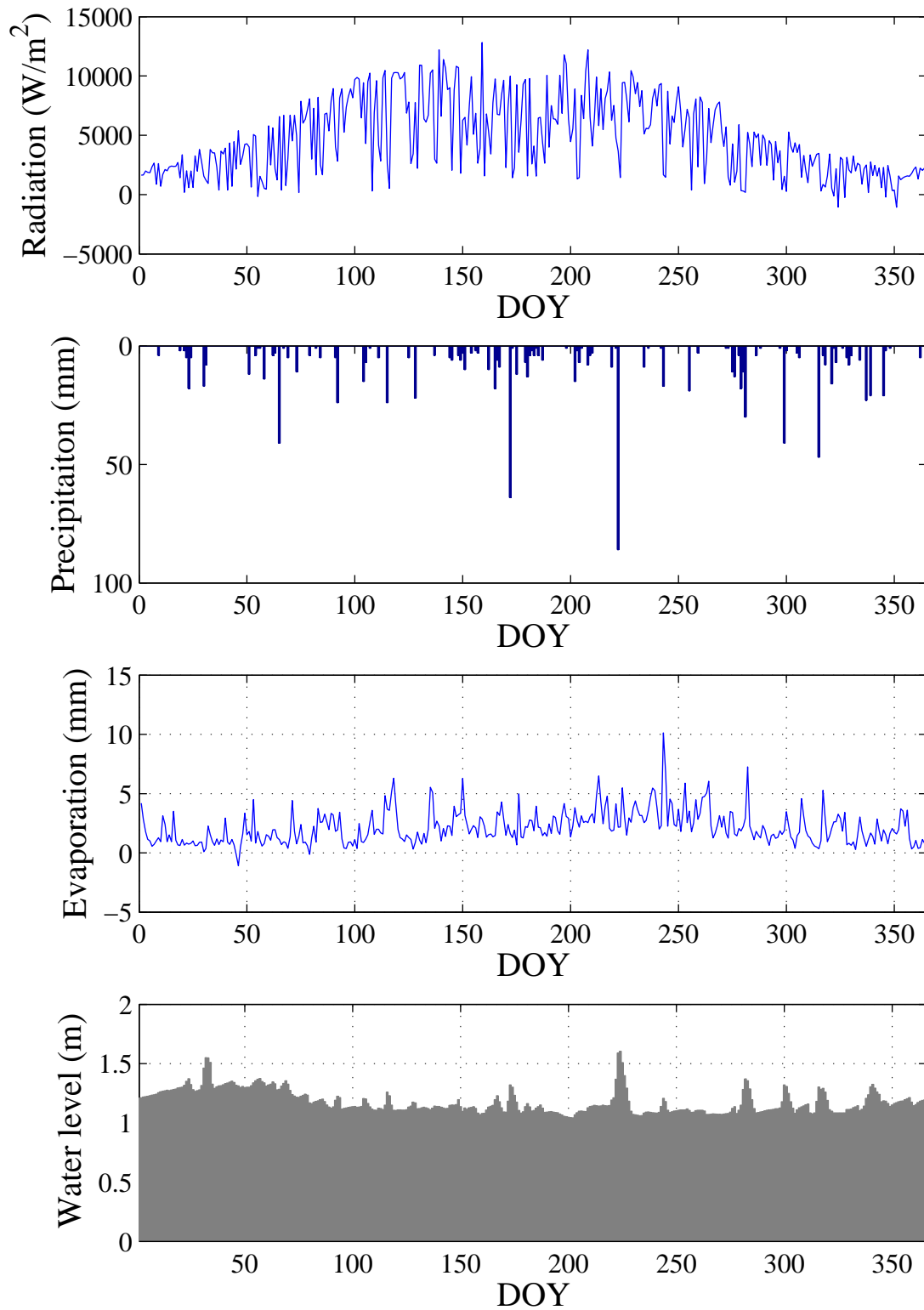


Fig 6.8 Daily sum of net radiation, precipitation, evaporation and daily averaged water level:

2009

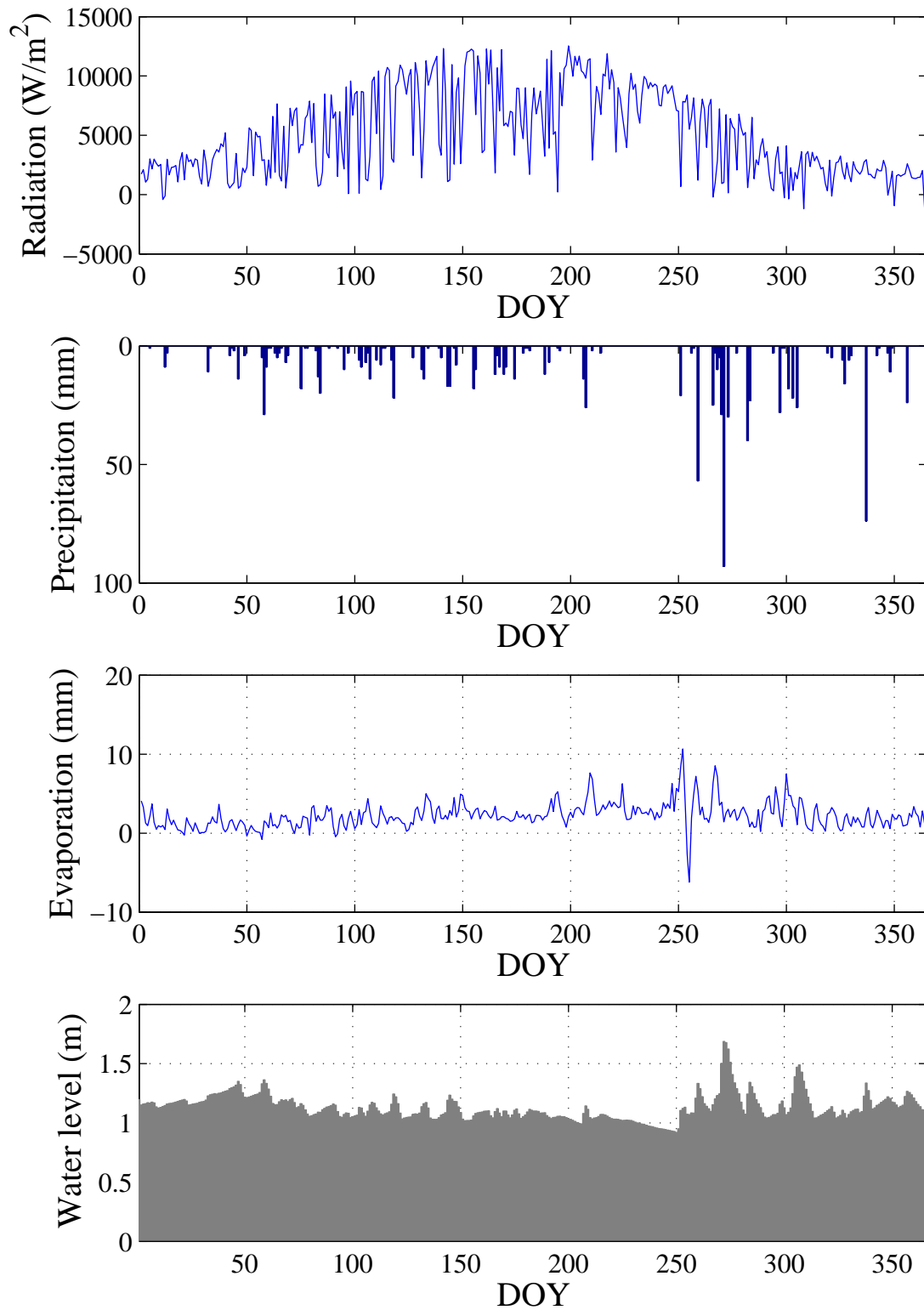


Fig 6.9 Daily sum of net radiation, precipitation, evaporation and daily averaged water level:

2010

7 Conclusions

This study investigated the exchanges of water vapor, heat and momentum over a lake. The bulk coefficients were estimated under pure locally generated turbulence condition. Under weak wind speed region, the characteristics of the bulk transfer coefficients of momentum C_{dn} and of water vapor and heat have been studied with emphasis on the possible influence of the large-scale convection to surface fluxes. Increase of C_{dn} when mean wind speed U becomes smaller in the range of $u < 4$ m/s was found. By applying the cospectral and ogive analysis, a possible of this increase was the influence of convective circulation, as manifested by the mismatch of characteristic time scale of the flux (2nd moment) and mean wind speed (1st moment). Possible solutions to this the mismatch of time scale under weak wind speed was studied which include adaptation of the effective wind speed U_e instead of the traditional vector-averaged mean wind speed. However, complete solution is not likely available since this problem arises from ill-defined nature of C_{dn} under light wind condition. It was also focused on the wave's influence on the momentum flux over lake surface. Fluxes at 10-m is only controlled by the locally generate turbulence. The wave information is not necessary in estimating fluxes at 10-m over lake surface. In detail, it was concluded as the followings.

Chapter 1 aimed to introduce the interaction among lake-land-atmosphere. We pointed out the importance of turbulence in the exchanges. We explained the reasons why the bulk transfer method is selected, and what we need to pay attention when using this method. In this chapter, the main results of the previous studies were summarized and future perspectives were mentioned.

In chapter 2, we described the study site, introduced the hydrology and meteorology condition of the study area. A detail list of observation items was outlined. The wave information, fluxes and atmospheric condition data have been collected since July 2007; Pilot balloon observation was done to understand the CBL depth more clearly.

In chapter 3, we introduced the eddy correlation method and bulk transfer method. The bulk coefficients were calculated from the eddy correlation data. Several data quality tests were investigated to give a more reliable dataset.

By applying stationarity test and integral turbulence characteristic test, the bulk coefficients were calculated and found in agreement with previous studies in chapter 4. For momentum, the drag coefficient increased with increasing wind speed ($C_{dn} = (0.0767U + 0.6931)/1000U^2$). On the contrary, the temperature and moisture bulk coefficient showed a constant value of 0.0011 which is independent on the wind speed. The impact of stability was also focused on. Over water surface, the heat fluxes were relatively small, z/L or Ri was almost dominated by the friction velocity or wind speed and resulted in a slight unstable atmospheric condition for most of the time. The stability was shown limited effect on bulk coefficients in our data set. Therefore, neglecting the stability effect and assuming a smooth surface under weak wind speed (since the measurement may be influenced by the large scale convection and/or water surface state, we did not have any reliable data), the bulk transfer methods related to local generated turbulence were given by

$$\overline{u'w'} = \begin{cases} 1.08U^2/1000U^2 & U < 2.2m/s \\ (0.0767U + 0.6931)/1000U^2 & U \geq 2.2m/s \end{cases} \quad (7.1)$$

$$\overline{w't'} = \begin{cases} 1.185U^{-0.15}/1000U dt & U < 2.2m/s \\ 1.1/1000U dt & U \geq 2.2m/s \end{cases} \quad (7.2)$$

$$\overline{u'w'} = \begin{cases} 1.185U^{-0.15}/1000U dt & U < 2.2m/s \\ 1.1/1000U dt & U \geq 2.2m/s \end{cases} \quad (7.3)$$

The remained issue was about temperature bulk coefficient increased with increasing wind speed when $U > 9$ m. The possible causes about this issue were discussed. The probable error analysis showed huge error when $U > 9$. We pointed out the water surface temperature and air temperature measurement error could be occurred due to several physical causes (spray, downward longwave radiation and patches of foam). Recent study showed flux measurement error is also a potential cause. Hence, it is unable to identify the precise reason. More accurate measurements of temperature appear to be necessary.

Chapter 5 contained a review of research on lake current concerning both experimental and modelling study. Lake current related to bulk transfer method was introduced. The measurement showed that the lake current was mainly derived from wind speed and quite small. The lake surface current is two orders of magnitude smaller than that of the wind speed. Since the lake current is small and negligible in bulk transfer method, it could not be used to explain that the drag coefficient increased with decreasing wind speed under weak wind speed region ($U < 2$ m/s).

In chapter 5, bulk transfer method related to large-scale convection was investigated. The higher value of C_{dn} was found at higher radiation and lower wind speed condition which indicated strong unstable condition. The convection circulation which is playing a very important role under such condition was verified by the cospectral and ogive analysis. For high wind speed cases, the result of cospectral showed similar curve with the standard cospectral well. For weak wind speed, an obvious peak was not found. This indicated that the cospectral gap may be fixed by the energy which comes from large scale convection. By utilizing ogive analysis, the match and mismatch of time scale between the flux and wind speed are found in strong and weak wind cases, respectively. For high wind speed, the energy mainly came from the locally generate turbulence but for weak wind speed, the large-scale convection played very important role. Since the averaging length chosen must encompass or capture all the scales of motion, the large eddy (large scale convection) need much longer time than small eddy (locally generated turbulence) to converge at a constant value. To solve the mismatch of time scale under weak wind speed, a general approach presented by Godfrey and Beljaars (1991) who suggested that using an effective wind speed U_e instead of the vector-averaged mean wind speed was visited. In order to estimate U_e , a simplified slab model for estimating CBL depth was presented. The model was validated by the pilot balloon experiment and lidar simulation. An alternative method which is using the scalar averaged wind speed instead of the vector averaged wind speed was also investigated. Both methods were found improved the bulk coefficients estimation under weak wind speed. A scalar averaged wind speed was suggested for estimating fluxes and evaporation under strong convective conditions. However, complete solution is not likely available since this problem arises from ill-defined nature of C_{dn} under light wind condition. Some alternative method evaluating the impact of large scale convection in the bulk transfer method were hoped in further study.

The wave influence on the air-lake exchange was investigated as well. Wave boundary layer was introduced to explain the wave age influence on the turbulence. The parameters of wave were found having a high correlation with wind speed. Assuming that the wing profile method is valid by applying several corrections, the wave age influencing on the roughness length and correction function were investigated. For a rough surface ($Rr > 0.13$), the roughness length is dominated by the gravity wave and expressed as Charnock equation. A constant Charnock parameter ($a = 0.032$) is found to adequately describe the momentum roughness length. On the contrary, the wave ages dependent momentum roughness length was not found in our study. A wave age dependence correction function was also not necessary. These findings confirmed that the dynamics of the

water surface exchanges were predominantly controlled by the atmospheric flow over lake surface.

Incorporating bulk transfer method and eddy correlation measurement, the energy variation and evaporation were estimated to clearly understand hydrological characteristics in the lake Kasumigaura during 2008-2010. The latent heat flux and sensible heat were always positive. The storage of energy in the lake is very important, which is different from over the land. The variable depth's water temperature was measured monthly, the measurement indicated the water in different depth was well mixed. Temperature gradient was not found during observation months. The daily averaged water level was not changed through the years about 1.3 m on average. Higher radiation and evaporation were found in summer but no seasonal variation of precipitation was shown. The annual amount of rainfall was about 929 mm, 996 mm and 1112 mm. 721 mm, 781 mm and 813 mm were found for evaporation respectively.

Acknowledgements

I would like to thank to my supervisor Prof. Michiaki Sugita for his considerable support throughout my master studies. He has provided me with a lot of help, support and encouragement. Thanks to his patience, kindness, encouragement and good advice, I can finish my master course. Thanks also to Prof. Asanuma, who has contributed with his expertise during seminar and lecture. Thanks to Prof. Yamanaka, Prof. Tsujimura and Prof. Tase for their valuable suggestion and encouragement for my research. Thanks to all the advisers in Hydrology, University of Tsukuba.

I also thank my colleagues of hydrological science, University of Tsukuba, Mr. Pei Wang, Ms. Yapin Liu, and Ms. Wenchao Ma. Without their help, I can not successfully finish my thesis. Thanks to Mr. Matsuno, Mr. Shimizu, Mr Yamanoto, Mr. Minh, Mr. Tsuji and all the member in Sugita lab.

I am very grateful to Kanto Regional Development Bureau, Ministry of Land, Infrastructure, Transport and Tourism. Thank them provided us abundant high quality data. Thanks to the staff from Yokogawa Denshikiki Co., Ltd. With their help in fieldwork and care in many practical matters such as instruments, measurements and data analysis.

At last, thanks also to all my other friends who gave me unforgettable experience in my life. Thanks to my brother, without his help, I could not imagine how I can live through the last two years. At the same time, I would like to thank my parents. They gave me life, and spent countless love on me.

References

- Abdella, K. and D'Alessio, S.: 2003, A parameterization of the roughness length for the air-sea interface in free convection, *Environmental Fluid Mechanics* **3**, 55–77.
- Andreas, E.: 2011, Fallacies of the enthalpy transfer coefficient over the ocean in high winds, *Journal of the Atmospheric Sciences* **68**, 1435–1445.
- Ann-Sofi, S., Ulf, S., Erik, H. and Cecilia, J.: 2007, Critical re-evaluation of the bulk transfer coefficient for sensible heat over the ocean during unstable and neutral conditions, *Quarterly Journal of the Royal Meteorological Society* **133**, 227–250.
- Ataktürk, S. and Katsaros, K.: 1999, Wind stress and surface waves observed on lake washington, *Journal of physical oceanography* **29**, 633–650.
- Blanken, P., Rouse, W., Culf, A., Spence, C., Boudreau, L., Jasper, J., Kochtubajda, B., Schertzer, W., Marsh, P. and Verseghy, D.: 2000, Eddy covariance measurements of evaporation from great slave lake, northwest territories, canada, *Water Resources Research* **36**, 1069–1077.
- Bourassa, M., Vincent, D. and Wood, W.: 1999, A flux parameterization including the effects of capillary waves and sea state, *Journal of the Atmospheric Sciences* **56**, 1123–1139.
- Bradley, E., Coppin, P. and Godfrey, J.: 1991, Measurements of sensible and latent heat flux in the western equatorial pacific ocean, *Journal of Geophysical Research Supplement* **96**, 3375.
- Brut, A., Butet, A., Durand, P., Caniaux, G. and Planton, S.: 2005, Air–sea exchanges in the equatorial area from the equalant99 dataset: Bulk parametrizations of turbulent fluxes corrected for airflow distortion, *Quarterly Journal of the Royal Meteorological Society* **131**, 2497–2538.
- Brutsaert, W.: 1973, Similarity functions for turbulence in neutral air above swell, *Journal of Physical Oceanography* **3**, 479–481.

- Brutsaert, W.: 1982, *Evaporation into the atmosphere: Theory, history, and applications*, Reidel Dordrecht, Boston, London.
- Brutsaert, W.: 1992, Stability correction functions for the mean wind speed and temperature in the unstable surface layer, *Geophysical Research Letters* **19**, 469–472.
- Brutsaert, W.: 2005, *Hydrology: an introduction*, Cambridge University Press.
- Burns, S., Horst, T., Blanken, P. and Monson, R.: 2012, Using sonic anemometer temperature to measure sensible heat flux in strong winds, *Atmospheric Measurement Techniques Discussions* **5**, 447–469.
- Businger, J.: 1973, A note on free convection, *Boundary-Layer Meteorology* **4**, 323–326.
- Businger, J., Wyngaard, J., Izumi, Y. and Bradley, E.: 1971, Flux-profile relationships in the atmospheric surface layer, *Journal of the Atmospheric Sciences* **28**, 181–189.
- Charnock, H.: 1955, Wind stress on a water surface, *Quarterly Journal of the Royal Meteorological Society* **81**, 639–640.
- Cheng, I. and Brutsaert, W.: 1972, Wave effect and eddy diffusivity in the air near a water surface, *Water Resources Research* **8**, 1439–1443.
- Deardorff, J.: 1970, Convective velocity and temperature scales for the unstable planetary boundary layer and for rayleigh convection, *Journal of the Atmospheric Sciences* **27**, 1211–1213.
- Deardorff, J.: 1979, Prediction of convective mixed-layer entrainment for realistic capping inversion structure, *Journal of the Atmospheric Sciences* **36**, 424–436.
- DeCosmo, J., Katsaros, K., Smith, S., Anderson, R., Oost, W., Bumke, K. and Chadwick, H.: 1996, Air-sea exchange of water vapor and sensible heat: The humidity exchange over the sea (hexos) results, *Journal of Geophysical Research* **101**, 12001–12.
- Derecki, J.: 1975, Evaporation from lake erie, *Technical report*, U.S. Department of Commerce, National Oceanic and Atmospheric Administration, Environmental Research Laboratories.
- Donelan, M., Dobson, F., Smith, S. and Anderson, R.: 1993, On the dependence of sea surface roughness on wave development, *Journal of Physical Oceanography* **23**, 2143–2149.

- Downing, J., Prairie, Y., Cole, J., Duarte, C., Tranvik, L., Striegl, R., McDowell, W., Kortelainen, P., Caraco, N., Melack, J. et al.: 2006, The global abundance and size distribution of lakes, ponds, and impoundments, *Limnology and Oceanography* **51**, 2388–2397.
- Drennan, W., Graber, H., Hauser, D. and Quentin, C.: 2003, On the wave age dependence of wind stress over pure wind seas, *Journal of Geophysical Research* **108**, 8062.
- Dupuis, H., Taylor, P., Weill, A. and Katsaros, K.: 1997, Inertial dissipation method applied to derive turbulent fluxes over the ocean during the surface of the ocean, fluxes and interactions with the atmosphere/atlantic stratocumulus transition experiment (sofia/astex) and structure des echanges mer-atmosphere, proprietes des heterogeneites oceaniques: Recherche experimentale (semaphore) experiments with low to moderate wind speeds, *Journal of Geophysical Research* **102**, 21115–21.
- Dyer, A.: 1974, A review of flux-profile relationships, *Boundary-Layer Meteorology* **7**, 363–372.
- Ellis, C., Champlin, J. and Stefan, H.: 1997, Density current intrusions in an ice-covered urban lake, *Journal of the American Water Resources Association* **33**, 1363–1374.
- Esbensen, S. K. and McPhaden, M. J.: 1996, Enhancement of tropical ocean evaporation and sensible heat flux by atmospheric mesoscale systems, *Collections* .
- Fairall, C., Bradley, E., Hare, J., Grachev, A. and Edson, J.: 2003, Bulk parameterization of air-sea fluxes: Updates and verification for the coare algorithm, *Journal of Climate* **16**, 571–591.
- Fairall, C., Bradley, E., Rogers, D., Edson, J. and Youngs, G.: 1996, Bulk parameterization of air-sea fluxes for tropical ocean-global atmosphere coupled-ocean atmosphere response, *Journal of Geophysical Research* **101**, 3747–3764.
- Foken, T., G^ockede, M., Mauder, M., Mahrt, L., Amiro, B. and Munger, W.: 2005, Post-field data quality control, in X. Lee, W. Massman and B. Law (eds), *Handbook of Micrometeorology*, Atmospheric and Oceanographic Sciences Library, Springer Netherlands, pp. 181–208.
- Foken, T. and Wichura, B.: 1996, Tools for quality assessment of surface-based flux measurements, *Agricultural and Forest Meteorology* **78**, 83–105.
- Garratt, J. et al.: 1992, The atmospheric boundary layer. cambridge atmospheric and space science series, *Cambridge University Press, Cambridge* **416**, 444.

- Geernaert, G., Davidson, K., Larsen, S. and Mikkelsen, T.: 1988, Wind stress measurements during the tower ocean wave and radar dependence experiment, *Journal of Geophysical Research* **93**, 13913–13.
- Gibson, J.: 2002, Short-term evaporation and water budget comparisons in shallow arctic lakes using non-steady isotope mass balance, *Journal of Hydrology* **264**, 242–261.
- Godfrey, J. and Beljaars, A.: 1991, On the turbulent fluxes of buoyancy, heat and moisture at the air-sea interface at low wind speeds, *Journal of Geophysical Research* **96**, 22043–22.
- Grachev, A., Fairall, C., Hare, J., Edson, J. and Miller, S.: 2003, Wind stress vector over ocean waves, *Journal of Physical Oceanography* **33**, 2408–2429.
- Green, T. and Terrell, R.: 1978, The surface temperature structure associated with the keweenaw current in lake superior, *Journal of Geophysical Research* **83**, 419–426.
- Hamed, K. H.: 2008, Trend detection in hydrologic data: The mann–kendall trend test under the scaling hypothesis, *Journal of Hydrology* **349**(3), 350–363.
- Heikinheimo, M., Kangas, M., Tourula, T., Venäläinen, A. and Tattari, S.: 1999, Momentum and heat fluxes over lakes tämnaren and råkssjö determined by the bulk-aerodynamic and eddy-correlation methods, *Agricultural and Forest Meteorology* **98**, 521–534.
- Hino, M.: 1977, *Spectral analysis*, Asakura Shoten.
- Högström, U., Smedman, A., Sahlée, E., Drennan, W., Kahma, K., Pettersson, H. and Zhang, F.: 2009, The atmospheric boundary layer during swell: A field study and interpretation of the turbulent kinetic energy budget for high wave ages, *Journal of the Atmospheric Sciences* **66**, 2764–2779.
- Howell, J. and Mahrt, L.: 1997, Multiresolution flux decomposition, *Boundary-Layer Meteorology* **83**(1), 117–137.
- Ikura, H.: 2010, *Estimation of evaporation distribution over lake kasumigaura using satellite data*, Master's thesis, University of Tsukuba.
- Janssen, J.: 1997, Does wind stress depend on sea-state or not?—a statistical error analysis of hexmax data, *Boundary-Layer Meteorology* **83**, 479–503.

- Johnson, H., Højstrup, J., Vested, H. and Larsen, S.: 1998, On the dependence of sea surface roughness on wind waves, *Journal of Physical Oceanography* **28**, 1702–1716.
- Kader, B. and Yaglom, A.: 1990, Mean fields and fluctuation moments in unstably stratified turbulent boundary layers, *Journal of Fluid Mechanics* **212**, 637–662.
- Kaimal, J. and Finnigan, J.: 1994, *Atmospheric boundary layer flows: their structure and measurement*, Oxford University Press, USA.
- Kaimal, J., Wyngaard, J., Izumi, Y. and Cote, O.: 1972, Spectral characteristics of surface-layer turbulence, *Quarterly Journal of the Royal Meteorological Society* **98**, 563–589.
- Kendall, M. G.: 1975, *Rank correlation methods*, Griffin, London.
- Kondo, J.: 1975, Air-sea bulk transfer coefficients in diabatic conditions, *Boundary-Layer Meteorology* **9**, 91–112.
- Kraus, E. and Businger, J.: 1994, *Atmosphere-ocean interaction*, Oxford University Press, USA.
- Large, W., Morzel, J. and Crawford, G.: 1995, Accounting for surface wave distortion of the marine wind profile in low-level ocean storms wind measurements, *Journal of Physical Oceanography* **25**, 2959–2971.
- Law, B. and Verma, S.: 2005, Introduction, in X. Lee, W. Massman and B. Law (eds), *Handbook of Micrometeorology*, Vol. 29 of *Atmospheric and Oceanographic Sciences Library*, Springer Netherlands, pp. 1–5.
- Lee, C.: 1986, Simple model and climatological aspects of the structure of the convective boundary layer, *Atmospheric Environment (1967)* **20**, 705–714.
- Lee, X., Finnigan, J. and Paw U, K.: 2005, Coordinate systems and flux bias error, in X. Lee, W. Massman and B. Law (eds), *Handbook of Micrometeorology*, Vol. 29 of *Atmospheric and Oceanographic Sciences Library*, Springer Netherlands, pp. 33–66.
- Lee, X. and Massman, W.: 2011, A perspective on thirty years of the webb, pearman and leuning density corrections, *Boundary-Layer Meteorology* **139**, 37–59.
- Lenschow, D., Mann, J. and Kristensen, L.: 1994, How long is long enough when measuring fluxes and other turbulence statistics, *NCAR Technical Note* .

- Lenters, J., Kratz, T. and Bowser, C.: 2005, Effects of climate variability on lake evaporation: Results from a long-term energy budget study of sparkling lake, northern wisconsin (usa), *Journal of Hydrology* **308**(1), 168–195.
- Lilly, D.: 1968, Models of cloud-topped mixed layers under a strong inversion, *Quarterly Journal of the Royal Meteorological Society* **94**(401), 292–309.
- Liu, X. and Ohtaki, E.: 1997, An independent method to determine the height of the mixed layer, *Boundary-Layer Meteorology* **85**, 497–504.
- Lofgren, B. and Zhu, Y.: 2000, Surface energy fluxes on the great lakes based on satellite-observed surface temperatures 1992 to 1995, *Journal of Great Lakes Research* **26**, 305–314.
- Lumley, J. and Panofsky, H.: 1964, The structure of atmospheric turbulence, *Interscience Monographs and Texts in Physics and Astronomy, New York: Wiley, 1964* **1**, 239.
- Maat, N., Kraan, C. and Oost, W.: 1991, The roughness of wind waves, *Boundary-Layer Meteorology* **54**, 89–103.
- Mahrt, L., Moore, E., Vickers, D. and Jensen, N.: 2001, Dependence of turbulent and mesoscale velocity variances on scale and stability, *Journal of Applied Meteorology* **40**(3), 628–641.
- Mahrt, L. and Sun, J.: 1995, Dependence of surface exchange coefficients on averaging scale and grid size, *Quarterly Journal of the Royal Meteorological Society* **121**, 1835–1852.
- Mahrt, L., Vickers, D., Andreas, E. and Khelif, D.: 2012, Sensible heat flux in near-neutral conditions over the sea, *Journal of Physical Oceanography* **42**, 1134–1142.
- Mahrt, L., Vickers, D., Howell, J., Hojstrup, J., Wilczak, J., Edson, J. and Hare, J.: 1996, Sea surface drag coefficients in the risø air sea experiment, *Journal of Geophysical Research* **101**, 14,327–14,335.
- Makin, V. and Mastenbroek, C.: 1996, Impact of waves on air-sea exchange of sensible heat and momentum, *Boundary-Layer Meteorology* **79**, 279–300.
- Marmorino, G. and Smith, G.: 2005, Bright and dark ocean whitecaps observed in the infrared, *Geophysical R* **32**, L11604.

- Metzger, M. and Holmes, H.: 2008, Time scales in the unstable atmospheric surface layer, *Boundary-Layer Meteorology* **126**, 29–50.
- Monbaliu, J.: 1994, On the use of the donelan wave spectral parameter as a measure for the roughness of wind waves, *Boundary-Layer Meteorology* **67**, 277–291.
- Moncrieff, J., Clement, R., Finnigan, J. and Meyers, T.: 2005, Averaging, detrending, and filtering of eddy covariance time series, in X. Lee, W. Massman and B. Law (eds), *Handbook of Micrometeorology*, Vol. 29 of *Atmospheric and Oceanographic Sciences Library*, Springer Netherlands, pp. 7–31.
- Moncrieff, J., Malhi, Y. and Leuning, R.: 2006, The propagation of errors in long-term measurements of land-atmosphere fluxes of carbon and water, *Global Change Biology* **2**, 231–240.
- Muraoka, K. and Fukushima, T.: 1981, Lake current of kasumigaura, *Res. Rep. Nat. Inst. Envir. Stud* **19**, 150.
- Nikuradse, J.: 1933, Laws of flow in rough pipes, *VDI Forschungsheft* **361**.
- Oncley, S., Friehe, C., Larue, J., Businger, J., Itsweire, E. and Chang, S.: 1996, Surface-layer fluxes, profiles, and turbulence measurements over uniform terrain under near-neutral conditions, *Journal of the Atmospheric Sciences* **53**, 1029–1044.
- Oost, W., Jacobs, C. and Van Oort, C.: 2000, Stability effects on heat and moisture fluxes at sea, *Boundary-Layer Meteorology* **95**, 271–302.
- Oost, W., Komen, G., Jacobs, C. and Van Oort, C.: 2002, New evidence for a relation between wind stress and wave age from measurements during asgamage, *Boundary-Layer Meteorology* **103**, 409–438.
- Panofsky, H., Tennekes, H., Lenschow, D. and Wyngaard, J.: 1977, The characteristics of turbulent velocity components in the surface layer under convective conditions, *Boundary-Layer Meteorology* **11**, 355–361.
- Paulson, C.: 1970, The mathematical representation of wind speed and temperature profiles in the unstable atmospheric surface layer, *Journal of Applied Meteorology* **9**, 857–861.
- Priestley, C. and Taylor, R.: 1972, On the assessment of surface heat flux and evaporation using large-scale parameters, *Monthly Weather Review* **100**, 81–92.

- Rannik, Ü. and Vesala, T.: 1999, Autoregressive filtering versus linear detrending in estimation of fluxes by the eddy covariance method, *Boundary-Layer Meteorology* **91**(2), 259–280.
- Read, J., Hamilton, D., Desai, A., Rose, K., MacIntyre, S., Lenters, J., Smyth, R., Hanson, P., Cole, J., Staehr, P. et al.: 2012, Lake-size dependency of wind shear and convection as controls on gas exchange, *Geophysical Research Letters* **39**, L09405.
- Redelsperger, J., Guichard, F. and Mondon, S.: 2000, A parameterization of mesoscale enhancement of surface fluxes for large-scale models, *Journal of Climate* **13**, 402–421.
- Rosenberry, D., Winter, T., Buso, D. and Likens, G.: 2007, Comparison of 15 evaporation methods applied to a small mountain lake in the northeastern usa, *Journal of Hydrology* **340**, 149–166.
- Rutgersson, A., Carlsson, B. and Smedman, A.: 2007, Modelling sensible and latent heat fluxes over sea during unstable, very close to neutral conditions, *Boundary-Layer Meteorology* **123**, 395–415.
- Saito., M.: 2007, *Characteristics of vertical heat and water vapor transport at around Spectral gap scales over land Surface*, PhD thesis, University of Tsukuba.
- Sakai, R. K., Fitzjarrald, D. R. and Moore, K. E.: 2001, Importance of low-frequency contributions to eddy fluxes observed over rough surfaces, *Journal of Applied Meteorology* **40**(12), 2178–2192.
- Saotome, T.: 2009, *Mixed layer depth estimation using mie lidar : an example of tsukuba (in japanese)*, Master's thesis, University of Tsukuba.
- Schertzer, W.: 1978, Energy budget and monthly evaporation estimates for lake superior, 1973, *Journal of Great Lakes Research* **4**, 320–330.
- Schumann, U.: 1988, Minimum friction velocity and heat transfer in the rough surface layer of a convective boundary layer, *Boundary-Layer Meteorology* **44**, 311–326.
- Sjoblom, A. and Smedman, A.-S.: 2003, Vertical structure in the marine atmospheric boundary layer and its implication for the inertial dissipation method, *Boundary-Layer Meteorology* **109**, 1–25.

- Smedman, A., Högström, U., Hunt, J. and Sahlée, E.: 2007, Heat/mass transfer in the slightly unstable atmospheric surface layer, *Quarterly Journal of the Royal Meteorological Society* **133**, 37–51.
- Smedman, A., Högström, U., Sahlée, E., Drennan, W., Kahma, K., Pettersson, H. and Zhang, F.: 2009, Observational study of marine atmospheric boundary layer characteristics during swell, *Journal of the Atmospheric Sciences* **66**, 2747–2763.
- Smedman, A., Larsén, X., Högström, U., Kahma, K. and Pettersson, H.: 2003, Effect of sea state on the momentum exchange over the sea during neutral conditions, *Journal of Geo* **108**, 3367.
- Smedman, A., Tjernström, M. and Högström, U.: 1994, The near-neutral marine atmospheric boundary layer with no surface shearing stress: A case study., *Journal of Atmospheric Sciences* **51**, 3399–3411.
- Smith, S., Anderson, R., Oost, W., Kraan, C., Maat, N., De Cosmo, J., Katsaros, K., Davidson, K., Bumke, K., Hasse, L. et al.: 1992, Sea surface wind stress and drag coefficients: the hexos results, *Boundary-Layer Meteorology* **60**, 109–142.
- Smith, S. D., Anderson, R. J., Hertzman, O., Oost, W. A., W.Kohsiek, de Leeuw, G. and Kunz, G. J.: 1995, New measurements of eddy fluxes at the sea surface in asgasex, *Selected papers from the Proceedings of the Third International Symposium on Air-Water Gas Transfer* pp. 703–712.
- Stull, R.: 1988, *An introduction to boundary layer meteorology*, Vol. 13 of *Atmospheric and Oceanographic Sciences Library*, Springer.
- Stull, R.: 1994, A convective transport theory for surface fluxes, *Journal of the Atmospheric Sciences* **51**, 3–22.
- Sugita, M., Hiyama, T., Endo, N. and Tian, S.: 1995, Flux determination over a smooth surface under strongly unstable conditions, *Boundary-Layer Meteorology* **73**, 145–158.
- Sun, J., Howell, J., Esbensen, S., Mahr, L., Greb, C., Grossman, R. and LeMone, M.: 1996, Scale dependence of air-sea fluxes over the western equatorial pacific, *Collections* **53**, 2997–3012.
- Sun, J., Lenschow, D., Mahrt, L., Crawford, T., Davis, K., Oncley, S., MacPherson, J., Wang, Q., Dobosy, R. and Desjardins, R.: 1997, Lake-induced atmospheric circulations during boreas, *Collections* **102**, 29155–29166.

- Sun, J. and Mahrt, L.: 1994, Spatial distribution of surface fluxes estimated from remotely sensed variables, *J. Appl. Meteor.* **33**, 1341–1353.
- Sykes, R., Henn, D. and Lewellen, W.: 1993, Surface-layer description under free-convection conditions, *Quarterly Journal of the Royal Meteorological Society* **119**, 409–421.
- Taylor, P. and Yelland, M.: 2001, The dependence of sea surface roughness on the height and steepness of the waves, *Journal of Physical Oceanography* **31**, 572–590.
- Toba, Y., Iida, N., Kawamura, H., Ebuchi, N. and Jones, I.: 1990, Wave dependence of sea-surface wind stress, *Journal of Physical Oceanography* **20**, 705–721.
- Toyota, A. K. M., Haginiwa, Y., Terzawa, K., Hikida, M., Furiya, T., Y. Miyabara and Tomidokuro, G.: 2006, Nonuniformity of wind distribution over lake suwa and their effect on lake current, *Journal of Japan Society of Civil Engineers* **50**, 1303–1308.
- Vallet-Coulomb, C., Legesse, D., Gasse, F., Travi, Y. and Chernet, T.: 2001, Lake evaporation estimates in tropical africa (lake ziway, ethiopia), *Journal of Hydrology* **245**, 1–18.
- Vercauteren, N.: 2011, *Water Vapor and Heat Exchange over Lakes*, PhD thesis, ECOLE POLYTECHNIQUE FEDERALE DE LAUSANNE EPFL.
- Vercauteren, N., Bou-Zeid, E., Parlange, M., Lemmin, U., Huwald, H., Selker, J. and Meneveau, C.: 2008, Subgrid-scale dynamics of water vapour, heat, and momentum over a lake, *Boundary-Layer Meteorology* **128**, 205–228.
- Vesala, T., Eugster, W. and Ojala, A.: 2012, Eddy covariance measurements over lakes, in M. Aubinet, T. Vesala and D. Papale (eds), *Eddy Covariance*, Springer Atmospheric Sciences, Springer Netherlands, pp. 365–376.
- Vickers, D. and Mahrt, L.: 1997, Fetch limited drag coefficients, *Boundary-Layer Meteorology* **85**, 53–79.
- Vickers, D. and Mahrt, L.: 2003, The cospectral gap and turbulent flux calculations, *Journal of atmospheric and oceanic technology* **20**(5), 660–672.
- Wilson, K., Goldstein, A., Falge, E., Aubinet, M., Baldocchi, D., Berbigier, P., Bernhofer, C., Ceulemans, R., Dolman, H., Field, C. et al.: 2002, Energy balance closure at fluxnet sites, *Agricultural and Forest Meteorology* **113**(1), 223–243.

- Wu, J.: 1980, Wind-stress coefficients over sea surface near neutral conditions-a revisit, *Journal of Physical Oceanography* **10**, 727–740.
- Wu, J.: 1994, The sea surface is aerodynamically rough even under light winds, *Boundary-Layer Meteorology* **69**, 149–158.
- Yue, S. and Wang, C.: 2004, The mann-kendall test modified by effective sample size to detect trend in serially correlated hydrological series, *Water Resources Management* **18**(3), 201–218.
- Zhang, W., Perrie, W. and Li, W.: 2006, Impacts of waves and sea spray on midlatitude storm structure and intensity, *Monthly Weather Review* **134**, 2418–2442.

Appendix A

The bulk coefficient estimated from eddy correlation method and follow the Monin-Obukhov similarity theory. The dimensionless gradients of the wind speed, temperature and humidity can be expressed by

$$\begin{aligned}\frac{kz}{u_*} \frac{d\bar{U}}{dz} &= \phi_m\left(\frac{z}{L}\right) \\ -\frac{kz}{T_*} \frac{d\bar{T}}{dz} &= \phi_h\left(\frac{z}{L}\right) \\ -\frac{kz}{q_*} \frac{d\bar{q}}{dz} &= \phi_q\left(\frac{z}{L}\right)\end{aligned}$$

Assumed that $d\bar{U} = U_{10} - U_m$, $d\bar{T} = T_{10} - T_m$, $d\bar{q} = q_{10} - q_m$, then the integral form of them can be expressed as follow:

$$\begin{aligned}U_{10} - U_m &= \frac{u_*}{k} \left[\ln\left(\frac{10}{z_m}\right) - \psi_m\left(\frac{10}{L}\right) + \psi_m\left(\frac{z_m}{L}\right) \right] \\ t_{10} - t_m &= \frac{t_*}{k} \left[\ln\left(\frac{10}{z_m}\right) - \psi_h\left(\frac{10}{L}\right) + \psi_h\left(\frac{z_m}{L}\right) \right] \\ q_{10} - q_m &= \frac{q_*}{k} \left[\ln\left(\frac{10}{z_m}\right) - \psi_q\left(\frac{10}{L}\right) + \psi_q\left(\frac{z_m}{L}\right) \right]\end{aligned}$$

where the stability function is defined by the dimensionless gradient function ϕ_x

$$\psi_x\left(\frac{z}{L}\right) = \int_0^{z/L} [1 - \phi_x(y)] dy/y$$

y is the dummy integration variable. 10-m parameters can be estimated by transposition of measured parameters

$$\begin{aligned}U_{10} &= U_m + \frac{u_*}{k} \left[\ln\left(\frac{10}{z_m}\right) - \psi_m\left(\frac{10}{L}\right) + \psi_m\left(\frac{z_m}{L}\right) \right] \\ t_{10} &= t_m + \frac{t_*}{k} \left[\ln\left(\frac{10}{z_m}\right) - \psi_h\left(\frac{10}{L}\right) + \psi_h\left(\frac{z_m}{L}\right) \right] \\ q_{10} &= q_m + \frac{q_*}{k} \left[\ln\left(\frac{10}{z_m}\right) - \psi_q\left(\frac{10}{L}\right) + \psi_q\left(\frac{z_m}{L}\right) \right]\end{aligned}$$

The bulk coefficients at 10m are computed from the wind measured at height z as

$$C_d = \frac{u_*^2}{U_{10}^2} = \frac{u_*^2}{\left\{ U_m + \frac{u_*}{k} \left[\ln \left(\frac{10}{z_m} \right) - \psi_m \left(\frac{10}{L} \right) + \psi_m \left(\frac{z_m}{L} \right) \right] \right\}^2}$$

$$C_d = \frac{k^2}{\left\{ \ln \left(\frac{z}{z_{0m}} \right) - \Psi_m \left(\frac{z_m}{L} \right) \right\}^2}$$

$$C_h = \frac{\overline{w't'}}{U_{10}\Delta t} = \frac{u_*}{U_m + \frac{u_*}{k} \left[\ln \left(\frac{10}{z_m} \right) - \psi_m \left(\frac{10}{L} \right) + \psi_m \left(\frac{z_m}{L} \right) \right]} \frac{t_*}{\left\{ t_m + \frac{t_*}{k} \left[\ln \left(\frac{10}{z_m} \right) - \psi_h \left(\frac{10}{L} \right) + \psi_h \left(\frac{z_m}{L} \right) \right] \right\} - t_s}$$

$$C_h = \frac{k^2}{\left\{ \ln \left(\frac{10}{z_{0m}} \right) - \Psi_m \left(\frac{10}{L} \right) \right\} \left\{ \ln \left(\frac{10}{z_{0h}} \right) - \Psi_h \left(\frac{10}{L} \right) \right\}}$$

$$C_e = \frac{\overline{w'q'}}{U_{10}\Delta q} = \frac{u_*}{U_m + \frac{u_*}{k} \left[\ln \left(\frac{10}{z_m} \right) - \psi_q \left(\frac{10}{L} \right) + \psi_q \left(\frac{z_m}{L} \right) \right]} \frac{q_*}{\left\{ q_m + \frac{q_*}{k} \left[\ln \left(\frac{10}{z_m} \right) - \psi_q \left(\frac{10}{L} \right) + \psi_q \left(\frac{z_m}{L} \right) \right] \right\} - q_s}$$

$$C_e = \frac{k^2}{\left\{ \ln \left(\frac{10}{z_{0m}} \right) - \Psi_m \left(\frac{10}{L} \right) \right\} \left\{ \ln \left(\frac{10}{z_{0q}} \right) - \Psi_q \left(\frac{10}{L} \right) \right\}}$$

Since the bulk coefficient clearly depend on the measurement height and the atmospheric stratification, it is customary to choose a neutral atmosphere as standard condition, therefore the neutral bulk coefficients are introduced. The neutral bulk coefficients are calculated from the neutral wind, neutral temperature difference and neutral humidity difference

$$C_{dn} = \frac{u_*^2}{U_{10n}^2} = \frac{u_*^2}{\left\{ U_m - \frac{u_*}{k} \left[\ln \left(\frac{z_m}{10} \right) - \psi_m \left(\frac{z_m}{L} \right) \right] \right\}^2}$$

$$C_{hn} = \frac{\overline{w't'}}{U_{10n}\Delta t_{10n}} = \frac{\overline{w't'}}{\left\{ U_m - \frac{u_*}{k} \left[\ln \left(\frac{z_m}{10} \right) - \psi_m \left(\frac{z_m}{L} \right) \right] \right\} \left\{ \Delta t + \frac{t_*}{k} \left[\ln \left(\frac{z_m}{10} \right) - \psi_h \left(\frac{z_m}{L} \right) \right] \right\}}$$

$$C_{en} = \frac{\overline{w'q'}}{U_{10n}\Delta q_{10n}} = \frac{\overline{w'q'}}{\left\{ U_m - \frac{u_*}{k} \left[\ln \left(\frac{z_m}{10} \right) - \psi_m \left(\frac{z_m}{L} \right) \right] \right\} \left\{ \Delta q + \frac{q_*}{k} \left[\ln \left(\frac{z_m}{10} \right) - \psi_q \left(\frac{z_m}{L} \right) \right] \right\}}$$

Where the neutral wind is expressed as

$$U_{10n} = U_{10} + \frac{u_*}{k} \psi_m \left(\frac{10}{L} \right)$$

$$U_{10n} = U_m + \frac{u_*}{k} \left[\ln \left(\frac{10}{z_m} \right) + \psi_m \left(\frac{z_m}{L} \right) \right]$$

$$U_{10n} = U_m - \frac{u_*}{k} \left[\ln \left(\frac{z_m}{10} \right) - \psi_m \left(\frac{z_m}{L} \right) \right]$$

and the neutral humidity is given by

$$q_{10} = \frac{q_*}{k} \left[\ln \left(\frac{10}{z_{0h}} \right) - \psi_q \left(\frac{10}{L} \right) \right]$$

$$q_{10n} = q_{10} + \frac{q_*}{k} \psi_q \left(\frac{10}{L} \right)$$

$$q_{10n} = q_m + \frac{q_*}{k} \left[\ln \left(\frac{10}{z_m} \right) + \psi_q \left(\frac{z_m}{L} \right) \right]$$

the neutral temperature is expressed as

$$t_{10} = \frac{t_*}{k} \left[\ln \left(\frac{10}{z_{0h}} \right) - \psi_t \left(\frac{10}{L} \right) \right]$$

$$t_{10n} = t_{10} + \frac{t_*}{k} \psi_h \left(\frac{10}{L} \right)$$

$$t_{10n} = q_m + \frac{q_*}{k} \left[\ln \left(\frac{10}{z_m} \right) + \psi_h \left(\frac{z_m}{L} \right) \right]$$

The neutral humidity difference is given as follows

$$\Delta q_{10n} = q_s - \left(q_m + \frac{q_*}{k} \left[\ln \left(\frac{10}{z_m} \right) + \psi_q \left(\frac{z_m}{L} \right) \right] \right)$$

$$\Delta q_{10n} = \Delta q - \frac{q_*}{k} \left[\ln \left(\frac{10}{z_m} \right) + \psi_q \left(\frac{z_m}{L} \right) \right]$$

$$\Delta q_{10n} = \Delta q + \frac{q_*}{k} \left[\ln \left(\frac{z_m}{10} \right) - \psi_q \left(\frac{z_m}{L} \right) \right]$$

Similarity, the neutral humidity difference is expressed as

$$\Delta t_{10n} = t_s - \left(t_m + \frac{t_*}{k} \left[\ln \left(\frac{10}{z_m} \right) + \psi_h \left(\frac{z_m}{L} \right) \right] \right)$$

$$\Delta t_{10n} = \Delta t - \frac{t_*}{k} \left[\ln \left(\frac{10}{z_m} \right) + \psi_h \left(\frac{z_m}{L} \right) \right]$$

$$\Delta t_{10n} = \Delta t + \frac{t_*}{k} \left[\ln \left(\frac{z_m}{10} \right) - \psi_h \left(\frac{z_m}{L} \right) \right]$$

Appendix B

The coordinate system for the three components are introduced as follow: the measured three components wind speed u_1, v_1 and w_1 (30 min averaged) are rotated by several steps.

The first step swings the x_1, y_1 axis around z_1 to produce a new axis x_2, y_2, z_2 , this step forces the lateral component $v = 0$.

$$u_2 = u_1 \cos \theta + v_1 \sin \theta$$

$$v_2 = -u_1 \sin \theta + v_1 \cos \theta$$

$$w_2 = w_1$$

where

$$\theta = \tan^{-1} \left(\frac{v_1}{u_1} \right)$$

apply to covariance matrix, the wind components are given by

$$u_2 u_2 = u_1 u_1 \cos^2 \theta + v_1 v_1 \sin^2 \theta + 2u_1 v_1 \sin \theta \cos \theta$$

$$v_2 v_2 = u_1 u_1 \sin^2 \theta + v_1 v_1 \cos^2 \theta - 2u_1 v_1 \sin \theta \cos \theta$$

$$w_2 w_2 = w_1 w_1$$

$$u_2 v_2 = -u_1 u_1 \sin \theta \cos \theta + v_1 v_1 \sin \theta \cos \theta + u_1 v_1 (\cos^2 \theta - \sin^2 \theta)$$

$$u_2 w_2 = u_1 w_1 \cos \theta + v_1 w_1 \sin \theta$$

$$v_2 w_2 = -u_1 w_1 \sin \theta + v_1 w_1 \cos \theta$$

$$u_2 t_2 = u_1 t_1 \cos \theta + v_1 t_1 \sin \theta$$

$$v_2 t_2 = -u_1 t_1 \sin \theta + v_1 t_1 \cos \theta$$

$$w_2 t_2 = w_1 t_1$$

The same procedure can be applied for the humidity covariance. Ideally the wind flow should be horizontal and the mean value of w should be zero. Therefore ,the second rotation swings x_2, z_2 about y_2 into new direction x_3, y_3 and z_3 in order to force $w_3 = 0$. The u_3, v_3 and w_3 are given by

$$u_3 = u_2 \cos \phi + w_2 \sin \phi$$

$$v_3 = v_2$$

$$w_3 = -u_2 \sin \phi + w_2 \cos \phi$$

where

$$\phi = \tan^{-1} \left(\frac{w_2}{u_2} \right)$$

apply to covariance matrix, the fluxes are calculated by

$$u_3 u_3 = u_2 u_2 \cos^2 \phi + w_2 w_2 \sin^2 \phi + 2u_2 w_2 \sin \phi \cos \phi$$

$$v_3 v_3 = v_2 v_2$$

$$w_3 w_3 = u_2 u_2 \sin^2 \phi + w_2 w_2 \cos^2 \phi - 2u_2 w_2 \sin \phi \cos \phi$$

$$u_3 w_3 = (w_2 w_2 - u_2 u_2) \sin \phi \cos \phi + u_2 w_2 (\cos^2 \phi - \sin^2 \phi)$$

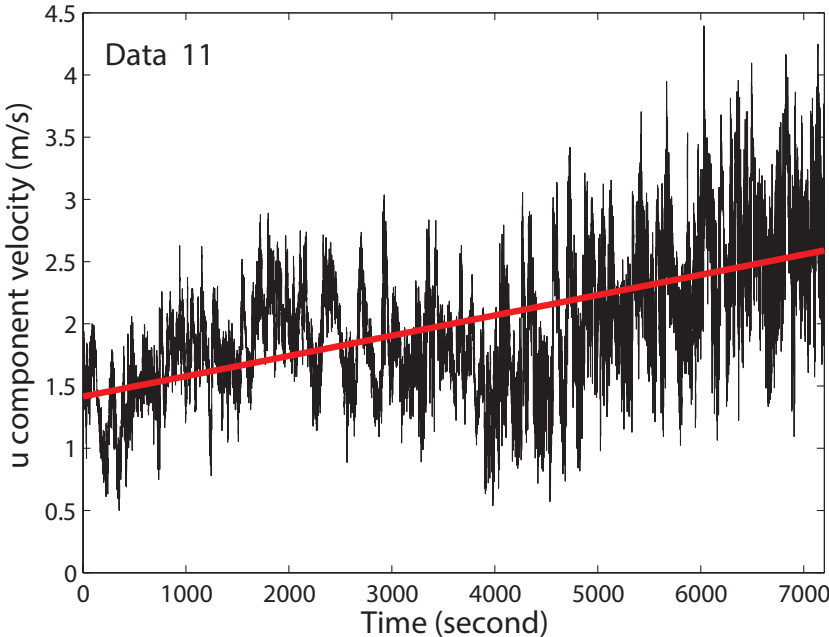
$$v_3 w_3 = -u_2 w_2 \sin \phi + v_2 w_2 \cos \phi$$

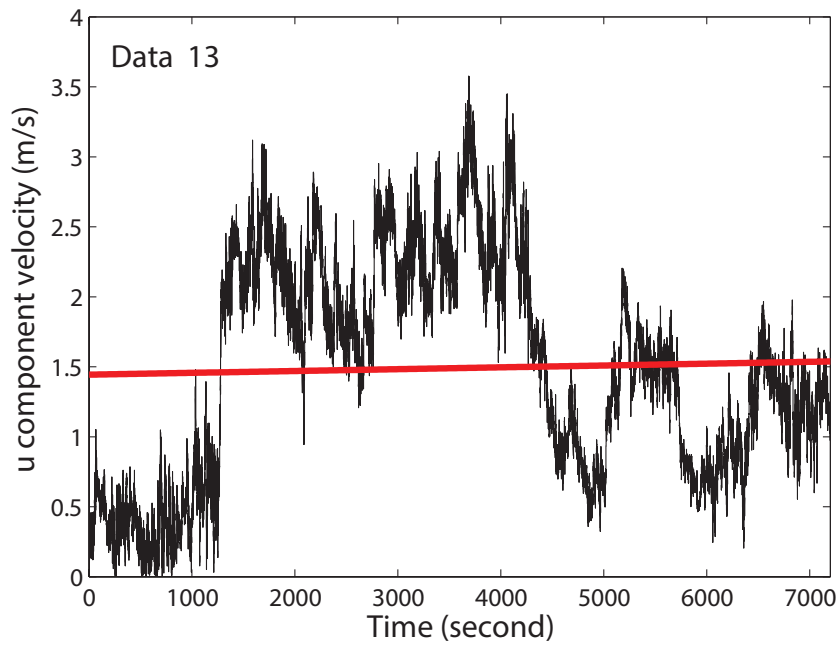
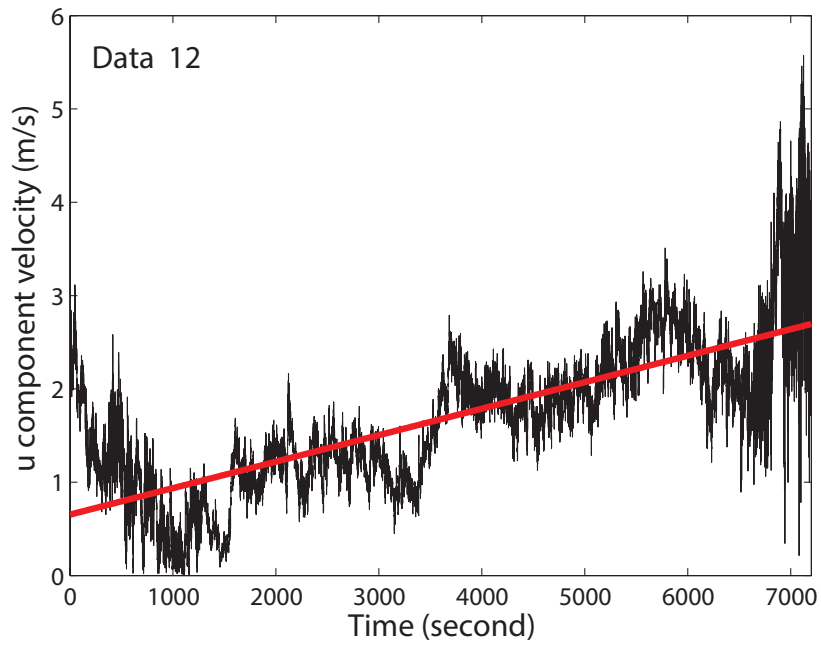
$$w_3 t_3 = -u_2 t_2 \sin \phi + w_2 t_2 \cos \phi$$

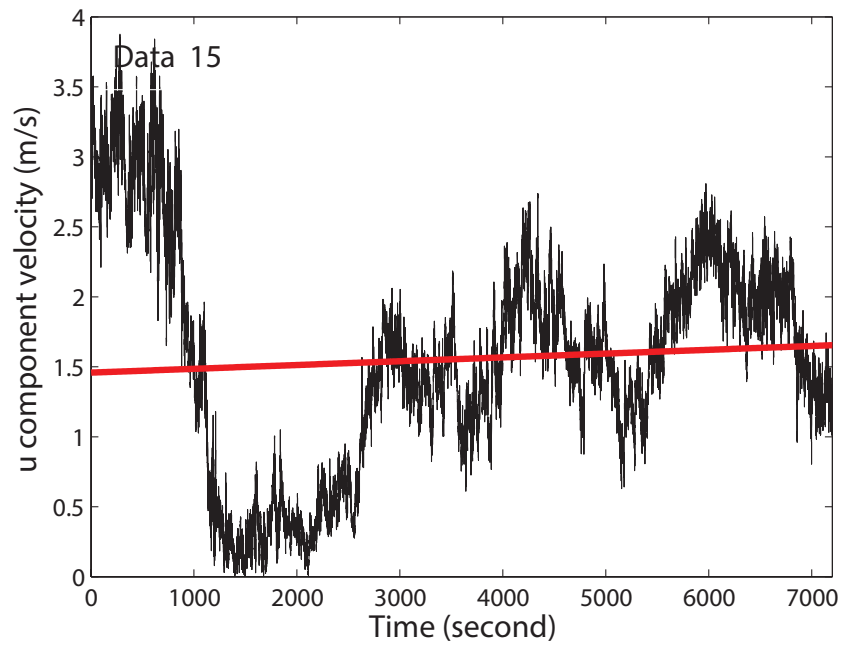
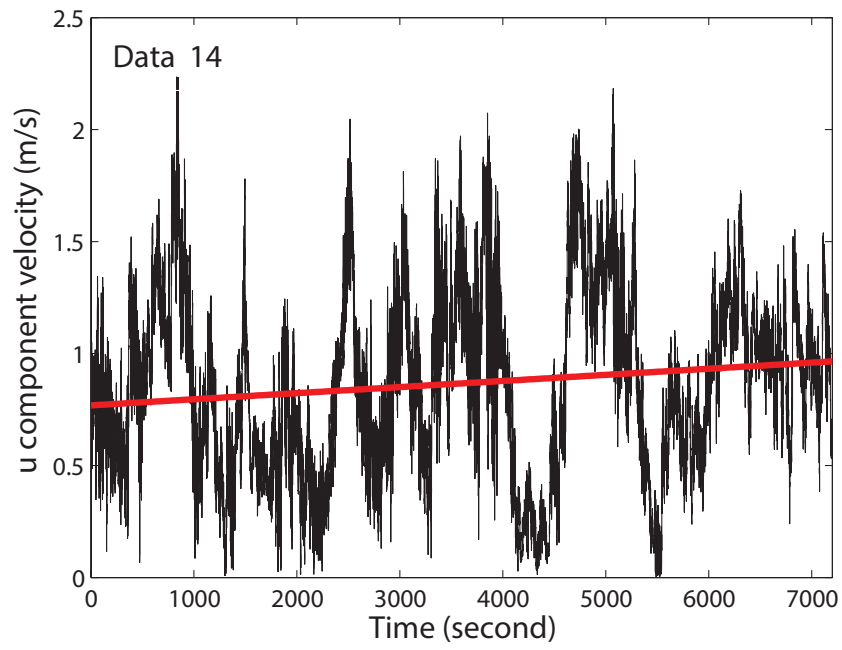
$$w_3 q_3 = -u_2 q_2 \sin \phi + w_2 q_2 \cos \phi$$

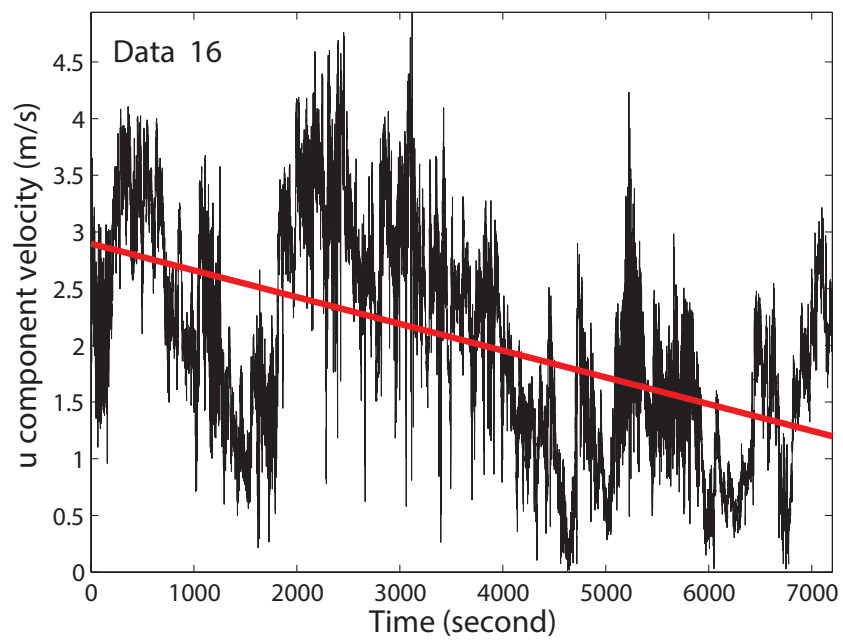
Appendix C

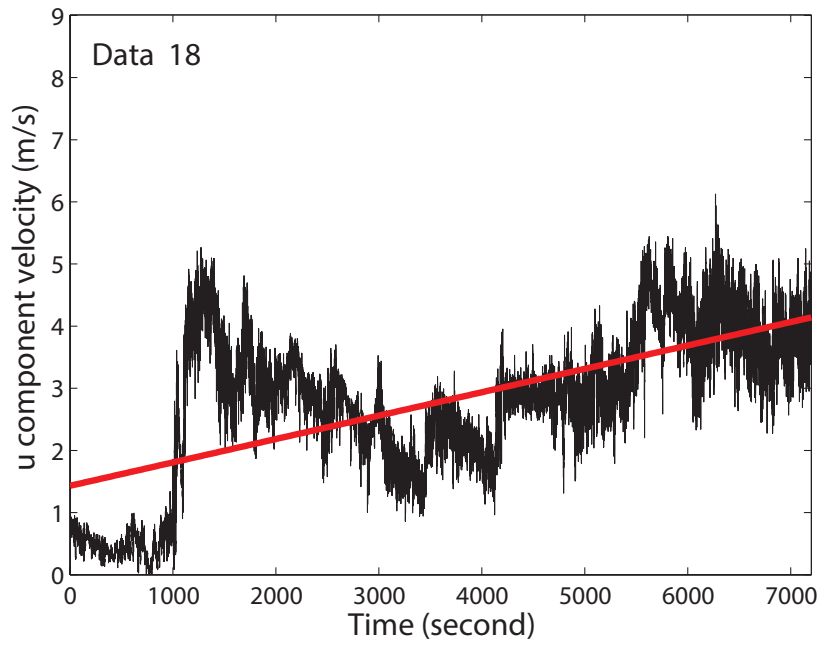
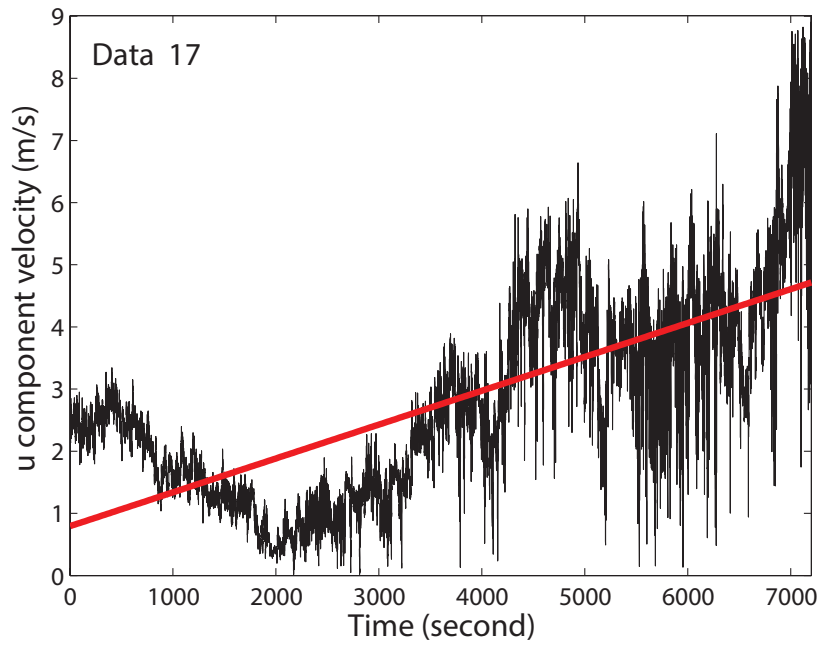
The trends in ogive data analysis for low wind speed cases are described as follows: For U component, we have:

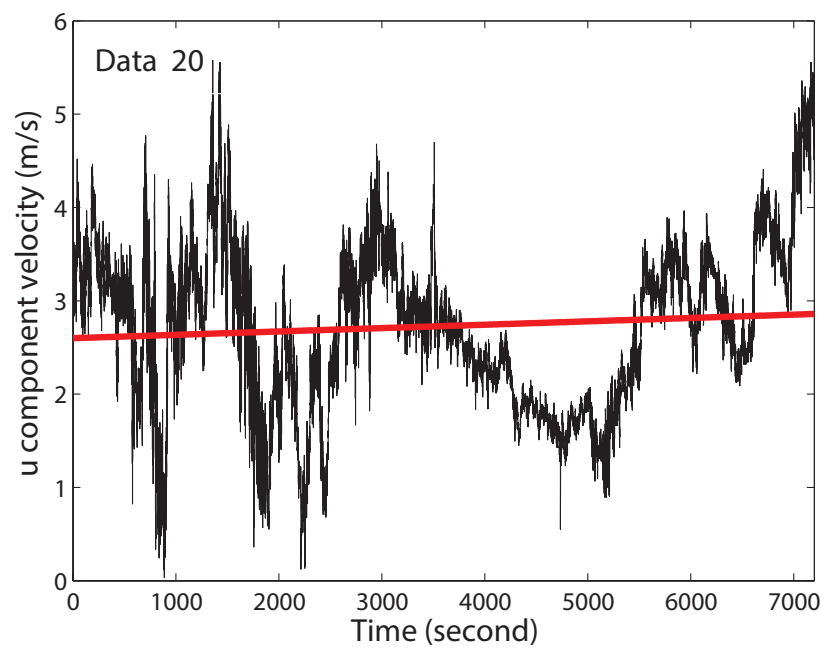
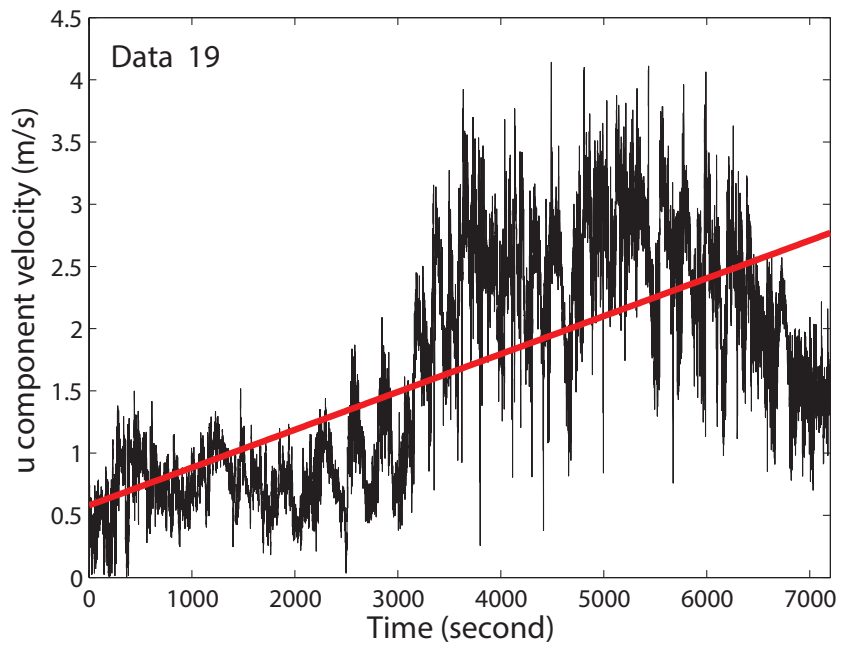




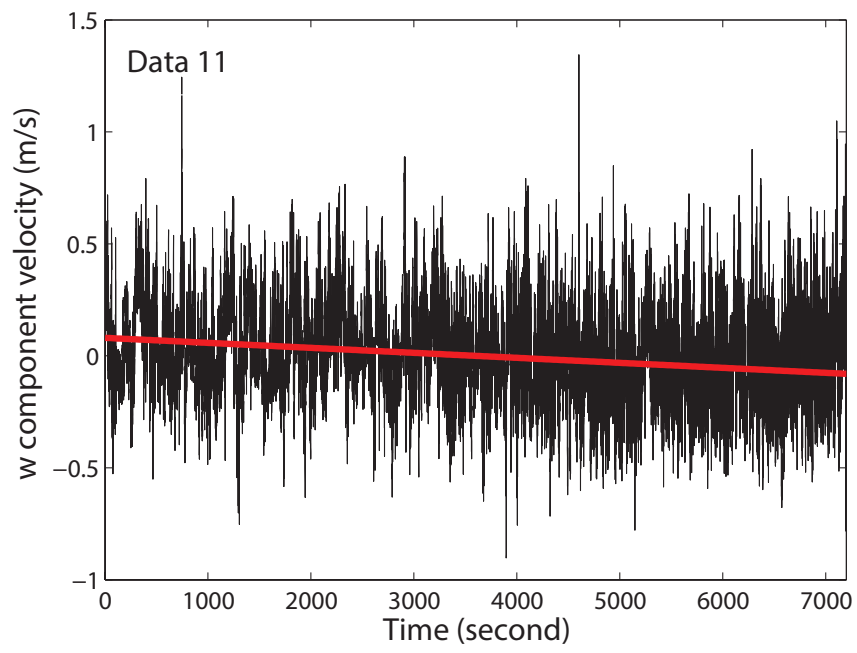


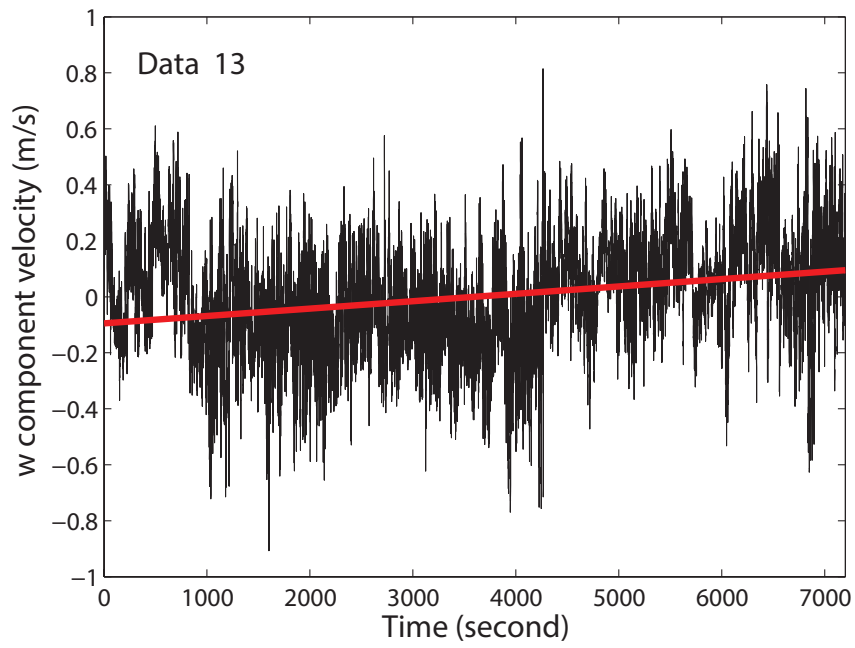
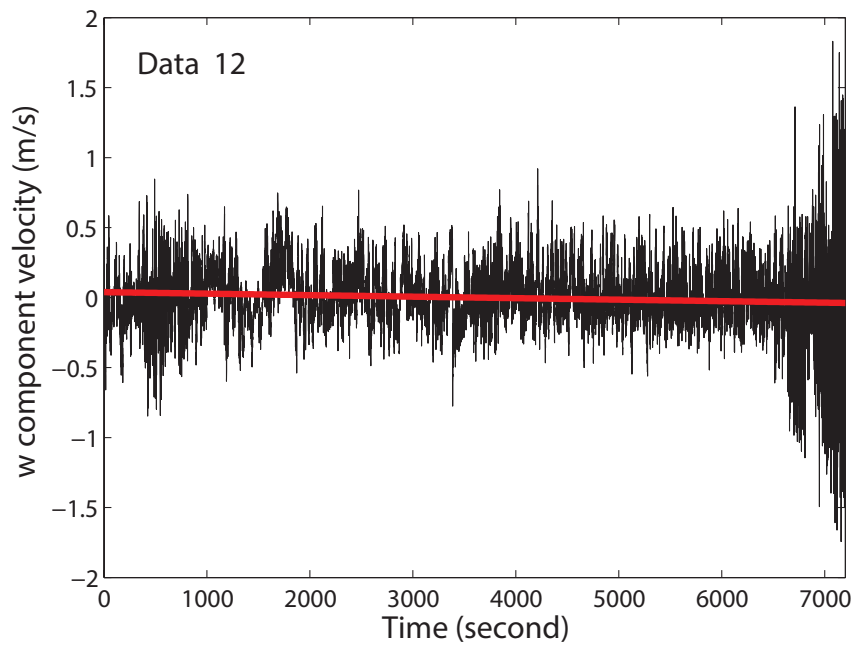


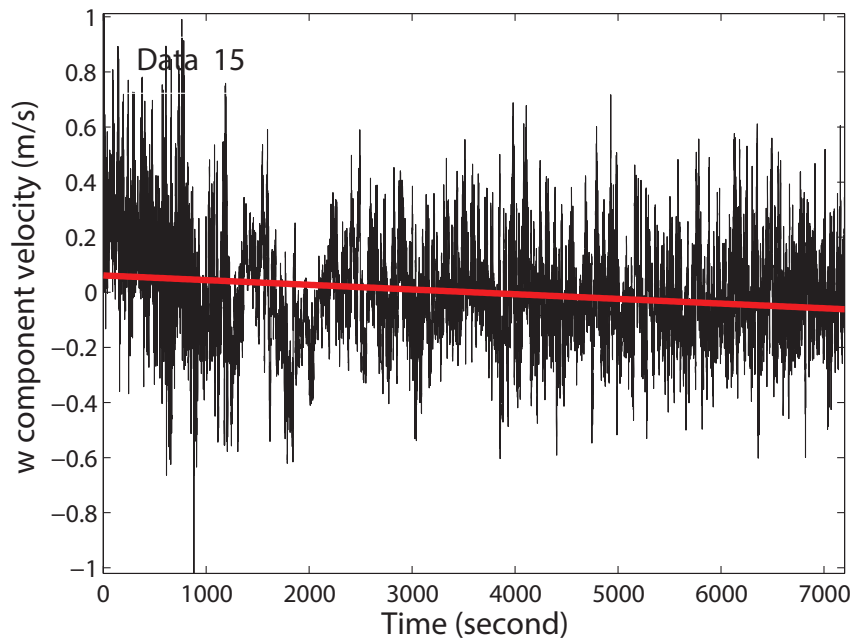
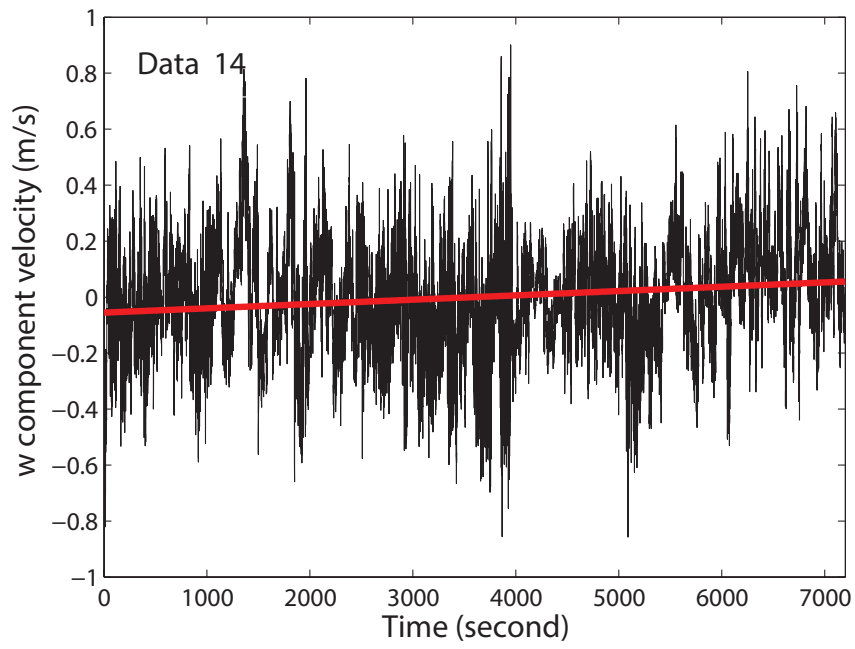


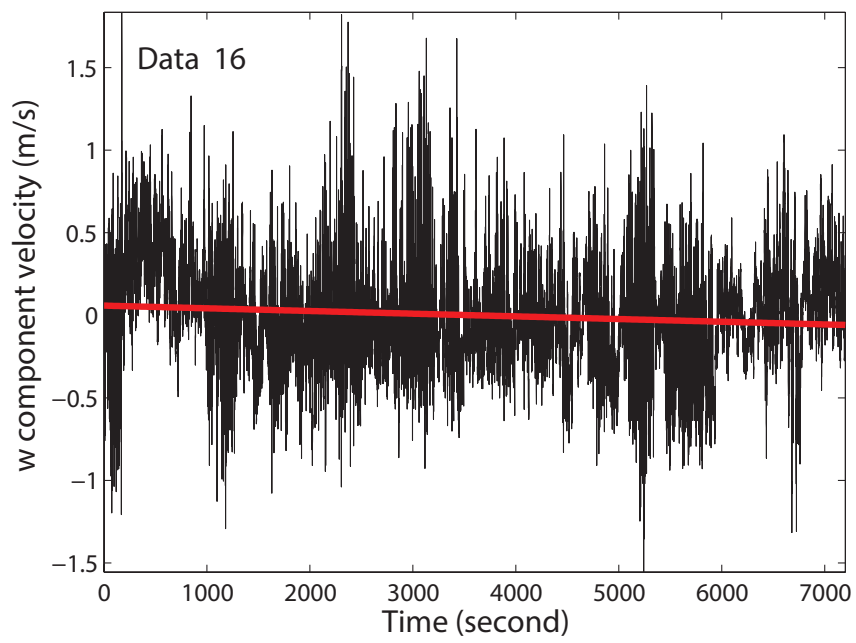


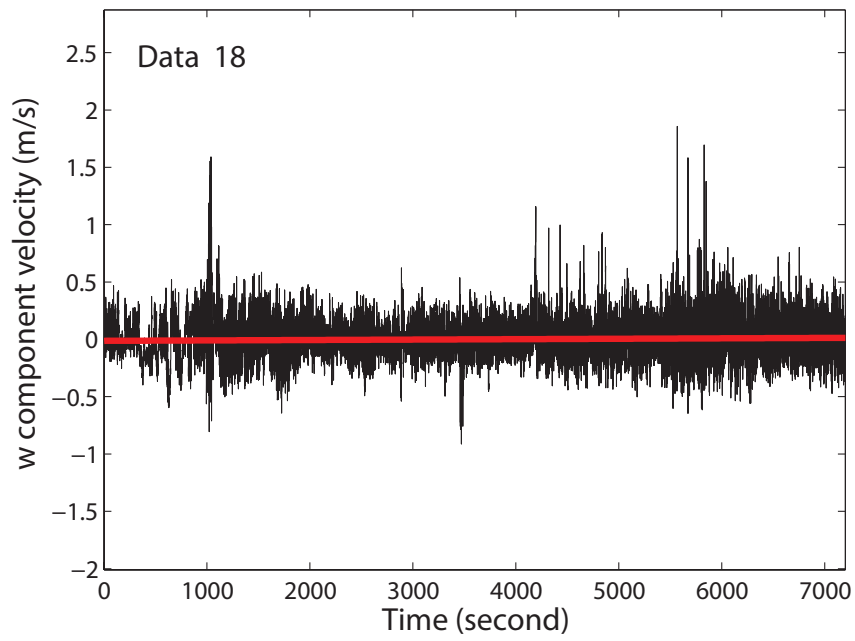
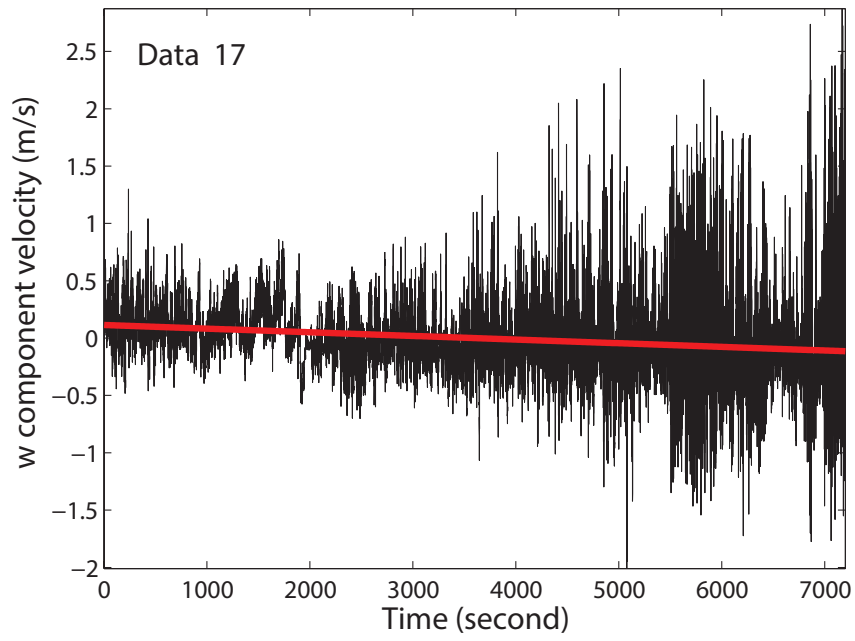
For w component, we have:

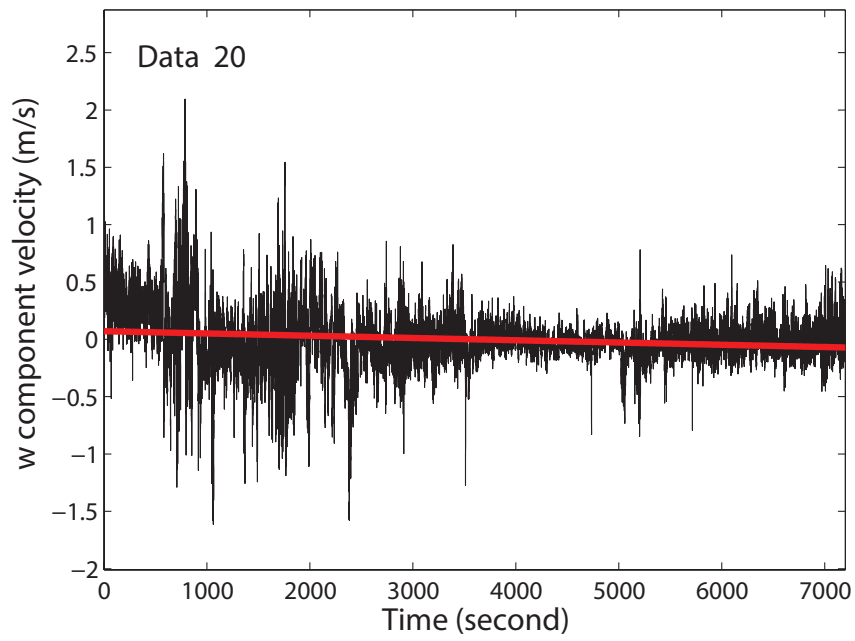
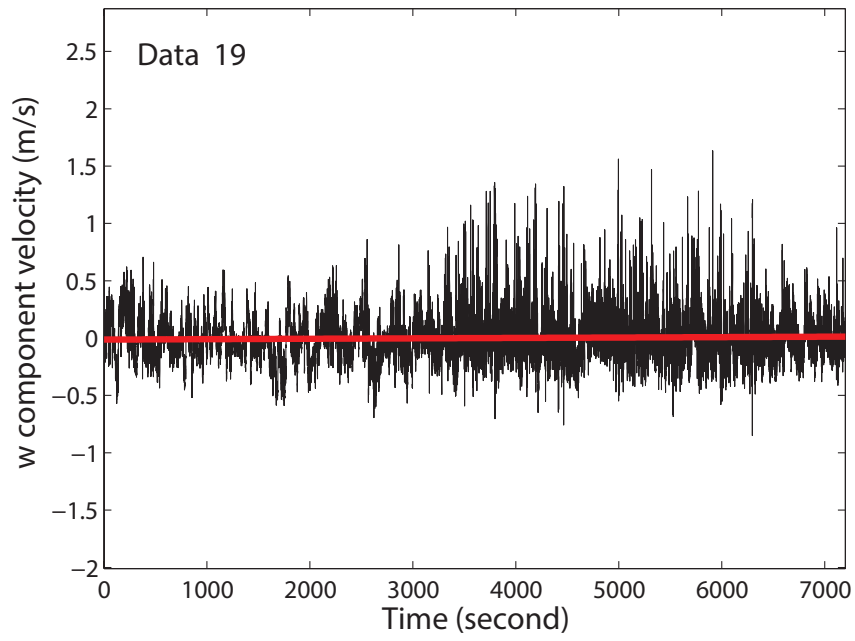




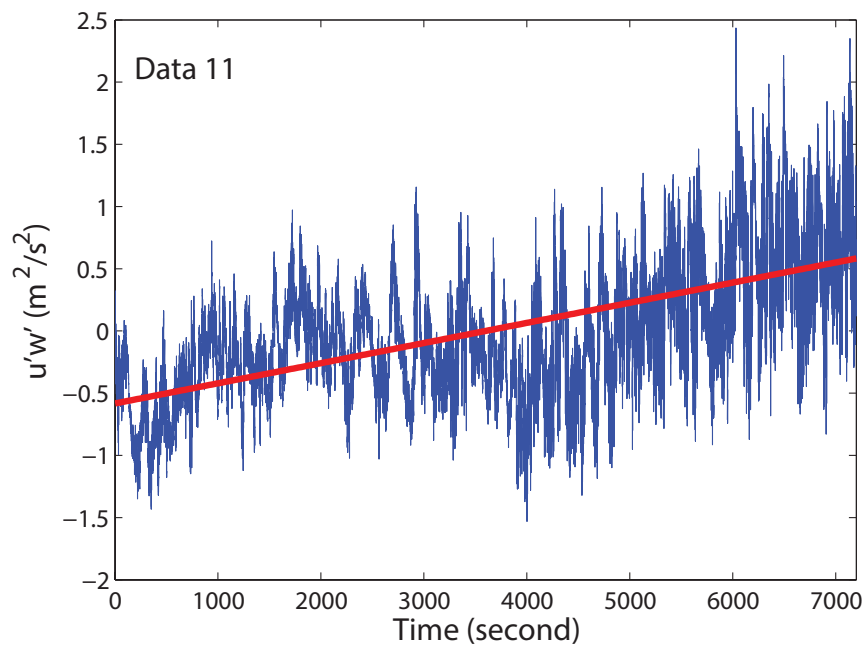


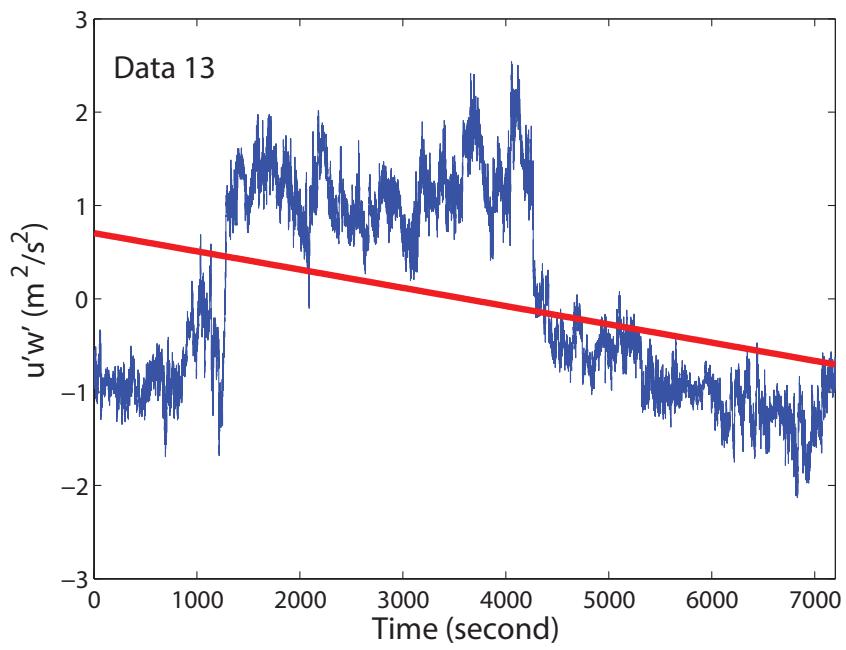
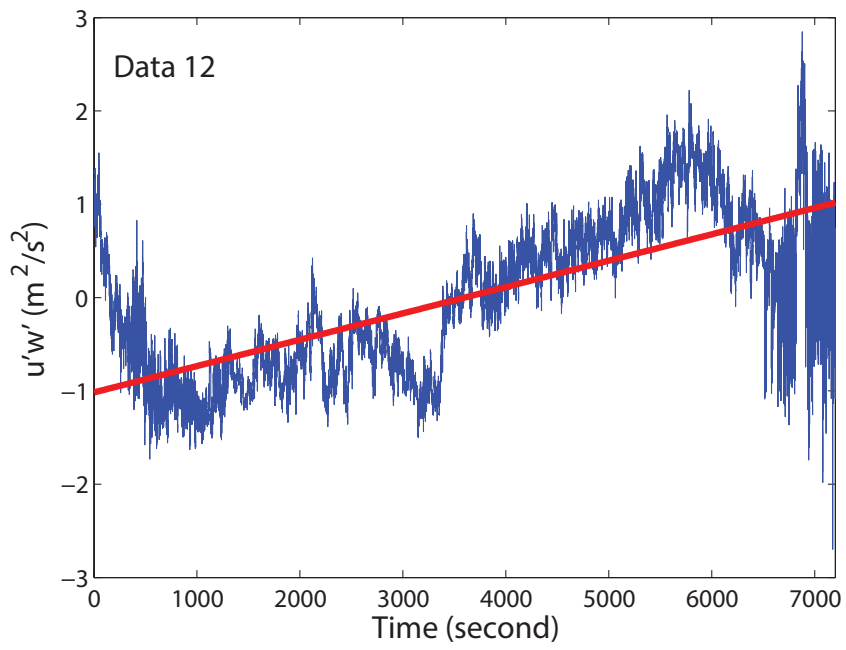


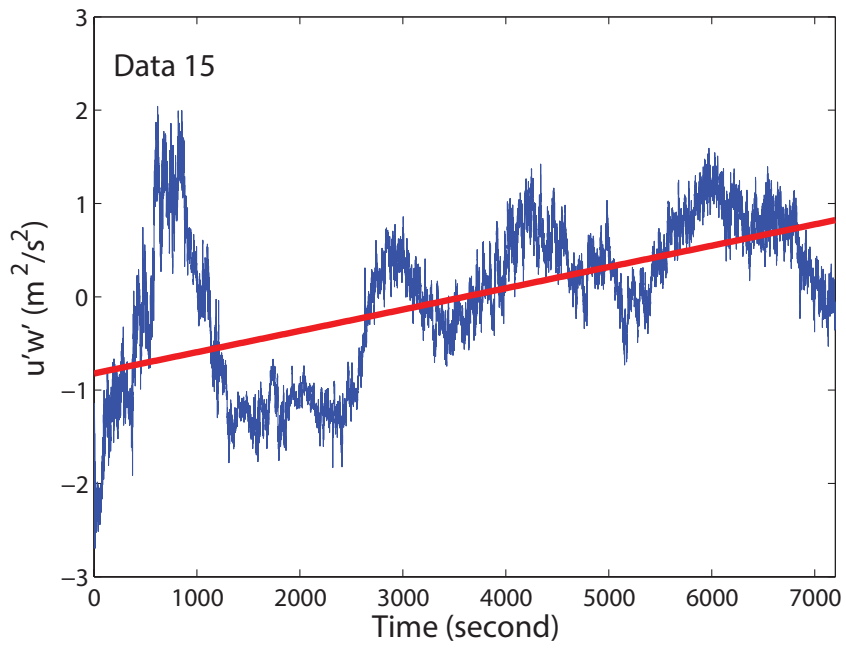
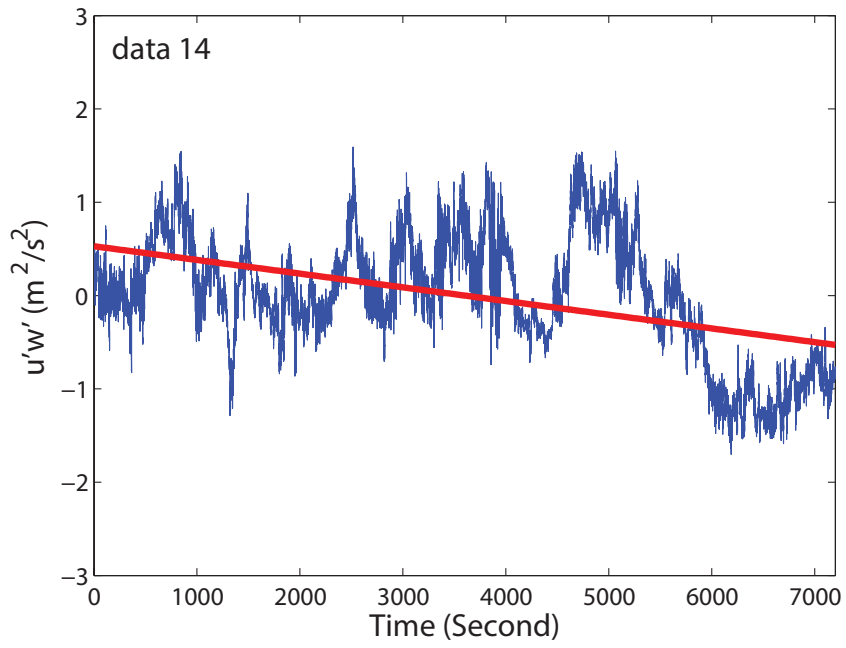


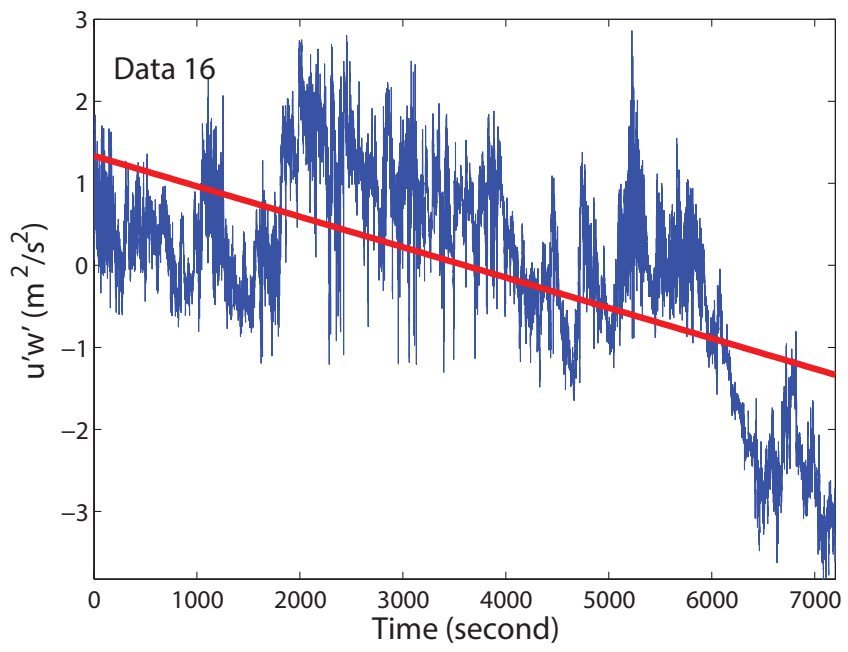


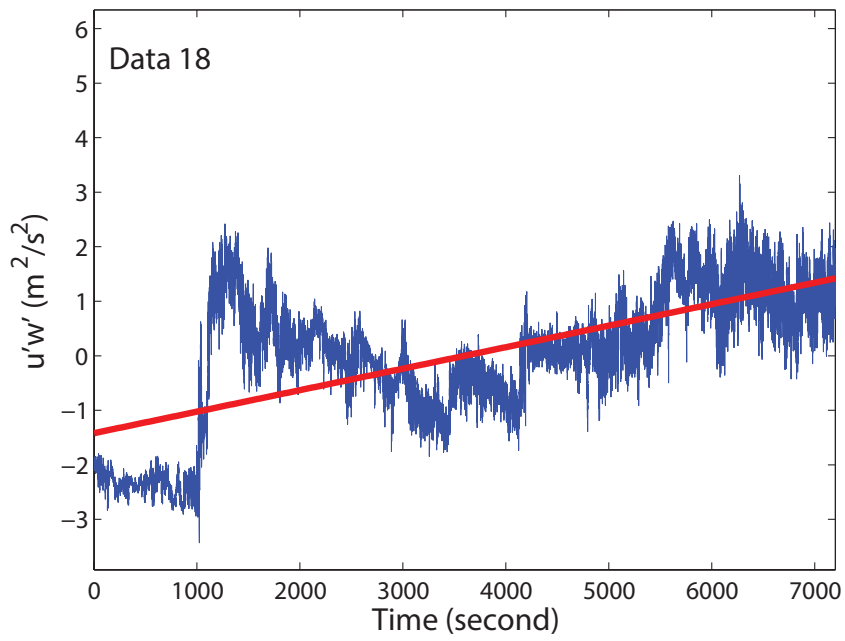
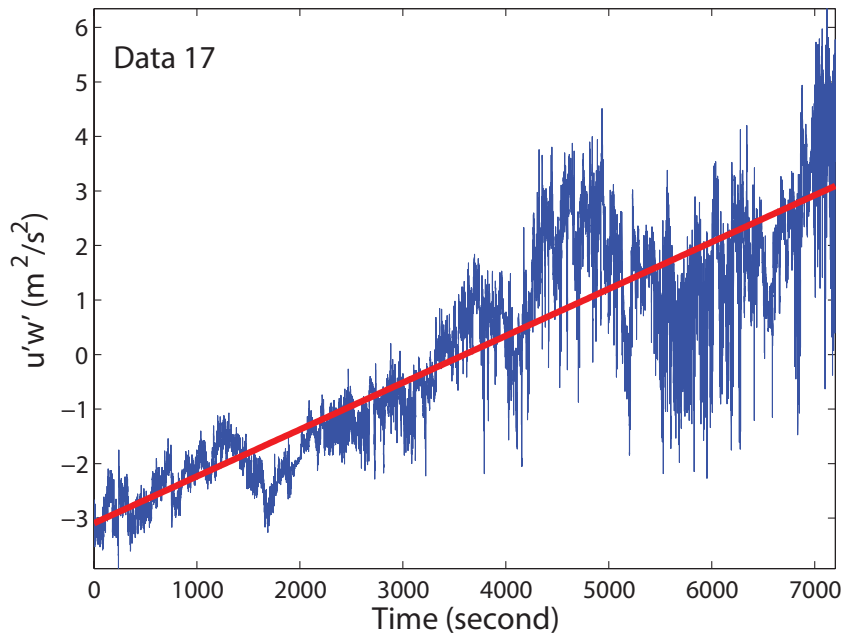
For $u'w'$ component, we have:

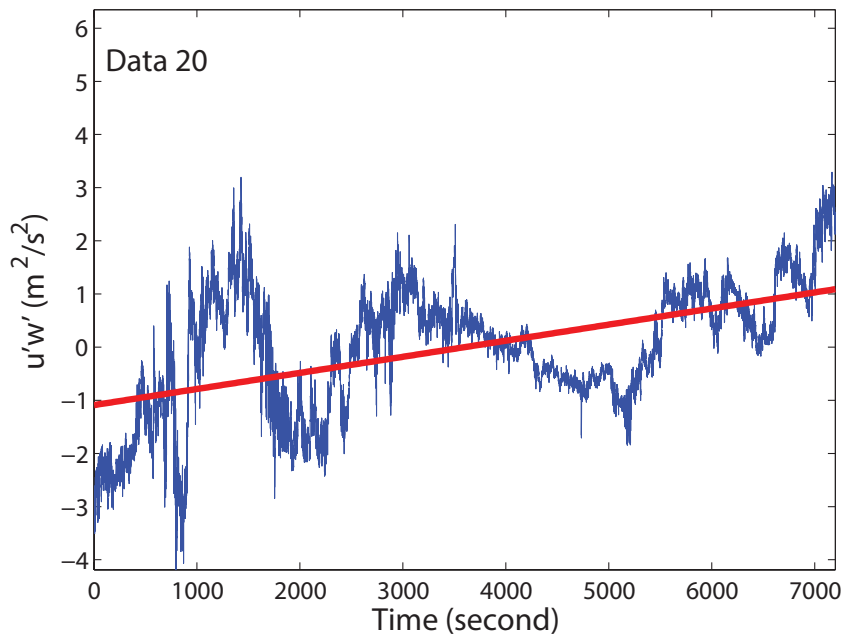
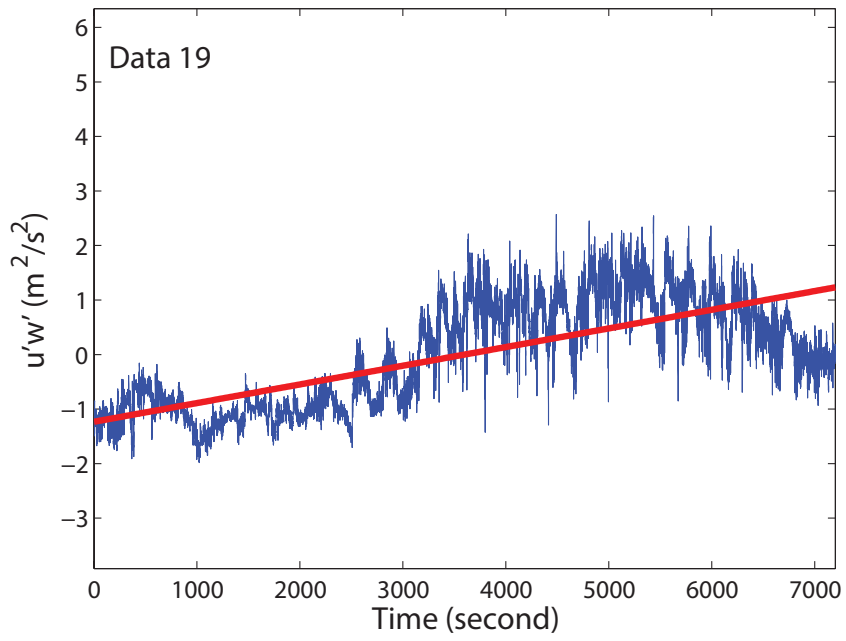






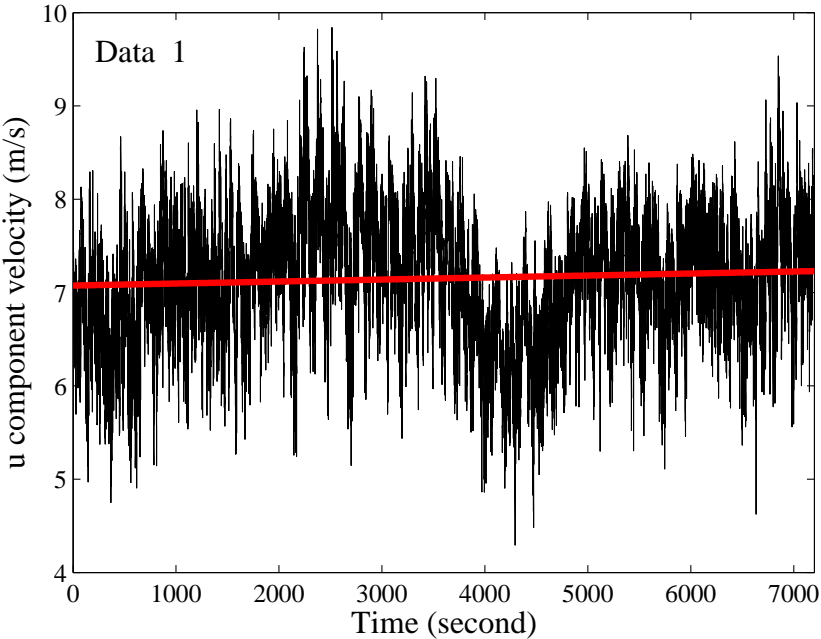


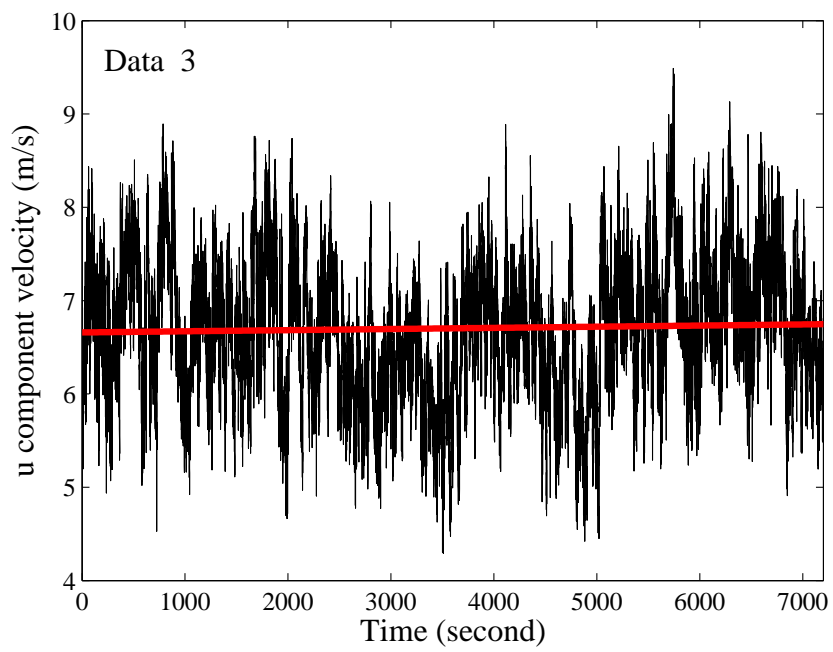
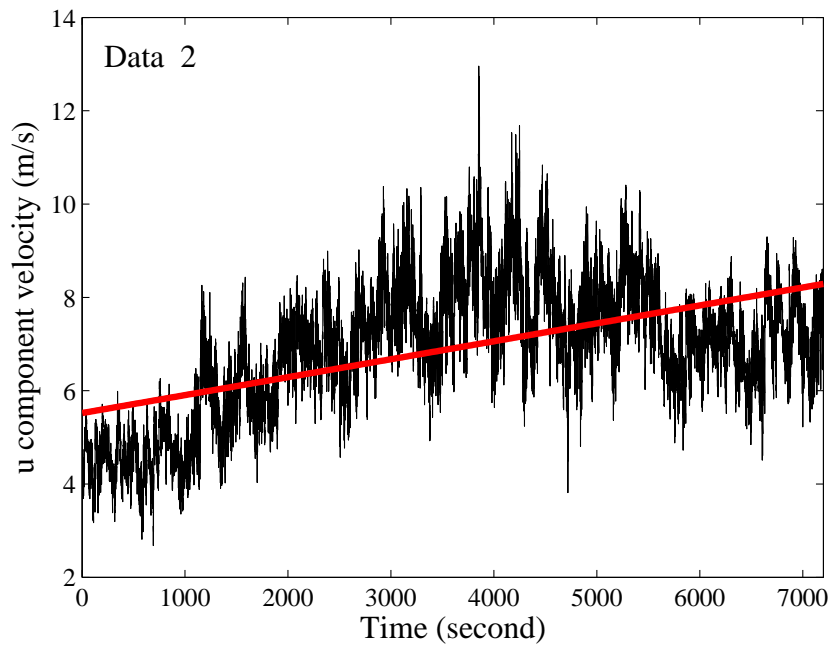


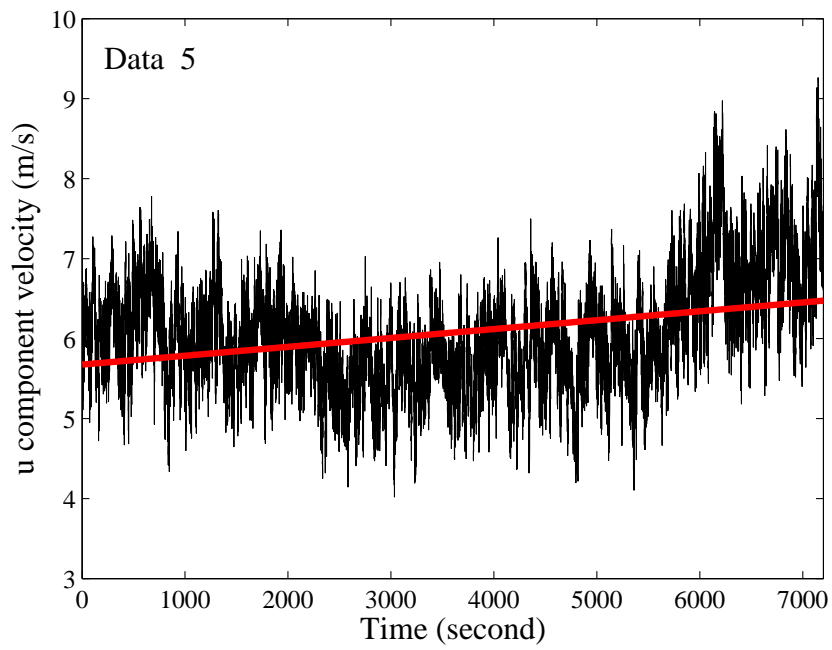
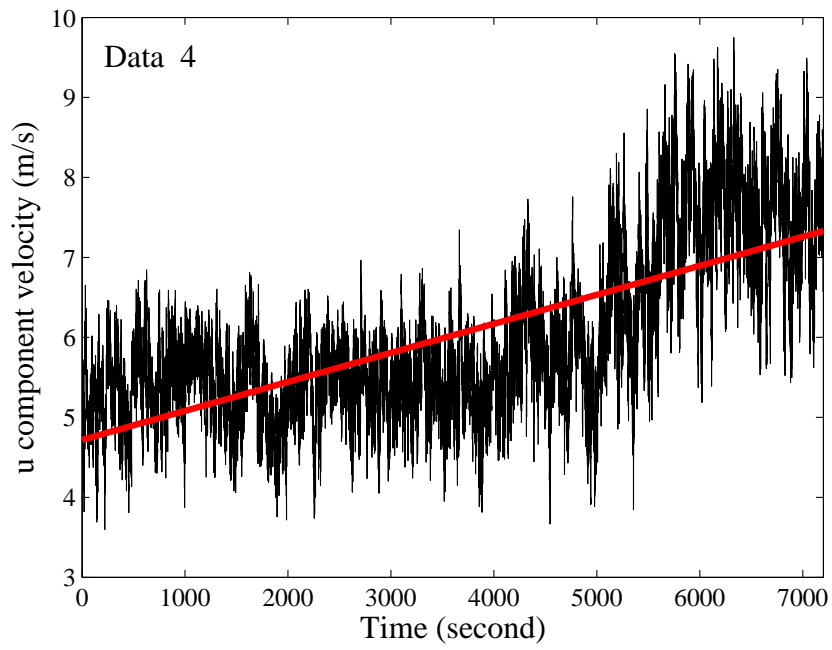


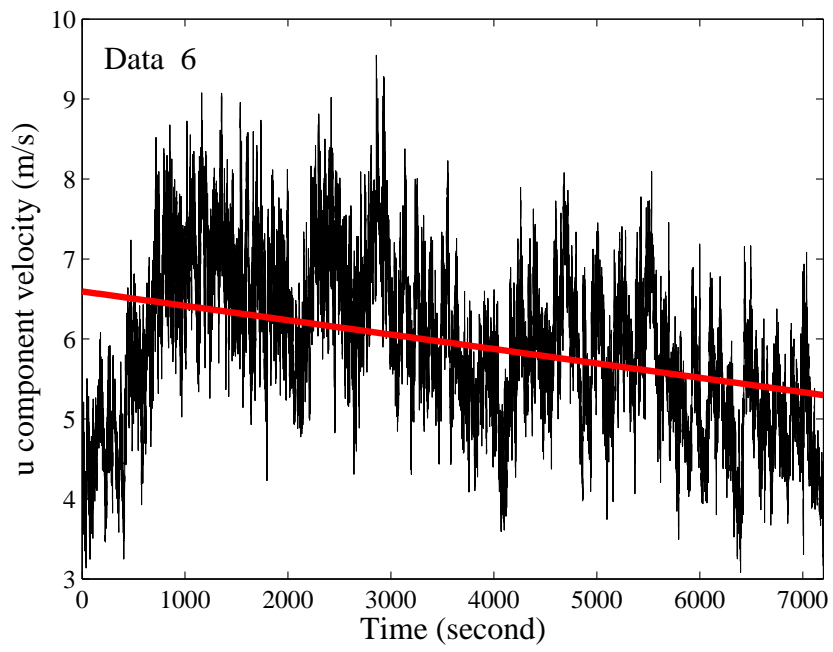
Appendix D

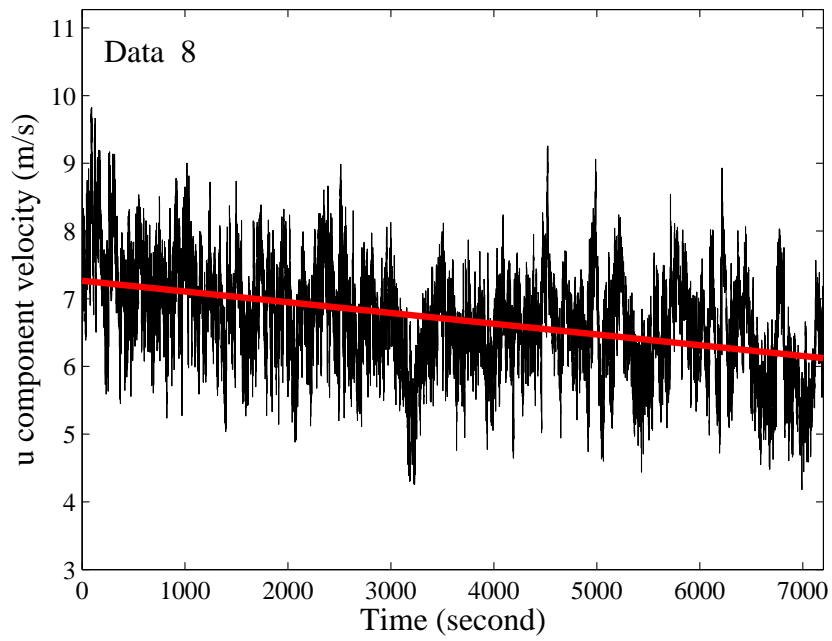
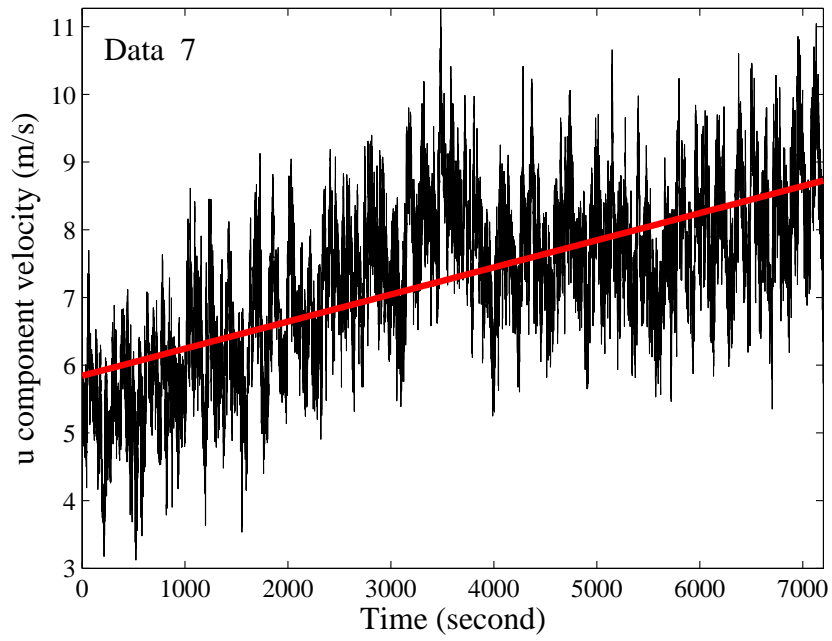
The trends in ogive data analysis for high wind speed cases are described as follows: For U component, we have:

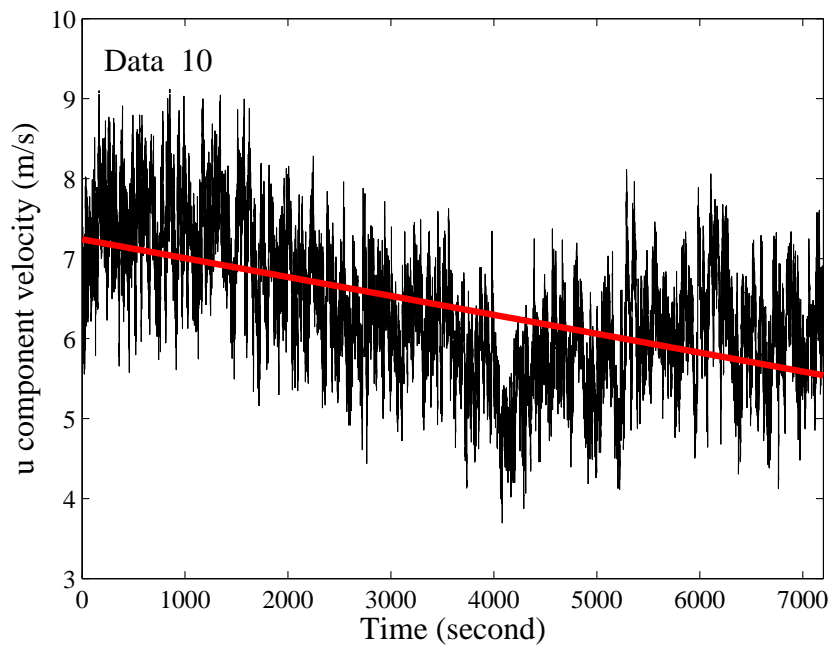
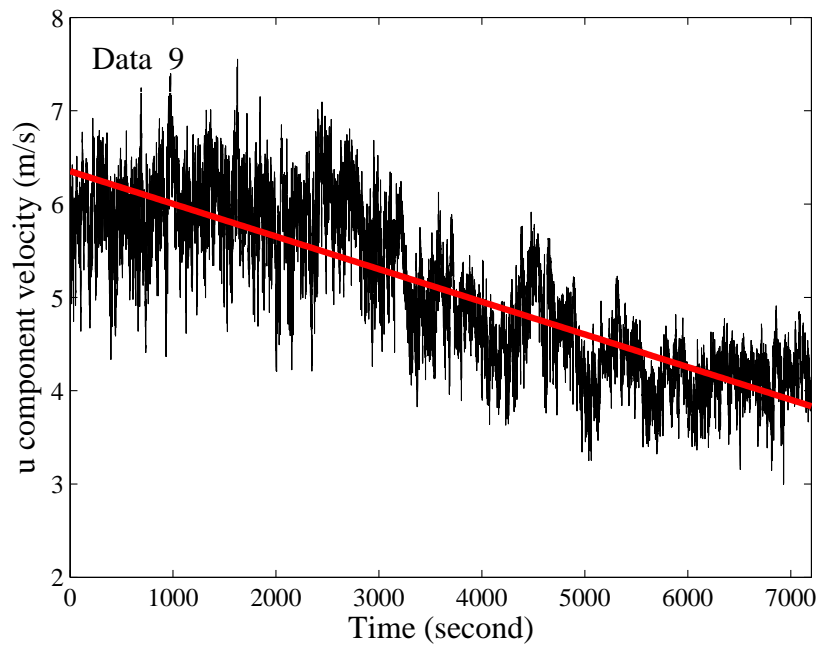




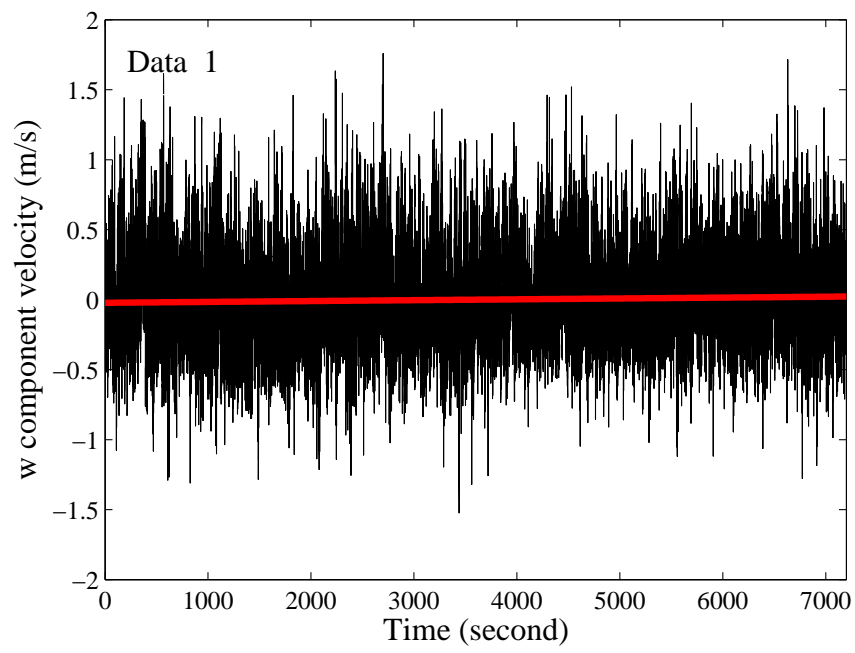


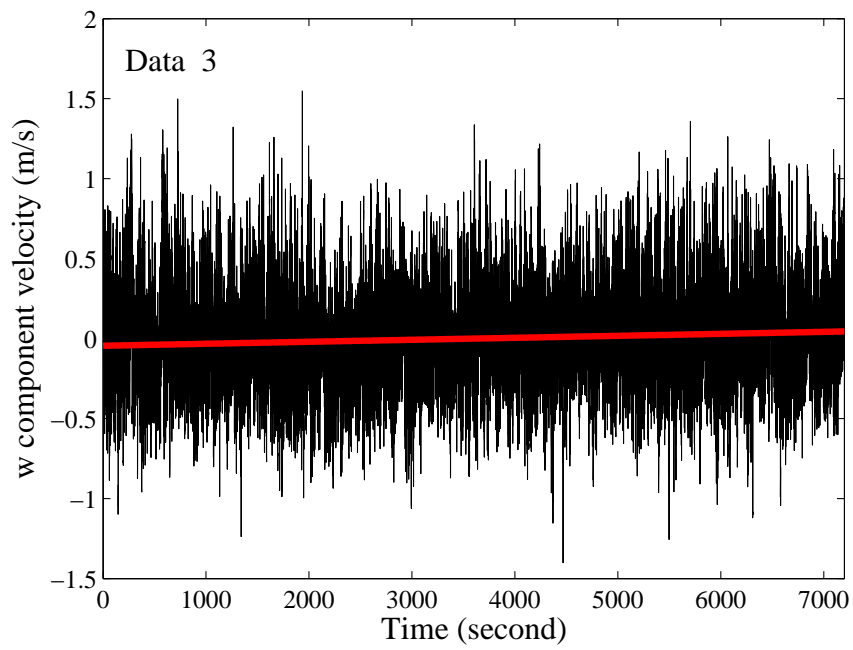
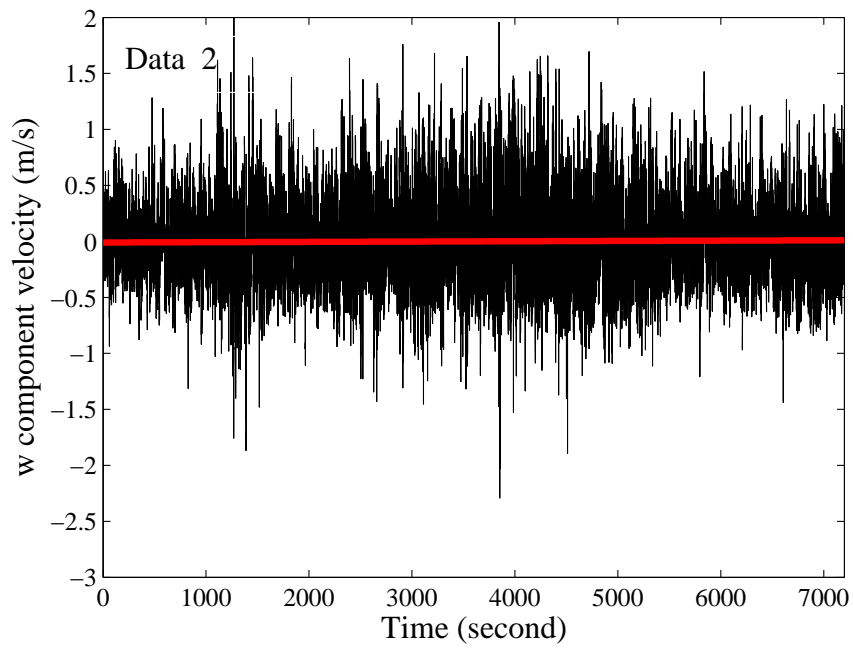


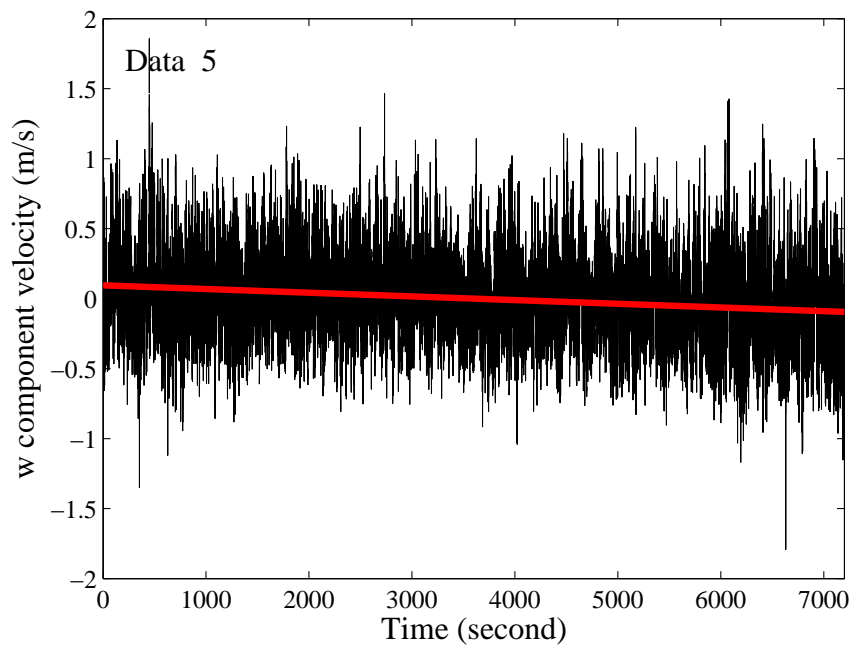
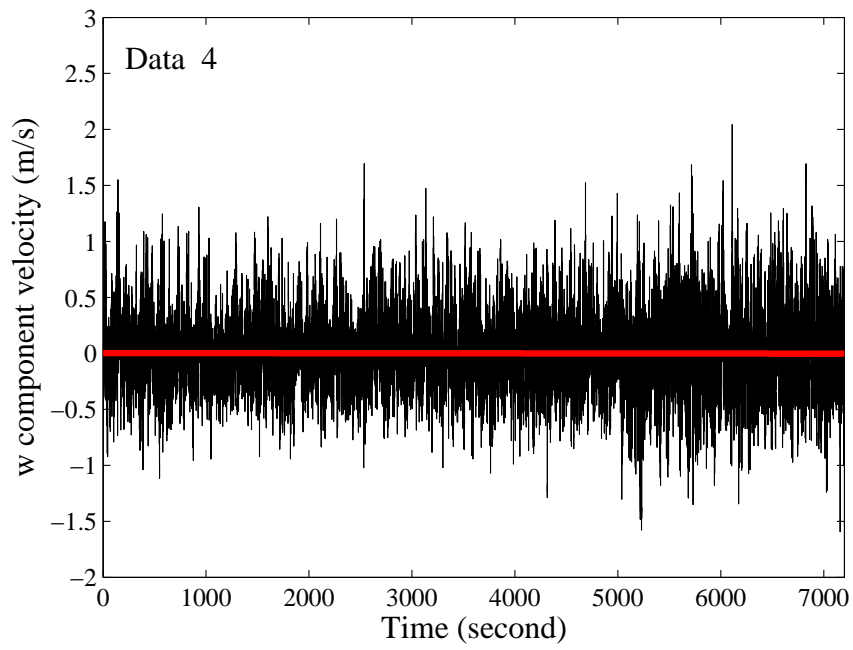


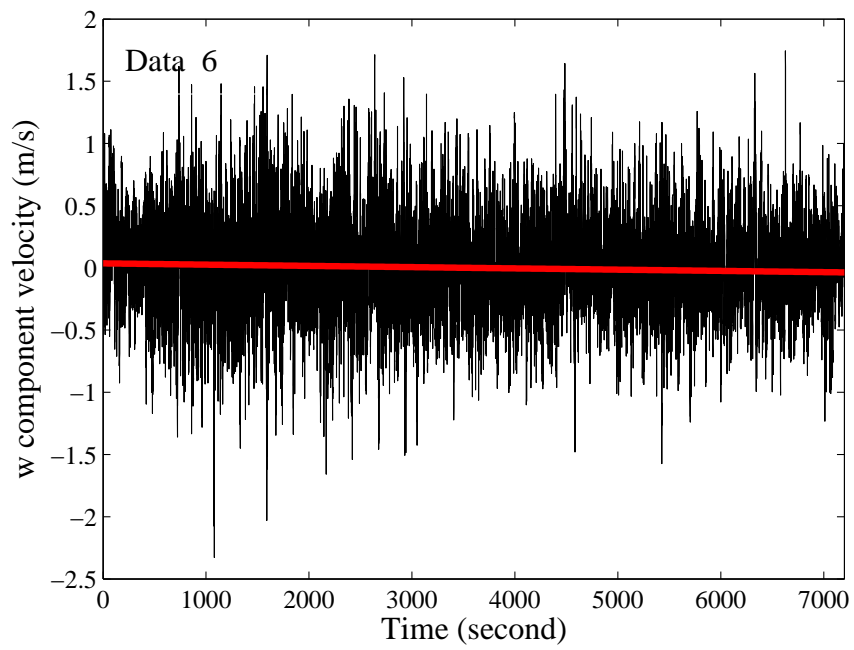


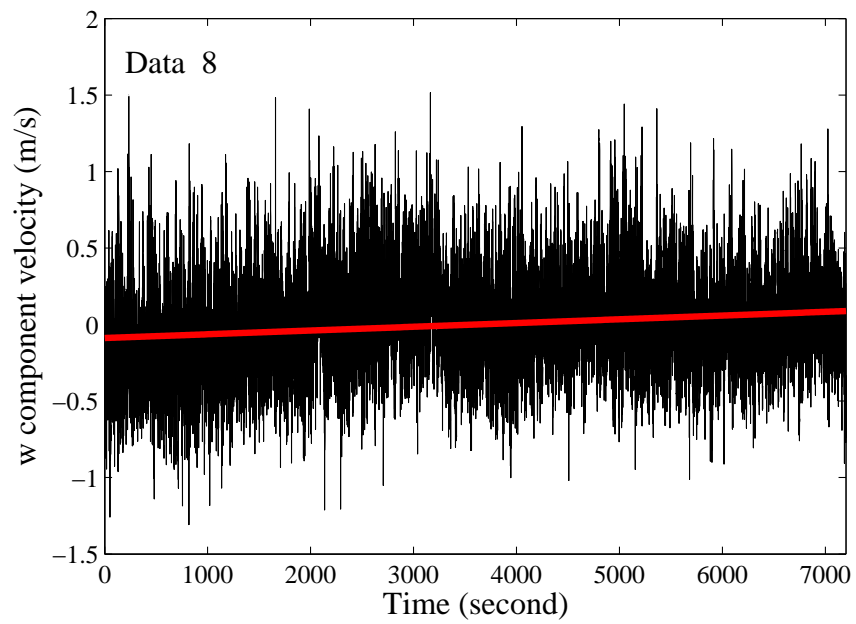
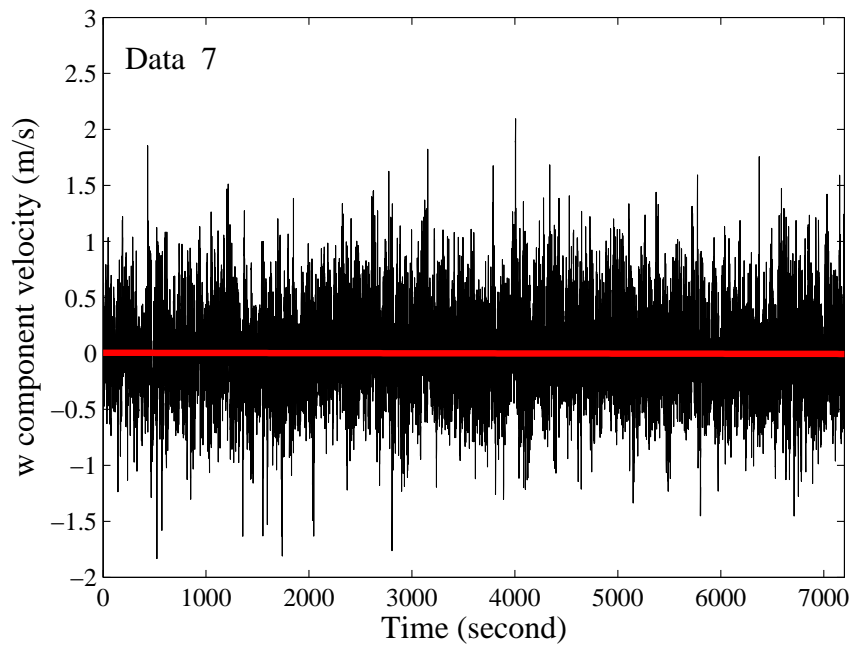
For w component, we have:

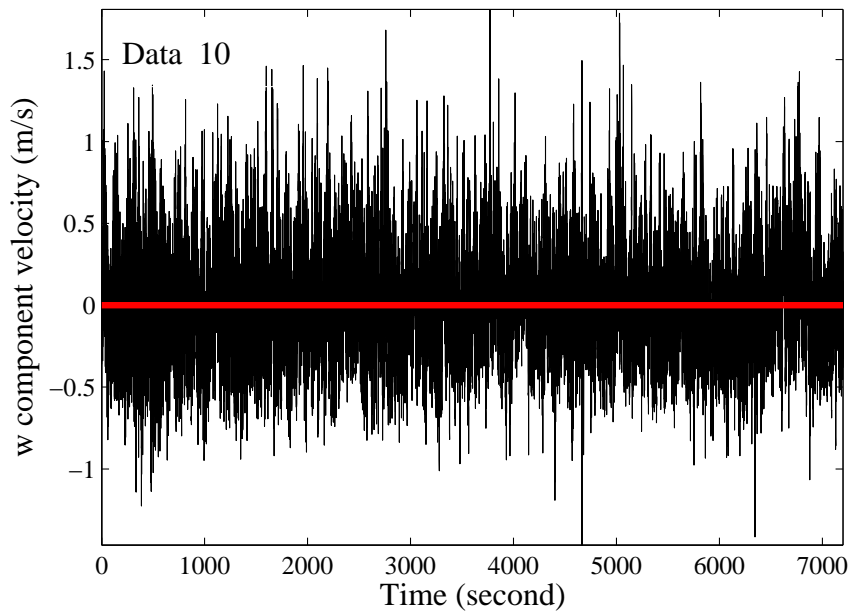
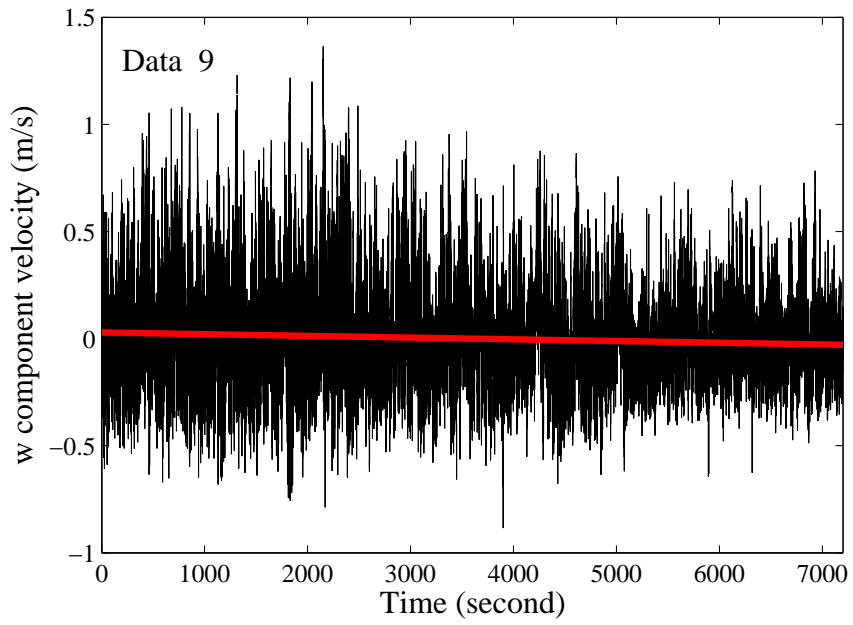












For $u'w'$ component, we have:

